CONTROL OF NETWORKED LAGRANGIAN SYSTEMS WITH DELAYS

BY

ERICK J. RODRÍGUEZ-SEDA

DISSERTATION

Submitted in partial fulfillment of the requirements
for the degree of Doctor of Philosophy in Electrical and Computer Engineering
in the Graduate College of the
University of Illinois at Urbana-Champaign, 2011

Urbana, Illinois

Doctoral Committee:

Professor Mark W. Spong, Chair
Professor Seth A. Hutchinson
Associate Professor Daniel M. Liberzon
Associate Professor Dušan M. Stipanović

ABSTRACT

In sync with the accelerated integration of communication and control systems, this dissertation presents theoretical and experimental results on the robust control of networked Lagrangian systems with discrete-delayed inputs and uncertain information. Within this context, we present novel solutions to the control of nonlinear systems, coordination of multiple agents, bilateral teleoperation, and collision avoidance over unreliable communication channels. We start with the introduction of a passivity-based Model Reference Robust Control framework that guarantees delay-independent asymptotic stability and state convergence of dissipative, nonlinear Lagrangian systems with input and state measurement delays. Then, the proposed control methodology is extended to networks of multiple heterogeneous systems. We demonstrate that stability, formation, and cooperative motion coordination can be attained independently of arbitrarily large constant input delays. We next treat the control problem of single-master-single-slave bilateral teleoperation. Using concepts of passivity theory and input-to-state stability, we design a control strategy that passively compensates for position errors that arise during contact tasks and achieves delay-independent stability and transparency when alternating between unobstructed and obstructed environments. Likewise, we address the case of single-master-multi-slave teleoperation and propose a distributed control law that synthesizes the use of a proportional-derivative controller and the avoidance functions to enforce closed-loop stability, slaves-to-master motion coordination, formation control, static force reflection, and collision avoidance of a group of slave robots with bounded communication delays. We further investigate the topic of collision avoidance and formulate cooperative and noncooperative control strategies that guarantee the safe navigation of multiple Lagrangian systems with limited, unreliable sensing range. Along with the theoretical formulation of the control solutions, this dissertation presents simulation and experimental results with robotic manipulators and unmanned coaxial helicopters utilizing the proposed control strategies.

To my parents

ACKNOWLEDGMENTS

I delightfully devote the following lines to articulate my most sincere gratitude to the many people who in some way or another contributed to the completion of this dissertation (although words will never suffice).

First, I would like to thank my adviser, Dr. Mark W. Spong, for granting me the privilege to conduct my research under his profound knowledge, fueling my research work with interesting ideas, and providing me the perfect balance between direction and freedom that allowed me to venture into diverse research arenas. I am deeply thankful to him for introducing me to the world of robotics, for seeding me with the importance of being practical, and for his unwearying support throughout all these six years.

I will be eternally indebted to Dr. Dušan M. Stipanović or simply Dušan, as he humbly preferred to be called. He has been a true advocate of my work and abilities, seeing in me what I sometimes have failed to see. His dedication and savvy advice throughout the last years have been truly significant on my young career.

I would also like to thank Dr. Seth A. Hutchinson and Dr. Daniel Liberzon for their valuable feedback through the completion of this dissertation. I have also been inspired by the many courses I have taken with Daniel Liberzon, which have meaningfully contributed to the theoretical foundation from which I can now claim to be a control theorist.

I am also thankful to Dr. Charles A. Erignac and Dr. James J. Troy from Boeing Research and Technology for allowing me to conduct experiments at their facilities and for providing me a rich environment to thrive in. I am grateful for the fruitful discussions on control applications over the last two and a half years. Many thanks also go to Paul and Marie Murray for fostering the nicest working atmosphere while I was at The Boeing Company.

I also thank The Boeing Company for providing me with material and financial support for part of this dissertation through the Information Trust Institute. I am also grateful to the National

Science Foundation, the SURGE Fellowship, and the DFI Fellowship for supporting financially my graduate studies and my research work at different stages of my academic journey. However, the results and opinions in this dissertation do not necessarily reflect those of the aforementioned organizations.

My heartfelt gratitude goes to my colleagues and friends at the Coordinated Science Laboratory (CSL) and the Department of Electrical and Computer Engineering for their good sense of camaraderie through all these years. I thank Aaron, Bobby, Chad, Emmanuel, Gökhan, John, Juan, Kunal, Nikhil C., Nikhil S., Peter, Oscar, Sam, Silvia, and Wilfredo. I specially thank Jae-Sung, who has shared the same space at CSL for the last six years and who has become an unexpected pillar through the writing stages of this dissertation. Similarly, I would like to thank my friends at Champaign-Urbana for making this place feel like home and aiding me to dissipate the stress that typically comes with being a graduate student. I restrain myself to include any of their names in this thesis, as I am afraid to leave out some names of this terrific family that keeps on growing. I will make certain to personally thank them.

I would like to thank my best friend for the last several years and whom I deeply admire, Pedro. His frank (and sometimes derisive) criticism and philosophical discussions have challenged me to dream larger.

Special gratitude goes to my self-acquired brothers: Gaby, Alexis, Jonathan, Julio, and Jayson, of whom I feel proud and treasure to have them after all the time we have spent apart.

Finally, I would like to thank my family. Many thanks to Jarice, my courageous sister, and Talo, my well-motivated brother, whose examples have sparked the love towards engineering on their younger brother. I immensely thank my parents, Neftalí Rodríguez and Mildred Seda, because their love, support, and encouragement have yet to meet a boundary. I thank them for keeping my spirit high and for showing me the value of humbleness, hard work, and strong ambitions. I have been enviably blessed to have them. *A ustedes, mis padres, les dedico esta tesis.*

Erick J. Rodríguez-Seda

December 2010

TABLE OF CONTENTS

LIST OF FIGURES viii

CHAPTER 1 INTRODUCTION 1
1.1 Brief History of the Control of Time Delay Systems 2
1.2 Time Delay Effects on Stability 3
1.3 Why Lagrangian Systems? 4
1.4 Research Topics and Related Work 5
1.5 Thesis Outline and Contributions 10

CHAPTER 2 LAGRANGIAN SYSTEMS AND PASSIVITY 14
2.1 Notation 14
2.2 Lagrangian Systems 14
2.3 Passivity 16

CHAPTER 3 CONTROL OF NONLINEAR SYSTEMS WITH INPUT DELAYS 19
3.1 System Dynamics 20
3.2 Passivity-Based Model Reference Robust Control Framework 21
3.3 Stability Analysis and State Convergence 23
3.4 Numerical Example: A 2-DOF Planar Manipulator 29
3.5 Experimental Example: A Coaxial Helicopter 32
3.6 Comments 36

CHAPTER 4 FORMATION CONTROL OF MULTIPLE SYSTEMS WITH INPUT AND STATE MEASUREMENT DELAYS 37
4.1 Multi-Agent System 37
4.2 Control Framework 38
4.3 Stability and Formation Control 40
4.4 Illustrative Example 44

CHAPTER 5 BILATERAL TELEOPERATION: STABILITY AND TRANSPARENCY . . 49
5.1 Time-Delay Bilateral Teleoperation 49
5.2 Stability and Transparency 50
5.3 Modeling the Teleoperator 52
5.4 Towards Transparency Compensation 52
5.5 Simulation and Experimental Results 60

CHAPTER 6 BILATERAL TELEOPERATION OF MULTIPLE AGENTS 67
6.1 Problem Statement and Objectives 67
6.2 Coordination Control 68
6.3 Collision Avoidance Control 74
6.4 Experimental Setup 76
6.5 Experimental Results 81

CHAPTER 7 COLLISION AVOIDANCE CONTROL: TWO-AGENT SYSTEMS 87
7.1 Problem Formulation 88
7.2 Collision Avoidance Control 91
7.3 Collision Avoidance under Bounded Uncertainties 93
7.4 Simulation Examples 101
7.5 A Cooperative Collision Avoidance Experimental Example 106

CHAPTER 8 COLLISION AVOIDANCE CONTROL: MULTI-AGENT SYSTEMS 109
8.1 Multi-Lagrangian System with Bounded Control Inputs and Sensing Uncertainties . 109
8.2 Control Objective and Definitions 110
8.3 Control Framework 111
8.4 Collision Avoidance Analysis 116
8.5 Example: Collision Avoidance with Detection Delays 118
8.6 Example: Collision Avoidance without Sensing Uncertainties 122

CHAPTER 9 CONCLUSIONS AND RECOMMENDATIONS 125
9.1 Conclusions 125
9.2 Recommended Future Research Directions 127

REFERENCES 129

LIST OF FIGURES

1.1 Networked control system with delays. 3
1.2 Configuration of a teleoperation system. 7
1.3 Raymond Goertz operating a mechanical teleoperator. 8

2.1 Negative feedback connection of two passive systems. 18

3.1 Nonlinear plant and controller with input and state measurement delays. 20
3.2 Proposed MRRC framework. 23
3.3 Planar manipulator. 30
3.4 Response of proximal and distal links with the proposed MRRC framework without utilizing the full state compensator for $T_1 = 1.0$ s and $T_2 = 0.5$ s. 31
3.5 Response of proximal and distal links with the proposed MRRC framework using the full state compensator for $T_1 = 1.0$ s and $T_2 = 0.5$ s. 32
3.6 Available energy for compensation. 32
3.7 Coaxial helicopter. 33
3.8 Position and orientation response of the coaxial helicopter with proposed controller for $T_1 = 0.50$ s and $T_2 = 0.03$ s. 35
3.9 Norm of the position and orientation errors. 36

4.1 Multi-vehicle system with control communication delays. 37
4.2 Proposed multi-MRRC framework. 39
4.3 Omnidirectional vehicle. 45
4.4 Cartesian position (x, y) of the four vehicles. 46
4.5 Norm of the position error. 46
4.6 Norm of the heading angle error. 47
4.7 Cartesian position (x, y) of the four vehicles for a time-varying formation. 47
4.8 Norm of the position error for a time-varying formation. 48
4.9 Norm of the heading angle error for a time-varying formation. 48

5.1 Scheme of a bilateral teleoperation system with local delays T_{1_i} and T_{2_i}, and interconnection delays T_m and T_s. 50
5.2 Position of master and slave robot with constant $b_m(t) = b_{free}$. 61
5.3 Position of master and slave robot with time-varying $b_m(t)$. 61
5.4 Evolution of the Wave Impedance $b_m(t)$. 62
5.5 Experimental testbed. 63
5.6 Position of master and slave robot with constant $b_m(t) = b_{free}$. 64
5.7 Position of master and slave robot with time-varying $b_m(t)$. 64

5.8 $\mathcal{L}_2$ norm of the position error. 65
5.9 Force tracking and wave impedance. 66

6.1 Detection (radius R) and avoidance (radius r) regions. 74
6.2 Experimental workspace. 77
6.3 Master and slave agents. 77
6.4 (a) Orientation of the rotational angles (θ, ϕ, ψ) with respect to the Cartesian coordinates (x, y, z). (b) Virtual coupling between master and slave agents. 79
6.5 A 3-D image generated by the MoCap System using Vicon iQ2.5 graphical display. . 80
6.6 Sequential motion of slave agents with fixed formation in an unobstructed environment. 82
6.7 Position error for an unobstructed environment and a fixed formation. 82
6.8 Sequential motion of slave agents with fixed formation in an obstructed environment. 83
6.9 Position error for an obstructed environment and a fixed formation. 84
6.10 Sequential motion of slave agents with dynamic formation in an obstructed environment. 85
6.11 Position error for an obstructed environment and dynamic formation. 86

7.1 Antitarget $(\mathcal{T})$, Avoidance (Ω), Conflict $(\mathcal{W}_i)$, and Detection $(\mathcal{D}_i)$ Regions for the ith agent. 90
7.2 Hypothetical motion of $\mathbf{q}_j(\tau)$ with respect to $\mathbf{q}_i(\tau)$ for $t_\delta \leq \tau \leq t_f$. 94
7.3 Extreme case in Lemma 7.3.1. 95
7.4 Noncooperative collision avoidance example. 103
7.5 Distance between agents for the noncooperative collision avoidance example. 103
7.6 Cooperative collision avoidance example. 105
7.7 Distances among agents for the cooperative collision avoidance example. 106
7.8 Two E-Flite μ-CX coaxial helicopters. 107
7.9 Cooperative collision avoidance experimental example. 108
7.10 Norm of the distance between the two helicopters. 108

8.1 Bounded avoidance function and bounded avoidance control. 113
8.2 Multi-agent collision avoidance example with sensing uncertainties. 120
8.3 Distances among agents with sensing uncertainties. 121
8.4 Norm of the difference between the position of the vehicles and their desired configuration. 121
8.5 Multi-agent collision avoidance example with perfect sensing. 123
8.6 Distances between agents with perfect sensing. 124
8.7 Norm of the error between the position of the agents and their desired configuration. 124

CHAPTER 1

INTRODUCTION

Recent advances in electronics and integrated communications have allowed the development of a new generation of control systems technology, namely networked control [1–4]. Nowadays, sensors, actuators, controllers, and processes (which we will refer to as *agents*) are no longer restricted to being physically connected, not even proximal to one another. Instead, in a networked control system (NCS), agents can asynchronously operate from remote locations and share information through a wireless communication network. This spatially distributed configuration mitigates implementation and maintenance costs and provides scalability, redundancy, and robustness in the control process. Such advantages make NCSs appealing for several applications including space and underwater exploration, search and rescue, coverage control, data mining, power distribution (e.g., smart grids), traffic control, remote diagnostic, and teleoperation.

Although NCS technology has significantly matured over the recent years [5], there are many control and communication challenges to overcome [6]. One of these challenges is to guarantee stability and reliable performance of the overall system independently of inherent network-induced delays. Time delays can originate and develop as a result of congested communication networks, complex transmission protocols, large separation distances between agents, and limited hardware and software update rates. For instance, the sampling process of the variable being regulated, the computation of the control command, and the time it takes for the control signal to travel from the controller to the actuator or plant in a NCS may add a significant delay to the control loop. If the presence of this delay is not carefully considered, the overall system may exhibit a poor performance and, in the worst scenario, instability [1, 7]. Therefore, it is crucial to design control frameworks that guarantee the overall stability and safety of the networked system independently of delays.

Inspired by the need for reliable and robust control frameworks for NCSs, we now present different theoretical and experimental results for the control of time delay systems. Herein, we focus on

the robust control of mobile networked Lagrangian systems, including unmanned vehicles and manipulators, and present control ideas mainly based on stability, motion coordination, and collision avoidance under communication delays. In some instances, we will extend our analysis to address other important issues within NCSs such as stability, safety, and convergence when the control's communication network induces data transmission errors and quantization (e.g., Section 3.3.1 and Chapters 7 and 8).

1.1 Brief History of the Control of Time Delay Systems

The study of time delay systems can be traced back as far as the 18th century with the pioneering work of prestigious scientists and mathematicians[1] working on delayed differential equations and formalized later with the mathematical analysis of the delay effects on biological [8] and mechanical systems [9,10] in the early 20th century. Yet, it was not until the 1930s that the effects of delays in a system were explicitly visited from a control perspective [11]. The work of Callender *et al.* [12] on the design of stable controllers considering time-lags (delays) in the mid 1930s and the engineering review [13] published in 1937 in the periodical *The Engineer* relating the effect of delays with the introduction of negative damping, seeded the interest for what would become a long line of research in the control of time delay systems. Here, we cite a few relevant results that followed, starting with the work of Minorsky [14], who investigated problems related to ship stabilization; Tsypkin [15], who provided sufficient conditions for delay-independent stability in the frequency domain; and Myshkis [16], who properly defined the use of functional (delay) differential equations. The following decades experienced considerable attention on the control of delay systems (see [11,17] for historical references), from which we emphasize the work of Smith [18] in *eliminating* the delay from the feedback loop and the separate work of Razumikhin [19] and Krasovskii [20] in extending Lyapunov stability theory to systems with delays. For a more exhaustive survey on this topic, the reader can refer to [11, 17, 21, 22].

Nowadays, the study of control systems with delays has regained momentum, owed in part to the recent popularity of NCSs [2, 3, 23] as well as its many derived applications such as teleoperation [24, 25], mobile sensors [26], and cooperative tasking [27]. In this context, the stabilization and control of linear NCSs has been treated for constant delays [1] as well as for time-varying delays

[1] We especially note the work of Daniel Bernouilli, Leonhard Euler, Joseph-Louis Lagrange, Pierre-Simon Laplace, and Nicolas de Condorcet.

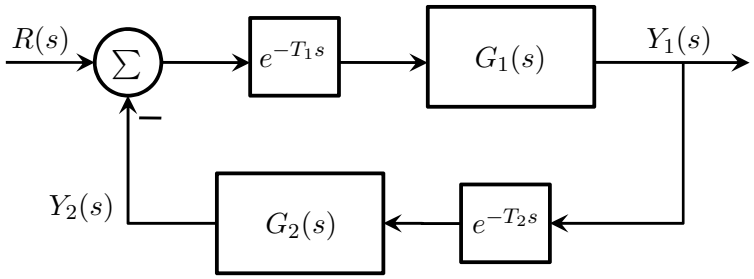

Figure 1.1: Networked control system with delays.

[28–30]. The control of networked systems with nonlinear dynamics has also been addressed in [31–33]. Similarly, there has been a great amount of effort to minimize the delay or mitigate its effects in the control loop [34–36]. For some further reading on NCS research, the reader can consult [5, 6, 23, 37–39].

1.2 Time Delay Effects on Stability

The classical hypothesis in the control of most dynamical systems has been to assume that the evolution of the states does not depend on information from their past. Although this assumption is suitable for many engineering processes, there exists a wide range of control systems for which the effects of delays cannot be ignored. As an example, let us consider the two interconnected linear systems depicted in Figure 1.1, where $G_i(s)$ and $T_i \geq 0$ represent the Laplace transfer functions and the associated delays for the first ($i = 1$) and second ($i = 2$) system, respectively. The total transfer function from the input $R(s)$ to the output $Y_1(s)$ can be computed as

$$G(s) = \frac{Y_1(s)}{R(s)} = \frac{G_1(s)e^{-T_1 s}}{1 + G_1(s)G_2(s)e^{-(T_1+T_2)s}} \,. \tag{1.1}$$

From the above equation and denominator, the dependence of the stable and unstable poles on the round-trip delay value becomes evident. More importantly, we have that for a positive round trip delay, i.e., $T_1 + T_2 > 0$, the closed-loop system has an infinite number of poles. Therefore, conventional control linear analysis is not sufficient to fully comprehend the behavior of (1.1).

In order to show the potential effect of delays on stability, let us consider the following example. Let $G_1(s) = k\frac{1}{s}$ and $G_2(s) = 1$ where k is a control parameter. Then, the characteristic equation

of (1.1) is given by

$$s + ke^{-(T_1+T_2)s} = 0. \tag{1.2}$$

For no delay, we may easily check that the closed-loop system is stable for any $k > 0$. However, once there is a positive delay in the control loop, one can always find a positive value of k for which the system will become unstable. Indeed, the system is unstable for any round-trip delay satisfying [11] the following inequalities

$$T_1 + T_2 > \frac{\pi}{2k}, \qquad k > 0. \tag{1.3}$$

The previous example demonstrates the appearance of instability on delay-free stable systems due to feedback delays. The reverse case is also possible: Unstable or marginally stable systems can be stabilized by delayed output feedback [40]. In fact, time delay systems may exhibit infinite switches of stability according to the control parameters and the size of the delay [41]. This latter topic, as well as the stabilization of unstable systems via delayed feedback, will not be further investigated in this thesis.

1.3 Why Lagrangian Systems?

Arguably, most control theories and analytical tools for the study and control of time delay systems have been developed with linear systems in mind. Yet, the vast majority of systems are nonlinear in nature, and although we can certainly force nonlinear system to behave linearly by canceling nonlinearities using active control or by operating the system near its equilibrium point, these techniques are not sufficiently robust or do not properly capture the system's complex behavior. Thereby, throughout this thesis we'll presume systems are nonlinear and use the Euler-Lagrange (i.e., Lagrangian) formalism to represent them. We opt for the Euler-Lagrange formalism over other nonlinear representations for diverse reasons. Some of these reasons are listed below.

- The Lagrangian formulation derives from the minimization of an energy function. Hence, we can expect the system to satisfy some energy-related properties. One of these properties is *passivity*, which will play a central role in assessing the stability of the system and the development of the control ideas proposed in this dissertation.

- The Euler-Lagrange formulation allows us to easily synthesize systems of different nature (e.g., electrical, electromagnetic, and mechanical systems).
- The Euler-Lagrange equations are invariant with respect to coordinates.
- The Lagrangian structure is conserved under feedback interconnection [42]. This avails us to divide a complex system into the interconnection of smaller and simpler ones.
- The motion of most practical mechanical and electrical systems, such as robotic manipulators and omni-directional vehicles, can be modeled using Euler-Lagrange equations.

1.4 Research Topics and Related Work

As previously stated, we study the stabilization and safe control of networked systems with time delays whose dynamics can be described by nonlinear Euler-Lagrange equations. Specifically, we address problems of stability, motion coordination, trajectory tracking, bilateral teleoperation, and collision avoidance of mobile networked systems with discrete delayed[2] inputs. The following is a literature review of the research areas covered in this document.

1.4.1 Control of Nonlinear Systems with Input Delays

We study the control of Euler-Lagrange nonlinear systems with parametric uncertainties and constant input delays. Whereas the case of time delay linear systems has been well studied and documented in the literature [11, 21, 22], the robust control of time delay nonlinear systems has received relatively little attention from the control community. Moreover, the few existing control frameworks for nonlinear systems typically constrict their scope to plants with linear norm-bounded nonlinearities, known constant delays, or well-known dynamics. Some efficient but yet restrictive, recent examples include a model reference adaptive control that enforces stability and state tracking for a known-structured nonlinear system with bounded nonlinearities and known input delays [43]; a backstepping design technique that guarantees stability for a class of well-defined nonlinear systems with arbitrary-large, known, constant delays [44]; and a delayed output feedback control that

[2] A system is said to have discrete delays if the evolution of the states depends on a finite and discrete set of information from its past. In contrast, a system is said to have distributed delays if the evolution of the states depends on information from its past over a finite set of continuous bounded intervals of time.

achieves asymptotic stability for a family of systems with linear norm-bounded-in-state and in-control nonlinearities [45]. Although all these examples solve the stability issue induced by delays for specific sets of families of nonlinear systems, the control ideas presented therein are not easily adapted to more general classes of nonlinear systems, such as nonlinear Lagrangian processes.

Recently, the control of a larger class of nonlinear plants with delayed output feedback was addressed through the use of the scattering transformation, a conventional approach in the tele-operation field [46]. In references [33, 47, 48], it was shown that the utilization of the scattering transformation to couple the plant with the controller can stabilize passive and non-passive, static-output-feedback-stabilizable plants independently of any constant delays and uncertain system parameters. Later in [49], the stability of interconnected systems satisfying an inequality condition of small $\mathcal{L}_2$ gain (or a similar inequality constraint in the case of output strictly passive systems [50, 51]) was established through the use of the scattering transformation and extended to time-varying delays. Similarly, in [52], the use of the scattering transformation to stabilize passive systems was explored for losses in the controller-to-plant communication channel. Although the aforementioned efforts are applicable to a broad class of nonlinear systems, their scope is still limited to systems with no measurement delays since instantaneous local state values are required to construct the scattering transformation outputs.

1.4.2 Control of Multiple Agents with Input Delays

Many advanced applications, such as surveillance tasks, military operations [53], mobile sensors [54], and rescue missions [55], can be executed faster, more efficiently, and less expensively by a team of simpler machines rather than a single complex one. Due in part to its modularity and flexibility, a team of simple and cost-effective agents can replace a single robotic system and complete multiple tasks in shorter time, cover large-scaled areas, and adapt more easily to single point failures. Moreover, diversifying the group and scaling down the agents promotes multitasking abilities as well as mobility through diverging paths and/or obstructed spaces where the use of an individual, larger robot might be restricted. Such advantages of multiple networked systems over single machines have continuously fueled research on the control of multi-agent systems over the last decades [53].

Among the many control ideas developed for cooperative control of multi-agent systems, the most popular formalisms include behavioral-based approaches [56], optimization-based techniques [57], passivity-based formulations [58], and others more nature-inspired, such as the nearest neighbor

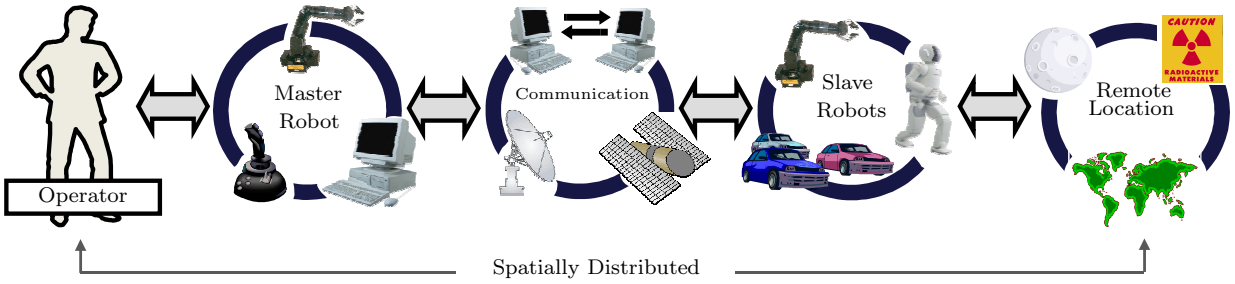

Figure 1.2: Configuration of a teleoperation system.

rule [59,60]. Some of these control formulations have also been applied to coordination and consensus problems considering coupling communication delays among near agents and between agent and controller. For instance, in [61] a control framework based on the nearest neighbor rule for cooperative control of multiple vehicles with communication delays is presented. Similarly, in [62,63] passivity-based properties of the nonlinear agents are exploited to guarantee convergence between agents independently of communication constant delays. Other examples include [64–71] and [72–75], where the last group of references are special applications on bilateral teleoperation.

The discussed cooperative control frameworks for systems with interconnection delays are either exclusive to linear systems or do not consider delays in the local control loop, i.e., where each agent has instantaneous access to its own state information. This leaves open the research question on how to control and coordinate the behavior of more complex, nonlinear multi-agent systems with control input and communication delays.

1.4.3 Bilateral Teleoperation with Communication Delays

In principle, a teleoperation system is a multi-robotic set that enables a human operator to manipulate, sense, and physically interact with a distant environment (see Figure 1.2 for a representation). In such system, the desired manipulation or task is performed remotely by one or multiple slave robots that track the motion of a locally human-controlled master robot. The master robot and the slave robots are typically coupled via a communication network. Ideally, this coupling should be transparent to the operator, meaning that he/she should feel as if being directly active in the remote location. This is generally attained by transmitting remote slave information (e.g., position, velocity, and force) to the master robot in what is called a bilateral connection.

Achieving transparency (commonly measured in terms of motion coordination, impedance match-

Figure 1.3: Raymond Goertz operating a mechanical teleoperator. He later invented the first electro-mechanical master/slave teleoperator. (Source: Argonne National Laboratory).

ing, and force reflection) and stability of bilateral teleoperation systems has proved to be difficult and more than often, a conflicting task due to time delays in the control loop [76, 77]. Time delays typically arise from the separation distance between master and slave robots in addition to the communication medium (e.g., Internet, satellite, and wireless) and may range from a few milliseconds to several seconds as it is the case for outer space exploration [78]. Independently of their size and nature, time delays may degrade the performance of a bilateral teleoperator and even lead to instability.

Research on time delay bilateral teleoperation can be traced back as far as the 1940s with the invention of the first modern single-master-single-slave (SMSS) teleoperator for manipulation of radioactive materials by Raymond C. Goertz at Argonne National Laboratory (see Figure 1.3). Ever since, the field of teleoperation has found application in a wide range of arenas that range from manipulation of nanoscale systems [79] to that of heavy duty hydraulic machines [80]. Similarly, today's teleoperators have been embraced by different scientific and industrial sectors that include medicine [81, 82], entertainment [83], agriculture [84], and education [85]. In general, we can argue that SMSS teleoperation systems have enjoyed considerable interest over the last 60 years, and for comprehensive reviews on the topic, the reader can refer to [25, 86, 87].

In contrast to the arguably mature state of SMSS teleoperation, single-master-multi-slave (SMMS) systems remains relatively new in the control community. The ability to remotely coordinate and bilaterally control multiple mobile agents through a single master robot under constant and time-varying communication delays has been previously attained in [72–74, 88, 89]. These control methodologies were later extended to include collision avoidance algorithms in [90, 91]. Similarly, in [92] formation control and obstacle avoidance for a linear SMMS system is addressed under time-

varying delayed communication lines. Finally, in [93] a control framework for bilateral teleoperation of multiple nonholonomic vehicles with collision avoidance is presented.

1.4.4 Collision Avoidance with Sensing Delays and Uncertainties

Mobile networked agents, such as unmanned vehicles, typically rely on navigation and localization sensors to estimate the location of nearby agents and obstacles or on wireless communication networks for the broadcast of position coordinates among agents. These sensing mechanisms, in which we include communication networks, may inaccurately estimate the position of obstacles and agents as a result of process delays, interferences, noise, and quantization. For instance, obstacle's position measurements, sampled by vision-based sensing mechanisms on many mobile robotic systems, are easily affected by weather conditions and light variations [94]. Underwater localization equipment, such as sonar radars and inertial measurements units, may also experience substantial delays, slow sampling rates, and additive measurement errors [95]. In fact, 12 kHz Long Baseline acoustic navigation, the standard approach for full depth ocean navigation [95], typically operates at update rates periods of up to 20 s [96] and with a precision of 0.1-10 m [97]. Alternatively, widely used Global Positioning Systems for localization of ground and aerial vehicles may experience temporary interruptions when traveling through occluded spaces or because of the interference with radio signals [98]. Therefore, collision avoidance strategies for vehicle navigation must provide robustness to sensing delays as well as uncertainties.[3]

Collision avoidance strategies for multi-vehicle systems can be classified as noncooperative or cooperative. In a noncooperative policy, each agent assumes the worst case scenario in which other agents do not apply any collision avoidance strategy. Within this perspective, several control ideas have been proposed. For instance, Leitmann and Skowronski [99] established sufficient conditions for collision avoidance between two agents in a noncooperative scenario using Lyapunov-based analysis. Alternatively, Mitchell *et al.* [100] studied the problem of collision avoidance for two agents applying level set methods [101] to compute the solutions of Hamilton-Jacobi-Isaacs partial differential equations. On the other hand, in a cooperative scenario, all agents collaborate to solve the potential conflict. For instance, in [102], a control strategy for collision avoidance of multiple agents in a cooperative scenario is presented based on the concept of avoidance functions

[3]Many sources of uncertainties, such as sporadic interference and ephemeral interruptions, can be modeled as delays. Similarly, the error induced by sensing delays can be considered as a bounded uncertainty. More details will be provided in Chapter 7.

introduced in [99]. This method has been extended to nonholonomic vehicles [103] and Lagrangian systems with bounded control input disturbances [104] and has been successfully tested on multiple ground [103] and aerial vehicles [75]. Cooperative collision avoidance strategies have also been studied using navigation functions on systems with integrator dynamics [105] and on unicycle models with constant speed [106]. Similarly, collision avoidance laws have been formulated based on potential field functions for double-integrators [107] and for single-integrators with bounded control [108] and unicycle models [109].

The aforementioned collision avoidance strategies are strictly for systems with accurate and immediate position information. In fact, collision avoidance control laws (cooperative or noncooperative) for the case of accurate obstacle position estimation abound in the literature (see [99,110–112] and references therein for examples). This sharply contrasts with the opposite case of safe navigation under sensing uncertainties which has not been comprehensively studied from a control perspective. Instead, the orthodox solution in the presence of sensing uncertainties has been to improve sensory perception [113–115]. Some of the few examples that effectively deal with inaccurate obstacle position estimation from a control perspective include the certainty grid [116] and the occupancy grid [117], which are equivalent techniques based on probabilistic methods, and a noncooperative strategy for unicycle models [118] based on the concept of reachable sets [100]. However, these strategies do not address collision avoidance with moving obstacles. Recently in [119], a noncooperative collision avoidance algorithm based on the velocity occupancy space, a variation of the occupancy grid, was proposed to guarantee the safe navigation of vehicles interacting with dynamic obstacles. Yet, the performance of the avoidance algorithm in the case of time-varying speed obstacles, such as other agents, was not explicitly investigated.

1.5 Thesis Outline and Contributions

As the foundation for the theoretical treatment of the control problems addressed in this dissertation, we start with a brief mathematical background on Lagrangian systems in Chapter 2. First, we formulate the Euler-Lagrange equations of motion for mechanical systems and introduce some relevant properties of Lagrangian systems. Then, we define the concept of passivity and highlight its connection to Lyapunov's stability. This connection will be instrumental in analyzing the stability of the control algorithms proposed herein.

In Chapter 3, we commence the treatment of networked Lagrangian systems with delays. We

introduce a passivity-based model reference robust control framework that achieves asymptotic stability and provides satisfactory trajectory tracking for nonlinear Lagrangian systems with dynamic uncertainties and arbitrarily large input and state measurement constant delays. The proposed control law builds on the assumption that the Lagrangian system is dissipative in order to establish delay-independent stability (i.e., the control parameters are independent of the size of the delay). In addition, the model reference robust control framework explicitly guarantees position convergence under communication and computation errors as opposed to most common passivity-based control approaches reported in the literature. Simulation and experimental results with a coaxial helicopter and a robot manipulator with constant input and state feedback delays are presented to validate the proposed controller. Results relating to this topic have been reported in [120].

We then extend the model reference robust control framework introduced in Chapter 3 to the general case of multi-agent systems in Chapter 4. We specifically consider the research problem of controlling the formation and state trajectory of a group of n-dimensional, possibly heterogeneous nonlinear systems with constant input and state feedback delays. It is shown that the formation and state trajectory control problem can be cooperatively solved independently of the magnitude of the individual round-trip delays. Numerical examples with a group of omni-directional vehicles are presented.

In Chapter 5 we continue with the control of NCSs molded to the topic of bilateral teleoperation. Using passivity-based control and the wave scattering transformation, we design a novel control framework that guarantees stability, master-to-slave position convergence, and static force reflection for SMSS bilateral teleoperators with constant coupling delays. Our main contribution within this topic lies in the effective passive compensation of position errors that inherently arise during contact tasks and in the conservation of stability and transparency when alternating between unobstructed (free) and obstructed (contact) environments. The proposed control framework exploits the wave impedance independent passivity property of the scattering transformation to guarantee both control objectives by gradually switching between a low wave impedance, ideal for free motion, and a sufficiently large impedance, suitable for contact tasks. Specifically, the passive controller adapts the wave impedance online according to contact forces at the remote environment, enabling satisfactory transparency compensation. By utilizing input-to-state stability analysis we are able to demonstrate that the position error between master and slave decays to zero as we passively increase the wave impedance or attenuate external forces. The validity of the control framework is

verified through simulations and experiments on a pair of nonlinear robots. The work presented in Chapter 5 has been reported in [121].

We then cover the research problem of bilaterally teleoperating multiple slave agents with a single master robot. The main control objectives for SMMS bilateral teleoperation systems are summarized as follows: (1) stability of the overall closed-loop system, (2) formation control among slave agents, (3) slaves-to-master trajectory tracking, (4) force reflection of environmental forces to the human operator, and (5) collision avoidance in the case of mobile agents. In order to achieve these objectives, we present in Chapter 6 a distributed, bilateral control framework that guarantees stability and coordinated motion (i.e., formation control and trajectory tracking) between master and slave agents under arbitrary constant communication delays, as well as a safe interaction between slave agents and surrounding obstacles. We first design a passivity-based proportional-derivative (PD) controller that enforces motion tracking, static force reflection, and formation control of master and slave vehicles under constant, bounded communication delays. Then, we incorporate the use of avoidance functions [102] to guarantee collision-free transit through obstructed spaces and cooperative collision evasion between neighboring agents. The effectiveness of the proposed controller is finally tested through experiments with two coaxial helicopters as slave agents and a haptic force-feedback device as the master robot. The theoretical and experimental results reported here have been published in [75].

Following with the notion of collision avoidance, we devote Chapters 7 and 8 to the design of decentralized collision avoidance strategies for Lagrangian agents with bounded sensing delays and sensing uncertainties. First, we consider the simpler case of a pair of dynamical systems with double integrator dynamics[4] in Chapter 7. Within this context, we develop cooperative and noncooperative avoidance policies based on the use of avoidance functions [99, 102]. We show, using Lyapunov-based analysis, that if a sufficiently large safety neighborhood around each agent is defined and avoidance control strategies are developed according to this region, collision-free trajectories for nonlinear systems with bounded inputs and limited, unreliable sensing range can be guaranteed. Furthermore, the collision avoidance control laws proposed herein can be appended to any other stable control law (e.g., set-point regulation and trajectory tracking) and are exclusively active when an obstacle or other agents are close to the controlled vehicles. Along with the theoretical treatment, we present a set of cooperative and noncooperative simulation examples to illustrate

[4]We demonstrate that the collision avoidance strategies presented in Chapter 7 can be extended to nonlinear Lagrangian systems via the use of inverse dynamics control.

the effectiveness of the proposed controller. Experimental results with two coaxial helicopters are also presented. Results in this chapter has been reported in [122].

In Chapter 8 we extend the previous collision avoidance formulation to a network of multiple agents with nonlinear Lagrangian dynamics. We consider a group of N vehicles with bounded inputs and develop cooperative collision avoidance strategies based on finite Lyapunov functions that can be easily synthesized with other stable control laws. The avoidance control strategy is validated via a simulation example with sensing delays.

Finally, in Chapter 9, we conclude with a set of final remarks and future research directions associated with the control problems discussed in this dissertation.

CHAPTER 2

LAGRANGIAN SYSTEMS AND PASSIVITY

In this chapter, we define the equations of motion for a Lagrangian system and introduce some relevant properties exploited throughout the thesis, including the notion of passivity.

2.1 Notation

As standard notation, $\Re^n$ stands for the n-dimensional Euclidean space. The p-norm of a vector $\mathbf{x} = [x_1, \cdots, x_n]^T \in \Re^n$ is denoted by $\|\mathbf{x}\|_p := (|x_i|^p + \cdots + |x_n|^p)^{1/p}$ for $1 \leq p < \infty$ and $\|\mathbf{x}\|_p = \max_i |x_i|$ for $p = \infty$, where $|x_i|$ is the absolute value of a real scalar x_i. We define the induce p-norm of a matrix $A \in \Re^{m \times n}$ as $\|A\|_p := \sup_{\mathbf{x} \neq \mathbf{0}} \frac{\|A\mathbf{x}\|_p}{\|\mathbf{x}\|_p}$. For the 2-norm of a vector or matrix we use the simpler notation $\|\cdot\|$. We also say that a n-dimensional piecewise continuous function $\mathbf{y} : [0, \infty) \to \Re^n$ belongs to $\mathcal{L}_p$ if $\|\mathbf{y}(t)\|_{\mathcal{L}_p} = \left(\int_0^\infty \|\mathbf{y}\|^p\right)^{1/p} < \infty$ for $1 \leq p < \infty$ and to $\mathcal{L}_\infty$ if $\|\mathbf{y}(t)\|_{\mathcal{L}_\infty} = \sup_{t \geq 0} \|\mathbf{y}(t)\| < \infty$. As a shorthand for a matrix $A \in \Re^{m \times n}$ we use $[a_{kl}]_{m \times n}$, where a_{kl} is the klth entry of A. Additional notation might be introduced as new concepts appear in the following chapters. For simplicity, we will omit time dependence of signals except when considered necessary.

2.2 Lagrangian Systems

An n-degree-of-freedom (DOF) Lagrangian system, with generalized coordinates $\mathbf{q} = \mathbf{q}(t) \in \Re^n$ and external forces $\tilde{\boldsymbol{\tau}} = \tilde{\boldsymbol{\tau}}(t) \in \Re^n$, is one that satisfies the following Euler-Lagrange equations of motion [42]

$$\frac{d}{dt}\left(\frac{\partial \mathcal{L}(\mathbf{q}, \dot{\mathbf{q}})}{\partial \dot{\mathbf{q}}}\right) - \frac{\partial \mathcal{L}(\mathbf{q}, \dot{\mathbf{q}})}{\partial \mathbf{q}} = \tilde{\boldsymbol{\tau}} \tag{2.1}$$

where

$$\mathcal{L}(\mathbf{q}, \dot{\mathbf{q}}) = \mathcal{K}(\mathbf{q}, \dot{\mathbf{q}}) - \mathcal{P}(\mathbf{q})$$

is known as the Lagrangian function. The kinetic energy function of the system, $\mathcal{K}(\mathbf{q}, \dot{\mathbf{q}})$, is assumed to be of the form

$$\mathcal{K}(\mathbf{q}, \dot{\mathbf{q}}) = \frac{1}{2}\dot{\mathbf{q}}^T M(\mathbf{q})\dot{\mathbf{q}}$$

where $M(\mathbf{q}) \in \Re^{n\times n}$ represents the positive definite inertia matrix, while the potential energy function, $\mathcal{P}(\mathbf{q})$, is assumed to be bounded from below, i.e., $\exists c \in \Re$ such that $\mathcal{P}(\mathbf{q}) \geq c$ for all $\mathbf{q} \in \Re^n$. In addition, we suppose that the system is fully-actuated and that external forces are comprised of three types

$$\tilde{\boldsymbol{\tau}} = \mathbf{u} + \mathbf{f} - \frac{\partial \mathcal{F}(\dot{\mathbf{q}})}{\partial \dot{\mathbf{q}}}$$

where $\mathbf{u} \in \Re^n$, $\mathbf{f} \in \Re^n$, and $\mathcal{F}(\dot{\mathbf{q}}) \in \Re^n$ are the control inputs, the environmental/disturbance forces, and the Rayleigh dissipation function, respectively. We will further assume that dissipative forces satisfy the following condition

$$\dot{\mathbf{q}}^T \frac{\partial \mathcal{F}(\dot{\mathbf{q}})}{\partial \dot{\mathbf{q}}} \geq \rho \left\|\dot{\mathbf{q}}\right\|^2, \qquad \text{for } \rho \geq 0. \tag{2.2}$$

Then, it is easy to show that the Euler-Lagrange equations of motion in (2.1) reduce to

$$M(\mathbf{q})\ddot{\mathbf{q}} + C(\mathbf{q}, \dot{\mathbf{q}})\dot{\mathbf{q}} + \frac{\partial \mathcal{F}(\dot{\mathbf{q}})}{\partial \dot{\mathbf{q}}} + \mathbf{g}(\mathbf{q}) = \mathbf{u} + \mathbf{f} \tag{2.3}$$

where the jkth element of the centrifugal and Coriolis matrix, $C(\mathbf{q}, \dot{\mathbf{q}}) \in \Re^{n\times n}$, are univocally computed as

$$C_{jk}(\mathbf{q}, \dot{\mathbf{q}}) = \sum_{l=1}^{n} \frac{1}{2}\left[\frac{\partial M_{jk}}{\partial q_l} + \frac{\partial M_{jl}}{\partial q_k} - \frac{\partial M_{kl}}{\partial q_l}\right]\dot{q}_l \tag{2.4}$$

and where

$$\mathbf{g}(\mathbf{q}) = \frac{\partial \mathcal{P}(\mathbf{q})}{\partial \mathbf{q}}$$

defines the n-dimensional vector of gravitational forces.

Throughout this thesis, unless otherwise stated, we will further assume that the Lagrangian systems (2.3) satisfy the following properties.[1]

Property 2.2.1 (Skew-Symmetry)**.** $\dot{M}(\mathbf{q}) = C(\mathbf{q}, \dot{\mathbf{q}}) + C^T(\mathbf{q}, \dot{\mathbf{q}})$.

Property 2.2.2 (Uniform Boundedness)**.** $\exists$ *positive constants* $\underline{\lambda}$ *and* $\overline{\lambda}$ *such that* $\underline{\lambda} I \leq M(\mathbf{q}) \leq \overline{\lambda} I$*, where* $I \in \Re^{n \times n}$ *is the identity matrix.*

Property 2.2.3 (Boundedness of C-matrix)**.** *The matrix* $C(\mathbf{q}, \dot{\mathbf{q}})$ *is bounded in* $\mathbf{q}$ *and linear in* $\dot{\mathbf{q}}$*, and so,* $\|C(\mathbf{q}, \dot{\mathbf{q}})\| \leq k_c \|\dot{\mathbf{q}}\|$ *for some* $k_c \geq 0$.

The skew-symmetric property is a consequence of (2.4) [124]. The second property, although more restrictive, is satisfied by many different configurations of robotics systems [125]. For instance, it trivially holds when the system has linear dynamics. Finally, the last property is a direct result of Property 2.2.2.

2.3 Passivity

The Euler-Lagrange formalism to derive the equations of motion is based on the minimization of an energy function (e.g., difference between kinetic and potential energy functions). Therefore, it is consequential to question if Lagrangian systems satisfy energy-based properties. One of such properties is called passivity.

Definition 2.3.1. [126] *A system with input* $\mathbf{u}$ *and output* $\mathbf{y}$ *is said to be passive if*

$$\int_0^t \mathbf{y}^T \mathbf{u} d\theta \geq -\kappa + \nu \int_0^t \mathbf{u}^T \mathbf{u} d\theta + \rho \int_0^t \mathbf{y}^T \mathbf{y} d\theta \tag{2.5}$$

for some nonnegative constants κ, ν*, and* ρ*. Moreover, it is said to be lossless if equality persists and* $\nu = \rho = 0$*, input strictly passive if* $\nu > 0$*, and output strictly passive if* $\rho > 0$.

[1] For additional common properties of Lagrangian systems, the reader can consult [123].

Theorem 2.3.1. *The Euler-Lagrange system (2.3) with* $\mathbf{f} \equiv 0$ *is passive with respect to input* $\mathbf{u}$ *and output* $\dot{\mathbf{q}}$*. Furthermore, if* $\rho > 0$*, then (2.3) is output strictly passive.*

Proof. Consider the following positive definite function

$$\mathcal{H} = \frac{1}{2}\dot{\mathbf{q}}^T M(\mathbf{q})\dot{\mathbf{q}} + \mathcal{P}(\mathbf{q}) - c \geq 0$$

Then, taking the time derivative of $\mathcal{H}$ we obtain

$$\begin{aligned}\dot{\mathcal{H}} &= \dot{\mathbf{q}}^T M(\mathbf{q})\ddot{\mathbf{q}} + \frac{1}{2}\dot{\mathbf{q}}^T \dot{M}(\mathbf{q})\dot{\mathbf{q}} + \dot{\mathbf{q}}^T \frac{\partial \mathcal{P}(\mathbf{q})}{\partial \mathbf{q}} \\ &= \dot{\mathbf{q}}^T \left(\mathbf{u} - C(\mathbf{q}, \dot{\mathbf{q}})\dot{\mathbf{q}} - \frac{\partial \mathcal{F}(\dot{\mathbf{q}})}{\partial \dot{\mathbf{q}}} - \mathbf{g}(\mathbf{q}) \right) + \frac{1}{2}\dot{\mathbf{q}}^T \dot{M}(\mathbf{q})\dot{\mathbf{q}} + \dot{\mathbf{q}}^T \mathbf{g}(\mathbf{q})\end{aligned}$$

and recalling the skew-symmetry Property 2.2.2 we have

$$\dot{\mathcal{H}} = \dot{\mathbf{q}}^T \mathbf{u} - \dot{\mathbf{q}}^T \frac{\partial \mathcal{F}(\dot{\mathbf{q}})}{\partial \dot{\mathbf{q}}}. \tag{2.6}$$

Now, integrating both sides of (2.6) yields

$$\int_0^t \dot{\mathbf{q}}^T \mathbf{u} d\theta = \int_0^t \dot{\mathbf{q}}^T \frac{\partial \mathcal{F}(\dot{\mathbf{q}})}{\partial \dot{\mathbf{q}}} d\theta + \mathcal{H}(t) - \mathcal{H}(0) \geq \rho \int_0^t \dot{\mathbf{q}}^T \dot{\mathbf{q}} d\theta - \mathcal{H}(0) \tag{2.7}$$

where we used (2.2) and the fact that $\mathcal{H}(\theta) \geq 0 \; \forall \theta \Rightarrow \mathcal{H}(t) - \mathcal{H}(0) \geq -\mathcal{H}(0)$. Then, passivity and output strictly passivity follow from $\kappa = \mathcal{H}(0)$ and $\rho > 0$. □

Remark 2.3.1. *Note that from (2.6) we have that the total energy of the system* $\mathcal{H}$ *is non-increasing for* $\mathbf{u} \equiv 0$*. Therefore, the unforced system (2.3) is stable in the sense of Lyapunov.*

In addition, we have the following nice result for the interconnection of passive systems.

Theorem 2.3.2. *The negative feedback interconnection of two passive systems is passive.*

Proof. Consider the two interconnected passive systems in Figure 2.1. Since G_1 and G_2 are passive, we have that

$$\int_0^t \mathbf{y}_i^T \mathbf{e}_i d\theta \geq -\kappa_i, \qquad\qquad \kappa_i \geq 0.$$

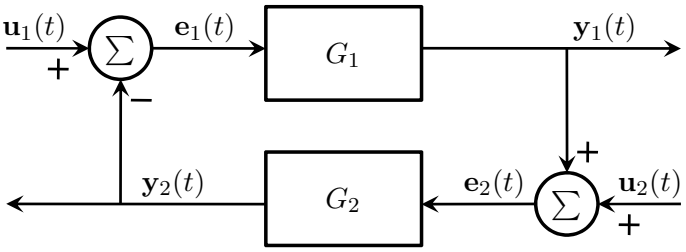

Figure 2.1: Negative feedback connection of two passive systems.

Hence,

$$\begin{aligned}
\int_0^t \mathbf{y}_1^T \mathbf{e}_1 d\theta + \int_0^t \mathbf{y}_2^T \mathbf{e}_2 d\theta &\geq \kappa_1 + \kappa_2 \\
\int_0^t \mathbf{y}_1^T (\mathbf{u}_1 - \mathbf{y}_2) d\theta + \int_0^t \mathbf{y}_2^T (\mathbf{u}_2 + \mathbf{y}_1) d\theta &\geq \kappa_1 + \kappa_2 \\
\int_0^t (\mathbf{y}_1^T \mathbf{u}_1 + \mathbf{y}_2^T \mathbf{u}_2) d\theta &\geq \kappa_1 + \kappa_2 \\
\int_0^t \mathbf{y}^T \mathbf{u} d\theta &\geq \kappa
\end{aligned}$$

and we conclude that the overall system with input $\mathbf{u}^T = [\mathbf{u}_1^T, \mathbf{u}_2^T]$ and output $\mathbf{y}^T = [\mathbf{y}_1^T, \mathbf{y}_2^T]$ is also passive for $\kappa = \kappa_1 + \kappa_2 \geq 0$. □

CHAPTER 3

CONTROL OF NONLINEAR SYSTEMS WITH INPUT DELAYS

Due to diverse natural factors (e.g., propagation and transport phenomena) and implementation requirements (e.g., discretization and networking), time delays may appear in control systems. For instance, control of chemical processes, such as chemical reactors [127] and heat exchangers [128], typically experience time delays in the control loop as the result of mass transport and heat transfer phenomena. Similarly, data transmission in analog and digital communication-based NCSs inherently suffers from positive propagation delays due to the time it takes for the transmitted signal to travel from one end-point to another. In these scenarios, the presence of time delays in the control loop can degrade the performance of the control process and even lead to instability. Therefore, it is of great significance to formulate control algorithms conformed to time delay models.

Following the research line of [33, 47–52], we now present the design of a model reference robust control (MRRC) framework that combines the use of the wave-based scattering transformation [46] to guarantee asymptotic stability of nonlinear dissipative Lagrangian systems[1] with dynamic uncertainties and arbitrary large input and state measurement constant delays. The proposed control law assumes that the unforced (i.e., zero input control) system is exponentially stable[2] or, equivalently, output strictly passive in order to establish delay-independent stability of the controlled system. The design of the controller is comprised of two parts: a linear reference model and a scattering transformation block. The first is designed according to a desired input-to-output property that the delayed system must mimic, while the latter is used to stabilize the delayed coupling between the plant and the controller. In addition, the outputs of the scattering transformation are passively modified to enable explicit full state tracking between controller (i.e., reference model) and plant independently of dissimilar and unknown initial conditions as well as losses in the transmission lines, a recurring problem with scattering transformation-based techniques. The overall framework

[1] The results presented in this chapter can be extended to more general classes of nonlinear systems [120].

[2] For time delay control frameworks based on exponential stability of the unforced system or similar assumptions, see [11, 43, 44].

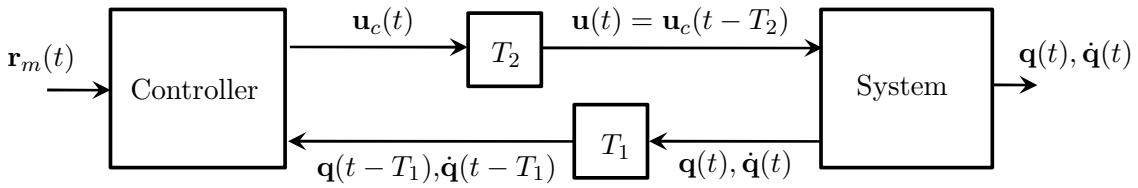

Figure 3.1: Nonlinear plant and controller with input and state measurement delays. The signals $\mathbf{r}_m(t)$ and $\mathbf{u}_c(t)$ represent the input and output of the controller, respectively.

is then validated via a numerical example. To the best of our knowledge, nonlinear systems (including Lagrangian systems) with explicit state measurement delays have not been addressed applying the passivity-based scattering formulation.

3.1 System Dynamics

We consider an n-DOF nonlinear Lagrangian system with equations of motion given by

$$M(\mathbf{q})\ddot{\mathbf{q}} + C(\mathbf{q}, \dot{\mathbf{q}})\dot{\mathbf{q}} = \mathbf{u} - \frac{\partial \mathcal{F}(\dot{\mathbf{q}})}{\partial \dot{\mathbf{q}}} \tag{3.1}$$

where gravitational effects have been either neglected or canceled through constant control (i.e., gravitational forces are constant) and where dissipative forces are assumed to satisfy the following inequality

$$\dot{\mathbf{q}}^T \frac{\partial \mathcal{F}(\dot{\mathbf{q}})}{\partial \dot{\mathbf{q}}} \geq \rho \left\| \dot{\mathbf{q}} \right\|^2 \tag{3.2}$$

for some $\rho > 0$. In addition, the positive inertia matrix M and centrifugal and Coriolis matrix C are assumed to satisfy Properties 2.2.1 to 2.2.3, while the control input $\mathbf{u}$ is assumed to be a delayed state feedback function depending on $\mathbf{q}(t - T_1 - T_2)$ and $\dot{\mathbf{q}}(t - T_1 - T_2)$, where $T_1 \geq 0$ and $T_2 \geq 0$ correspond to the measurement and plant-to-controller communication delay and the controller-to-plant communication delay, respectively. The system and controller are portrayed in Figure 3.1.

3.2 Passivity-Based Model Reference Robust Control Framework

The proposed control framework is comprised of two elements: the reference model and the wave-based scattering transformation block. The reference model is designed according to some ideal input-to-output (or equivalently, input-to-state) properties that we would like the time delay nonlinear plant to mimic. The scattering transformation is designed such that the delayed coupling transmission lines between controller and plant are passified. The passivation of the transmission lines will then be exploited to guarantee delay-independent stability of the overall system.

3.2.1 Reference Model

We design, for simplicity, an asymptotically stable linear reference model as

$$\begin{aligned} \ddot{\mathbf{q}}_m(t) = &\quad A_m\dot{\mathbf{q}}_m(t) + \mathbf{u}_m(t) + \mathbf{r}_m(t) \\ \mathbf{y}_m(t) = &\quad \dot{\mathbf{q}}_m(t) \end{aligned} \tag{3.3}$$

where $\mathbf{q}_m(t), \dot{\mathbf{q}}_m(t) \in \Re^n$ are the state vectors, $\mathbf{y}_m(t) \in \Re^n$ is the output vector, $\mathbf{u}_m(t) \in \Re^n$ is the control input, and $A_m \in \Re^{n\times n}$ is a symmetric Hurwitz matrix. The reference signal $\mathbf{r}_m(t) \in \Re^n$ is given by

$$\mathbf{r}_m(t) = K_d(\mathbf{q}_d - \mathbf{q}_m(t)) \tag{3.4}$$

where $K_d \in \Re^{n\times n}$ is a positive-definite constant matrix and $\mathbf{q}_d \in \Re^n$ is the desired state constant vector.

3.2.2 Scattering Transformation

If the reference model and the time delay nonlinear system are to be directly coupled through their delayed outputs $\mathbf{q}_m(t-T_2)$ and $\mathbf{q}(t-T_1)$ and/or $\dot{\mathbf{q}}_m(t-T_2)$ and $\dot{\mathbf{q}}(t-T_1)$, it can be shown that the communication channel may act as a nonpassive coupling element (i.e., may generate energy), potentially leading the system to instability [46]. In order to passify the communication channel and avoid instability, we propose the use of the wave-based scattering transformation. The wave variables $\mathbf{w}_m(t)$ and $\mathbf{v}(t)$, and the new control inputs $\mathbf{u}_m(t) = -\boldsymbol{\tau}_m(t)$ and $\mathbf{u}(t) = \boldsymbol{\tau}(t)$ are then

computed as

$$\boldsymbol{\tau}_m(t) = b\dot{\mathbf{e}}_m(t) + K_m\mathbf{e}_m(t) \tag{3.5}$$

$$\mathbf{w}_m(t) = \sqrt{\frac{2}{b}}\boldsymbol{\tau}_m(t) - \mathbf{v}_m(t) \tag{3.6}$$

$$\dot{\mathbf{q}}_{md}(t) = \frac{1}{b}\left(\boldsymbol{\tau}_m(t) - \sqrt{2b}\mathbf{v}_m(t)\right) \tag{3.7}$$

$$\mathbf{q}_{md}(t) = \int_0^t \dot{\mathbf{q}}_{md}(\theta)d\theta \tag{3.8}$$

$$\mathbf{e}_m(t) = \mathbf{q}_m(t) - \mathbf{q}_{md}(t) \tag{3.9}$$

for the reference model and

$$\boldsymbol{\tau}(t) = \sqrt{2b}\mathbf{w}(t) \tag{3.10}$$

$$\mathbf{v}(t) = \mathbf{w}(t) - \sqrt{2b}\dot{\mathbf{q}}(t) \tag{3.11}$$

for the nonlinear system; where the wave impedance b is a positive constant, K_m is a symmetric positive definite matrix, and

$$\mathbf{v}_m(t) = \mathbf{v}(t - T_1) \tag{3.12}$$

$$\mathbf{w}(t) = \mathbf{w}_m(t - T_2). \tag{3.13}$$

The implementation of the scattering transformation and the reference model is schematized in Figure 3.2.

The importance of the scattering transformation lies in the passivation of the communication channel independently of any arbitrary large constant round-trip delays. To demonstrate this statement, let us verify that the communication channel is, in fact, passified. Manipulating (3.5)-(3.13) we can easily show that

$$\dot{\mathbf{q}}_{md}^T\boldsymbol{\tau}_m - \dot{\mathbf{q}}^T(\boldsymbol{\tau} - b\dot{\mathbf{q}}) = \frac{1}{2}\left(\mathbf{w}_m^T\mathbf{w}_m - \mathbf{w}^T\mathbf{w} + \mathbf{v}^T\mathbf{v} - \mathbf{v}_m^T\mathbf{v}_m\right). \tag{3.14}$$

Then, integrating (3.14) we respect to time yields

$$\int_0^t (\dot{\mathbf{q}}_{md}^T\boldsymbol{\tau}_m - \dot{\mathbf{q}}^T(\boldsymbol{\tau} - b\dot{\mathbf{q}}))d\theta = \frac{1}{2}\int_{t-T_2}^t \mathbf{w}_m^T\mathbf{w}_m d\theta + \frac{1}{2}\int_{t-T_1}^t \mathbf{v}^T\mathbf{v}d\theta \geq 0 \tag{3.15}$$

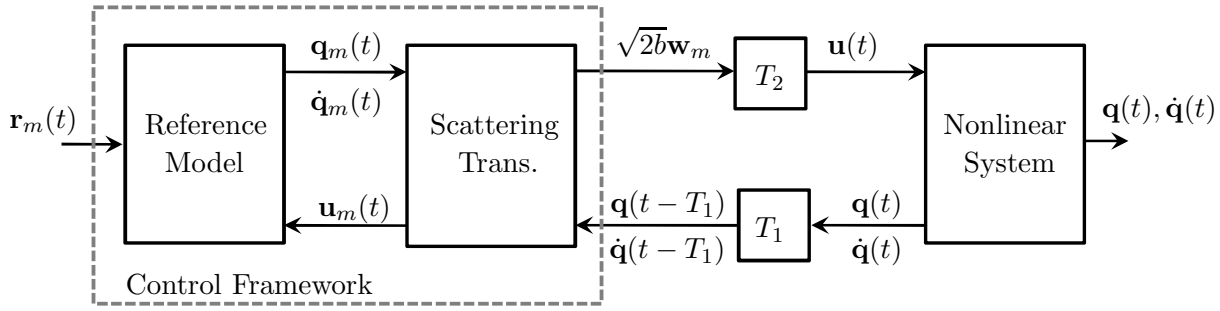

Figure 3.2: Proposed MRRC framework.

which confirms the passivity claim. The lower bound in (3.15) implies that the energy is temporarily stored in the transmission lines and, therefore, the communication channel is passified independently of the size of T_1 and T_2.

Remark 3.2.1. *The definition of the scattering transformation proposed here differs from its typical implementation [33, 46–52] in the sense that the current states of the time delay nonlinear plant are assumed to be unaccessible to the local plant and, therefore, cannot be used when computing the transformation variables. Consequently, all scattering transformation variables are computed at the same location in the network (see Figure 3.2), as opposed to their conventional bisected (or mirror) implementation.*

3.3 Stability Analysis and State Convergence

Having established the control framework and the passivation of the communication channel, we now proceed to claim asymptotic stability of (3.1) and state convergence independently of arbitrary large input and state measurement delays. The following theorem represents one of the main results of this chapter.

Theorem 3.3.1. *Consider the time delay nonlinear system (3.1) coupled to the reference model (3.3) via the scattering transformation (3.5-3.13) and let $b < \rho$. Then, for all initial conditions we have the following results.*

i. *All signals $\mathbf{q}_m(t), \mathbf{q}(t), \mathbf{e}_m(t), \dot{\mathbf{q}}_m(t), \dot{\mathbf{q}}(t), \dot{\mathbf{e}}_m(t)$, $\ddot{\mathbf{q}}_m(t)$, and $\ddot{\mathbf{q}}(t)$ are bounded $\forall t \geq 0$ and the velocities $\dot{\mathbf{q}}_m(t), \dot{\mathbf{e}}_m(t)$, and $\dot{\mathbf{q}}(t)$ converge to zero.*

ii. *The error signals $\mathbf{e}_m(t)$ and $\mathbf{q}_m(t) - \mathbf{q}_d$ converge asymptotically to zero.*

Proof. Consider the following Lyapunov candidate function

$$V(t) = V(\mathbf{q}_m(t), \mathbf{e}_m(t), \dot{\mathbf{q}}_m(t), \dot{\mathbf{q}}(t)) = \frac{1}{2}\dot{\mathbf{q}}^T M(\mathbf{q})\dot{\mathbf{q}} + \frac{1}{2}(\mathbf{q}_d - \mathbf{q}_m)^T K_d(\mathbf{q}_d - \mathbf{q}_m) + \frac{1}{2}\dot{\mathbf{q}}_m^T\dot{\mathbf{q}}_m + \frac{1}{2}\mathbf{e}_m^T K_m \mathbf{e}_m + \int_0^t (\dot{\mathbf{q}}_{md}^T\boldsymbol{\tau}_m - \dot{\mathbf{q}}^T(\boldsymbol{\tau} - b\dot{\mathbf{q}}))d\theta. \quad (3.16)$$

Its time derivative is given by

$$\begin{aligned}\dot{V} \leq & -\rho\dot{\mathbf{q}}^T\dot{\mathbf{q}} + \dot{\mathbf{q}}^T\boldsymbol{\tau} - \dot{\mathbf{q}}_m^T K_d(\mathbf{q}_d - \mathbf{q}_m) + \dot{\mathbf{q}}_m^T(A_m\dot{\mathbf{q}}_m - \boldsymbol{\tau}_m + K_d(\mathbf{q}_d - \mathbf{q}_m)) \\ & + \dot{\mathbf{e}}_m^T K_m\mathbf{e}_m + \dot{\mathbf{q}}_{md}^T\boldsymbol{\tau}_m - \dot{\mathbf{q}}^T\boldsymbol{\tau} + b\dot{\mathbf{q}}^T\dot{\mathbf{q}} \\ = & -\rho\dot{\mathbf{q}}^T\dot{\mathbf{q}} + \dot{\mathbf{q}}^T\boldsymbol{\tau} + \dot{\mathbf{q}}_m^T A_m\dot{\mathbf{q}}_m - \dot{\mathbf{q}}_m^T\boldsymbol{\tau}_m + \dot{\mathbf{e}}_m^T K_m\mathbf{e}_m + \dot{\mathbf{q}}_{md}^T\boldsymbol{\tau}_m - \dot{\mathbf{q}}^T\boldsymbol{\tau} + b\dot{\mathbf{q}}^T\dot{\mathbf{q}} \\ = & -\rho\dot{\mathbf{q}}^T\dot{\mathbf{q}} + \dot{\mathbf{q}}_m^T A_m\dot{\mathbf{q}}_m + b\dot{\mathbf{q}}^T\dot{\mathbf{q}} + \dot{\mathbf{e}}_m^T K_m\mathbf{e}_m - \dot{\mathbf{q}}_m^T(b\dot{\mathbf{e}}_m + K_m\mathbf{e}_m) + \dot{\mathbf{q}}_{md}^T(b\dot{\mathbf{e}}_m + K_m\mathbf{e}_m).\end{aligned}$$

Since $b < \rho$ and A_m is Hurwitz, we have that

$$\dot{V} \leq -(\rho - b)\|\dot{\mathbf{q}}\|^2 - \mu\|\dot{\mathbf{q}}_m\|^2 - b\|\dot{\mathbf{e}}_m\|^2 \leq 0 \quad (3.17)$$

where $\mu > 0$ is the smallest eigenvalue of $-A_m$. Therefore, the overall system is stable in the sense of Lyapunov. Moreover, we can invoke LaSalle's Invariance Principle for delay systems [17] and conclude that $\dot{\mathbf{q}}_m, \dot{\mathbf{q}}, \dot{\mathbf{e}}_m$, and hence $\dot{\mathbf{q}}_{md}$ (from (3.9)), converge to zero.

Now, in order to demonstrate boundedness of all signals, let us consider the inequality in (3.17). Integrating at both sides of the inequality, we obtain that $V(t) \leq V(0) < \infty$, which implies that $\mathbf{q}_m, \mathbf{q}_{md}, \mathbf{e}_m, \dot{\mathbf{q}}_m, \dot{\mathbf{q}} \in \mathcal{L}_\infty$. Similarly, from the scattering transformation equations (3.5) to (3.11) and the transmission equation (3.13) we can verify that

$$\boldsymbol{\tau}(t) = b\dot{\mathbf{q}}_m(t - T_2) + K_m\mathbf{e}_m(t - T_2) \quad (3.18)$$

is also bounded. Now, substituting (3.18) and (3.12) into (3.7) yields

$$2b\dot{\mathbf{q}}_{md}(t) = b\dot{\mathbf{q}}_m(t) + K_m\mathbf{e}_m(t) + 2\dot{\mathbf{q}}(t - T_1) - b\dot{\mathbf{q}}_m(t - T) - K_m\mathbf{e}_m(t - T) \quad (3.19)$$

where $T = T_1 + T_2$, and, therefore, $\dot{\mathbf{q}}_{md}$ and $\dot{\mathbf{e}}_m$ are bounded. Similarly, rewriting (3.5) gives us

that

$$\boldsymbol{\tau}_m(t) = \frac{b}{2}\left(\dot{\mathbf{q}}_m(t) + \dot{\mathbf{q}}_m(t-T)\right) + \frac{K_m}{2}\left(\mathbf{e}_m(t) + \mathbf{e}_m(t-T)\right) - b\dot{\mathbf{q}}(t-T_1). \tag{3.20}$$

Boundedness of $\mathbf{e}_m(t), \dot{\mathbf{q}}_m$, and $\dot{\mathbf{q}}$ then implies that $\boldsymbol{\tau}_m \in \mathcal{L}_\infty$ and from the definition of the reference model (3.3) we obtain that $\ddot{\mathbf{q}}_m$ is also bounded. Furthermore, integrating (3.19) with respect to time yields

$$\int_0^t \dot{\mathbf{q}}_{md}(\theta)d\theta = \int_0^t \dot{\mathbf{q}}(\theta)d\theta + \frac{1}{2}\int_{t-T}^t \dot{\mathbf{q}}_m(\theta)d\theta + \frac{K_m}{2b}\int_{t-T}^t \mathbf{e}_m(\theta)d\theta \tag{3.21}$$

and re-arranging the above equation we obtain that

$$\mathbf{q}(t) = \mathbf{q}(0) + \mathbf{q}_{md}(t) - \mathbf{q}_{md}(0) + \mathbf{q}_m(t) - \mathbf{q}_m(t-T) + \frac{K_m}{2b}\int_{t-T}^t \mathbf{e}_m(\theta)d\theta. \tag{3.22}$$

Since all terms in (3.22) are bounded (recall that the integral of a bounded function over a finite interval is also bounded), we can conclude that $\mathbf{q} \in \mathcal{L}_\infty$. Similarly, let us solve (3.1) for $\ddot{\mathbf{q}}$ as

$$\ddot{\mathbf{q}} = M^{-1}(\mathbf{q})\left(\boldsymbol{\tau} - \frac{\partial \mathcal{F}(\dot{\mathbf{q}})}{\partial \dot{\mathbf{q}}} - C(\mathbf{q}, \dot{\mathbf{q}})\dot{\mathbf{q}}\right) \tag{3.23}$$

where M^{-1} exists and is bounded owing to Property 2.2.2. Likewise, since $\dot{\mathbf{q}} \in \mathcal{L}_\infty$ we have that C (from Property 2.2.3) and $\frac{\partial \mathcal{F}(\dot{\mathbf{q}})}{\partial \dot{\mathbf{q}}}$ are bounded. These last results, combined with the boundedness of $\boldsymbol{\tau}$, yields that $\ddot{\mathbf{q}} \in \mathcal{L}_\infty$, which completes the proof for the first part of the theorem.

Now, in order to prove the second statement in the theorem, let us rewrite (3.20) as

$$\boldsymbol{\tau}_m(t) = \frac{b}{2}\left(\dot{\mathbf{q}}_m(t) + \dot{\mathbf{q}}_m(t-T)\right) + \frac{K_m}{2}\int_{t-T}^t \dot{\mathbf{e}}_m(\theta)d\theta - b\dot{\mathbf{q}}(t-T_1). \tag{3.24}$$

Since all signals at the right-hand side of (3.24) vanish, we have that $\boldsymbol{\tau}_m \to 0$, which implies that $\mathbf{e}_m \to 0$. Then, computing the time derivative of (3.20) yields that

$$\dot{\boldsymbol{\tau}}_m(t) = \frac{b}{2}\left(\ddot{\mathbf{q}}_m(t) + \ddot{\mathbf{q}}_m(t-T)\right) + \frac{K_m}{2}\left(\dot{\mathbf{e}}_m(t) + \dot{\mathbf{e}}_m(t-T)\right) - b\ddot{\mathbf{q}}(t-T_1) \tag{3.25}$$

and due to the fact that all signals at the right-hand side of the above equation are bounded, we obtain that $\dot{\boldsymbol{\tau}}_m(t)$ is also bounded. Likewise, by taking the time derivative at both sides of (3.3), we can easily verify that $\dddot{\mathbf{q}}_m$ is also bounded. Then, since $\int_0^t \ddot{\mathbf{q}}_m(\theta)d\theta \to -\dot{\mathbf{q}}_m(0) < \infty$ as $t \to \infty$,

we can apply Barbalat's Lemma [129] and conclude that $\ddot{\mathbf{q}}_m \to 0$. Finally, using (3.3) and the convergence results for $\dot{\mathbf{q}}_m, \ddot{\mathbf{q}}_m$, and $\boldsymbol{\tau}_m$, we obtain that $\mathbf{r}_m \to 0 \Rightarrow \mathbf{q}_m - \mathbf{q}_d \to 0$, which completes the proof. □

Remark 3.3.1. *Note that the only requirement for stability in the controller design is knowledge of a lower bound on ρ.*

The above theorem is important in the sense that it establishes global asymptotic stability and boundedness of the states for any time delay nonlinear system described by (3.1) as well as convergence of the reference model to the desired state, i.e., $\mathbf{q}_m(t) \to \mathbf{q}_d$. However, Theorem 3.3.1 does not guarantee full state tracking between reference model and nonlinear plant, that is, $\mathbf{q}(t) \to \mathbf{q}_m(t)$ remains in question. To demonstrate the ability of the proposed MRRC framework to achieve full state tracking, let us consider (3.21). Under steady-state conditions, we have that $\dot{\mathbf{q}}_m(t), \mathbf{e}_m(t)$ converge to zero and $\mathbf{q}_{md}(t) \to \mathbf{q}_m(t) \to \mathbf{q}_d$ as $t \to \infty$ (from Theorem 3.3.1). Therefore, taking the limit of (3.21) as $t \to \infty$ yields

$$\mathbf{q}_m(t) - \mathbf{q}_{md}(0) \to \mathbf{q}(t) - \mathbf{q}(0). \tag{3.26}$$

The above equation implies that $\mathbf{q}(t) \to \mathbf{q}_m(t) \to \mathbf{q}_d$ if $\mathbf{q}_{md}(0) = \mathbf{q}(0)$. Thus, the proposed control framework guarantees state convergence of the time delay nonlinear system to the desired state if the initial conditions for the system are known.

In practice, the initial conditions of the time delay system are generally uncertain. Consequently, the matching of the initial states between controller and plant might be unfeasible. Moreover, differentiation techniques to compute the states $\dot{\mathbf{q}}(t)$ (e.g., velocities) necessary for the scattering transformation are typically subjected to numerical errors, whereas the transmission of state information via the communication lines may as well suffer from losses – two conditions that may cause state drifts between the reference model and the plant even when initial conditions are matched. Motivated by these practical limitations, we propose a compensation technique that modifies the scattering transformation output $\mathbf{v}_m$ such that full state convergence can be explicitly enforced independently of dissimilar initial conditions and transmission losses. The compensation technique preserves the passivity of the communication channel and, hence, stability of the system is guaranteed.

3.3.1 Full State Tracking Compensator

To preserve passivity of the transmission lines, we must first ensure that the new scattering transformation output does not violate the passivity condition in (3.15). This means that the energy in the transmission lines, given by

$$E_i(t) = \int_0^t (v_i^2(\theta - T_1) - v_{m_i}^2(\theta))d\theta, \qquad \forall\, i \in \{1, \cdots, n\} \tag{3.27}$$

must never become negative, where v_i is the ith scalar component of the output vector $\mathbf{v}$ and v_{m_i} is the ith element of $\mathbf{v}_m$. According to this requirement, we propose to modify the previous transmission equation (3.12) for v_{m_i} as

$$v_{m_i}(t) = \begin{cases} \text{sign}\{\bar{v}_{m_i}(t)\} \min\{||\bar{v}_{m_i}(t)||, ||v_i(t - T_1)||\} & \text{if } E_i(t) \leq \sigma_i \\ v_i(t - T_1) + \phi_i(t)\left(q_{m_i}(t) - q_i(t - T_1)\right) & \text{otherwise} \end{cases} \tag{3.28}$$

$$\phi_i(t) = \frac{\gamma_i \left(1 - e^{-\delta_i E_i(t)}\right)}{\alpha_i \left(||\dot{\mathbf{q}}_m(t)|| + ||\dot{\mathbf{q}}(t - T_1)||\right) + 1} \tag{3.29}$$

where σ_i, γ_i, δ_i, and α_i are positive constants and

$$\bar{v}_{m_i}(t) = v_i(t - T_1) + \frac{\gamma_i \left(1 - e^{-\delta_i \sigma_i}\right)}{\alpha_i \left(||\dot{\mathbf{q}}_m(t)|| + ||\dot{\mathbf{q}}(t - T_1)||\right) + 1}(q_{m_i}(t) - q_i(t - T_1)). \tag{3.30}$$

We now prove, by the following theorem, that the utilization of the full state compensator, governed by (3.28), (3.29), and (3.30), enforces full state convergence of the system state vector $\mathbf{q}(t)$ to the desired trajectory $\mathbf{q}_d$.

Theorem 3.3.2. *Consider the time delay nonlinear system (3.1) coupled to the reference model (3.3) via the scattering transformation (3.5-3.11) and (3.13) and full state compensator (3.28). Suppose that $\exists t_0 \geq 0$ such that $E_i(t) > \sigma_i$ for all $i \in \{1, \cdots, n\}$ and $t \geq t_0$. Let $b < \rho$. Then, for all initial conditions, we have the following results.*

i. All signals $\mathbf{q}_m(t), \mathbf{e}_m(t), \dot{\mathbf{q}}_m(t), \dot{\mathbf{q}}(t), \mathbf{w}_m(t)$, $\mathbf{w}(t), \mathbf{v}(t), \boldsymbol{\tau}(t)$ and $\ddot{\mathbf{q}}$ are bounded $\forall t \geq t_0$ and the velocities $\dot{\mathbf{q}}_m(t), \dot{\mathbf{e}}_m(t)$, and $\dot{\mathbf{q}}(t)$ converge to zero.

ii. If $\partial M(\mathbf{q})/\partial \mathbf{q}_i, \partial^2 M(\mathbf{q})/\partial \mathbf{q}_i \partial \mathbf{q}_j$ are bounded $\forall i, j$ and $K_m = b^2 I$, where I is the $n \times n$ identity matrix, then the error signals $\mathbf{e}_m(t)$, $\mathbf{q}_m(t) - \mathbf{q}_d$, and $\mathbf{q}_m(t) - \mathbf{q}(t)$ converge asymptotically to zero.

Proof. Assume that there exists a constant $t_0 \geq 0$ such that $E_i(t) > \sigma_i \ \forall\, i \in \{1, \cdots, n\}, t \geq t_0$ and consider once again the candidate Lyapunov function given in (3.16). Since $E_i(t) > \sigma_i$, $V(t)$ is positive definite for $(\mathbf{q}_m(t) - \mathbf{q}_d, \mathbf{e}_m(t), \dot{\mathbf{q}}_m(t), \dot{\mathbf{q}}(t)) \neq \mathbf{0}$. Taking the time derivative of (3.16) yields (3.17), from which we obtain that $\mathbf{q}_m, \mathbf{e}_m, \dot{\mathbf{q}}_m, \dot{\mathbf{q}} \in \mathcal{L}_\infty$. Then, solving (3.10) via the transmission equation (3.13), it is easy to show that

$$\begin{aligned} \boldsymbol{\tau}(t) =& 2\boldsymbol{\tau}_m(t - T_2) - \sqrt{2b}\mathbf{v}_m(t - T_2) && (3.31) \\ =& b\dot{\mathbf{q}}_m(t - T_2) + K_m\mathbf{e}_m(t - T_2). && (3.32) \end{aligned}$$

Therefore, $\boldsymbol{\tau}$ is bounded and so are $\mathbf{w}_m(t)$, $\mathbf{w}(t)$, and $\mathbf{v}(t)$. Now, invoking LaSalle's Invariance Principle for delay systems as in Theorem 3.3.1, we can conclude that solutions of the overall system converge to the largest invariance set of points for which $\dot{V} = 0$ and, hence, $(\dot{\mathbf{q}}_m(t), \dot{\mathbf{e}}_m(t), \dot{\mathbf{q}}(t)) \to \mathbf{0}$ as $t \to \infty$. Finally, from (3.23) we have that boundedness of $\mathbf{q}$ and $\boldsymbol{\tau}$ implies boundedness of $\ddot{\mathbf{q}}$. This completes the proof for the first claim.

To prove the second statement, let $K_m = b^2 I$. Taking the time derivative of (3.32) yields

$$\dot{\boldsymbol{\tau}}(t) = b\ddot{\mathbf{q}}_m(t - T_2) + b^2\dot{\mathbf{e}}_m(t - T_2). \tag{3.33}$$

Then, substituting (3.3) into (3.33) gives us that

$$\begin{aligned} \dot{\boldsymbol{\tau}}(t) =& bA_m\dot{\mathbf{q}}_m(t - T_2) - b^2\dot{\mathbf{e}}_m(t - T_2) - b^3\mathbf{e}_m(t - T_2) + bK_d(\mathbf{q}_d - \mathbf{q}_m(t - T_2)) + b^2\dot{\mathbf{e}}_m(t - T_2) \\ =& bA_m\dot{\mathbf{q}}_m(t - T_2) - b^3\mathbf{e}_m(t - T_2) + bK_d(\mathbf{q}_d - \mathbf{q}_m(t - T_2)) && (3.34) \end{aligned}$$

from which we conclude that $\dot{\boldsymbol{\tau}}$ is also bounded. Now, let us take the time derivative of (3.23). The assumptions that $\partial M(\mathbf{q})/\partial \mathbf{q}_i$ and $\partial^2 M(\mathbf{q})/\partial \mathbf{q}_i \partial \mathbf{q}_j$ are bounded imply that $dM^{-1}(\mathbf{q})/d\mathbf{q}_i$ and $dC(\mathbf{q}, \dot{\mathbf{q}})/dt$ are bounded, respectively [130]. Hence, $\dddot{\mathbf{q}} \in \mathcal{L}_\infty$. Then, since $\int_0^t \ddot{\mathbf{q}}(\theta)d\theta \to -\dot{\mathbf{q}}(0) < \infty$ as $t \to \infty$, we can apply Barbalat's Lemma and conclude that $\ddot{\mathbf{q}} \to 0$. Therefore, $\boldsymbol{\tau} \to 0$, which implies that $\mathbf{e}_m(t) \to 0$ (from (3.33)) and $\mathbf{v} \to 0$ (from (3.11) and (3.10)). Similarly from (3.5), we obtain that $\boldsymbol{\tau}_m \to 0$.

Now, by manipulating the equations of the scattering transformation, it is easy to obtain that

$$\begin{aligned} 2b\dot{\mathbf{q}}_{md}(t) = & \, b\left(\dot{\mathbf{q}}_m(t) - \dot{\mathbf{q}}_m(t-T)\right) + 2b\dot{\mathbf{q}}(t-T_1) \\ & + b^2(\mathbf{e}_m(t) - \mathbf{e}_m(t-T)) - \sqrt{2b}\Phi(t)(\mathbf{q}_m(t) - \mathbf{q}(t-T_1)) \end{aligned} \tag{3.35}$$

where Φ is a diagonal matrix with iith entries given by ϕ_i. Then, since $\left(1 - e^{-\delta_i E_i(t)}\right) \in (1 - e^{-\delta_i \sigma_i}, 1)$, from (3.29) we have that $\Phi(t)$ is both lower and upper bounded by finite positive constants. Therefore, $(\dot{\mathbf{q}}_{md}, \dot{\mathbf{q}}_m, \dot{\mathbf{q}}, \dot{\mathbf{e}}_m) \to \mathbf{0} \Rightarrow \mathbf{q}_m(t) - \mathbf{q}(t-T_1) \to 0$ which for finite delay T_1 implies that $\mathbf{q}_m(t) - \mathbf{q}(t) \to 0$ as $t \to \infty$. This last result and the fact that $\mathbf{q}_m(t) - \mathbf{q}(t-T_1)$ is uniformly continuous further imply that $\mathbf{q}_m(t) - \mathbf{q}(t-T_1)$ is bounded. Likewise, from (3.35) we obtain that $\dot{\mathbf{q}}_{md}$ and $\dot{\mathbf{e}}_m$ are also bounded. Then, by taking the time derivative of (3.34) we can show that

$$\begin{aligned} \ddot{\boldsymbol{\tau}}(t) = & bA_m^2\dot{\mathbf{q}}_m(t-T_2) + b^2(A_m + bI)\dot{\mathbf{e}}_m(t-T_2) - b^3A_m\mathbf{e}_m(t-T_2) \\ & + bA_mK_d(\mathbf{q}_d - \mathbf{q}_m(t-T_2)) - K_d\dot{\mathbf{q}}_m(t-T_2)) \end{aligned}$$

is bounded. Finally, using Barbalat's Lemma and noting that $\int_0^t \dot{\boldsymbol{\tau}}(\theta)d\theta \to -\boldsymbol{\tau}(0) < \infty$ we can conclude that $\dot{\boldsymbol{\tau}}(t) \to \mathbf{0}$, which further implies that $\ddot{\mathbf{q}}_m(t) \to \mathbf{0}$ (from 3.33). Then, from the definition of the reference model we obtain that $\mathbf{r}_m(t) \to \mathbf{0} \Rightarrow \mathbf{q}_d - \mathbf{q}_m(t) \to \mathbf{0}$, and the proof is complete. □

Remark 3.3.2. *Theorem 3.3.2 requires $E_i(t) > \sigma_i \; \forall t \geq t_0$ to guarantee state convergence between reference model and plant. If this requirement is not satisfied, then we cannot claim convergence of $\mathbf{q}_m(t) - \mathbf{q}(t)$ except that it is bounded. Nevertheless, we can make $E_i(t)$ increase the sufficient amount to perform complete compensation by avoiding the system from reaching steady-state before the compensation task is consumed. Therefore, it is appealing to investigate properties on $\mathbf{r}_m(t)$ that will guarantee state convergence before all signals in the system reach a steady-state value.*

3.4 Numerical Example: A 2-DOF Planar Manipulator

To illustrate the proposed controller let us consider the following nonlinear example.

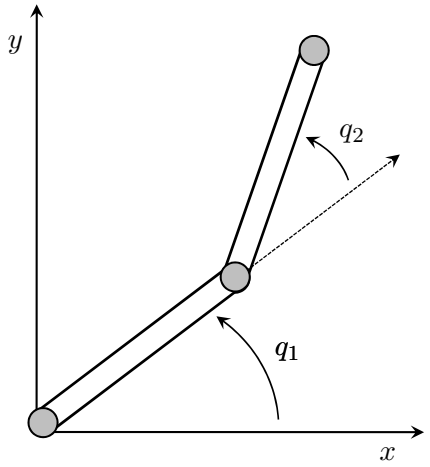

Figure 3.3: Planar manipulator.

3.4.1 System Dynamics and Control Objective

Consider the 2-DOF revolute-joint planar manipulator portrayed in Figure 3.3 with measurement delay $T_1 = 1.0$ s and input delay $T_2 = 0.5$ s. The dynamics of the manipulator, neglecting constant gravitational effects, is given by (3.1) with

$$M(\mathbf{q}) = \begin{bmatrix} m_1 & m_2 \\ m_2 & m_3 \end{bmatrix}, \qquad C(\mathbf{q}, \dot{\mathbf{q}}) = \begin{bmatrix} h\dot{q}_2 & h(\dot{q}_1 + \dot{q}_2) \\ -h\dot{q}_1 & 0 \end{bmatrix}, \qquad \frac{\partial \mathcal{F}(\dot{\mathbf{q}})}{\partial \dot{\mathbf{q}}} = \begin{bmatrix} \rho\dot{q}_1 & 0 \\ 0 & \rho\dot{q}_2 \end{bmatrix}$$

where $m_1 = (52.72 + 5.85\cos(x_2)) \times 10^{-2}$ kg $\cdot$ m^2, $m_2 = (3.27 + 2.92\cos(x_2)) \times 10^{-2}$ kg $\cdot$ m^2, $m_3 = (3.27) \times 10^{-2}$ kg $\cdot$ m^2, $h = (-2.92\sin(x_2)) \times 10^{-2}$ kg $\cdot$ m^2 [131], and $\rho = 0.50$ kg $\cdot$ m^2. The reference model and the reference control law are designed according to (3.3) and (3.4) with

$$A_m = \begin{bmatrix} -10 & 0 \\ 0 & -10 \end{bmatrix}, \qquad K_d = \begin{bmatrix} 4 & 0 \\ 0 & 4 \end{bmatrix}.$$

The control task is to drive the nonlinear manipulator from an unknown initial position $\mathbf{q}(0\text{ s}) = [q_1(0\text{ s}), q_2(0\text{ s})]^T = [-\frac{1}{2}, -\frac{\pi}{4}]^T$ rad to the desired configuration $\mathbf{q}_d = [q_{d1}, q_{d2}] = [\pi, \pi]^T$ rad.

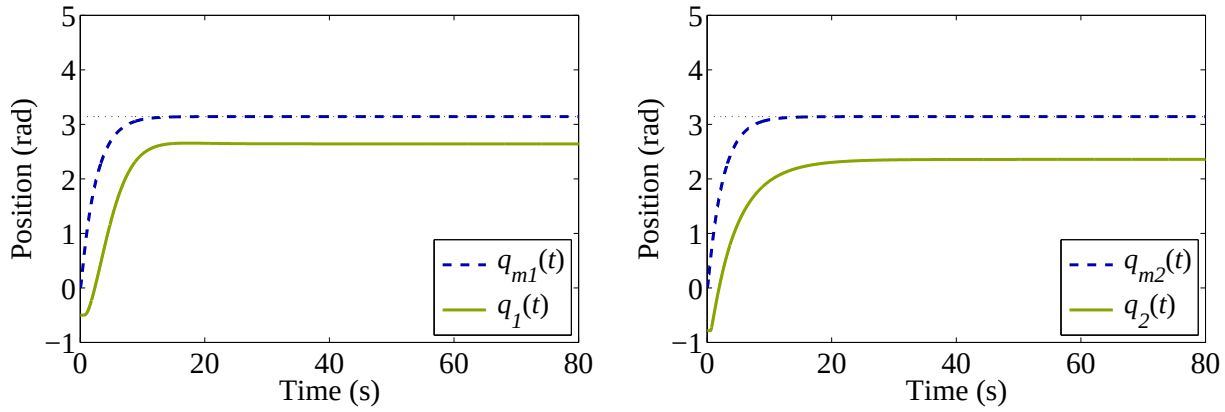

(a) Position of Proximal Link

(b) Position of Distal Link

Figure 3.4: Response of proximal and distal links with the proposed MRRC framework without utilizing the full state compensator for $T_1 = 1.0$ s and $T_2 = 0.5$ s. The fine dotted line at π rad denotes the desired state value.

3.4.2 Simulation Results

The first simulated experiment consisted of applying the proposed MRRC framework with no state compensator. The design parameters for the scattering transformation were chosen as $b = 0.30$ and $K_m = b^2 I = 0.09I$ while initial state values for the controller were set to zero, i.e., $\mathbf{q}_m(0\text{ s}) = \mathbf{q}_{md}(0\text{ s}) = \mathbf{0}$ rad. The response of the system is depicted in Figure 3.4. As noted in the plots, the state of the reference model converged to the desired configuration and the position error between the reference model and the time delay system stabilized at a constant value. Yet, the error did not converge to zero as both reference model and nonlinear system were not initialized at the same configuration, i.e., $\mathbf{q}_m(t) - \mathbf{q}(t) \to \mathbf{q}_m(0\text{ s}) - \mathbf{q}(0\text{ s}) = [\frac{1}{2}, \frac{\pi}{4}]^T$ rad.

We next simulated the response of the overall system employing the full state compensator. The parameters for the scattering transformation and the initial states for the controller were designed as in the previous example. The parameters for the state compensator were chosen as $\boldsymbol{\gamma} = [2, 10]^T, \boldsymbol{\delta} = [2, 10]^T, \boldsymbol{\sigma} = [\frac{1}{100}, \frac{1}{10000}]^T$, and $\boldsymbol{\alpha} = [6, 25]^T$. The position response for the proximal ($i = 1$) and distal ($i = 2$) links are illustrated in Figure 3.5. As it is shown in both plots, the time delay nonlinear plant was able to track the motion of the reference system and converged to the desired configuration even when the initial conditions between controller and nonlinear plant were different and the delays were relatively large.

Finally, Figure 3.6 illustrates how the available energy to perform the compensation technique evolved over time. Note that after some interval of time, the system built enough energy to modify

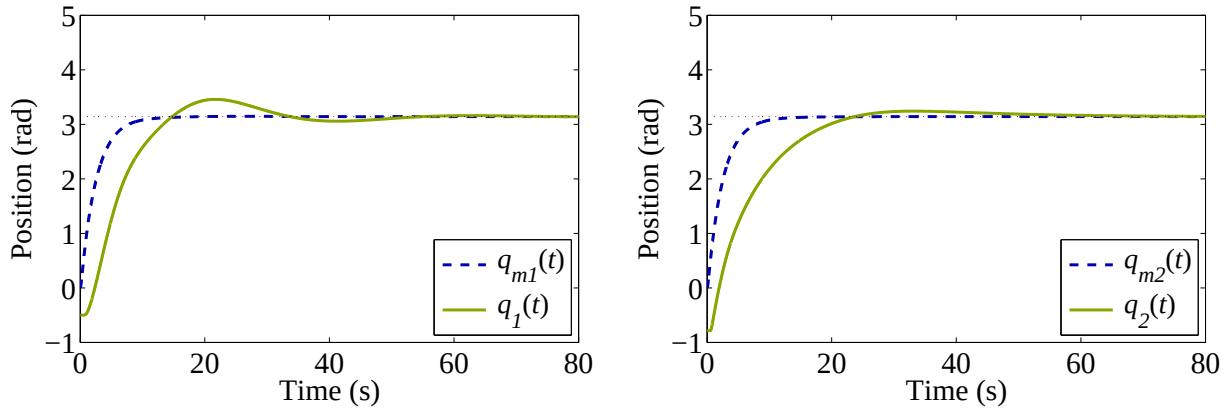

(a) Position of Proximal Link

(b) Position of Distal Link

Figure 3.5: Response of proximal and distal links with the proposed MRRC framework using the full state compensator for $T_1 = 1.0$ s and $T_2 = 0.5$ s.

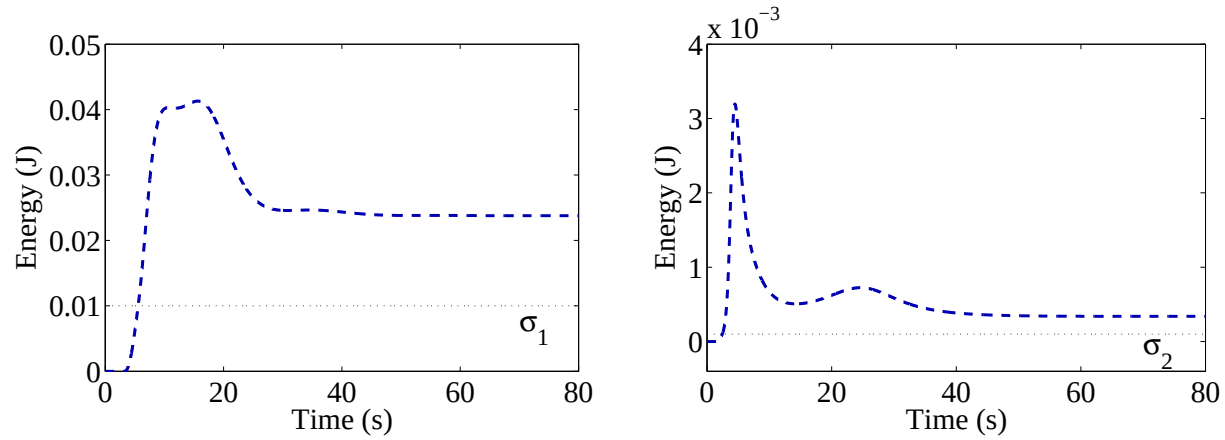

(a) $E_1(t)$

(b) $E_2(t)$

Figure 3.6: Available energy for compensation.

the scattering output such that position convergence, as stated by Theorem 3.3.2, was achieved.

3.5 Experimental Example: A Coaxial Helicopter

3.5.1 Testbed

Besides simulations, we tested the proposed controller on an unmanned vehicle. The vehicle, illustrated in Figure 3.7(a), is an E-Flite μ-CX coaxial helicopter with 28 g of net weight, 19 cm of

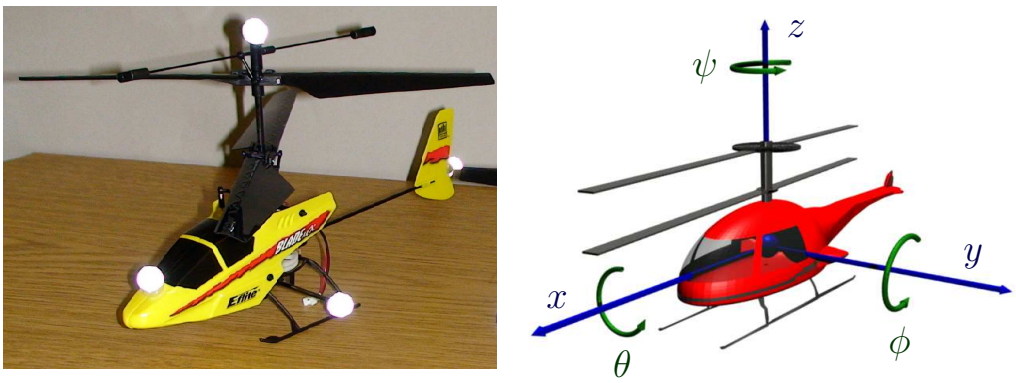

(a) E-Flite μ-CX helicopter. Copyright © 2010 Boeing. All rights reserved.

(b) Cartesian coordinate system and rotational angles.

Figure 3.7: Coaxial helicopter.

rotor diameter, and 20 cm of length. The simplified equations of motion for the μ-CX are given by

$$m\ddot{\mathbf{q}} = -\tilde{\mathbf{f}}(\dot{\mathbf{q}}) + \mathbf{u} \tag{3.36}$$

where gravitational forces have been compensated by a constant control (i.e., constant trim control values), m is the net weight of the helicopter, and $\mathbf{u}$ is the control input. The dissipation vector function $\tilde{\mathbf{f}}$ accounts for drag forces and damping effects on the rotors and servos, and is known to satisfy the following inequality [132]

$$\dot{\mathbf{q}}^T\tilde{\mathbf{f}}(\dot{\mathbf{q}}), \geq \rho \left\|\dot{\mathbf{q}}\right\|^2 \qquad \text{for some } \rho > 0. \tag{3.37}$$

In addition, the μ-CX helicopter is considered to have four controllable variables

$$\mathbf{q} = [x, y, z, \psi]^T \tag{3.38}$$

where (x, y, z) correspond to the position of the center of mass of the helicopter in Cartesian coordinates and ψ is the rotational angle around the z axis, namely yaw. A pictorial representation describing the relation and orientation of the rotational angles with respect to the Cartesian coordinates is given in Figure 3.7(b), where the roll (θ) and pitch (ϕ) angles are also illustrated.

Position and orientation recognition of the helicopter is owed to a Motion Capture (MoCap) system comprised of multiple high speed infrared cameras strategically located around the navigation room while state velocities were digitally computed. For more details on the experimental testbed,

the reader must refer to [133, 134] as well as Section 6.4.

3.5.2 Controller Design

We consider the coaxial helicopter mathematically described by (3.36) and coupled to the proposed controller with delays $T_1 = 0.50$ s and $T_2 = 0.03$ s. The controller was designed according to Section 3.2 with the reference model given by

$$A_m = \begin{bmatrix} -15 & 0 & 0 & 0 \\ 0 & -15 & 0 & 0 \\ 0 & 0 & -15 & 0 \\ 0 & 0 & 0 & -15 \end{bmatrix}, \qquad K_d = \begin{bmatrix} -15 & 0 & 0 & 0 \\ 0 & -15 & 0 & 0 \\ 0 & 0 & -15 & 0 \\ 0 & 0 & 0 & -15 \end{bmatrix}$$

and with the parameters of the scattering transformation being empirically chosen as

$$b = 0.5, \qquad K_m = \begin{bmatrix} 0.25 & 0 & 0 & 0 \\ 0 & 0.25 & 0 & 0 \\ 0 & 0 & 0.25 & 0 \\ 0 & 0 & 0 & 0.25 \end{bmatrix}. \tag{3.39}$$

Similarly, the state compensator was empirically designed with parameters $\gamma_i = 2.0$, $\delta_i = 1.0$, $\sigma_i = 0.05$, and $\alpha_i = 0.001$ $\forall i$. Finally, the selected control task was to drive the helicopter from an unknown initial position and orientation to a desired configuration given by

$$\mathbf{q}_d(t) = \begin{cases} [1.0 \text{ m}, & 0.9 \text{ m}, & 0.9 \text{ m}, & 0 \text{ rad}]^T & \text{if } t < 40 \text{ s} \\ [0.0 \text{ m}, & 0.0 \text{ m}, & 0.4 \text{ m}, & \pi \text{ rad}]^T & \text{if } t \geq 40 \text{ s} \end{cases} \tag{3.40}$$

3.5.3 Experimental Results

The response of the coaxial helicopter with the proposed controller is depicted in Figure 3.8, where the controller and the nonlinear system have been initialized at different configurations (i.e., $\mathbf{q}(0 \text{ s}) - \mathbf{q}_{md}(0 \text{ s}) = [0.2 \text{ m}, 0.2 \text{ m}, 0.2 \text{ m}, 0 \text{ rad}]^T$). As illustrated in the plots, the helicopter does not converge to the exact desired position but stays oscillating relatively close to the desired trajectory. This oscillatory response might be attributed to different factors such as environmental

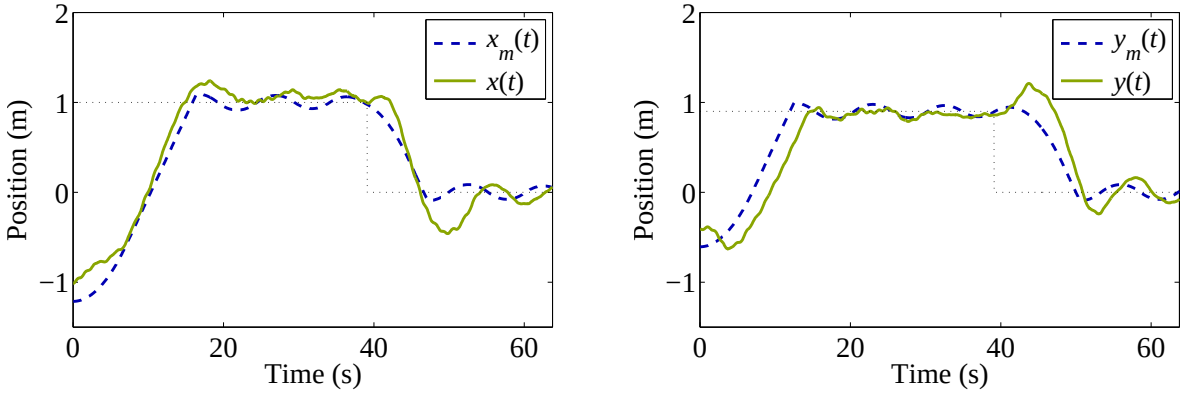

(a) $x(t)$

(b) $y(t)$

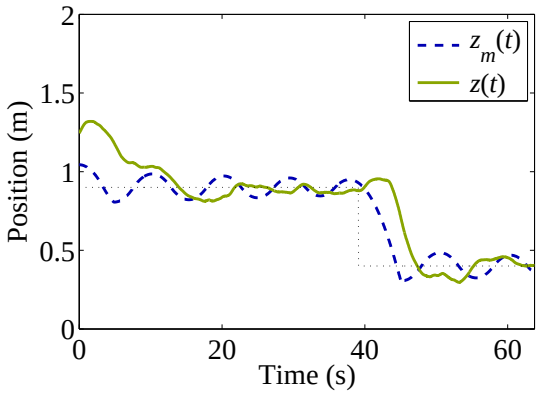

(c) $z(t)$

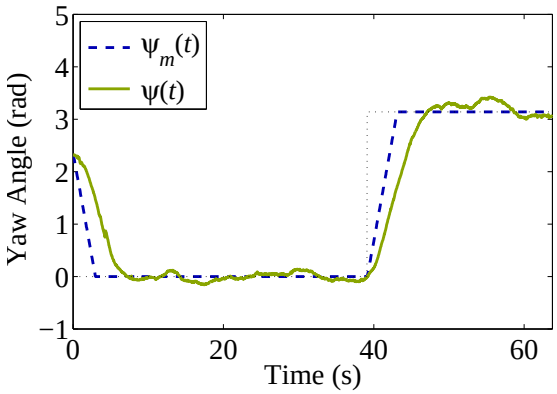

(d) $\psi(t)$

Figure 3.8: Position and orientation response of the coaxial helicopter with proposed controller for $T_1 = 0.50$ s and $T_2 = 0.03$ s. The fine dotted line denotes the desired trajectory.

disturbances (e.g., low weight of helicopter makes its motion vulnerable to any air flows), wave reflections [46], inaccurate trim values, and ignored dynamics. Despite the oscillatory response, it can be noticed that the error remains bounded and the vehicle tracks the desired trajectory. To clearly illustrate the last statement, Figure 3.9 graphs the norm of the position and orientation errors, where the error signals are shown to remain inside a small, bounded neighborhood around zero near steady-state conditions.

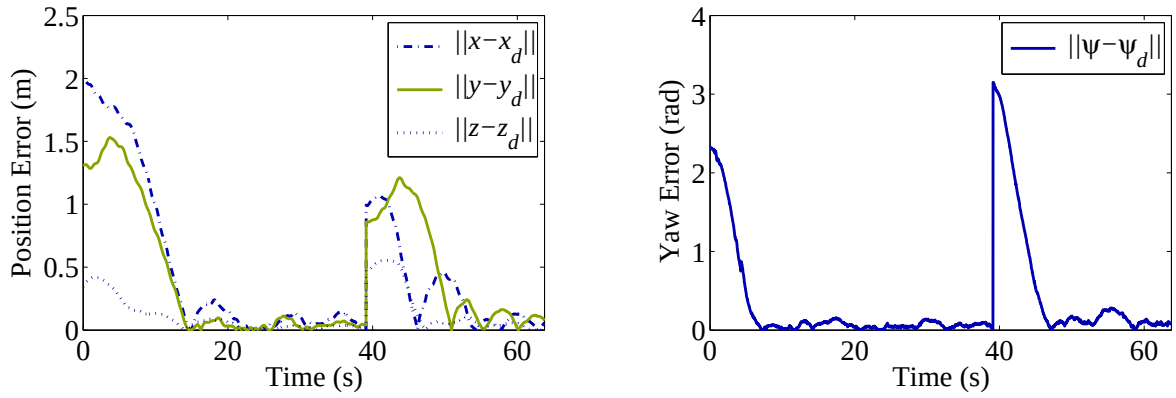

(a) Cartesian Coordinates

(b) $\psi(t)$

Figure 3.9: Norm of the position and orientation errors.

3.6 Comments

The proposed controller implicitly assumes that the delayed wave variable $\mathbf{w}_m(t-T)$ is known or that, at least, it can be decoded from the output of the system. Specifically, we assumed that $\mathbf{w}_m(t-T)$ is available when computing (3.11) and (3.12), i.e.,

$$\mathbf{v}_m(t) = \mathbf{v}(t-T_1) = \mathbf{w}_m(t-T) - \sqrt{2b}\dot{\mathbf{q}}(t-T_1). \tag{3.41}$$

In case that $\mathbf{w}_m(t-T)$ is unknown or unavailable, knowledge of the round-trip delay value is required to reconstruct $\mathbf{w}_m(t-T)$.

It is worth mentioning that knowledge of the delay or $\mathbf{w}_m(t-T)$ is not required to design the values of the parameters for the reference model, scattering transformation, and state compensator; that is, A_m, K_d, and b are all independent of T_1 and T_2.

CHAPTER 4

FORMATION CONTROL OF MULTIPLE SYSTEMS WITH INPUT AND STATE MEASUREMENT DELAYS

The scope of the passivity-based MRRC framework for nonlinear Lagrangian systems with input and state measurement delays, introduced in Chapter 3, is now extended to enclose multi-vehicle systems, such as the one illustrated in Figure 4.1. The results presented herein focus on motion coordination, cooperative formation control, and stability of multiple heterogeneous nonlinear agents coupled to a centralized controller via a communication network with constant delays.

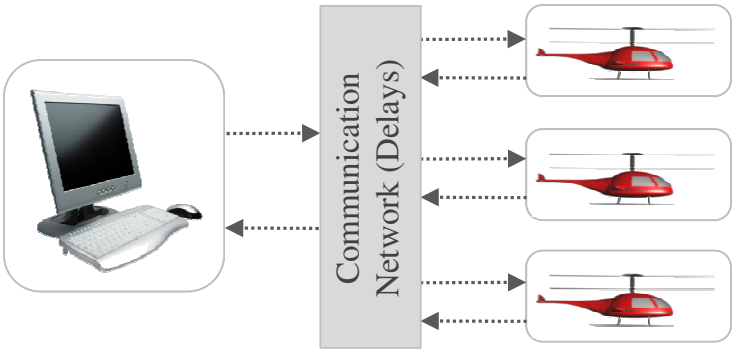

Figure 4.1: Multi-vehicle system with control communication delays.

4.1 Multi-Agent System

In this chapter, we aim to control a group of N n-DOF nonlinear Lagrangian system[1] with equations of motion given by

$$M_i(\mathbf{q}_i)\ddot{\mathbf{q}}_i + C_i(\mathbf{q}_i, \dot{\mathbf{q}}_i)\dot{\mathbf{q}}_i = \mathbf{u}_i - \frac{\partial \mathcal{F}_i(\dot{\mathbf{q}}_i)}{\partial \dot{\mathbf{q}}_i}, \qquad \text{for } i = \{1, \cdots, N\} \tag{4.1}$$

[1] Gravitational forces have been either neglected or canceled through constant control.

where dissipative forces are assumed to satisfy the following inequality

$$\dot{\mathbf{q}}_i^T \frac{\partial \mathcal{F}_i(\dot{\mathbf{q}}_i)}{\partial \dot{\mathbf{q}}_i} \geq \rho_i \left\| \dot{\mathbf{q}}_i \right\|^2, \qquad \text{for } \rho_i > 0. \tag{4.2}$$

The positive inertia matrices M_i and centrifugal and Coriolis matrices C_i are assumed to satisfy Properties 2.2.1 to 2.2.2 whereas the control input $\mathbf{u}_i$ is a delayed state feedback function depending on $\mathbf{q}_i(t - T_{1_i} - T_{2_i})$ and $\dot{\mathbf{q}}_i(t - T_{1_i} - T_{2_i})$, where $T_{1_i} \geq 0$ and $T_{2_i} \geq 0$ correspond to the measurement and plant-to-controller communication delay and the controller-to-plant communication delay, respectively.

4.2 Control Framework

As part of the control objectives, we identify two main goals. First, the overall system must be stable, meaning that all trajectories must remain bounded; and second, the agents must converge to the desired state (e.g., position and orientation) within the formation whereas the formation's center of mass must converge to the desired trajectory. Mathematically, we would like $\mathbf{q}_i(t) \to \mathbf{q}_d + \boldsymbol{\gamma}_i \ \forall i$ and $\frac{1}{N}\sum_{i=1}^{N} \mathbf{q}_i(t) \to \mathbf{q}_d$ as $t \to \infty$, where $\mathbf{q}_d$ is the desired trajectory of the formation's centroid and $\boldsymbol{\gamma}_i$ is the desired relative distance and orientation of the ith agent from the center of the formation satisfying, without loss of generality, the following conditions

$$\boldsymbol{\gamma}_i \neq \boldsymbol{\gamma}_j, \ \ \forall i \neq j \ \text{ and } \ \sum_{i=1}^{N} \boldsymbol{\gamma}_i = 0, \ \ \forall t \geq 0. \tag{4.3}$$

According to these objectives, we propose the use of a passivity-based control framework, comprising a reference model coupled to the time delay nonlinear systems via the implementation of N scattering transformation blocks. A pictorial representation is given in Figure 4.2.

For simplicity, the reference model is a linear system with dynamics given by

$$\begin{aligned} \ddot{\mathbf{q}}_m(t) = &\quad A_m \dot{\mathbf{q}}_m(t) + \mathbf{u}_m(t) + \mathbf{r}_m(t) \\ \mathbf{y}_m(t) = &\quad \dot{\mathbf{q}}_m(t) \end{aligned} \tag{4.4}$$

where $\mathbf{q}_m(t), \dot{\mathbf{q}}_m(t) \in \Re^n$ are the state vectors, $\mathbf{y}_m(t) \in \Re^n$ is the output vector, $\mathbf{u}_m(t) \in \Re^n$ is the control input, and $A_m \in \Re^{n \times n}$ is a symmetric Hurwitz matrix. The reference signal $\mathbf{r}_m(t) \in \Re^n$ is

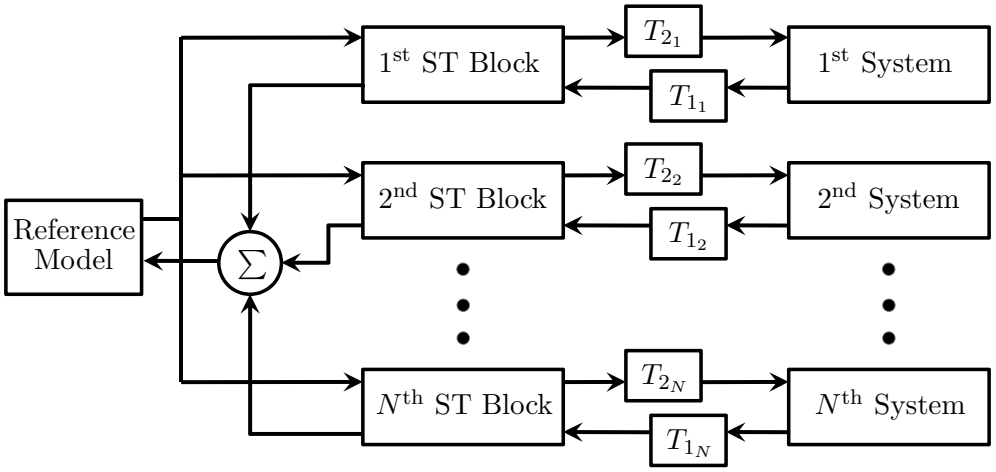

Figure 4.2: Proposed multi-MRRC framework. ST stands for scattering transformation.

governed by

$$\mathbf{r}_m(t) = K_d(\mathbf{q}_d - \mathbf{q}_m(t)) \tag{4.5}$$

where $K_d \in \Re^{n\times n}$ is a positive-definite constant matrix.

The scattering transformation blocks are employed to stabilize the coupling between the reference model and the nonlinear agents. The scattering transformation equations are given as

$$\boldsymbol{\tau}_{m_i}(t) = b_i\dot{\mathbf{e}}_{m_i}(t) + K_{m_i}\mathbf{e}_{m_i}(t) \tag{4.6}$$

$$\mathbf{w}_{m_i}(t) = \sqrt{\frac{2}{b_i}}\boldsymbol{\tau}_{m_i}(t) - \mathbf{v}_{m_i}(t) \tag{4.7}$$

$$\dot{\mathbf{q}}_{md_i}(t) = \frac{1}{b_i}\left(\boldsymbol{\tau}_{m_i}(t) - \sqrt{2b_i}\mathbf{v}_{m_i}(t)\right) \tag{4.8}$$

$$\mathbf{q}_{md_i}(t) = \int_0^t \dot{\mathbf{q}}_{md_i}(\theta)d\theta \tag{4.9}$$

$$\mathbf{e}_{m_i}(t) = \mathbf{q}_m(t) - \mathbf{q}_{md_i}(t) \tag{4.10}$$

$$\boldsymbol{\tau}_i(t) = \sqrt{2b_i}\mathbf{w}_i(t) \tag{4.11}$$

$$\mathbf{v}_i(t) = \mathbf{w}_i(t) - \sqrt{2b_i}\dot{\mathbf{q}}_i(t) \tag{4.12}$$

where b_i, namely the wave impedances, are positive constants,[2] K_{m_i} are symmetric positive definite

[2]The same results hold if b_i are positive definite matrices.

matrices, and

$$\mathbf{v}_{m_i}(t) = \mathbf{v}_i(t - T_{1_i}) \tag{4.13}$$

$$\mathbf{w}_i(t) = \mathbf{w}_{m_i}(t - T_{2_i}) \tag{4.14}$$

are known as the transmission equations. The control inputs to the reference model and the nonlinear plants are then given as $\mathbf{u}_m(t) = -\boldsymbol{\tau}_m(t)$ and $\mathbf{u}_i(t) = \boldsymbol{\tau}_i(t)$, respectively, where

$$\boldsymbol{\tau}_m(t) = \sum_{i=1}^{N} \boldsymbol{\tau}_{m_i}(t). \tag{4.15}$$

Remark 4.2.1. *The above controller represents a cooperative control algorithm since, although the agents do not directly share state information among each other, the state of the ith agent affects the behavior of the reference model which, in turn, directly affects the state and command of all other agents.*

4.3 Stability and Formation Control

We now proceed to claim the attainment of the control objectives by the proposed controller. The following theorem will be used to establish stability of the overall system whereas the later corollary will guarantee state convergence and formation control.

Theorem 4.3.1. *Consider the group of time delay nonlinear systems (4.1) coupled to the reference model (4.4) via the scattering transformation blocks (4.6-4.14) and let $b_i < \rho_i$ for $i = \{1, \cdots, N\}$. Then, $\forall i$ and for all initial conditions we have the following results.*

i. All signals $\mathbf{q}_m(t), \mathbf{q}_i(t), \mathbf{e}_{m_i}(t), \dot{\mathbf{q}}_m(t), \dot{\mathbf{q}}_i(t), \dot{\mathbf{e}}_{m_i}(t)$, $\ddot{\mathbf{q}}_m(t)$, and $\ddot{\mathbf{q}}_i(t)$ are bounded $\forall t \geq 0$ and the velocities $\dot{\mathbf{q}}_m(t), \dot{\mathbf{e}}_{m_i}(t)$, and $\dot{\mathbf{q}}_i(t)$ converge to zero.

ii. The error signals $\mathbf{e}_{m_i}(t)$ and $\mathbf{q}_m(t) - \mathbf{q}_d$ converge asymptotically to zero.

Proof. The proof follows similar to that of Theorem 3.3.1. Consider the group of agents described by (4.1) and coupled via the scattering transformation equations (4.6) to (4.14). Let the following Lyapunov candidate function be given by

$$
\begin{aligned}
V(t) =& V(\mathbf{q}_m(t), \dot{\mathbf{q}}_m(t), \mathbf{e}_{m_1}(t), \cdots, \mathbf{e}_{m_N}(t), \dot{\mathbf{q}}_i(t), \cdots, \dot{\mathbf{q}}_N(t)) \\
=& \frac{1}{2}\sum_{i=1}^{N} \dot{\mathbf{q}}_i^T M_i(\mathbf{q}_i)\dot{\mathbf{q}}_i + \frac{1}{2}(\mathbf{q}_d - \mathbf{q}_m)^T K_d(\mathbf{q}_d - \mathbf{q}_m) + \frac{1}{2}\dot{\mathbf{q}}_m^T \dot{\mathbf{q}}_m \\
&+ \frac{1}{2}\sum_{i=1}^{N} \mathbf{e}_{m_i}^T K_{m_i}\mathbf{e}_{m_i} + \sum_{i=1}^{N}\int_0^t (\dot{\mathbf{q}}_{md_i}^T \boldsymbol{\tau}_{m_i} - \dot{\mathbf{q}}_i^T(\boldsymbol{\tau}_i - b_i\dot{\mathbf{q}}_i))d\theta.
\end{aligned} \tag{4.16}
$$

Then, taking the time derivative of (4.16) yields

$$
\begin{aligned}
\dot{V} \leq& \sum_{i=1}^{N}\left(-\rho_i \dot{\mathbf{q}}_i^T\dot{\mathbf{q}}_i + \dot{\mathbf{q}}_i^T\boldsymbol{\tau}_i\right) - \dot{\mathbf{q}}_m^T K_d(\mathbf{q}_d - \mathbf{q}_m) + \dot{\mathbf{q}}_m^T(A_m\dot{\mathbf{q}}_m - \boldsymbol{\tau}_m + K_d(\mathbf{q}_d - \mathbf{q}_m)) \\
&+ \sum_{i=1}^{N}\dot{\mathbf{e}}_{m_i}^T K_{m_i}\mathbf{e}_{m_i} + \sum_{i=1}^{N}\left(\dot{\mathbf{q}}_{md_i}^T\boldsymbol{\tau}_{m_i} - \dot{\mathbf{q}}_i^T\boldsymbol{\tau}_i + b_i\dot{\mathbf{q}}_i^T\dot{\mathbf{q}}_i\right) \\
=& -\sum_{i=1}^{N}(\rho_i - b_i)\dot{\mathbf{q}}_i^T\dot{\mathbf{q}}_i + \dot{\mathbf{q}}_m^T A_m\dot{\mathbf{q}}_m - \dot{\mathbf{q}}_m^T\sum_{i=1}^{N}\boldsymbol{\tau}_{m_i} + \sum_{i=1}^{N}\dot{\mathbf{e}}_{m_i}^T K_{m_i}\mathbf{e}_{m_i} + \sum_{i=1}^{N}\dot{\mathbf{q}}_{md_i}^T\boldsymbol{\tau}_{m_i} \\
=& -\sum_{i=1}^{N}(\rho_i - b_i)\dot{\mathbf{q}}_i^T\dot{\mathbf{q}}_i + \dot{\mathbf{q}}_m^T A_m\dot{\mathbf{q}}_m + \sum_{i=1}^{N}\dot{\mathbf{e}}_{m_i}^T K_{m_i}\mathbf{e}_{m_i} - \sum_{i=1}^{N}\dot{\mathbf{q}}_m^T\left(b_i\dot{\mathbf{e}}_{m_i} + K_{m_i}\mathbf{e}_{m_i}\right) \\
&+ \sum_{i=1}^{N}\dot{\mathbf{q}}_{md_i}^T\left(b_i\dot{\mathbf{e}}_{m_i} + K_{m_i}\mathbf{e}_{m_i}\right) \\
\leq& -\sum_{i=1}^{N}(\rho_i - b_i)\dot{\mathbf{q}}_i^T\dot{\mathbf{q}}_i - \mu\dot{\mathbf{q}}_m^T\dot{\mathbf{q}}_m - \sum_{i=1}^{N}b_i\dot{\mathbf{e}}_{m_i}^T\dot{\mathbf{e}}_{m_i}
\end{aligned}
$$

where $\mu > 0$ is the smallest eigenvalues of $-A_m$. Since $b_i < \rho_i \; \forall\, i$ we have that

$$
\dot{V} \leq -\mu\left\|\dot{\mathbf{q}}_m\right\|^2 - \sum_{i=1}^{N}(\rho_i - b_i)\left\|\dot{\mathbf{q}}_i\right\|^2 - \sum_{i=1}^{N}b_i\left\|\dot{\mathbf{e}}_{m_i}\right\|^2 \leq 0 \tag{4.17}
$$

and, therefore, the overall multi-agent system is stable in the sense of Lyapunov. Moreover, we can invoke LaSalle's Invariance Principle for delay systems and conclude that $\dot{\mathbf{q}}_m, \dot{\mathbf{q}}_i, \dot{\mathbf{e}}_{m_i}$, and hence $\dot{\mathbf{q}}_{md_i}$, converge to zero for all i.

Now, in order to demonstrate boundedness of all signals, let us consider once again the (4.17) inequality. Integrating at both sides of (4.17) we obtain that $V(t) \leq V(0) < \infty$, which implies that $\mathbf{q}_m, \mathbf{q}_{md_i}, \mathbf{e}_{m_i}, \dot{\mathbf{q}}_m, \dot{\mathbf{q}}_i$ are all bounded. Similarly, from the scattering transformation equations (4.6)

to (4.12) and the transmission equation (4.14) we can easily verify that

$$\boldsymbol{\tau}_i(t) = b_i\dot{\mathbf{q}}_m(t - T_{2_i}) + K_{m_i}\mathbf{e}_{m_i}(t - T_{2_i}) \tag{4.18}$$

is also bounded $\forall\, i$. Then, substituting (4.18) and (4.13) into (4.8) yields

$$2b_i\dot{\mathbf{q}}_{md_i}(t) = b_i\dot{\mathbf{q}}_m(t) + K_{m_i}\mathbf{e}_{m_i}(t) + 2\dot{\mathbf{q}}_i(t - T_{1_i}) - b_i\dot{\mathbf{q}}_m(t - T_i) - K_{m_i}\mathbf{e}_{m_i}(t - T_i) \tag{4.19}$$

where $T_i = T_{1_i} + T_{2_i}$, and, therefore, $\dot{\mathbf{q}}_{md_i}$ and $\dot{\mathbf{e}}_{m_i}$ are bounded. Similarly, rewriting (4.6) gives us that

$$\boldsymbol{\tau}_{m_i}(t) = \frac{b_i}{2}\left(\dot{\mathbf{q}}_m(t) + \dot{\mathbf{q}}_m(t - T_i)\right) + \frac{K_{m_i}}{2}\left(\mathbf{e}_{m_i}(t) + \mathbf{e}_{m_i}(t - T_i)\right) - b_i\dot{\mathbf{q}}_i(t - T_{1_i}) \tag{4.20}$$

Boundedness of $\mathbf{e}_{m_i}(t), \dot{\mathbf{q}}_m$, and $\dot{\mathbf{q}}_i$ then implies that $\boldsymbol{\tau}_{m_i} \in \mathcal{L}_\infty$ and from the definition of the reference model (4.4) and (4.15) we obtain that $\ddot{\mathbf{q}}_m$ is also bounded. Furthermore, integrating (4.19) with respect to time yields

$$\int_0^t \dot{\mathbf{q}}_{md_i}(\theta)d\theta = \int_0^t \dot{\mathbf{q}}_i(\theta)d\theta + \frac{1}{2}\int_{t-T_i}^t \dot{\mathbf{q}}_m(\theta)d\theta + \frac{K_{m_i}}{2b_i}\int_{t-T_i}^t \mathbf{e}_{m_i}(\theta)d\theta \tag{4.21}$$

and re-arranging the above equation we obtain that

$$\mathbf{q}(t)_i = \mathbf{q}_i(0) + \mathbf{q}_{md_i}(t) - \mathbf{q}_{md_i}(0) + \mathbf{q}_{m_i}(t) - \mathbf{q}_{m_i}(t - T_i) + \frac{K_{m_i}}{2b_i}\int_{t-T_i}^t \mathbf{e}_{m_i}(\theta)d\theta. \tag{4.22}$$

Since all terms in (4.22) are bounded, we can conclude that $\mathbf{q}_i \in \mathcal{L}_\infty$.

Finally, let us solve (4.1) for $\ddot{\mathbf{q}}_i$ as

$$\ddot{\mathbf{q}}_i = M_i^{-1}(\mathbf{q})\left(\boldsymbol{\tau}_i - \frac{\partial \mathcal{F}_i(\dot{\mathbf{q}}_i)}{\partial \dot{\mathbf{q}}_i} - C_i(\mathbf{q}_i, \dot{\mathbf{q}}_i)\dot{\mathbf{q}}_i\right). \tag{4.23}$$

where M_i^{-1} exist and are bounded $\forall i$ due to Property 2.2.2. Similarly, from boundedness of $\dot{\mathbf{q}}_i$ we have that C_i (from Property 2.2.3) and $\frac{\partial \mathcal{F}_i(\dot{\mathbf{q}}_i)}{\partial \dot{\mathbf{q}}_i}$ are bounded, which in addition to boundedness of $\boldsymbol{\tau}_i$, lead us to the conclusion that $\ddot{\mathbf{q}}_i \in \mathcal{L}_\infty$.

Now, let us prove the second statement in the theorem. Consider equation (4.20) rearranged as

$$\boldsymbol{\tau}_{m_i}(t) = \frac{b_i}{2}\left(\dot{\mathbf{q}}_m(t) + \dot{\mathbf{q}}_m(t-T)\right) + \frac{K_{m_i}}{2}\int_{t-T_i}^{t} \dot{\mathbf{e}}_{m_i}(\theta)d\theta - b_i\dot{\mathbf{q}}_i(t-T_{1_i}). \tag{4.24}$$

Due to the fact that all signals at the right-hand side of (4.24) go to zero, we have that $\boldsymbol{\tau}_{m_i} \to 0$, which similarly implies that $\mathbf{e}_{m_i} \to 0$. Then, computing the time derivative of (4.20) yields that

$$\dot{\boldsymbol{\tau}}_{m_i}(t) = \frac{b_i}{2}\left(\ddot{\mathbf{q}}_m(t) + \ddot{\mathbf{q}}_m(t-T_i)\right) + \frac{K_{m_i}}{2}\left(\dot{\mathbf{e}}_{m_i}(t) + \dot{\mathbf{e}}_{m_i}(t-T_i)\right) - b_i\ddot{\mathbf{q}}(t-T_{1_i}). \tag{4.25}$$

Noticing that all signals at the right-hand side of (4.25) are bounded, we obtain that $\dot{\boldsymbol{\tau}}_{m_i}(t)$ are also bounded. Likewise, by taking the time derivative at both sides of (4.4), we can easily verify that $\dddot{\mathbf{q}}_m$ is also bounded. Then, since $\int_0^t \ddot{\mathbf{q}}_m(\theta)d\theta \to -\dot{\mathbf{q}}_m(0) < \infty$ as $t \to \infty$, we can apply Barbalat's Lemma and conclude that $\ddot{\mathbf{q}}_m \to 0$. Finally, using (4.4) and the convergence results for $\dot{\mathbf{q}}_m, \ddot{\mathbf{q}}_m$, and $\boldsymbol{\tau}_m$, we obtain that $\mathbf{r}_m \to 0 \Rightarrow \mathbf{q}_m - \mathbf{q}_d \to 0$, which completes the proof. □

Corollary 4.3.1. *If* $\mathbf{q}_{md_i}(0) = \mathbf{q}_i(0) - \boldsymbol{\gamma}_i \ \forall i$, *then* $\mathbf{q}_i(t) \to \mathbf{q}_d + \boldsymbol{\gamma}_i$ *and* $\frac{1}{N}\sum_{i=1}^{N} \mathbf{q}_i(t) \to \mathbf{q}_d$ *as* $t \to \infty$.

Proof. Consider equation (4.21). From Theorem 4.3.1 we have that $\dot{\mathbf{q}}_m(t)$ and $\mathbf{e}_{m_i}(t)$ vanish as $t \to \infty$. Hence, (4.21) reduces to

$$\mathbf{q}_{md_i}(t) - \mathbf{q}_{md_i}(0) \to \mathbf{q}_i(t) - \mathbf{q}_i(0). \tag{4.26}$$

Now, from Theorem 4.3.1 we also have that $\mathbf{q}_{md_i}(t) \to \mathbf{q}_m(t) \to \mathbf{q}_d$, which yields that $\mathbf{q}_i(t) \to \mathbf{q}_d - \mathbf{q}_{md_i}(0) + \mathbf{q}_i(0)$. Therefore, if $\mathbf{q}_{md_i}(0) = \mathbf{q}_i(0) - \boldsymbol{\gamma}_i \ \forall i$, we obtain that

$$\mathbf{q}_i(t) \to \mathbf{q}_d + \boldsymbol{\gamma}_i. \tag{4.27}$$

Similarly, from (4.27) we have that

$$\sum_{i=1}^{N} \mathbf{q}_i(t) \to \sum_{i=1}^{N} \mathbf{q}_d + \sum_{i=1}^{N} \boldsymbol{\gamma}_i = \sum_{i=1}^{N} \mathbf{q}_d. \tag{4.28}$$

which reduces to $\frac{1}{N}\sum_{i=1}^{N} \mathbf{q}_i(t) \to \mathbf{q}_d$. □

4.4 Illustrative Example

To illustrate the utility of the proposed MRRC framework for multi-vehicle systems, let us consider the following example.

4.4.1 System Dynamics and Control Design

We consider a group of four omnidirectional vehicles with nonlinear Lagrangian dynamics given by [135]

$$\begin{bmatrix} m_{p_i}+\frac{3I_r}{2r_i^2} & 0 & 0 \\ 0 & m_{p_i}+\frac{3I_r}{2r_i^2} & 0 \\ 0 & 0 & I_p+\frac{3I_rL_i^2}{r_i^2} \end{bmatrix} \begin{bmatrix} \ddot{x}_i \\ \ddot{y}_i \\ \ddot{\phi}_i \end{bmatrix} + \begin{bmatrix} 0 & -\frac{3I_r}{2r_i^2}\dot{\phi}_i & 0 \\ \frac{3I_r}{2r_i^2}\dot{\phi}_i & 0 & 0 \\ 0 & 0 & 0 \end{bmatrix} \begin{bmatrix} \dot{x}_i \\ \dot{y}_i \\ \dot{\phi}_i \end{bmatrix} =$$
$$-\begin{bmatrix} m_{p_i}g\mu_1 & 0 & 0 \\ 0 & m_{p_i}g\mu_1 & 0 \\ 0 & 0 & m_{p_i}g\mu_2 \end{bmatrix} \begin{bmatrix} \dot{x}_i \\ \dot{y}_i \\ \dot{\phi}_i \end{bmatrix} + \begin{bmatrix} -\sin(\theta+\phi_i) & -\sin(\theta-\phi_i) & \cos\phi_i \\ \cos(\theta+\phi_i) & -\cos(\theta-\phi_i) & \sin\phi_i \\ L_i & L_i & L_i \end{bmatrix} \hat{\mathbf{u}}_i \quad (4.29)$$

where effects of friction have been considered [136]. An illustration of the ith vehicle is given in Figure 4.3. The state vectors $\mathbf{q}_i = [x_i, y_i, \phi_i]^T$ are comprised of the Cartesian coordinates of the center of mass (x_i, y_i) and the heading angle (ϕ_i) of the vehicles $\forall i$, whereas the control inputs are computed as

$$\begin{aligned} \hat{\mathbf{u}}_i(t) =& B(\phi_i(t-T_i))^{-1}\mathbf{u}_i(t) \\ =& \begin{bmatrix} -\sin(\theta+\phi_i(t-T_i)) & -\sin(\theta-\phi_i(t-T_i)) & \cos\phi_i(t-T_i) \\ \cos(\theta+\phi_i(t-T_i)) & -\cos(\theta-\phi_i(t-T_i)) & \sin\phi_i(t-T_i) \\ L_i & L_i & L_i \end{bmatrix}^{-1} \mathbf{u}_i(t). \end{aligned} \quad (4.30)$$

It is assumed that $\phi_i(t)$ is a slow time-varying state, such that $\hat{\mathbf{u}}_i(t) = B(\phi_i(t))B(\phi_i(t-T_i))^{-1}\mathbf{u}_i(t) \approx \mathbf{u}_i(t)$.

The system parameters are $I_r = 0.52$ kg $\cdot$ m^2, $I_p = 0.17$ kg $\cdot$ m^2, $g = 9.81$ kg $\cdot$ m/s^2, $\mu_1 = 0.25$, $\mu_2 = 0.1$, and $\theta = 0$ rad for all vehicles; $m_{p_i} = 9.58$ kg, $r_i = 0.079$ m, and $L_i = 0.205$ m for the first and second vehicles; and $m_{p_i} = 11.58$ kg, $r_i = 0.089$ m, and $L_i = 0.305$ m for the third and fourth vehicles.

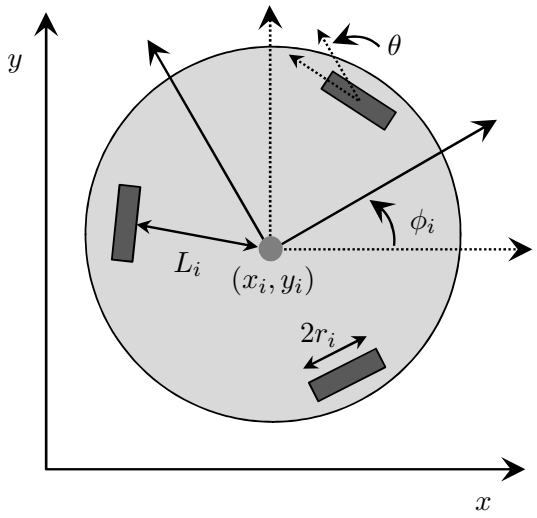

Figure 4.3: Omnidirectional vehicle.

The reference model was design according to (4.4) and (4.5) with

$$A_m = \begin{bmatrix} -10 & 0 & 0 \\ 0 & -10 & 0 \\ 0 & 0 & -10 \end{bmatrix}, \qquad K_d = \begin{bmatrix} 20 & 0 & 0 \\ 0 & 20 & 0 \\ 0 & 0 & 2 \end{bmatrix}.$$

while the scattering transformation parameters were similarly chosen as

$$b_i = \begin{bmatrix} 5 & 0 & 0 \\ 0 & 5 & 0 \\ 0 & 0 & 1 \end{bmatrix}, \; b_j = \begin{bmatrix} 4 & 0 & 0 \\ 0 & 4 & 0 \\ 0 & 0 & \frac{4}{5} \end{bmatrix}, \; K_{m_i} = \begin{bmatrix} 250 & 0 & 0 \\ 0 & 250 & 0 \\ 0 & 0 & 1 \end{bmatrix}, \; K_{m_j} = \begin{bmatrix} 150 & 0 & 0 \\ 0 & 150 & 0 \\ 0 & 0 & 1 \end{bmatrix}$$

for $i \in \{1, 2\}$ and $j \in \{3, 4\}$. The coupling delays were assigned different for each vehicle and were given as $T_{1_1} = 0.6$ s, $T_{2_1} = 0.4$ s, $T_{1_2} = 0.8$ s, $T_{2_2} = 0.4$ s, $T_{1_3} = 0.5$ s, $T_{2_3} = 0.5$ s, $T_{1_4} = 0.5$ s, and $T_{2_4} = 0.7$ s.

4.4.2 Simulation Results

The first simulated experiment consisted of commanding the state agents to converge to a static formation centered at $\mathbf{q}_d = [5.0 \text{ m}, 5.0 \text{ m}, 0.0 \text{ rad}]^T$. The desired formation was a trapezoid with vertices $\boldsymbol{\gamma}_1 = [-0.5 \text{ m}, 1.5 \text{ m}, 0.0 \text{ rad}]^T$, $\boldsymbol{\gamma}_2 = [0.5 \text{ m}, 0.65 \text{ m}, 0.0 \text{ rad}]^T$, $\boldsymbol{\gamma}_3 = [0.5 \text{ m}, -0.65 \text{ m}, 0.0 \text{ rad}]^T$, and $\boldsymbol{\gamma}_4 = [-0.5 \text{ m}, -1.5 \text{ m}, 0.0 \text{ rad}]^T$. The response of the overall system in the xy Cartesian plane

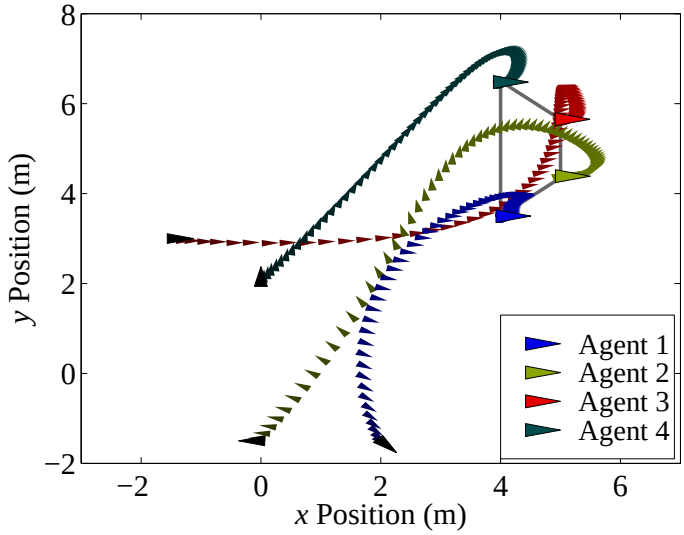

Figure 4.4: Cartesian position (x, y) of the four vehicles. The heading of each vehicle is denoted by the triangle pointing direction. Each position mark is distanced by intervals of 0.5 s.

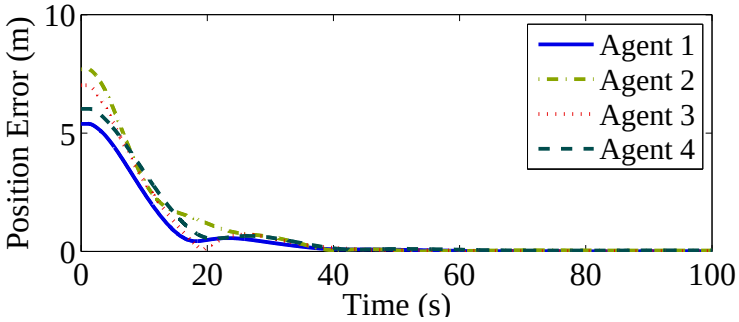

Figure 4.5: Norm of the position error.

is illustrated in Figure 4.4, where the four triangles indicate the position and orientation of the vehicles. As can be noticed from the plot, the four vehicles started from a configuration (i.e., position and orientation) different from the desired formation. Yet, the vehicles are able to converge to desired formation delineated by the trapezoid in gray color.

Figures 4.5 and 4.6 show the norm of the position error ($\|(x_d + \gamma_{i_1}, y_d + \gamma_{i_2}) - (x_i, y_i)\|$) and the heading error ($\|\phi_d + \gamma_{i_3} - \phi_i\|$), respectively, for the four vehicles. Both figures confirm convergence of the error signals to zero.

In the second simulated experiment, the same trapezoid formation was enforced, but the center of the formation was time-varying and given by $\mathbf{q}_d(t) = [\frac{t}{20}\ \text{m/s}, 5.0\ \text{m}, 0.0\ \text{rad}]^T$. Figure 4.7 illustrates the trajectory of the four vehicles, which were initialized at the same position and orientation as the previous simulated experiment. Note that the four vehicles converged to the desired trapezoid

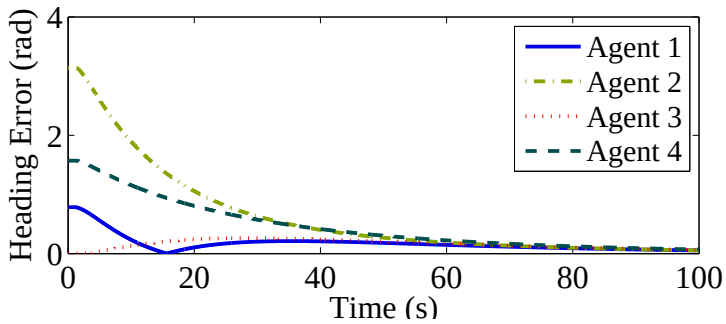

Figure 4.6: Norm of the heading angle error.

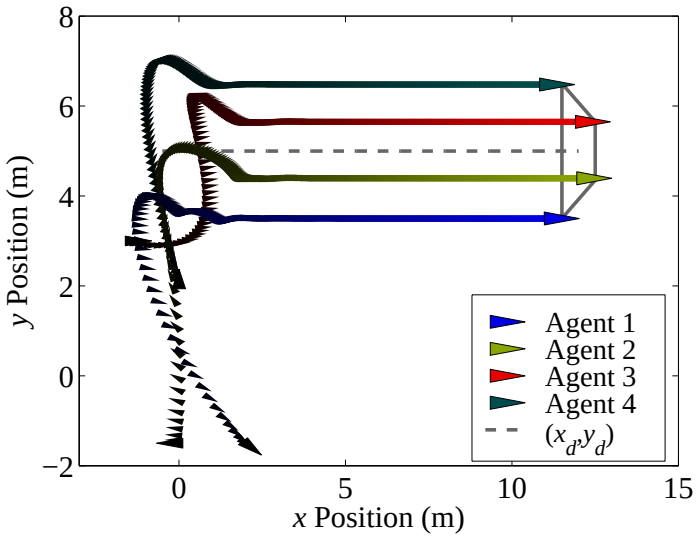

Figure 4.7: Cartesian position (x, y) of the four vehicles for a time-varying formation. The heading of each vehicle is denoted by the triangle pointing direction. Each position mark is distanced by intervals of 0.5 s.

formation and were able to follow in unison the desired trajectory even though it was time-varying. Figures 4.8 and 4.9 confirm the fact the agents satisfactory followed the desired trajectory. The nonzero constant error in Figure 4.9 for all vehicles is due to the fact the desired trajectory does not converge to a static configuration but diverges at a constant rate.

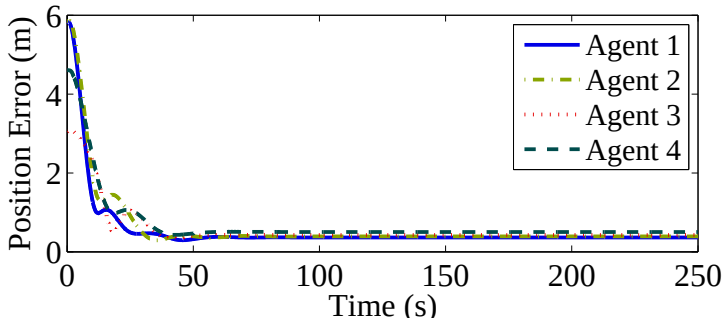

Figure 4.8: Norm of the position error for a time-varying formation.

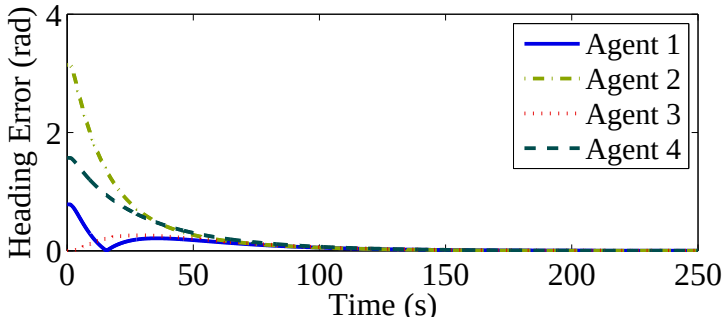

Figure 4.9: Norm of the heading angle error for a time-varying formation.

CHAPTER 5

BILATERAL TELEOPERATION: STABILITY AND TRANSPARENCY

In continuation of the previous chapters, where stability and coordination of nonlinear systems with interconnection delays was addressed, we now center our attention on the special problem of time delay bilateral teleoperation. In principle, a teleoperation system is a dual (or multi) robotic set that enables a human operator to manipulate, sense, and physically interact with a distant environment. In such systems, the desired manipulation or task is performed remotely by a slave robot which tracks the motion of a locally human-controlled master robot. The master and slave robot are coupled through a communication channel that, ideally, should be *transparent* to the operator, meaning that he or she should feel as if being directly active in the remote location [76]. This is generally achieved by transmitting remote slave information (e.g., position, velocity, and force) to the master robot in what is called a bilateral connection. Unfortunately, bilateral configurations can potentially yield a teleoperation system unstable due to delays [137] and data losses [138] experienced in the communication network.

5.1 Time-Delay Bilateral Teleoperation

A bilateral teleoperator is a NCS with a *human-in-the-loop*. Therefore, network-induced delays associated with NCSs are also of concern in a bilateral teleoperator (see Figure 5.1). However, in a teleoperation system, time delays in the master's and slave's local control loop are typically less significant than interconnection delays between the local and remote site (i.e., $T_{j_i} << T_i$, for $i \in \{m, s\}, j \in \{1, 2\}$). Therefore, it is standard to ignore local delays (i.e., assume $T_1 = T_2 = 0$) and consider only the presence of interconnection delays between master and slave. From now on, we will follow this convention when addressing bilateral teleoperators.

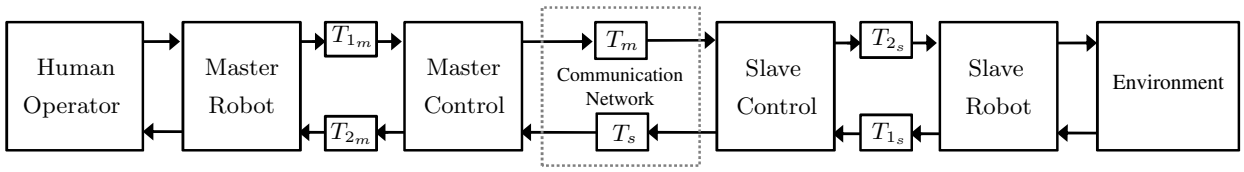

Figure 5.1: Scheme of a bilateral teleoperation system with local delays T_{1_i} and T_{2_i}, and interconnection delays T_m and T_s.

5.2 Stability and Transparency

The destabilizing effects of time delays and delayed force feedback in teleoperation systems were first reported by Ferrell [137,139] in 1965 and 1966. Thereafter, most research efforts were directed toward the design of control schemes that aimed for a stable and reliable performance of time delayed teleoperators. One breakthrough in this topic came in 1988 when passivity-based control and scattering theory, derived from network theory, were combined to guarantee the stability of force feedback teleoperators independently of any sized constant delay [140]. Ever since, the scattering and passivity formulation (reformulated later with the notion of wave variables [46]) has arguably become one of the fundamental control approaches for stabilizing bilateral teleoperators. Other parallel research approaches for stability not based on passivity include H_∞-optimization [141], sliding mode control [142], and compliant control [143] (refer to [25] for a review on bilateral control frameworks).

Aside from stability issues, time delays are also known to affect transparency. According to [76], transparency is achieved when the transmitted impedance to the operator equals the environmental impedance. An alternative interpretation is given in [144], where a system is said to be transparent if the position of the slave equals the master's position and the human force is equal to the net environmental force. Based on either formulation, considerable research efforts have been aimed to conciliate transparency-based objectives while still enforcing time delay independent stability (see [76, 77, 144–148] for examples and further discussion).

5.2.1 Stable Transparency Compensation

Despite the fact that most force-feedback frameworks for bilateral teleoperation are designed to achieve both stability and transparency, their results generally depend on the dynamics of the environment which more than often is unknown or, at least, variable. Precisely, one of the still prevalent issues in bilateral frameworks is the failure to adjust transparency when transitioning

from an unobstructed (free movement) to an obstructed (rigid contact) environment, and vice versa. For instance, in wave-based approaches, transparency highly depends on the wave impedance: a control parameter specified by the designer [149]. For free motion, the ideal wave impedance should be infinitesimal such that the increase of inertia induced by the delay is barely perceived by the operator; whereas for rigid environments, the desired wave impedance should be infinitely large such that a stiff environment is felt by the operator [150]. Compromising the value of the wave impedance to best satisfy both scenarios would lead to a system that feels rather sluggish in free motion with substantial position errors (also referenced as position drifts [151]) when interacting with rigid environments. A similar behavior is also experienced when tuning traditional proportional-derivative (PD) architectures where, in general, control gains are limited by stability constrains and, consequently, position errors arise while in contact motion [147, 151, 152].

Stable time-varying compensation of position errors during contact tasks has been previously addressed in [153] via a wave-based scheme that introduces the notion of a variable rest length. The role of the variable rest length is to modify the desired target position according to the position drift and applied forces such that the error between the master and slave position converges to zero. A similar approach based on the variable rest length is presented in [154], where an energy tank replaces the dissipative element in the wave scattering transformation for impedance matching such that the energy is stored rather than dissipated. The stored energy is then used to adequately change the variable rest length without relying on the operator's energy as in [153]. In both of the above methods, the communication delay must be known in order to perform the position compensation.

In this chapter, we present a novel control strategy for position compensation during contact tasks where the wave impedance independent passivity property in the scattering transformation is exploited. The proposed control framework builds on the wave-based approach reported in [155] and introduces a time-varying wave impedance for transparency compensation when transitioning between unobstructed and obstructed environments. A similar strategy has been previously presented in [156], where the wave impedance alternates between two discrete values according to the current task, given that the mechanical and control systems dissipate enough energy to perform the transition and preserve passivity. In contrast, the control framework proposed herein gradually changes the wave impedance, allowing for passive (i.e., stable) and smooth switches between arbitrary small impedances (suitable for free environments) and sufficiently large impedances (ideal

for rigid contact).

5.3 Modeling the Teleoperator

We address the task of remotely controlling an n-DOF slave robot coupled bilaterally to an n-DOF master robot through a time delayed communication channel. The master and slave teleoperator have nonlinear Euler-Lagrangian dynamics given by

$$\begin{aligned} M_m(\mathbf{q}_m)\ddot{\mathbf{q}}_m + C_m(\mathbf{q}_m, \dot{\mathbf{q}}_m)\dot{\mathbf{q}}_m + \mathbf{g}_m(\mathbf{q}_m) =& \mathbf{f}_m + \bar{\boldsymbol{\tau}}_m \\ M_s(\mathbf{q}_s)\ddot{\mathbf{q}}_s + C_s(\mathbf{q}_s, \dot{\mathbf{q}}_s)\dot{\mathbf{q}}_s + \mathbf{g}_s(\mathbf{q}_s) =& \mathbf{f}_s + \bar{\boldsymbol{\tau}}_s \end{aligned} \tag{5.1}$$

where $\mathbf{q}_i \in \Re^n$ are the generalized coordinates, $M_i \in \Re^{n\times n}$ are the positive definite inertia matrices, $C_i \in \Re^{n\times n}$ are the centrifugal and Coriolis matrices, $\mathbf{g}_i$ are the gravitational forces, $\mathbf{f}_i \in \Re^n$ are the human and environmental forces, and $\bar{\boldsymbol{\tau}}_i \in \Re^n$ are the control inputs for the master ($i = m$) and slave robots ($i = s$). We assume that both systems satisfy Properties 2.2.1 to 2.2.3 and ignore previous restrictions regarding dissipative forces.

5.4 Towards Transparency Compensation

5.4.1 Control Objectives

The control goal is to design the inputs $\bar{\boldsymbol{\tau}}_i$ such that stability and transparency of the close-loop system in (5.1) are achieved. Explicitly, we would like $\bar{\boldsymbol{\tau}}_i$ to enforce position coordination for finite delays, i.e.,

$$\mathbf{q}_m(t) - \mathbf{q}_s(t) \to 0 \tag{5.2}$$

and static force reflection, i.e.,

$$\mathbf{f}_m(t) \to -\mathbf{f}_s(t) \tag{5.3}$$

as $\dot{\mathbf{q}}_i \to 0$, independently of the structure of the remote environment. Furthermore, we would like the operator to perceive low and high impedances when interacting with free and rigid environ-

ments, respectively.

Remark 5.4.1. *In the following analysis we make the assumption that delays on the transmission lines from master to slave, T_m, and from slave to master, T_s, are constant but not necessarily equal. Furthermore, we assume that the slave robot is equipped with force/torque sensors*[1] *and that it is able to communicate contact information to the master robot.*

5.4.2 Control Framework

In order to passivize and hence stabilize the teleoperator, we propose the design of the control inputs as

$$\bar{\boldsymbol{\tau}}_i = -M_i(\mathbf{q}_i)\Lambda\dot{\mathbf{q}}_i - C_i(\mathbf{q}_i,\dot{\mathbf{q}}_i)\Lambda\mathbf{q}_i + \mathbf{g}_i(\mathbf{q}_i) + \boldsymbol{\tau}_i \tag{5.4}$$

where $\Lambda \in \Re^{n\times n}$ is, without loss of generality, a diagonal positive definite constant matrix and $\boldsymbol{\tau}_i = \boldsymbol{\tau}_i(t) \in \Re^n$ are the coordination control inputs to be designed. Then, the dynamic equations of the system in (5.1) reduce to

$$\begin{aligned} M_m(\mathbf{q}_m)\dot{\mathbf{r}}_m + C_m(\mathbf{q}_m,\dot{\mathbf{q}}_m)\mathbf{r}_m &= \mathbf{f}_m + \boldsymbol{\tau}_m \\ M_s(\mathbf{q}_s)\dot{\mathbf{r}}_s + C_s(\mathbf{q}_s,\dot{\mathbf{q}}_s)\mathbf{r}_s &= \mathbf{f}_s + \boldsymbol{\tau}_s \end{aligned} \tag{5.5}$$

where

$$\mathbf{r}_i(t) = \dot{\mathbf{q}}_i(t) + \Lambda\mathbf{q}_i(t). \tag{5.6}$$

The control law in (5.4) is a passivity-based control method [130], which means that the master and slave teleoperators, with reduced dynamics (5.5), are passive with respect to the input $\mathbf{f}_i + \boldsymbol{\tau}_i$ and output $\mathbf{r}_i$. Mathematically,

$$\int_0^t (\mathbf{f}_i + \boldsymbol{\tau}_i)^T \mathbf{r}_i d\theta = \mathbf{r}_i^T(\theta)M_i(\mathbf{q}_i(\theta))\mathbf{r}_i(\theta)\big|_{\theta=0}^{\theta=t} \geq -\mathbf{r}_i^T(0)M_i(\mathbf{q}_i(0))\mathbf{r}_i(0).$$

Remark 5.4.2. *Note that the control law in (5.4) assumes complete knowledge of the dynamics of the master and slave robot. In [130, 155], a passivity-based adaptive law is suggested for the case where the parameters are unknown. Such an approach can be easily extended to our proposed*

[1] This assumption can be replaced with any other contact/proximity sensor.

control framework without altering the passivity and position convergence results presented in this dissertation.

Now, we are left to design the control inputs $\boldsymbol{\tau}_i$ such that the communication channel is passivized independently of the delay and that position and force tracking of the teleoperators are guaranteed. With this in mind, we propose the use of the scattering transformation and wave variables[2] $\mathbf{u}_i$ and $\mathbf{v}_i$. For the master side, the outputs of the scattering transformation are computed as

$$\mathbf{u}_m(t) = (2b_m(t))^{-\frac{1}{2}}(b_m(t)\mathbf{r}_{md}(t) - \boldsymbol{\tau}_m(t)) \tag{5.7}$$

$$\mathbf{r}_{md}(t) = (2b_m^{-1}(t))^{\frac{1}{2}}\mathbf{v}_m(t) - b_m^{-1}(t)\boldsymbol{\tau}_m(t) \tag{5.8}$$

where $b_m(t) \in \Re^{n\times n}$, the wave impedance, is a time-varying, positive definite matrix that will be designed under transparency concerns; and $\mathbf{v}_m(t) = \mathbf{v}_s(t - T_s)$ is the upcoming, delayed wave variable from the slave's scattering transformation. Then, the coordination control input can be given as

$$\boldsymbol{\tau}_m(t) = b_m(t)(\mathbf{r}_{md}(t) - \mathbf{r}_m(t)). \tag{5.9}$$

Likewise, for the slave side, the outputs of the scattering transformation are computed as

$$\mathbf{v}_s(t) = (2b_s(t))^{-\frac{1}{2}}(b_s(t)\mathbf{r}_{sd}(t) - \boldsymbol{\tau}_s(t)) \tag{5.10}$$

$$\mathbf{r}_{sd}(t) = (2b_s^{-1}(t))^{\frac{1}{2}}\mathbf{u}_s(t) - b_s^{-1}(t)\boldsymbol{\tau}_s(t) \tag{5.11}$$

where $b_s(t) = b_m(t - T_m)$ and $\mathbf{u}_s(t) = \mathbf{u}_m(t - T_m)$. Similar to the master case,

$$\boldsymbol{\tau}_s(t) = b_s(t)(\mathbf{r}_{sd}(t) - \mathbf{r}_s(t)). \tag{5.12}$$

We now show that passivity of the communication channel is achieved independently of delays and variance of the wave impedance. Manipulating (5.7) to (5.11), we obtain that

$$\begin{aligned}\boldsymbol{\tau}_m^T\mathbf{r}_{md} + \boldsymbol{\tau}_s^T\mathbf{r}_{sd} &= -2b_m^{-1}b_m\frac{\mathbf{u}_m - \mathbf{v}_m}{2}\frac{\mathbf{u}_m + \mathbf{v}_m}{2} - 2b_s^{-1}b_s\frac{\mathbf{v}_s - \mathbf{u}_s}{2}\frac{\mathbf{v}_s + \mathbf{u}_s}{2}\\ &= -\frac{1}{2}\left(\mathbf{u}_m^2 - \mathbf{v}_m^2 + \mathbf{v}_s^2 - \mathbf{u}_s^2\right)\end{aligned}$$

[2]In contrast to the two previous chapters, where a modified wave scattering transformation was employed, here we opt to use the traditional notation for the wave scattering variables, i.e., the pairs $\mathbf{u}$ and $\mathbf{v}$.

and integrating with respect to time,

$$-\int_0^t (\boldsymbol{\tau}_m^T \mathbf{r}_{md} + \boldsymbol{\tau}_s^T \mathbf{r}_{sd}) d\theta = \frac{1}{2}\int_{t-T_m}^t \mathbf{u}_m^2 d\theta + \frac{1}{2}\int_{t-T_s}^t \mathbf{v}_s^2 d\theta \geq 0 \tag{5.13}$$

where the negative sign in front of the integral is owed to the power inflow. The lower bound in (5.13) implies that the energy is temporarily stored in the transmission lines and, therefore, the communication channel is passive independently of delays. In addition, the reader can easily verify that using the scattering transformation and the coordination control inputs (5.9) and (5.12), (5.8) and (5.11) reduce to

$$\mathbf{r}_{md}(t) = \frac{1}{2}\left(\Gamma(t)\mathbf{r}_s(t-T_s) - \mathbf{r}_m(t)\right) \tag{5.14}$$

$$\mathbf{r}_{sd}(t) = \frac{1}{2}\left(\mathbf{r}_m(t-T_m) - \mathbf{r}_s(t)\right) \tag{5.15}$$

where $\Gamma(t) = b_m(t - T_m - T_s)^{\frac{1}{2}} b_m(t)^{-\frac{1}{2}}$. As we will show in Section 5.4.4, the above proposed control law guarantees position convergence and force reflection of the teleoperators in the sense of (5.2) and (5.3).

Remark 5.4.3. *The control law in (5.4), (5.9), and (5.12), in conjunction with the wave scattering formalism, resembles the control framework proposed in [155]. The difference lies on the use of a wave impedance that is time-varying rather than constant. This property, as will be shown in Section 5.4.4, will allow the proposed control framework to compensate for position errors during contact tasks.*

Up to now, we have designed the control inputs $\bar{\boldsymbol{\tau}}_i$ based on passivity and position coordination. We are yet to tune the control law such that transparency is achieved for both free and restricted environments. This task is left for the next subsection.

5.4.3 Tuning the Wave Impedance

Transparency in wave-based control frameworks, as previously discussed in Section 5.2.1, highly depends on the wave impedance, b_i. Ideally, we would like the wave impedance to alternate from a small value, b_{free}, when the slave is free to move, to a large value, b_{cont}, as soon as the slave robot makes contact with a rigid surface. For sake of simplicity, we will assume that $b_i(t) > 0$ are diagonal matrices.

We propose the update law for the diagonal jjth entry of the wave impedance matrix to be given as

$$\dot{b}_m^{jj}(t) = \begin{cases} \min\{\overline{\beta}^j(t), \hat{\Lambda}^{jj} b_m(t)\}, & \text{if } \left\| f_s^j(t - T_s) \right\| > 0 \\ -\underline{\beta}^j(t), & \text{otherwise} \end{cases}$$

$$b_s^{jj}(t) = b_m^{jj}(t - T_m) \tag{5.16}$$

where f_s^j is the jth component of $\mathbf{f}_s$, $\hat{\Lambda} < \Lambda$ is a $n \times n$ diagonal positive definite matrix with entries $\hat{\Lambda}^{jj}$, and $\overline{\beta}^j$ and $\underline{\beta}^j$ are nonnegative scalar functions that drive b_m^{jj} to b_{cont}^{jj} and b_{free}^{jj}, respectively.

5.4.4 Stability and Transparency Analysis

As aforementioned, the two foremost goals in bilateral teleoperation are stability and transparency. In this section we demonstrate that the proposed control framework achieves both objectives. We first evaluate the standard case where the human operator and remote environment are modeled as passive systems. Then, we prove our original claims as we relax this assumption on the operator.

Theorem 5.4.1. *Consider the teleoperation system in (5.1) with control law (5.4), (5.9), and (5.12). Suppose that the human operator and remote environment are passive with respect to (5.6), i.e., $\exists\ \kappa_i \in \Re$ such that*

$$-\int_0^t \mathbf{f}_i^T \mathbf{r}_i d\theta \geq -\kappa_i^2, \qquad \text{for } i \in \{m, s\}. \tag{5.17}$$

Then, for all arbitrary initial conditions, the closed-loop teleoperation system is stable, all signals are bounded, and the system achieves position coordination and static force reflection in the sense of (5.2) and (5.3).[3]

Proof. Define the slave's coordination error as

$$\mathbf{e}_s(t) = \mathbf{q}_s(t) - \mathbf{q}_m(t - T_m) \tag{5.18}$$

[3]This is a modified version of Theorem 4.1 in [155]. Here we show that $\mathbf{f}_m \to -\mathbf{f}_e$ as $(\ddot{\mathbf{q}}_i, \dot{\mathbf{q}}_i) \to 0$ and prove stability and position convergence for non-constant wave impedances.

and consider the following Lyapunov candidate function

$$V = \frac{1}{2}(\mathbf{r}_m^T M_m \mathbf{r}_m + \mathbf{r}_s^T M_s \mathbf{r}_s) + \frac{1}{4}\mathbf{e}_s^T \Lambda b_s \mathbf{e}_s + \kappa_m^2 + \kappa_s^2 - \int_0^t (\mathbf{f}_m^T \mathbf{r}_m + \mathbf{f}_s^T \mathbf{r}_s) d\theta - \int_0^t (\boldsymbol{\tau}_m^T \mathbf{r}_{md} + \boldsymbol{\tau}_s^T \mathbf{r}_{sd}) d\theta. \tag{5.19}$$

Taking the derivative of V with respect to time and applying the skew symmetric Property 2.2.1, we have

$$\begin{aligned}\dot{V} &= \boldsymbol{\tau}_m^T \mathbf{r}_m + \boldsymbol{\tau}_s^T \mathbf{r}_s + \frac{1}{2}\dot{\mathbf{e}}_s^T \Lambda b_s \mathbf{e}_s + \frac{1}{4}\mathbf{e}_s^T \Lambda \dot{b}_s \mathbf{e}_s - \boldsymbol{\tau}_m^T \mathbf{r}_{md} - \boldsymbol{\tau}_s^T \mathbf{r}_{sd} \\ &\leq \frac{1}{2}\dot{\mathbf{e}}_s^T \Lambda b_s \mathbf{e}_s + \frac{1}{4}\mathbf{e}_s^T \Lambda \dot{b}_s \mathbf{e}_s - (\mathbf{r}_{sd} - \mathbf{r}_s)^T b_s (\mathbf{r}_{sd} - \mathbf{r}_s) - (\mathbf{r}_{md} - \mathbf{r}_m)^T b_m (\mathbf{r}_{md} - \mathbf{r}_m).\end{aligned}$$

Now, using (5.15) and the fact that $\dot{b}_s(t) \leq \hat{\Lambda} b_s(t)\ \forall t \geq 0$ and $\mathbf{r}_s(t) - \mathbf{r}_m(t - T_m) = \dot{\mathbf{e}}_s + \Lambda \mathbf{e}_s$ we obtain

$$\dot{V} \leq -(\mathbf{r}_{md} - \mathbf{r}_m)^T b_m (\mathbf{r}_{md} - \mathbf{r}_m) - \frac{1}{4}\dot{\mathbf{e}}_s^T b_s \dot{\mathbf{e}}_s - \frac{1}{4}\mathbf{e}_s^T \Lambda \tilde{\Lambda} b_s \mathbf{e}_s \tag{5.20}$$

where $\tilde{\Lambda} = \Lambda - \hat{\Lambda} > 0$. Since $\dot{V}$ is negative semi-definite, we conclude that the teleoperation system is closed-loop stable in the sense of Lyapunov. Furthermore, we can also show that (5.19) is bounded and so $\mathbf{r}_i$ are also bounded. Using the Comparison Lemma [129], we can conclude that $\dot{\mathbf{q}}_i, \mathbf{q}_i \in \mathcal{L}_\infty$, and, therefore, the coordination error $\mathbf{q}_m - \mathbf{q}_s$ and its velocity are also bounded. Thus we are left to prove (5.2) and (5.3).

Invoking LaSalle's Invariance Principle [129], we have that $\dot{V} = 0 \Rightarrow (\dot{\mathbf{e}}_s, \mathbf{e}_s) \to 0$. Therefore, $\boldsymbol{\tau}_s \to 0$ and the slave's dynamics reduces to $M_s \dot{\mathbf{r}}_s + C_s \mathbf{r}_s = \mathbf{f}_s$. Consider now the following positive definite function

$$V_s = \mathbf{r}_s^T M_s \mathbf{r}_s - \int_0^t \mathbf{f}_s^T \mathbf{r}_s d\theta. \tag{5.21}$$

Then, we can show by taking its time-derivative that $\dot{V}_s(t) = 0$. Thus, $V_s(t) = V_s(0)\ \forall t \geq 0$ which implies that

$$\begin{aligned}V_s =& \mathbf{r}_s^T M_s \mathbf{r}_s - \int_0^t (\dot{\mathbf{r}}_s^T M_s \mathbf{r}_s + \mathbf{r}_s^T C_s \mathbf{r}_s) d\theta \\ =& \int_0^t (2\mathbf{r}_s^T C_s \mathbf{r}_s + \dot{\mathbf{r}}_s^T M_s \mathbf{r}_s) d\theta - \int_0^t \mathbf{r}_s^T C_s \mathbf{r}_s d\theta = \int_0^t \mathbf{f}_s^T \mathbf{r}_s d\theta = V_s(0).\end{aligned}$$

By boundedness of the inertia matrix [130], we can show that $\mathbf{r}_s^T M_s \mathbf{r}_s = 2V_s(0) \Rightarrow (\dot{\mathbf{q}}_s, \mathbf{q}_s) \rightarrow (0, \bar{\mathbf{q}}_s)$, where $\bar{\mathbf{q}}_s$ is a constant vector. Then, using the fact that $\mathbf{e}_s \rightarrow 0$ we have

$$\mathbf{q}_s(t) - \mathbf{q}_m(t - T_m) = \mathbf{q}_s(t - T_m) - \mathbf{q}_m(t - T_m) + \int_{(t-T_m)}^{t} \dot{\mathbf{q}}_s d\theta \rightarrow 0$$

which for finite T_m, gives $\mathbf{q}_s(t) - \mathbf{q}_m(t) \rightarrow 0$ and position convergence is established.

Now, consider the system under steady-state conditions, i.e., $(\ddot{\mathbf{q}}_i, \dot{\mathbf{q}}_i) = 0$ and $b_s = b_m$. Then, (5.5) simplifies to

$$2\mathbf{f}_m = -b_m \Lambda \left(\mathbf{q}_s - \mathbf{q}_m\right), \quad 2\mathbf{f}_s = -b_s \Lambda \left(\mathbf{q}_m - \mathbf{q}_s\right)$$

and it is easy to see that $\mathbf{f}_m(t) = -\mathbf{f}_s(t)$, which completes the proof. □

We just showed that, when the human operator and remote environment are modeled as passive systems, position and force tracking are enforced. We now relax this passivity assumption on the human operator and suppose that the environment is output strictly passive. This emulates the scenario in which the slave interacts with a rigid environment. We will show that the position error is bounded and that indeed, $\mathbf{q}_m - \mathbf{q}_s \rightarrow 0$ as $\|b_i\| \rightarrow \infty$ even for contact tasks.

Theorem 5.4.2. *Consider the teleoperation system in (5.1) with control law (5.4), (5.9), and (5.12). Suppose that (1) the remote environment is output strictly passive, i.e.,* $\exists\, \kappa_s, \rho_s \in \Re, \rho_s \neq 0$ *such that*

$$-\int_0^t \mathbf{f}_s^T \mathbf{r}_s d\theta \geq -\kappa_s^2 + \rho_s^2 \int_0^t \mathbf{r}_s^T \mathbf{r}_s d\theta \tag{5.22}$$

and (2) the human force is bounded, i.e., $\|\mathbf{f}_m\| < \eta$ *for some* $\eta \in (0, \infty)$*. Then, for all arbitrary initial conditions, the closed-loop teleoperation system is stable, static force reflection is achieved, and the slave's coordination error is uniformly ultimately bounded with ultimate bound inversely proportional to the wave impedance.*

The proof for static force reflection follows similar to Theorem 5.4.1; therefore, it will be omitted. We now proceed to demonstrate closed-loop stability and boundedness of the coordination error.

Proof. Consider the following Lyapunov candidate function

$$\tilde{V} = \frac{1}{2}(\mathbf{r}_m^T M_m \mathbf{r}_m + \mathbf{r}_s^T M_s \mathbf{r}_s) + \frac{1}{4}\mathbf{e}_s^T \Lambda b_s \mathbf{e}_s - \int_0^t \mathbf{f}_s^T \mathbf{r}_s d\theta + \kappa_s^2 - \rho_s^2 \int_0^{t-T_s} \mathbf{r}_s^T \mathbf{r}_s d\theta - \int_0^t (\boldsymbol{\tau}_m^T \mathbf{r}_{md} + \boldsymbol{\tau}_s^T \mathbf{r}_{sd}) d\theta.$$

Taking its derivative with respect to time and using (5.14), (5.15), and the fact that $\dot{b}_s(t) \leq \hat{\Lambda} b_s(t)\ \forall t \geq 0$ and $\mathbf{r}_s(t) - \mathbf{r}_m(t - T_m) = \dot{\mathbf{e}}_s + \Lambda \mathbf{e}_s$, we obtain

$$\dot{\tilde{V}} \leq -\frac{1}{4}\dot{\mathbf{e}}_s^T b_s \dot{\mathbf{e}}_s - \frac{1}{4}\mathbf{e}_s^T \Lambda \tilde{\Lambda} b_s(t) \mathbf{e}_s - \rho_s^2 \left\|\mathbf{r}_s(t - T_s)\right\|^2 - \frac{1}{4}(\mathbf{r}_m - \Gamma \mathbf{r}_s(t - T_s))^T b_m (\mathbf{r}_m - \Gamma \mathbf{r}_s(t - T_s)) + \mathbf{f}_m^T \mathbf{r}_m.$$

Now, let us define $\mathbf{e}_r(t) = \mathbf{r}_m(t) - \Gamma(t)\mathbf{r}_s(t - T_s)$. Notice that $\mathbf{f}_m^T \mathbf{r}_m = \mathbf{f}_m^T \mathbf{e}_r + \mathbf{f}_m^T \Gamma \mathbf{r}_s(t - T)$, where we can upper bound $\mathbf{f}_m^T \Gamma \mathbf{r}_s(t - T)$ by $\frac{1}{4\rho^2}\left\|\Gamma \mathbf{f}_m\right\|^2 + \rho^2 \left\|\mathbf{r}_s(t - T_s)\right\|^2$. Then,

$$\dot{\tilde{V}} \leq \mathbf{f}_m^T \mathbf{e}_r - \frac{1}{4}\mathbf{e}_r^T b_m \mathbf{e}_r + \frac{1}{4\rho^2}\left\|\Gamma \mathbf{f}_m\right\|^2 - \frac{1}{4}\dot{\mathbf{e}}_s^T b_s \dot{\mathbf{e}}_s - \frac{1}{4}\mathbf{e}_s^T \Lambda \tilde{\Lambda} b_s \mathbf{e}_s.$$

If we now denote $\underline{\sigma}(A)$ as the minimum eigenvalue of the matrix A, let $\epsilon \in (0, 1)$ be a constant, and recall that $\|\mathbf{f}_m\| \leq \eta$, then we can show that

$$\dot{\tilde{V}} \leq \eta \left\|\mathbf{e}_r\right\| - \frac{\epsilon}{4}\underline{\sigma}(b_m)\left\|\mathbf{e}_r\right\|^2 - \frac{1}{4}(1 - \epsilon)\underline{\sigma}(b_m)\left\|\mathbf{e}_r\right\|^2 - \frac{1}{4}\underline{\sigma}(b_s)\left\|\dot{\mathbf{e}}_s\right\|^2 - \frac{1}{4}(1 - \epsilon^2)\underline{\sigma}(b_s)\underline{\sigma}(\Lambda\tilde{\Lambda})\left\|\mathbf{e}_s\right\|^2 - \frac{\epsilon^2}{4}\underline{\sigma}(b_s)\underline{\sigma}(\Lambda\tilde{\Lambda})\left\|\mathbf{e}_s\right\|^2 + \frac{\eta^2}{4\rho^2}\left\|\Gamma\right\|^2$$

and consequently,

$$\dot{\tilde{V}} \leq -\frac{1}{4}(1 - \epsilon)\underline{\sigma}(b_m)\left\|\mathbf{e}_r\right\|^2 - \frac{1}{4}\underline{\sigma}(b_s)\left\|\dot{\mathbf{e}}_s\right\|^2 - \frac{1}{4}(1 - \epsilon^2)\underline{\sigma}(b_s)\underline{\sigma}(\Lambda\tilde{\Lambda})\left\|\mathbf{e}_s\right\|^2 < 0$$

for $\|\mathbf{e}_s\| > \frac{\eta}{\epsilon}\delta(b_m)$, where

$$\delta(b_m) = \left(\frac{4}{\underline{\sigma}(b_m)^2} + \frac{\left\|\Gamma\right\|^2}{\rho_s^2 \underline{\sigma}(b_m(t - T_m))\underline{\sigma}(\Lambda\tilde{\Lambda})}\right)^{\frac{1}{2}}.$$

Since $\dot{\tilde{V}} < 0$ for sufficiently large $\|\mathbf{e}_s\|$, we conclude that the system is closed-loop stable and the

coordination error is uniformly ultimately bounded with ultimate bound given by $\frac{\eta}{\epsilon}\delta(b_m)$. □

In general, the above theorem states that the slave's coordination error converges to a ball of radius $\frac{\eta}{\epsilon}\delta(b_m)$. Therefore, $||\mathbf{e}_s|| \to 0$ as either $\underline{\sigma}(b_m(t)) \to \infty$ or $\eta \to 0$. We can even formulate a more precise bound under steady state conditions. For instance, suppose that $\dot{\mathbf{q}}_i \to 0$, $\mathbf{q}_i(t - T_i) \to \mathbf{q}_i(t)$, and $\Gamma(t) \to 1$. Then, the master dynamics (5.5) simplifies to $2\mathbf{f}_m = -b_m\Lambda(\mathbf{q}_s - \mathbf{q}_m)$, which implies that

$$\|\mathbf{q}_m - \mathbf{q}_s\| = 2\left\|(b_m\Lambda)^{-1}\mathbf{f}_m\right\| \leq 2\eta\left\|b_m\Lambda\right\|^{-1}.$$

Thus, it is easy to note that by increasing b_m, the error effectively goes to zero.

5.5 Simulation and Experimental Results

5.5.1 Example: Simulations

As a mean of validation, we simulated the response of two 1-DOF teleoperators with the proposed controller. Both master and slave robots have identical linear dynamics with $M_i = 1$ kg, $C_i = 0$ kg/s, and $g_i = 0$ N and are coupled through an asymmetric time-delayed communication channel with $T_m = 0.6$ s and $T_s = 0.4$ s. The environment is modeled as a stiff wall located at $q_s = 4$ m with a reaction force given by

$$f_s = \begin{cases} -10\dot{q}_s - 500(q_s - 4) \text{ N}, & \text{if } q_s \geq 4 \text{ m} \\ 0 \text{ N}, & \text{otherwise} \end{cases}$$

while the human operator is modeled as a constant force source for the first 30 s and then as a PD-type controller, i.e.,

$$f_m = \begin{cases} 12 \text{ N}, & \text{if } 0 \leq t \leq 30 \text{ s} \\ -20\dot{q}_m - 25q_m \text{ N}, & \text{if } t > 30 \text{ s}. \end{cases}$$

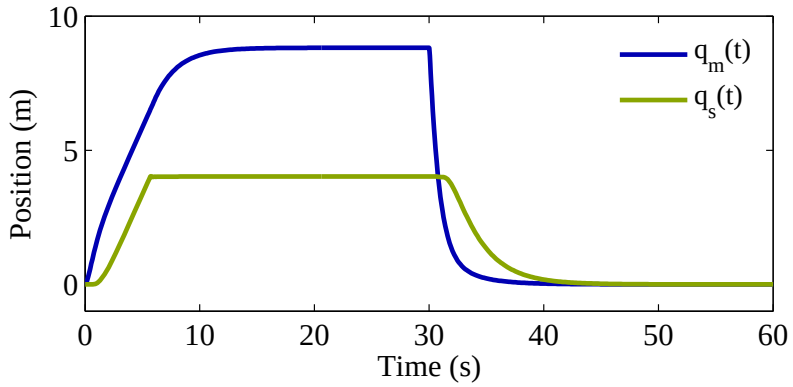

Figure 5.2: Position of master and slave robot with constant $b_m(t) = b_{free}$.

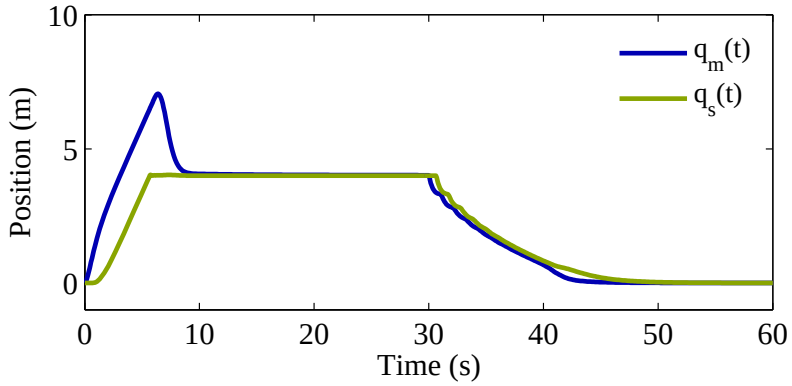

Figure 5.3: Position of master and slave robot with time-varying $b_m(t)$.

The control parameters and update law for the wave impedance are $\Lambda = 5\ \mathrm{s}^{-1}$ and

$$\overline{\beta}(t) = \begin{cases} 2, & \text{if } b_m(t) < b_{cont} \\ 0, & \text{if } b_m(t) = b_{cont} \end{cases}, \qquad \underline{\beta}(t) = \begin{cases} 2\left(5 - 4\frac{b_m(t) - b_{free}}{b_{cont}}\right), & \text{if } b_m(t) > b_{free} \\ 0, & \text{if } b_m(t) = b_{free} \end{cases}$$

where $b_{free} = 1\ \mathrm{N \cdot s/m}$ and $b_{cont} = 50\ \mathrm{N \cdot s/m}$.

We first simulated the system with a constant wave impedance tuned for free motion, i.e., $b_m(t) = b_{free}\ \forall t \geq 0$. The response is illustrated in Figure 5.2. Notice that the position error remains bounded and that position tracking is achieved once the slave retrieves from the wall. However, when the slave robot is in contact with the environment, a constant position error (i.e., position drift) of 4.800 m arises, which may mislead the remote perception of the operator.

The same conditions were then simulated employing the proposed control framework and the results are plotted in Figure 5.3. Notice that the position error during the contact task is drastically reduced to nearly 0.33% (0.016 m), which represents a subtantial improvement on position tracking

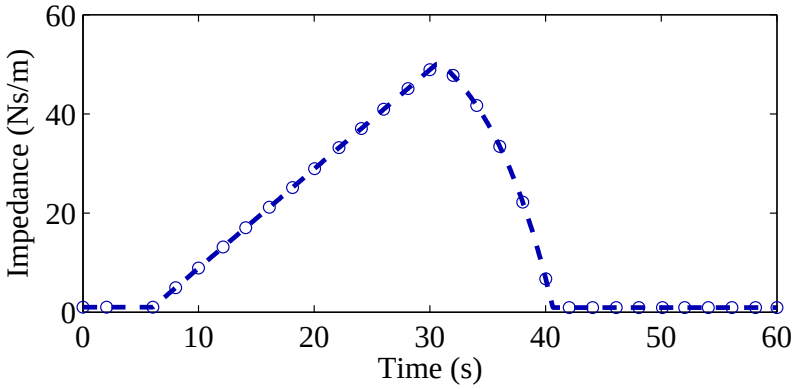

Figure 5.4: Evolution of the Wave Impedance $b_m(t)$.

from the previous case. Once the slave ceases contact with the wall, both master and slave positions converge to zero.

Note also that the settling time is slightly larger for the proposed controller. This is mainly caused by the transition from b_{cont} to b_{free} (illustrated in Figure 5.4) as governed by $\underline{\beta}(t)$. In general, a faster transition will allow for a shorter settling time as $\Gamma(t) \to 1$ in a small time. However, to do so may produce higher transient oscillations due to ephemeral large values of $\Gamma(t)$ in the control law. In practice, as will be shown through experiments, these transitions seem to have no drastic effect in the coordination error or settling time when compared to the constant wave impedance's case.

5.5.2 Example: Experiments

Besides simulations, we conducted experiments on a pair of 2-DOF identical planar-revolute-joint robots coupled through a simulated communication network with constant delays $T_m = 0.4$ s and $T_s = 0.3$ s. Both master and slave robots, which are illustrated in Figure 5.5, are equipped with a pair of optical encoders that measure the link's angular position and velocity (via digital estimation), and a force-torque sensor, located at the end-effector, that measures forces sensed/exerted by the operator/environment. The controllers and the communication network are implemented using Wincon 3.3 (a Windows application capable of running Simulink models in real time) with a sampling time of 0.004 s. The nonlinear dynamics of the teleoperators (5.1), with the gravitational

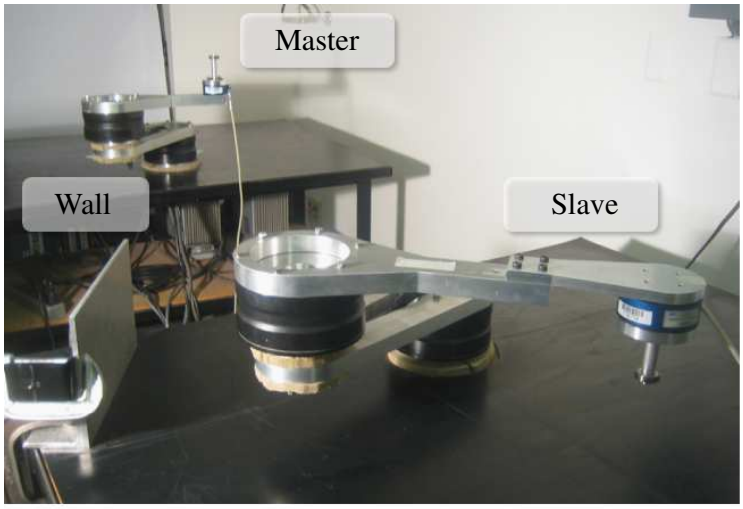

Figure 5.5: Experimental testbed.

torques neglected due to the system's planar configuration, is given by

$$M_i(\mathbf{q}_i) = \begin{bmatrix} \alpha_i & \beta_i \\ \beta_i & \gamma \end{bmatrix}, \qquad C_i(\mathbf{q}_i, \dot{\mathbf{q}}_i) = \begin{bmatrix} \delta_i \dot{q}_i^2 & \delta_i(\dot{q}_i^1 + \dot{q}_i^2) \\ -\delta_i \dot{q}_i^1 & 0 \end{bmatrix} \tag{5.23}$$

where $\dot{q}_i^1 \in \Re$ and $\dot{q}_i^2 \in \Re$ denote the angular velocities for the first and second links, respectively, and where $\alpha_i = (0.834 + 0.150\cos(q_i^2))$ kg $\cdot$ m^2, $\beta_i = (0.111 + 0.075\cos(q_i^2))$ kg $\cdot$ m^2, $\gamma = 0.111$ kg $\cdot$ m^2, and $\delta_i = -0.075\sin(q_i^2)$ kg $\cdot$ m^2. For more details on the experimental setup, consult [157].

The desired trajectory (or task) performed by the operator was the following: first, to displace the master teleoperator from the initial position $\mathbf{q}_0 = [0, -\pi]^T$ rad to $\mathbf{q}_c = [-0.4\pi, 0]^T$ rad; then, to hold the master's position around $\mathbf{q}_c$ for nearly 20 s; and finally, to return to the initial configuration $\mathbf{q}_0$. At the slave's environment, we placed a rigid aluminum wall at $\mathbf{q}_w = [-0.70, -1.52]^T$ rad in order to obstruct and lock the motion of the slave robot.

We first conducted the experiment with a constant wave impedance tuned for free motion, $(b_{free}^{11}, b_{free}^{22}) = (0.8, 0.6)$ N $\cdot$ s $\cdot$ m. The response of the system, with control parameters $\Lambda^{11} = 10$ s^{-1} and $\Lambda^{22} = 8$ s^{-1}, is reported in Figure 5.6. Despite the fact that the position error nearly converges to zero during free motion, a large position error arises for both links when the slave robot is in contact with the wall.

We then performed the same experiment for a time-varying wave impedance with $(b_{free}^{11}, b_{free}^{22}) =$

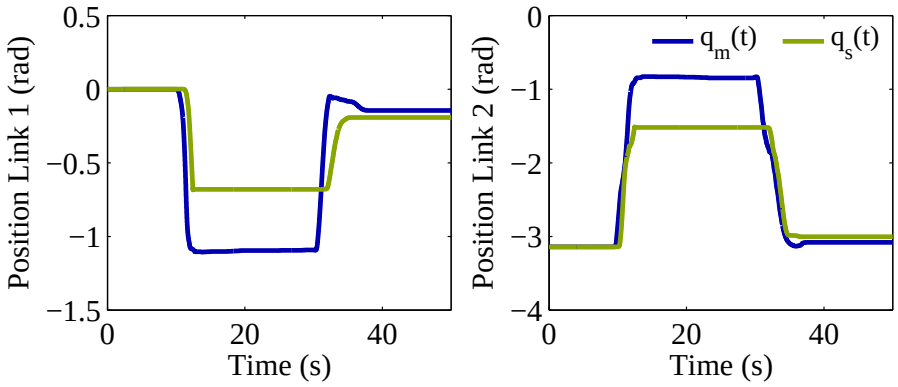

Figure 5.6: Position of master and slave robot with constant $b_m(t) = b_{free}$.

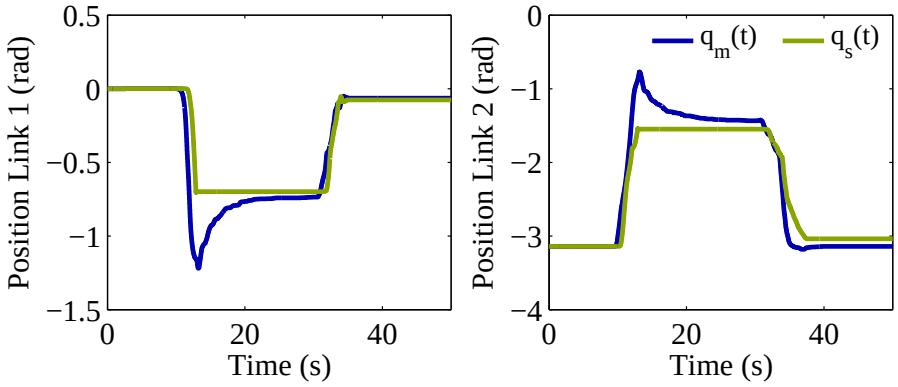

Figure 5.7: Position of master and slave robot with time-varying $b_m(t)$.

$(0.8, 0.6)$ N $\cdot$ s $\cdot$ m, $(b^{11}_{cont}, b^{22}_{cont}) = (12, 9)$ N $\cdot$ s $\cdot$ m, and update law given by

$$\overline{\beta}^j(t) = \|\mathbf{f}_e(t - T_s)\| \frac{b^{jj}_{cont} - b^{jj}_m(t)}{10}, \qquad \hat{\Lambda}^{jj} = \frac{\Lambda^{jj}}{1.01}$$
$$\underline{\beta}^j(t) = 1.65 \left(b^{jj}_m(t) - b^{jj}_{free}(t) \right)$$

where $\mathbf{f}_e(t) \in \Re^2$ is the environmental reaction force sensed at the tip of the slave's end-effector and is related to the $\mathbf{f}_s(t)$ through the Jacobian matrix $J_s(t)$ as $\mathbf{f}_s(t) = J_s^T(t)\mathbf{f}_e(t)$ [130]. The system response is shown in Figure 5.7. The position error between master and slave is considerably attenuated during contact with the wall and approaches zero when the slave is free to move.

Figure 5.8 contrasts the $\mathcal{L}_2$ norm of the coordination error (i.e., $||\mathbf{q}_m(t) - \mathbf{q}_s(t)||$) for the cases of a constant and a time-varying wave impedance. Notice that the steady-state error during contact is decreased from 0.79 rad to 0.12 rad when employing the time-varying wave impedance approach. When the slave retrieves from the wall, the behavior becomes similar in both cases with the position

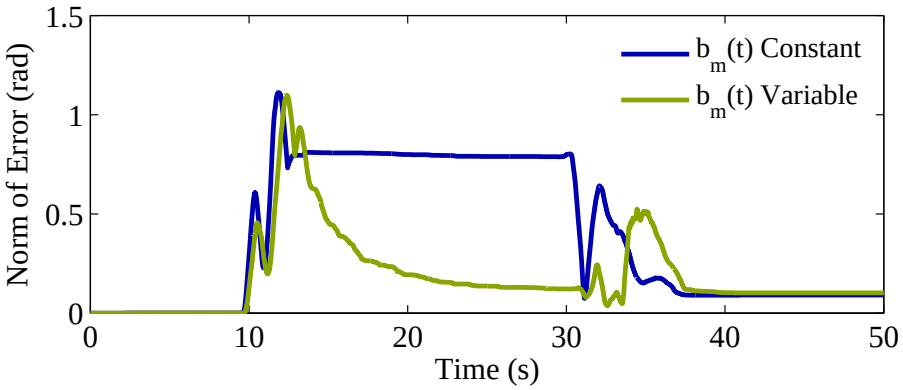

Figure 5.8: $\mathcal{L}_2$ norm of the position error.

error approaching zero. The fact that the coordination error does not converge exactly to zero in either case, while in free motion, can be attributed to considerable bearing friction suffered by the teleoperators as reported in [147, 158].

Similarly, Figure 5.9 compares the force applied at the master's and slave's end-effectors, i.e., $||\mathbf{f}_h||$ and $||\mathbf{f}_e||$, for both controllers. Observe that in the case of a time-varying wave impedance, the human operator applied a larger effort trying to retain the master position at $\mathbf{q}_c$. Despite the operator's larger effort, the coordination error was substantially attenuated. Notice also that, as the system achieves a steady-state, $||\mathbf{f}_h(t)||$ approaches[4] $||\mathbf{f}_e(t)||$.

Finally, Figure 5.9 also evidences a temporary difference on the force reflection by the time-varying wave impedance approach that lasted for several seconds while the slave was in contact with the wall. This contrast between the high-magnitude force perceived by the operator, which can also be interpreted as an indicator of the characteristic high-valued stiffness/impedance of the environment being remotely contacted, and the moderate sensed environmental force on the slave robot can be better explained by mathematically examining the net forces acting on the system. First, in the case of the slave robot, we have that its position is locked around $\mathbf{q}_w$. Therefore, $\dot{\mathbf{q}}_s = 0$. Using then (5.5) and (5.23), we can easily show that $J_s^T \mathbf{f}_e = \mathbf{f}_s = -\boldsymbol{\tau}_s$. On the other hand, in the case of the master teleoperator, $\dot{\mathbf{q}}_m \neq \mathbf{0}$ and, consequently,

$$J_m^T \mathbf{f}_h = \mathbf{f}_m = M_m(\mathbf{q}_m)\dot{\mathbf{r}}_m + C_i(\mathbf{q}_m, \dot{\mathbf{q}}_m)\mathbf{r}_m - \boldsymbol{\tau}_m. \tag{5.24}$$

[4]It is worth mentioning that, in general, $||\mathbf{f}_h||$ should not necessarily converge to $||\mathbf{f}_e||$, since the proposed control framework only guarantees force reflection with respect to $\mathbf{f}_m$ and $\mathbf{f}_s$ (joint space), or equivalently, $||J_m^T \mathbf{f}_h(t)|| \rightarrow ||J_s^T \mathbf{f}_e(t)||$. However, due to the fact that both master and slave have identical dynamics and that the coordination error becomes sufficiently small, the Jacobian matrix of both robots become nearly equal, i.e., $J_m \approx J_s$. Therefore, $||\mathbf{f}_h(t)|| \approx ||\mathbf{f}_e(t)||$.

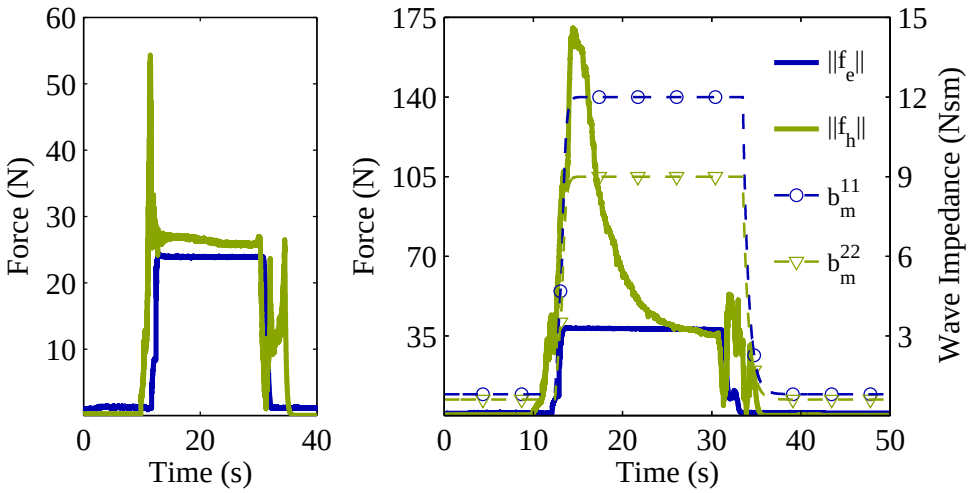

Figure 5.9: Force tracking and wave impedance. To the left, the human and environmental forces are plotted for the case of a constant wave impedance. To the right, the case of a time-varying wave impedance is illustrated. The green lines correspond to the human operator's force, whereas the blue lines plot the magnitude of the environmental force.

Thus, even though the wave impedance stabilizes at a constant value b_{cont} fast enough (as reported in Figure 5.9) and the control $\boldsymbol{\tau}_m \approx \boldsymbol{\tau}_s$; the force perceived by the operator $\mathbf{f}_m$ is still affected by the first two terms in (5.24); which in turn, exclusively depend on the velocities and accelerations of the master teleoperator. This means that the strong forces sensed at the operator's site are mostly owed to the slow attenuation of the position error. In fact, it is not until the system achieves an equilibrium (i.e., $(\ddot{\mathbf{q}}_i, \dot{\mathbf{q}}_i) \rightarrow (\mathbf{0}, \mathbf{0})$) that the first two terms in (5.24) vanish and force reflection (i.e., static) is ultimately achieved.

CHAPTER 6

BILATERAL TELEOPERATION OF MULTIPLE AGENTS

We formally introduced in the preceding chapter the concept of bilateral teleoperation and discussed the effects of delays on stability and transparency. We then presented a control solution aimed toward stability, accurate position convergence, and static force reflection of an SMSS teleoperator. In this chapter, we now present a bilateral control framework for an SMMS teleoperator. The control framework guarantees coordinated motion between master and multiple slave agents with nonlinear dynamics under constant communication delays, as well as a safe interaction between slave agents and surrounding environments. We extend the passivity-based PD control in [147], originally proposed for SMSS bilateral teleoperation, to enforce motion coordination of multiple slave vehicles and complement it with avoidance functions [102] to guarantee collision-free trajectories. Experimental results with two coaxial helicopters and a haptic force-feedback device validate the proposed control scheme.

6.1 Problem Statement and Objectives

This chapter is devoted to the task of remotely controlling a formation of N n-DOF slave agents coupled bilaterally through N constant time delayed communication channels to a single n-DOF master robot. The master and slave agents have nonlinear Lagrangian dynamics given by

$$\begin{aligned} M_m(\mathbf{q}_m)\ddot{\mathbf{q}}_m + C_m(\mathbf{q}_m, \dot{\mathbf{q}}_m)\dot{\mathbf{q}}_m &= \mathbf{f}_m + \boldsymbol{\tau}_m \\ M_1(\mathbf{q}_1)\ddot{\mathbf{q}}_1 + C_1(\mathbf{q}_1, \dot{\mathbf{q}}_1)\dot{\mathbf{q}}_1 &= \mathbf{f}_1 + \boldsymbol{\tau}_1 + \mathbf{u}_1 \\ \vdots \qquad\qquad & \qquad\qquad \vdots \\ M_N(\mathbf{q}_N)\ddot{\mathbf{q}}_N + C_N(\mathbf{q}_N, \dot{\mathbf{q}}_N)\dot{\mathbf{q}}_N &= \mathbf{f}_N + \boldsymbol{\tau}_N + \mathbf{u}_N \end{aligned} \tag{6.1}$$

where $\mathbf{q}_j \in \Re^n$ are the generalized coordinates, $M_j \in \Re^{n\times n}$ are the positive-definite inertia matrices, $C_j \in \Re^{n\times n}$ are the centrifugal and Coriolis matrices, $\mathbf{f}_j \in \Re^n$ are the human and environmental forces, $\boldsymbol{\tau}_j \in \Re^n$ are the coordination-based control inputs, and $\mathbf{u}_j \in \Re^n$ are the collision-free control inputs for master (i.e., $j = m$) and slave agents (i.e., $j \in \{1, \cdots, N\}$). The above nonlinear dynamic representation satisfies Properties 2.2.1 to 2.2.3 from Section 2.2 and assumes that gravitational forces are compensated by active control.

For the multi-agent teleoperation system (6.1), we identify three main control objectives. First, the system must be safe and stable, meaning that no damage should be inflicted to the operator, vehicles, and environment. Second, a coordinated motion between master and slave agents should be achieved: the slave vehicles must maintain a desired relative distance and orientation $\boldsymbol{\gamma}_i \in \Re^n$ from the formation's geometric center ($\frac{1}{N}\sum_{i=1}^{N} \mathbf{q}_i$) at all times while moving as a group along the trajectory commanded by the master robot. Without loss of generality, we consider formations with continuous constant (piecewise constant in the case of dynamic formations) functions $\boldsymbol{\gamma}_i(t)$ satisfying (4.3) given in page 38. Finally, a transparent interaction between operator and environment should be enforced, meaning that the net contribution of environmental forces should be reflected to the operator under steady-state conditions, i.e., $\mathbf{f}_m = -\frac{1}{N}\sum_{i=1}^{N} \mathbf{f}_i$.

In the following analysis, we assume that each slave agent can locate itself and nearby obstacles inside a detection region. In addition, we suppose that each slave vehicle can communicate its position and velocity to the master robot, and vice versa, through constant delayed communication channels.

6.2 Coordination Control

In general, we would like the system in (6.1) to be closed-loop stable while enforcing formation control, master-to-slaves position convergence, and static force reflection. By formation control we explicitly mean that the slave vehicles should maintain a relative position and orientation $\boldsymbol{\gamma}_i$ with respect to the formation's geometric center at all times, i.e., $\mathbf{q}_i \to \frac{1}{N}\sum_{j=1}^{N} \mathbf{q}_j + \boldsymbol{\gamma}_i \ \forall i$. Similarly, by master-to-slaves position tracking, we mean that the geometric center of the formation should converge to the position commanded by the master robot, i.e., $\frac{1}{N}\sum_{i=1}^{N} \mathbf{q}_i \to \mathbf{q}_m$. According to this formulation, we propose the use of the following PD-based control law for the master and slave

agents given as

$$\boldsymbol{\tau}_m(t) = \frac{1}{N}\sum_{i=1}^{N}\boldsymbol{\tau}_{m_i}(t)$$

$$\boldsymbol{\tau}_{m_i}(t) = -K_p(\mathbf{q}_m(t) - \mathbf{q}_i(t - T_{im})) - K_v(\dot{\mathbf{q}}_m(t) - \dot{\mathbf{q}}_i(t - T_{im})) - K_{di}\dot{\mathbf{q}}_m(t) \tag{6.2}$$

$$\boldsymbol{\tau}_i(t) = -K_p(\mathbf{q}_i(t) - \mathbf{q}_m(t - T_{mi}) - \boldsymbol{\gamma}_i(t - T_{mi})) - K_v(\dot{\mathbf{q}}_i(t) - \dot{\mathbf{q}}_m(t - T_{mi})) - K_{di}\dot{\mathbf{q}}_i(t) \tag{6.3}$$

where T_{mi}, T_{im} are the positive constant time delays on the communication channel from the master to the ith slave agent and vice versa, respectively, $K_p, K_v \in \Re^{n\times n}$ are positive definite matrices to be designed, and $K_{di} \geq \frac{(T_{mi}+T_{im})}{2}K_p \in \Re^{n\times n}$ are dissipative gain matrices.

We claim that the control law in (6.2) and (6.3) achieves stability, motion coordination, and force reflection for the system in (6.1). In order to prove our claim, we will first introduce the following result from [147].

Theorem 6.2.1. *Stability of SMSS Teleoperators ($N = 1$): Consider the teleoperation system in (6.1) with control law (6.2) and (6.3) for $N = 1$, $\mathbf{u}_1 \equiv \mathbf{0}$, and $\boldsymbol{\gamma}_1 \equiv \mathbf{0}$.*

i. Robust Passivity: *The closed-loop teleoperation system in (6.1) satisfies the* energetic passivity condition *[159],*

$$\int_0^t [\mathbf{f}_m^T(\theta)\dot{\mathbf{q}}_m(\theta) + \mathbf{f}_1^T(\theta)\dot{\mathbf{q}}_1(\theta)]d\theta \geq -d^2 \tag{6.4}$$

and the controller passivity condition *[159],*

$$\int_0^t [\boldsymbol{\tau}_m^T(\theta)\dot{\mathbf{q}}_m(\theta) + \boldsymbol{\tau}_1^T(\theta)\dot{\mathbf{q}}_1(\theta)]d\theta \leq c^2 \tag{6.5}$$

for some $d, c \in \Re$ and $t \geq 0$ regardless of parametric uncertainties.

ii. Coupled Stability: *If there exist finite constants $d_m, d_1 \in \Re$ such that $\forall t \geq 0$*

$$-\int_0^t \mathbf{f}_i^T(\theta)\dot{\mathbf{q}}_i(\theta)d\theta \geq -d_i^2, \qquad \text{for } i \in \{m, 1\} \tag{6.6}$$

then, $\dot{\mathbf{q}}_m, \dot{\mathbf{q}}_1 \in \mathcal{L}_\infty$ (i.e., if the energy generated by the human operator and the remote environment are bounded, then the velocities of the configurations are also bounded).

iii. Position Coordination: *Define the coordination error as $\mathbf{q}_E = \mathbf{q}_m - \mathbf{q}_1$. Suppose that $(M_i^{jk}(\mathbf{q}_i)$,*

$\partial M_i^{jk}(\mathbf{q}_i)/\partial q_i^l, \partial^2 M_i^{jk}(\mathbf{q}_i)/\partial q_i^l \partial q_i^m) \in \mathcal{L}_\infty$, *where* M^{jk} *and* q_i^l *are the* jk^{th} *and* l^{th} *components of the inertia matrices and configurations, respectively. Then, if* $(\mathbf{f}_m(t), \mathbf{f}_1(t)) = 0 \; \forall t \geq 0$, *the nonnegative quadratic functions*

$$\begin{aligned} E_p =& \frac{1}{2}\mathbf{q}_E^T K_p \mathbf{q}_E \in \mathcal{L}_\infty \\ E_v =& \frac{1}{2}\dot{\mathbf{q}}_m^T M_m(\mathbf{q}_m)\dot{\mathbf{q}}_m + \frac{1}{2}\dot{\mathbf{q}}_1^T M_1(\mathbf{q}_1)\dot{\mathbf{q}}_1 \to 0 \end{aligned}$$

and hence, $(\dot{\mathbf{q}}_m, \ddot{\mathbf{q}}_m, \dot{\mathbf{q}}_1, \ddot{\mathbf{q}}_1, \mathbf{q}_E, \dot{\mathbf{q}}_E) \to 0$.

iv. Static Force Reflection: *Suppose* $(\dot{\mathbf{q}}_m, \ddot{\mathbf{q}}_m, \dot{\mathbf{q}}_1, \ddot{\mathbf{q}}_1) \to 0$. *Then,* $\mathbf{f}_m \to -\mathbf{f}_1 \to -K_p(\mathbf{q}_m - \mathbf{q}_1)$.

Proof. Consult [147]. □

Remark 6.2.1. *The passivity conditions in (6.4) and (6.5) simply imply that the extractable energy from the human operator and environment and the generated energy by the controllers are bounded.*

Remark 6.2.2. *The negative sign in (6.6) is owed to the power inflows to the human and remote environment, i.e., the product of the reaction force* $-\mathbf{f}_j$ *times the interaction velocity* $\dot{\mathbf{q}}_j$.

In general, Theorem 6.2.1 states that for the case of SMSS teleoperation, the control law in (6.2) and (6.3) stabilizes the system under constant time delays, drives the coordination error ($\mathbf{q}_E$) to zero, and achieves static force reflection. In order to proceed to prove closed-loop stability and position coordination for a multi-agent system, i.e., $N \geq 2$, let us first redefine the representation of (6.1) as

$$\begin{aligned} M_m(\mathbf{q}_m)\ddot{\mathbf{q}}_m + C_m(\mathbf{q}_m, \dot{\mathbf{q}}_m)\dot{\mathbf{q}}_m &= \mathbf{f}_m + \boldsymbol{\tau}_m \\ M_i(\bar{\mathbf{q}}_i)\ddot{\bar{\mathbf{q}}}_i + C_i(\bar{\mathbf{q}}_i, \dot{\bar{\mathbf{q}}}_i)\dot{\bar{\mathbf{q}}}_i &= \mathbf{f}_i + \bar{\boldsymbol{\tau}}_i + \mathbf{u}_i, \qquad \text{for } i \in \{1, \cdots, N\} \end{aligned} \tag{6.7}$$

where $\bar{\mathbf{q}}_i(t) = \mathbf{q}_i(t) - \boldsymbol{\gamma}_i(t - T_{mi})$ and

$$\bar{\boldsymbol{\tau}}_i(t) = -K_p(\bar{\mathbf{q}}_i(t) - \mathbf{q}_m(t - T_{mi})) - K_v(\dot{\bar{\mathbf{q}}}_i(t) - \dot{\mathbf{q}}_m(t - T_{mi})) - K_{di}\dot{\bar{\mathbf{q}}}_i(t). \tag{6.8}$$

Theorem 6.2.2. *Stability of SMMS Teleoperators (*$N \geq 2$*): Consider the teleoperation system in (6.7) with control law (6.2) and (6.8) for* $N \geq 2$, $(\mathbf{u}_1, \cdots, \mathbf{u}_N) \equiv 0$, *and static formation.*

i. Robust Passivity: *The closed-loop teleoperation system in (6.7) is passive, i.e., satisfies the energetic passivity condition*

$$\sum_{i=1}^{N} \int_0^t [\mathbf{f}_m^T(\theta)\dot{\mathbf{q}}_m(\theta) + \mathbf{f}_i^T(\theta)\dot{\tilde{\mathbf{q}}}_i(\theta)]d\theta \geq -\bar{d}^2 \tag{6.9}$$

and the controller passivity condition

$$\sum_{i=1}^{N} \int_0^t [\boldsymbol{\tau}_{m_i}^T(\theta)\dot{\mathbf{q}}_m(\theta) + \bar{\boldsymbol{\tau}}_i^T(\theta)\dot{\tilde{\mathbf{q}}}_i(\theta)]d\theta \leq \bar{c}^2 \tag{6.10}$$

for some $\bar{d}, \bar{c} \in \Re$*, regardless of parametric uncertainties.*

ii. Coupled Stability: *If there exist finite constants* $d_i \in \Re$ *for* $i \in \{m, 1, \cdots, N\}$ *such that* $\forall t \geq 0$

$$-\int_0^t \mathbf{f}_i^T(\theta)\dot{\mathbf{q}}_i(\theta)d\theta \geq -d_i^2 \tag{6.11}$$

then, $\dot{\mathbf{q}}_m, \dot{\tilde{\mathbf{q}}}_1, \dot{\tilde{\mathbf{q}}}_2, \cdots, \dot{\tilde{\mathbf{q}}}_N \in \mathcal{L}_\infty$.

iii. Position Coordination: *Define the coordination errors as* $\bar{\mathbf{q}}_{E_i} = \mathbf{q}_m - \bar{\mathbf{q}}_i$ *for* $i \in \{1, \cdots, N\}$. *Suppose that* $(M_i^{jk}(\mathbf{q}_i),\ \partial M_i^{jk}(\mathbf{q}_i)/\partial q_i^l, \partial^2 M_i^{jk}(\mathbf{q}_i)/\partial q_i^l \partial q_i^m) \in \mathcal{L}_\infty$*, where* M_i^{jk} *and* q_i^l *are the* jk^{th} *and* l^{th} *components of the inertia matrices and configurations, respectively. Then, if* $(\mathbf{f}_m(t), \mathbf{f}_1(t), \cdots, \mathbf{f}_N(t)) \equiv 0\ \forall t \geq 0$*, the nonnegative quadratic functions*

$$\bar{E}_p = \frac{1}{2}\sum_{i=1}^{N} \bar{\mathbf{q}}_{E_i}^T K_p \bar{\mathbf{q}}_{E_i} \in \mathcal{L}_\infty \tag{6.12}$$

$$\bar{E}_v = \frac{1}{2}\sum_{i=1}^{N} [\dot{\mathbf{q}}_m^T M_m(\mathbf{q}_m)\dot{\mathbf{q}}_m + \dot{\tilde{\mathbf{q}}}_i^T M_i(\bar{\mathbf{q}}_i)\dot{\tilde{\mathbf{q}}}_i] \to 0 \tag{6.13}$$

and, hence, $(\dot{\mathbf{q}}_m, \ddot{\mathbf{q}}_m, \dot{\tilde{\mathbf{q}}}_i, \ddot{\tilde{\mathbf{q}}}_i, \bar{\mathbf{q}}_{E_i}, \dot{\tilde{\mathbf{q}}}_{E_i}) \to 0$*, which implies that*

$$\mathbf{q}_i \to \mathbf{q}_m + \boldsymbol{\gamma}_i \quad \text{and} \quad \mathbf{q}_m \to \frac{1}{N}\sum_{i=1}^{N} \mathbf{q}_i. \tag{6.14}$$

iv. Static Force Reflection: *Suppose* $(\dot{\mathbf{q}}_j, \ddot{\mathbf{q}}_j) \to 0$ *for* $j \in \{m, 1, \cdots, N\}$. *Then,*

$$\mathbf{f}_m \to -\frac{1}{N}\sum_{i=1}^{N} \mathbf{f}_i. \tag{6.15}$$

Proof. Part (i) Robust Passivity: Consider the passivity condition in (6.9). Applying directly Theorem 6.2.1 we have

$$\sum_{i=1}^{N}\int_0^t [\mathbf{f}_m^T(\theta)\dot{\mathbf{q}}_m(\theta) + \mathbf{f}_i^T(\theta)\dot{\tilde{\mathbf{q}}}_i(\theta)]d\theta \geq \sum_{i=1}^{N}(-\bar{d}_i^2) = -\bar{d}^2.$$

Similarly with (6.10), we can easily verify that

$$\sum_{i=1}^{N}\int_0^t [\boldsymbol{\tau}_{m_i}^T(\theta)\dot{\mathbf{q}}_m(\theta) + \bar{\boldsymbol{\tau}}_i^T(\theta)\dot{\tilde{\mathbf{q}}}_i(\theta)]d\theta \leq \sum_{i=1}^{N}\bar{c}_i^2 = \bar{c}^2,$$

for some $\bar{d}_i, \bar{c}_i \in \Re$. Therefore, using Proposition 1 in [159], we conclude that the closed-loop system in (6.7) is passive.

Part (ii) Coupled Stability: Consider the positive function in (6.13). Taking its derivative with respect to time and applying the skew-symmetric property for Lagrangian systems, we obtain

$$\dot{\bar{E}}_v(t) = N\mathbf{f}_m^T\dot{\mathbf{q}}_m + \sum_{i=1}^{N}\mathbf{f}_i^T\dot{\tilde{\mathbf{q}}}_i + N\boldsymbol{\tau}_m^T\dot{\mathbf{q}}_m + \sum_{i=1}^{N}\bar{\boldsymbol{\tau}}_i^T\dot{\tilde{\mathbf{q}}}_i. \tag{6.16}$$

Then, integrating (6.16) and using the passivity conditions in (6.10) and (6.11) give us

$$\bar{E}_v(t) \leq \bar{E}_v(0) + Nd_m^2 + \bar{c}^2 + \sum_{i=1}^{N}d_i^2 = B. \tag{6.17}$$

Now, since $\bar{E}_v(t)$ is bounded by B, from (6.13) we conclude that $\dot{\mathbf{q}}_m(t), \dot{\tilde{\mathbf{q}}}_1(t), \cdots, \dot{\tilde{\mathbf{q}}}_N(t)$ must be bounded as well.

Part (iii) Position Coordination: Suppose $(\mathbf{f}_m(t), \mathbf{f}_i(t)) = 0\ \forall t \geq 0$ and $i \in \{1, \cdots, N\}$. Assume that $(M_i^{jk}(\mathbf{q}_i),\ \partial M_i^{jk}(\mathbf{q}_i)/\partial q_i^l, \partial^2 M_i^{jk}(\mathbf{q}_i)/\partial q_i^l \partial q_i^m) \in \mathcal{L}_\infty$. Then, (6.12) and (6.13) are direct consequences of Theorem 6.2.1. Since all terms in (6.12) are bounded by Theorem 6.2.1, $\bar{E}_p$ must also be bounded, which implies that $\bar{\mathbf{q}}_{E_i}$ are also bounded. Similarly, all terms in (6.13) converge to zero; therefore, $(\bar{E}_v, \dot{\mathbf{q}}_m, \dot{\tilde{\mathbf{q}}}_1, \cdots, \dot{\tilde{\mathbf{q}}}_N) \to 0$.

Now we are left to prove that $(\ddot{\mathbf{q}}_m, \ddot{\tilde{\mathbf{q}}}_i) \to 0$ for $i \in \{1, \cdots, N\}$. From (6.7) we have

$$\begin{aligned}
\ddot{\mathbf{q}}_m &= M_m^{-1}(\mathbf{q}_m)C_m(\mathbf{q}_m, \dot{\mathbf{q}}_m)\dot{\mathbf{q}}_m + M_m^{-1}(\mathbf{q}_m)\boldsymbol{\tau}_m \\
\ddot{\tilde{\mathbf{q}}}_i &= M_i^{-1}(\bar{\mathbf{q}}_i)C_i(\bar{\mathbf{q}}_i, \dot{\bar{\mathbf{q}}}_i)\dot{\bar{\mathbf{q}}}_i + M_i^{-1}(\bar{\mathbf{q}}_i)\bar{\boldsymbol{\tau}}_i.
\end{aligned} \tag{6.18}$$

Since $\bar{\mathbf{q}}_{E_i}, \dot{\mathbf{q}}_m, \dot{\bar{\mathbf{q}}}_i \in \mathcal{L}_\infty$, $\boldsymbol{\tau}_m, \bar{\boldsymbol{\tau}}_i$ are bounded. By the assumption that $\partial M_*^{jk}(\mathbf{q}_*)/\partial q_*^l$ are bounded, $C_*(\mathbf{q}_*, \dot{\mathbf{q}}_*)$ are also bounded [130], and since M_* are positive-definite bounded matrices, M_*^{-1} exist and are also bounded. Therefore, from (6.18), we conclude that $\ddot{\mathbf{q}}_m, \ddot{\bar{\mathbf{q}}}_i \in \mathcal{L}_\infty$. Now, taking the time derivative of (6.18), we obtain that all terms at the right hand side are bounded: $\bar{\mathbf{q}}_{E_*}, \dot{\mathbf{q}}_*, \ddot{\mathbf{q}}_*, dM^{-1}/dt$ (by boundedness on $\partial M_*^{jk}/\partial q_*^l$), and dC_*/dt (by boundedness on $\partial^2 M_*^{jk}/\partial q_*^l \partial q_*^m$ [130]). Hence, $d^3\mathbf{q}_*/dt^3$ are also bounded, which implies that $\ddot{\mathbf{q}}_*$ are uniformly continuous. Applying then Barbalat's Lemma [129], we have that $(\ddot{\mathbf{q}}_m, \ddot{\bar{\mathbf{q}}}_i) \to 0$ as $(\dot{\mathbf{q}}_m, \dot{\bar{\mathbf{q}}}_i) \to 0$.

Consider once again the system in (6.7). Suppose $\mathbf{f}_m = \mathbf{f}_i = 0$. Then, since $(\ddot{\mathbf{q}}_*, \dot{\mathbf{q}}_*) \to 0$ holds,

$$\bar{\boldsymbol{\tau}}_i(t) = -K_p(\bar{\mathbf{q}}_i(t) - \mathbf{q}_m(t - T_{mi})) \to 0$$

which for finite T_{mi} gives

$$\bar{\mathbf{q}}_i(t) - \mathbf{q}_m(t) + \int_{-T_{mi}}^{0} \dot{\mathbf{q}}_m(t+\theta)d\theta \to \bar{\mathbf{q}}_i(t) - \mathbf{q}_m(t) \to 0.$$

Similarly for finite T_{im},

$$\boldsymbol{\tau}_m(t) = -K_p(\mathbf{q}_m(t) - \frac{1}{N}\sum_{i=1}^{N} \mathbf{q}_i(t - T_{im})) \to 0$$

implies that $\mathbf{q}_m(t) \to \frac{1}{N}\sum_{i=1}^{N} \mathbf{q}_i(t)$.

Part (iv) Static Force Reflection: Assume that $(\dot{\mathbf{q}}_m, \ddot{\mathbf{q}}_m, \dot{\mathbf{q}}_i, \ddot{\mathbf{q}}_i) \to 0$ for $i \in \{1, \cdots, N\}$. Then, from (6.7) we have that $\mathbf{f}_m + \boldsymbol{\tau}_m \to 0$ and $\mathbf{f}_i + \bar{\boldsymbol{\tau}}_i \to 0$, which imply

$$\mathbf{f}_i \to K_p(\mathbf{q}_i - \gamma_i - \mathbf{q}_m), \quad \mathbf{f}_m \to K_p(\mathbf{q}_m - \sum_{i=1}^{N} \frac{\mathbf{q}_i}{N}) \tag{6.19}$$

for $\mathbf{q}_*(t - T_*) \to \mathbf{q}_*(t)$. Now, using (4.3) and re-writing (6.19) we finally obtain

$$\mathbf{f}_m(t) \to \frac{1}{N}\sum_{i=1}^{N} K_p[\mathbf{q}_m(t) - \mathbf{q}_i(t) + \gamma_i] = -\frac{1}{N}\sum_{i=1}^{N} \mathbf{f}_i(t)$$

which completes the proof. □

Up to now, we have established closed-loop stability, motion tracking, formation control, and force reflection for the teleoperation system in (6.7) without addressing the possibility of collisions

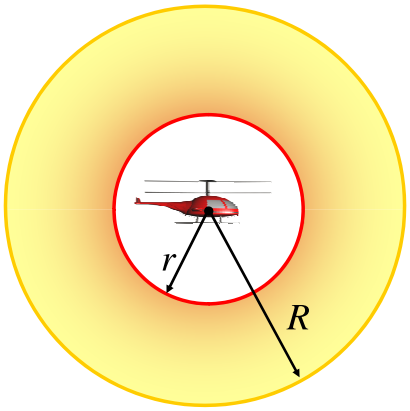

Figure 6.1: Detection (radius R) and avoidance (radius r) regions.

between slave vehicles and surrounding obstacles. This task will be discussed next.

6.3 Collision Avoidance Control

The overall goal in the teleoperation of multiple mobile robots is to achieve motion tracking and formation control of the slave vehicles while enforcing a minimum, safe distance between any two vehicles or obstacles at all times such that collisions are guaranteed never to occur. In general, we would like to define a safety region around each vehicle for which no other vehicle or obstacle is allowed to enter. According to this formulation, we proceed to introduce the following definitions.

We consider the motion of the ith slave vehicle from the group formation in (6.1) and define $\mathcal{N}_i$ as the set of obstacles (including other agents) in its vicinity. We assume that the ith slave agent can locate nearby obstacles and other agents inside a detection region (see Figure 6.1) given as

$$\mathcal{D}_{ij} = \left\{ \mathbf{q} : \mathbf{q} \in \Re^{2n}, r < \|\mathbf{q}_i - \mathbf{q}_j\| \leq R \right\} \tag{6.20}$$

where $\mathbf{q} = [\mathbf{q}_i^T, \mathbf{q}_j^T]^T$, $\mathbf{q}_j \in \Re^n$ are the coordinates of the jth obstacle in $\mathcal{N}_i$, and $R \in \Re$ is the detection radius. We also define an avoidance region for the ith slave as

$$\Omega_{ij} = \left\{ \mathbf{q} : \mathbf{q} \in \Re^{2n}, \|\mathbf{q}_i - \mathbf{q}_j\| \leq r \right\} \tag{6.21}$$

where $r \in \Re$ is the smallest safe distance from any other agent or obstacle and $0 < r < R$. Then the overall detection and avoidance regions for the system are $\mathcal{D} = \bigcup_{i \in N, j \in \mathcal{N}_i} \mathcal{D}_{ij}$ and $\Omega = \bigcup_{i \in N, j \in \mathcal{N}_i} \Omega_{ij}$, respectively, and the control goal is to design the collision-free control inputs $\mathbf{u}_i$ such

that the slave vehicles do not enter Ω at any time.

In order to achieve our control objective, we propose the use of avoidance functions [102]

$$V_{ij}(\mathbf{q}_i, \mathbf{q}_j) = \left(\min \left\{ 0, \frac{\|\mathbf{q}_i - \mathbf{q}_j\|^2 - R^2}{\|\mathbf{q}_i - \mathbf{q}_j\|^2 - r^2} \right\} \right)^2 \tag{6.22}$$

and the collision avoidance control input

$$\mathbf{u}_i = - \sum_{j \in \mathcal{N}_i} \frac{\partial V_{ij}(\mathbf{q}_i, \mathbf{q}_j)}{\partial \mathbf{q}_i} \tag{6.23}$$

where

$$\frac{\partial V_{ij}}{\partial \mathbf{q}_i} = \begin{cases} 0, & \text{if } \|\mathbf{q}_i - \mathbf{q}_j\| \geq R \\ \dfrac{4(R^2 - r^2)(\|\mathbf{q}_i - \mathbf{q}_j\|^2 - R^2)(\mathbf{q}_i - \mathbf{q}_j)^T}{(\|\mathbf{q}_i - \mathbf{q}_j\|^2 - r^2)^3}, & \text{if } r < \|\mathbf{q}_i - \mathbf{q}_j\| < R \\ \text{not defined}, & \text{if } \|\mathbf{q}_i - \mathbf{q}_j\| = r \end{cases} . \tag{6.24}$$

Theorem 6.3.1. *Consider the system in (6.7) with control law (6.2), (6.8), and (6.23) and let* $Q(t) = [\mathbf{q}_1^T(t), \cdots, \mathbf{q}_N^T(t), \cdots, \mathbf{q}_{N+\bar{N}}^T(t)]^T$*, where* $\bar{N}$ *is the number of obstacles and* $\mathbf{q}_{N+1}, \cdots, \mathbf{q}_{N+\bar{N}}$ *are their coordinates. Suppose that* $Q(0) \notin \Omega$*. Then, the closed-loop teleoperation system is stable and* $Q(t) \notin \Omega \; \forall t \geq 0$*.*

Proof. Suppose that $Q(0) \notin \Omega$ and consider the following Lyapunov-like function

$$W(t) = \bar{E}_v(t) + \frac{1}{2} \sum_{i=1}^{N} \sum_{j \in \mathcal{N}_i} V_{ij}(\mathbf{q}_i(t), \mathbf{q}_j(t)).$$

Taking its derivative with respect to time and noting that (6.22) are symmetric with respect to their arguments, i.e.,

$$\frac{\partial V_{ij}}{\partial \mathbf{q}_i} = \frac{\partial V_{ji}}{\partial \mathbf{q}_i} = -\frac{\partial V_{ij}}{\partial \mathbf{q}_j} = -\frac{\partial V_{ji}}{\partial \mathbf{q}_j},$$

we obtain

$$\dot{W} = N\mathbf{f}_m^T\dot{\mathbf{q}}_m + \sum_{i=1}^{N}\mathbf{f}_i^T\dot{\tilde{\mathbf{q}}}_i + N\boldsymbol{\tau}_m^T\dot{\mathbf{q}}_m + \sum_{i=1}^{N}\boldsymbol{\tau}_i^T\dot{\tilde{\mathbf{q}}}_i \\ \underbrace{-\sum_{i=1}^{N}\sum_{j\in\mathcal{N}_i}\frac{\partial V_{ij}}{\partial \mathbf{q}_i}\dot{\mathbf{q}}_i + \frac{1}{2}\sum_{i=1}^{N}\sum_{j\in\mathcal{N}_i}\left(\frac{\partial V_{ij}}{\partial \mathbf{q}_i}\dot{\mathbf{q}}_i + \frac{\partial V_{ij}}{\partial \mathbf{q}_j}\dot{\mathbf{q}}_j\right)}_{=0 \text{ by symmetry}}. \tag{6.25}$$

Then, integrating (6.25) yields

$$W(t) \leq W(0) + Nd_m^2 + \bar{c}^2 + \sum_{i=1}^{N} d_i^2 = B_W.$$

Now, assume $Q(t) \to \Omega$. This means that for some i, j, $V_{ij}(t) \to \infty \Rightarrow W(t) \to \infty$. However, $W(t)$ is bounded by B_W, which means that we reach a contradiction. Since the solutions of (6.7) are continuous, $Q(t)$ must never enter Ω. Furthermore, from the definition and boundedness on W, $\dot{\mathbf{q}}_m, \dot{\mathbf{q}}_i$ are also bounded, and from continuity of solutions and the fact that $Q(t) \not\to \Omega$, $\mathbf{u}_i(t)$ must be bounded. Therefore, we can consider the control inputs $\mathbf{u}_i(t)$ as external bounded forces and stability of the system and boundedness on the coordination errors follow from Theorem 6.2.2. □

Remark 6.3.1. *Note that the collision avoidance control is active (i.e., $\mathbf{u}_i(t) \neq 0$) only when $\mathbf{q}_i(t) \in \mathcal{D}_{ij}$ for some $j \in \mathcal{N}_i$. Thus outside of the detection region, all general conclusions from Theorem 6.2.2 apply. This leads us to prefer formations that satisfy $||\boldsymbol{\gamma}_i - \boldsymbol{\gamma}_j|| > R$ such that the collision avoidance control inputs do not represent a persistent conflict with the coordination goal.*

6.4 Experimental Setup

The control framework introduced in Sections 6.2 and 6.3 was tested in a SMMS environment (see Figure 6.2). The testbed consists of a haptic device (PHANTOM) with three actuated DOF to operate as the master robot, a pair of coaxial helicopters as slave mobile agents, a virtual interface, a Motion Capture (MoCap) system to gather position information from the slave vehicles, and a distributed network of computers for communication and local control. The helicopters were constrained to fly in a 5m long, 4m wide, and 1.7m tall room to which the operator had direct audio-visual access.

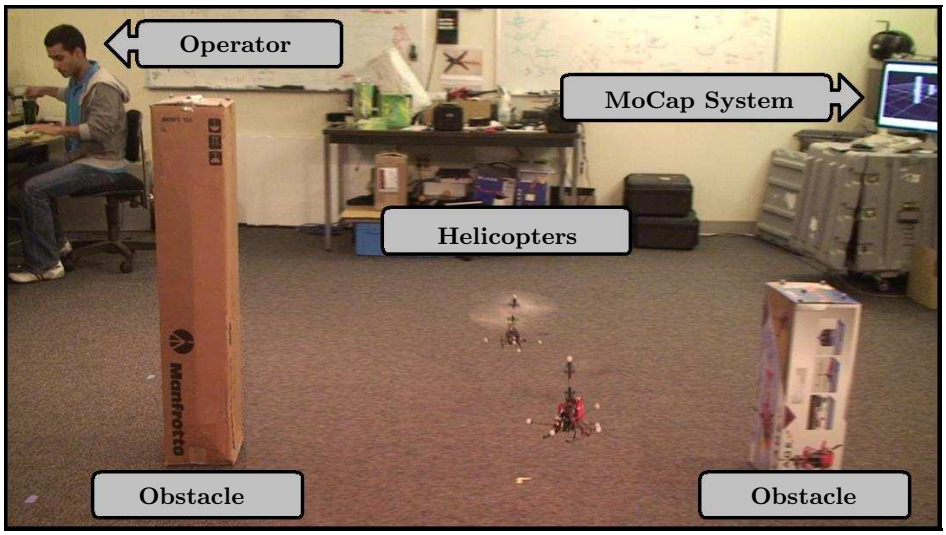

Figure 6.2: Experimental workspace. Copyright © 2010 Boeing. All rights reserved.

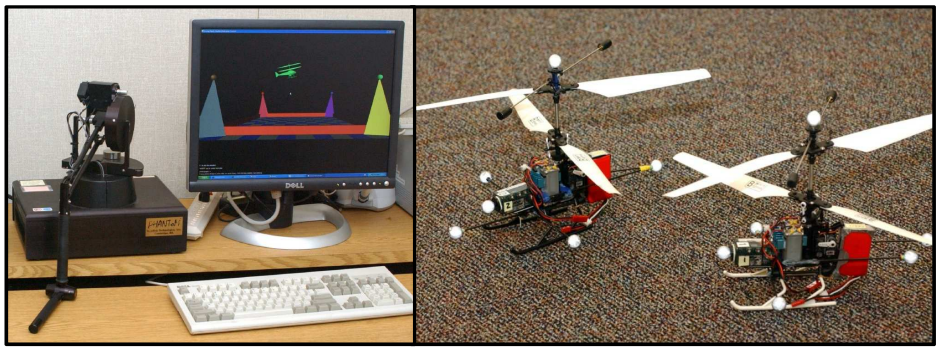

Figure 6.3: Master and slave agents. The left and right photos illustrate the PHANTOM haptic device and the coaxial helicopters, respectively. Copyright © 2010 Boeing. All rights reserved.

6.4.1 Haptic Device (Master Robot)

The haptic device, used as the master robot and illustrated in Figure 6.3, is the commercially available PHANTOM by SensAble Technologies, Inc. with 6-DOF of positional and rotational input and 6-DOF of force and torque output. Position and velocity commands to/from the slave agents are relative to the base of the PHANTOM's end-effector and are properly scaled to match with the mobility range of the haptic device. Rotational movements around the base of the end-effector are ignored, leaving the Cartesian coordinates, x, y, and z, as the only controllable DOF.

For the experiments, we used an update rate at the haptic interface of 1000Hz.

6.4.2 Coaxial Helicopters (Slave Robots)

The slave agents, shown in Figure 6.3, are two modified E-Flite Blade CX2 coaxial helicopters with multiple spherical retro-reflective markers for identification/localization purpose and cover removed to lower weight. Each vehicle weights 220 g and measures 340 mm of rotor diameter.[1] We assume that the CX2 helicopters have three controllable DOF corresponding to Cartesian x, y, and z motion,[2] while control of the yaw ψ angle is ignored. A pictorial representation of the relation between the rotational angles and the Cartesian coordinates is given in Figure 6.4(a).

The control parameters K_p, K_{di}, and K_v in (6.8) and the nominal control inputs for equilibrium of the helicopters, also known as trim values, were empirically found. The collision avoidance function for both helicopters was a sphere, such as in (6.22), with avoidance and detection radii of 400 mm and 900 mm, respectively.

6.4.3 Virtual Coupling

The slave controllers run on two separate off-board computers limited to a sampling rate of approximately 40 Hz due to wireless transmission's hardware constraints. That means that position and velocity data are communicated to the haptic device every 25 ms. Yet, a much higher update rate (e.g., 1000 Hz) on the haptic system is desirable in order to provide the operator with stable and realistic force feedback [160, 161].

A solution to overcome the constraint on the sampling rate and allow the haptic control to perform at a faster pace is to mediate the coupling between the haptic device and the helicopters via a virtual helicopter, as illustrated in Figure 6.4(b). The virtual helicopter is modeled as a frictionless 3-DOF second-order linear system with negligible mass in order to reduce the increase in inertia perceived by the operator. It is coupled to the master robot through a simple PD control [162] and to the slave agents through the control law in (6.8) where the virtual helicopter

[1] Note that the CX2 vehicle has larger dimensions and weight than the μ-CX model employed in Section 3.5.1.

[2] Cartesian motion of the CX2 helicopter is achieved by controlling pitch (ϕ), roll (θ), vertical thrust (ν), and yaw (ψ). However, we can assume that small changes in ϕ, θ, and ν proportionally translate into x, y, and z motion, respectively, whenever ψ is regulated at zero.

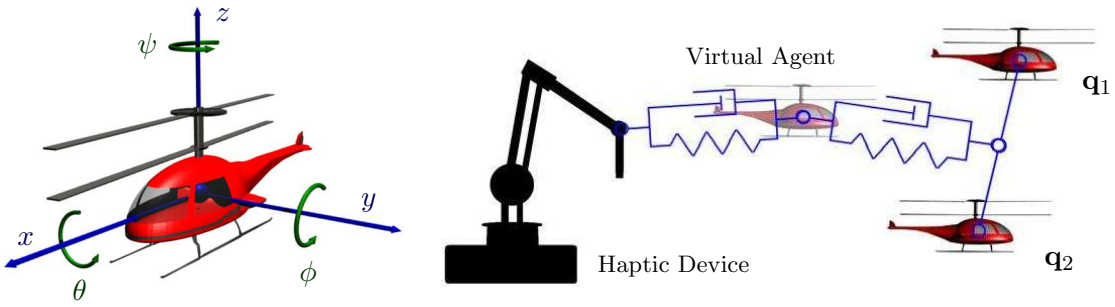

(a) CX2 local coordinate system. (b) Virtual coupling.

Figure 6.4: (a) Orientation of the rotational angles (θ, ϕ, ψ) with respect to the Cartesian coordinates (x, y, z). (b) Virtual coupling between master and slave agents.

is interpreted as the master robot. The dynamic model for the virtual agent is then given by

$$m_v \ddot{\mathbf{q}}_v = K_p \sum_{i=1}^{N} \frac{\mathbf{q}_i(t - T_{im})}{N} - K_p \mathbf{q}_v + K_v \sum_{i=1}^{N} \frac{\dot{\mathbf{q}}_i(t - T_{im})}{N} - K_v \dot{\mathbf{q}}_v - \sum_{i=1}^{N} K_{di} \frac{\dot{\mathbf{q}}_v}{N} + \bar{K}_p(\mathbf{q}_m - \mathbf{q}_v) + \bar{K}_v(\dot{\mathbf{q}}_m - \dot{\mathbf{q}}_v)$$

where $m_v \in \Re$ and $\mathbf{q}_v(t) \in \Re^3$ are the mass and the Cartesian coordinates of the virtual agent, respectively. The matrices $\bar{K}_p,\ \bar{K}_v \in \Re^{3\times 3}$ are symmetric positive-definite and computed such that the digital connection between the haptic and the virtual environment is passive [163]. Therefore, since the coupling between virtual agent and slave vehicles is passive (by Theorems 6.2.2 and 6.3.1) and the fact that the serial connection of passive two-ports systems is also passive (recall Theorem 2.3.2), we can conclude that the passivity of the overall system is preserved. Furthermore, the reader can easily verify that, for quasi-steady-state conditions $(\ddot{\mathbf{q}}_*, \dot{\mathbf{q}}_* \approx 0)$ and negligible mass $(m_v \approx 0)$, position coordination, as defined in (6.14), is achieved. Similarly, since the collision avoidance control inputs are independent of the master's dynamics, a safe interaction between agents and surrounding environment is also guaranteed.

The left side of Figure 6.3 offers a snapshot of the virtual interface, where a 3-dimensional (3-D) representation of the virtual helicopter (in green) can be observed.

6.4.4 MoCap System

Position tracking of the helicopters is performed off-board, meaning that the helicopters lack self-contained position and velocity sensors. Instead, the testbed employs a MoCap system [133] that

consists of multiple high speed cameras located in the remote environment and capable of tracking position and orientation of the slave agents in real-time by collecting two-dimensional visual data and constructing a three-dimensional representation through a photogrammetry-based technique. The cameras are able to sense and track unique configuration patterns of retro-reflective markers placed on the tracked vehicle or obstacle with a sub-millimeter accuracy at a sampling rate of 120Hz. The position and orientation of all vehicles and obstacles are then transmitted to each helicopter's control computer within less than 10ms such that every vehicle knows its own location and the location of nearby obstacles. Velocities of the agents are then computed locally by differentiation.

Figure 6.5 illustrates a 3-D representation of the workspace, including agents and obstacles, by the MoCap system's software.

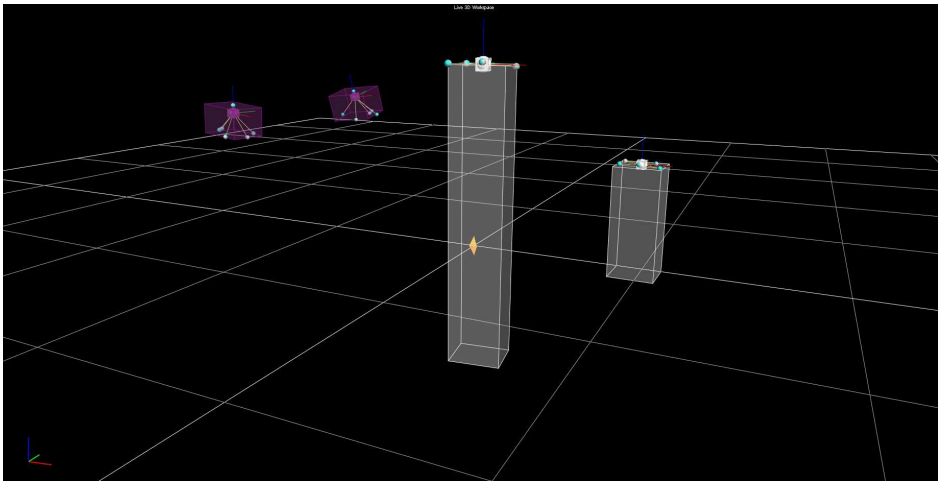

Figure 6.5: A 3-D image generated by the MoCap System using Vicon iQ2.5 graphical display. The small purple cubes represent the position and orientation of the two helicopters while the two gray rectangular prisms represent the position of the obstacles. Copyright © 2010 Boeing. All rights reserved.

6.4.5 Communication

Communication between agents and haptic device is achieved through TCP socket connections. Each agent transmits its Cartesian coordinates and velocities $(\mathbf{q}_i, \dot{\mathbf{q}}_i)$ to the virtual environment and receives from the virtual environment the coordinates and velocities of the virtual helicopter $(\mathbf{q}_v, \dot{\mathbf{q}}_v)$ and the corresponding offset for the desired formation $(\boldsymbol{\gamma}_i)$. Control inputs are computed locally.

The total average round trip delays for agents one and two were found to be 93 ms and 124 ms,

respectively, with a standard deviation of 1 ms, which means that fluctuations on the delays were negligible.

For more information on the experimental testbed, the reader is encouraged to consult [133,134].

6.5 Experimental Results

Three different experiments were performed. The first of these experiments was the teleoperation of both helicopters in a free (i.e., unobstructed) environment. The desired formation was a diagonal line with $\boldsymbol{\gamma}_1 = -\boldsymbol{\gamma}_2 = [500 \text{ mm}, -500 \text{ mm}, 0 \text{ mm}]^T$. Figures 6.6 and 6.7 illustrate, respectively, the resulting motion in the xy plane[3] and the Euclidean norm of the position error for the formation, where $\mathbf{e}_{cf}(t), \mathbf{e}_{\gamma_i}(t) \in \Re^3$ are given by

$$\begin{aligned}\mathbf{e}_{cf}(t) =& \mathbf{q}_v(t) - \frac{1}{2}(\mathbf{q}_1(t) + \mathbf{q}_2(t)) \\ \mathbf{e}_{\gamma_1}(t) =& \boldsymbol{\gamma}_1 - \frac{1}{2}(\mathbf{q}_2(t) - \mathbf{q}_1(t)) = -\mathbf{e}_{\gamma_2}(t).\end{aligned}$$

The two helicopters (red and blue markers), starting at opposite positions with respect to the desired formation, converged to the diagonal formation and followed thereafter the motion of the virtual helicopter (black line) without entering into each other's avoidance region. The commanded path by the virtual helicopter was a round trip from the right-back (i.e., negative (x, y) or third quadrant) to the left-front (i.e., positive (x, y) or first quadrant) corners of the workspace. As plotted in Figure 6.7, the agents converged to the desired formation in a short time (i.e., $t < 5$ s) and maintained the formation fairly well throughout the complete trajectory ($|\mathbf{e}_{\gamma_i}(t)| < 200$ mm $\forall t > 5$ s). Additionally, the vehicles were reported to track the master command with relative small error ($|\mathbf{e}_{cf}(t)| < 150$ mm $\forall t > 0$ s).

The second experiment consisted of teleoperating both agents through an obstructed environment. Two tall rectangular obstacles, modeled as three-dimensional cylindrical objects for collision avoidance's purpose, were placed near the center of the workspace. The helicopters were commanded to fly to the front of the room and then to return near the original position in the same fixed formation as in the first experiment. As can be seen in Figure 6.8, the helicopters were able to navigate safely around the obstacles tracking the virtual vehicle motion in the required diagonal

[3]Positive displacement along the Cartesian axes x, y, and z corresponds to motion of the helicopters to the front, left, and up directions, respectively. See Figure 6.4(a) for reference.

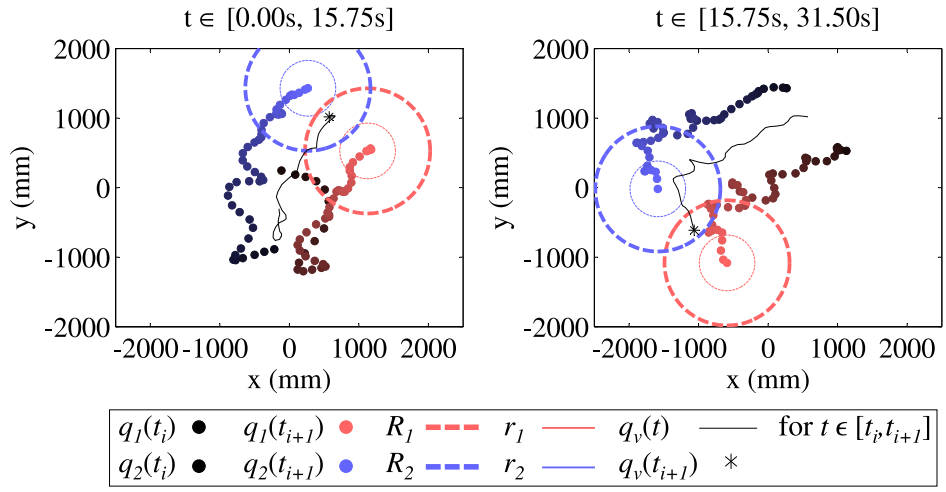

Figure 6.6: Sequential motion of slave agents with fixed formation in an unobstructed environment. The red and blue markers correspond to the first and second helicopter, respectively. The dashed-line, larger circles represent the detection regions while the solid-line circles represent the avoidance regions. Initial positions ($\mathbf{q}_*(t_i)$) are indicated by the darker, solid dots. The position of the virtual agent is traced by the fine, black line.

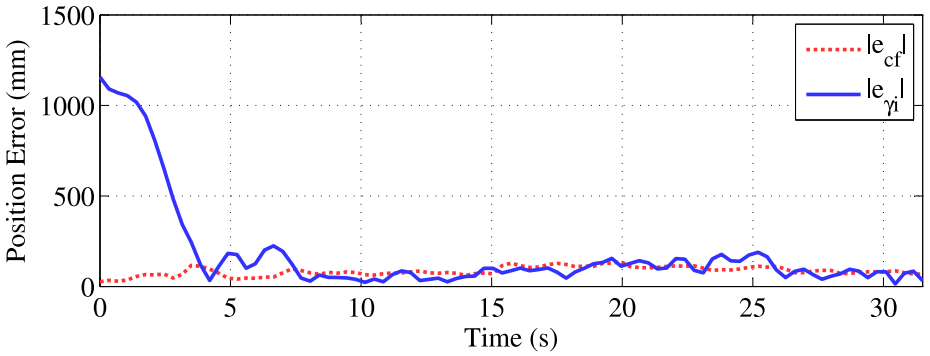

Figure 6.7: Position error for an unobstructed environment and a fixed formation.

formation. Figure 6.9 illustrates the coordination and formation errors where it can be observed that the formation error is in general higher (i.e., $|\mathbf{e}_{\gamma_i}(t)| < 350$ mm for all $t > 5$ s) than in the previous experiment, in particular at $t \in (5\text{ s}, 36\text{ s})$ where the agents come to the proximity of the static obstacles and the left virtual wall ($y = -2000$ mm). Nevertheless, the coordination error for the center of the formation remained small ($|\mathbf{e}_{cf}(t)| \approx 100$ mm $\forall t > 0$ s).

In the last experiment, the helicopters were commanded to fly from the back side of the workspace to the front side in a nearly parallel formation to the y axis with $\boldsymbol{\gamma}_{1_1} = -\boldsymbol{\gamma}_{2_1} = [250\text{ mm}, -550\text{ mm}, 0\text{ mm}]^T$. In addition, the operator had the ability to switch to a horizontal line formation ($\boldsymbol{\gamma}_{1_2} = -\boldsymbol{\gamma}_{2_2} = [550\text{ mm}, 0\text{ mm}, 0\text{ mm}]^T$) whenever he/she considered it preferable. Two rectangular obstacles were placed at $(x, y) = (457\text{ mm}, -738\text{ mm})$ and $(x, y) = (350\text{ mm}, 856\text{ mm})$ such that

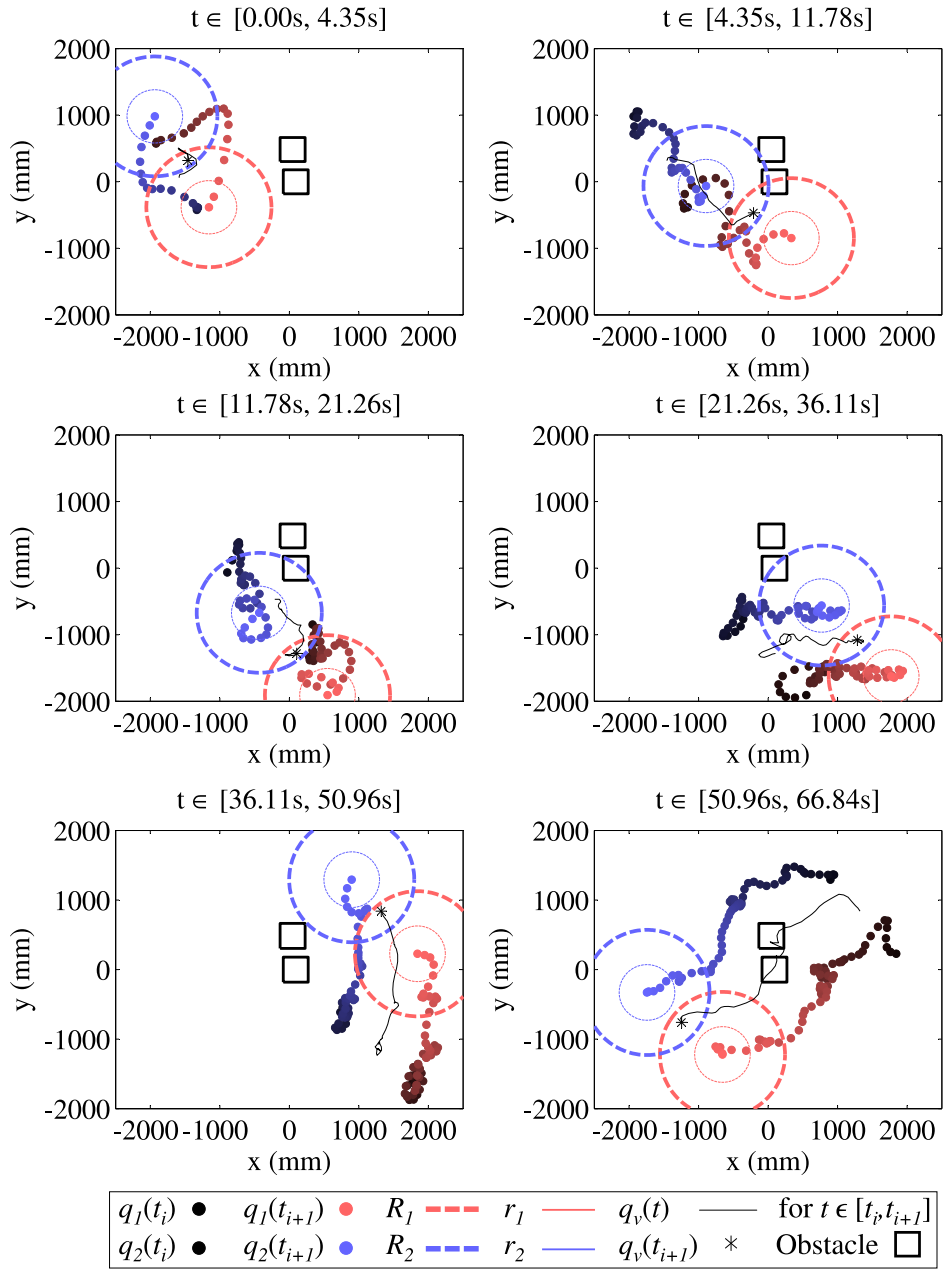

Figure 6.8: Sequential motion of slave agents with fixed formation in an obstructed environment.

the most feasible path for the agents was to travel between both obstacles. As depicted in Figure 6.10, the slave agents initially converged to the desired formation but encountered resistance to follow the virtual master's trajectory due to the presence of static obstacles. Once the operator switched to an horizontal line formation ($t = 26$ s), the helicopters were able to complete the path without collisions.

Figure 6.11 illustrates the coordination and formation errors for the last experiment. The peak

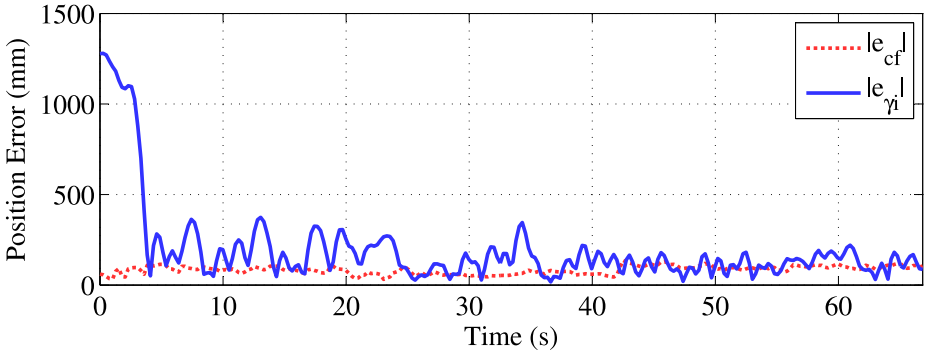

Figure 6.9: Position error for an obstructed environment and a fixed formation.

values at $t \in (10\text{ s}, 20\text{ s})$, $t = 26.0$ s, and $t = 37.9$ s correspond to the events at which the slave agents are unable to follow the master trajectory due to the detection of the static obstacles and to the change of formation from $\boldsymbol{\gamma}_{i_1}$ to $\boldsymbol{\gamma}_{i_2}$ and vice versa, respectively.

Position errors in the above experiments can be attributed to uncertainties on the trim values, nonlinearities in the helicopters' dynamics, and the frequent interaction between the helicopters, the virtual walls, and the static obstacles, among other disturbances. Despite this, the above experiments demonstrate the adeptness of the proposed control framework to enforce position convergence, formation control, and collision avoidance for a multi-agent system under constant time delays and obstructed environments.

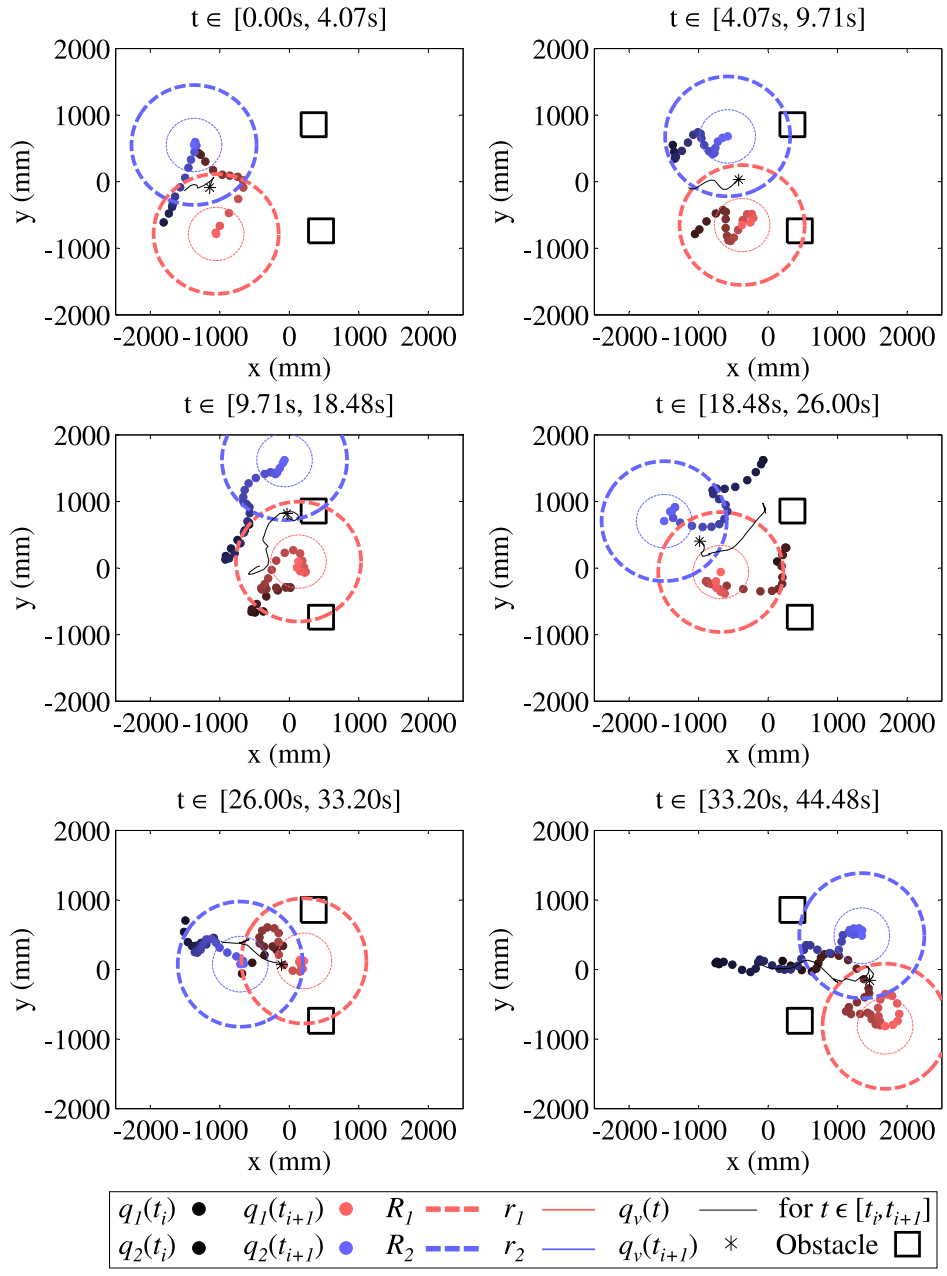

Figure 6.10: Sequential motion of slave agents with dynamic formation in an obstructed environment.

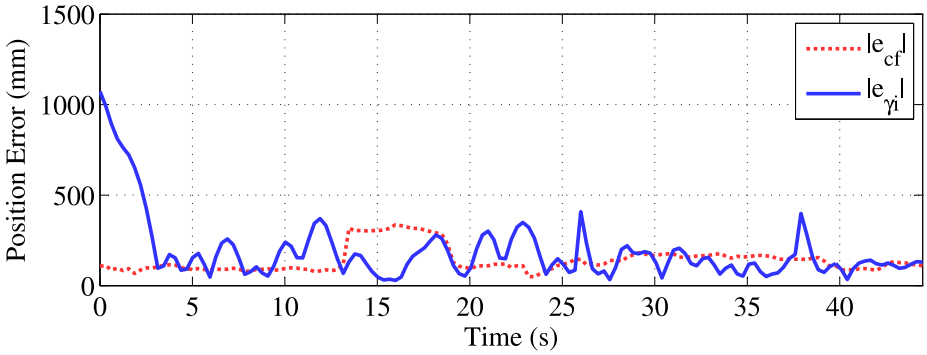

Figure 6.11: Position error for an obstructed environment and dynamic formation.

CHAPTER 7

COLLISION AVOIDANCE CONTROL: TWO-AGENT SYSTEMS

In the previous chapter, we developed a collision avoidance control law for a network of bilaterally teleoperated vehicles with unbounded control inputs and limited sensing range based on the use of avoidance functions. We assumed that position information from other agents and obstacles was accurate and immediate. Yet, in practice, the localization of other vehicles and obstacles might be subjected to measurement errors as well as communication and processing delays due to the presence of noise in the obstacle detection mechanism or unreliabilities in the broadcasting of coordinates among agents. For example, underwater localization equipment, such as sonar radars and inertial measurements units, may experience delays of up to 20s due to slow signal propagation and slow sampling rates [96] or additive measurement errors due to the use of dead reckoning as the position estimation algorithm [95]. Similarly, widely used Global Positioning Systems for localization of ground and aerial vehicles may experience temporary interruptions when traveling through occluded spaces or because of the interference with radio signals [98]. Therefore, control algorithms for autonomous and semi-autonomous vehicles must provide robustness to measurement uncertainties in order to guarantee the safety of the overall system.

Inspired by the need of robust strategies to guarantee the safe navigation of unmanned vehicles, we now devote this and the following chapter to the design of collision avoidance strategies for vehicles with sensing uncertainties including delays. Within this chapter, we formulate decentralized, cooperative and noncooperative collision avoidance strategies for a team of two vehicles with sensing uncertainties and limited sensing range. The control formulation relates to the concept of avoidance control presented in [99, 102, 104], yet the control inputs proposed herein are bounded. Advantages of the proposed avoidance strategies include the use of relative position information rather than absolute position and the robustness to time-varying delays, quantization, and other measurement errors. The strategies are also reactive (or real-time), meaning that collision avoidance control inputs are computed on-line as obstacles are detected, rather than computed according

to a predetermined (i.e., planned) collision-free trajectory. Furthermore, the avoidance control can be appended to any already designed, stable control law and is exclusively active when the vehicle is close to another agent. This implies that the agent's main objective, such as flocking, trajectory tracking, or set-point regulation, is unaffected when both agents (including obstacles) are safely apart. Two numerical examples and a real experiment with two coaxial helicopters illustrate the appropriateness of the proposed controller.

7.1 Problem Formulation

7.1.1 Dynamics of the Two-Agent System

In this chapter, we aim to control a pair of n-DOF agents with double-integrator dynamics given by

$$\ddot{\mathbf{q}}_i(t) = \mathbf{u}_i(t), \qquad \mathbf{q}_i \in \Re^n, \;\; \mathbf{u}_i \in \mathcal{U}_i \subset \Re^n \tag{7.1}$$

where $\mathbf{q}_i$ represents the position and $\mathcal{U}_i$ denotes the set of admissible control inputs $\mathbf{u}_i$ for the first ($i = 1$) and second ($i = 2$) agent. We assume the magnitudes of the control inputs are radially upper bounded by μ_i. The case where limits on the control inputs vary according to the Cartesian coordinates can be similarly covered by means of a coordinate transformation.

We also assume that each agent can locate the other agent within some margin of error. Specifically, we suppose that the ith agent is able to sense the jth agent as being located at $\hat{\mathbf{q}}_j(t) = \mathbf{q}_j(t) + \mathbf{d}_i(t)$, where $\mathbf{d}_i \in \Re^n$ is a time-varying vector representing the uncertainty on the localization process (e.g., delays, noise, and quantization) and which is considered to be upper bounded by some positive constant Δ_i, i.e., $\|\mathbf{d}_i(t)\| \leq \Delta_i, \; \forall t \geq 0$.

Remark 7.1.1. *Although the analysis in this chapter is centered on systems with double integrator dynamics, we can easily demonstrate that a nonlinear Lagrangian system satisfying Properties 2.2.1 to 2.2.3 can be reduced to the form of (7.1) via the use of inverse dynamics control [130]. To illustrate this statement, let us consider the equations of motion for a Lagrangian system*

$$M_i(\mathbf{q}_i)\ddot{\mathbf{q}}_i + C_i(\mathbf{q}_i, \dot{\mathbf{q}}_i)\dot{\mathbf{q}}_i + \mathbf{g}_i(\mathbf{q}_i) = \boldsymbol{\tau}_i, \qquad \|\boldsymbol{\tau}_i\| \leq U_i \tag{7.2}$$

where U_i is a limit on the magnitude of the control input $\boldsymbol{\tau}_i$. Since M_i is positive-definite, we have

that M_i^{-1} exists and we can rewrite (7.2) as

$$\ddot{\mathbf{q}}_i = M_i^{-1}(\mathbf{q}_i)\left(\boldsymbol{\tau}_i - C_i(\mathbf{q}_i, \dot{\mathbf{q}}_i)\dot{\mathbf{q}}_i - \mathbf{g}_i(\mathbf{q}_i)\right). \tag{7.3}$$

By choosing $\boldsymbol{\tau}_i = M_i(\mathbf{q}_i)\mathbf{u}_i + C_i(\mathbf{q}_i, \dot{\mathbf{q}}_i)\dot{\mathbf{q}}_i + \mathbf{g}_i(\mathbf{q}_i)$, we obtain that (7.3) reduces to (7.1), where $\mathbf{u}_i$ is the new control input. Moreover, if we assume (or force) the velocities of the ith agent to be bounded[1] *by some $\eta_i > 0$, i.e., $\|\dot{\mathbf{q}}_i\| \leq \eta_i$ and, in addition, we suppose gravitational forces are also bounded, i.e., $\exists G_i \geq 0$ such that $\|\mathbf{g}_i(\mathbf{q}_i)\| \leq G_i$, then we have that the magnitude of $\mathbf{u}_i$ is limited by*

$$\begin{aligned}
U_i &\geq \|M_i(\mathbf{q}_i)\mathbf{u}_i + C_i(\mathbf{q}_i, \dot{\mathbf{q}}_i)\dot{\mathbf{q}}_i + \mathbf{g}_i(\mathbf{q}_i)\| \\
U_i &\geq \|M_i(\mathbf{q}_i)\|\,\|\mathbf{u}_i\| + \|C_i(\mathbf{q}_i, \dot{\mathbf{q}}_i)\|\,\|\dot{\mathbf{q}}_i\| + \|\mathbf{g}_i(\mathbf{q}_i)\| \\
\|\mathbf{u}_i\| &\leq \frac{U_i - \|C_i(\mathbf{q}_i, \dot{\mathbf{q}}_i)\|\,\|\dot{\mathbf{q}}_i\| - \|\mathbf{g}_i(\mathbf{q}_i)\|}{\|M_i(\mathbf{q}_i)\|} \\
\|\mathbf{u}_i\| &\leq \frac{U_i - k_{c_i}\eta_i^2 - G_i}{\overline{\lambda}_i} = \mu_i
\end{aligned}$$

where k_{c_i} and $\overline{\lambda}_i$ are positive constants, deduced from Properties 2.2.1 to 2.2.3, and where μ_i is also positive if $k_{c_i}\eta_i^2 + G_i \leq U_i$.

7.1.2 Control Objective

Our main objective is to develop control strategies that enforce the completion of the agents' main tasks, such as flocking and trajectory tracking, while guaranteeing a safe separation between both agents at all times independently of bounded sensing delays and uncertainties. In general, we would like to define a safety region around each agent for which the other vehicle (or obstacle) is not allowed to enter. According to this formulation, and inspired by the concept of avoidance sets [99], we introduce the following definitions.

We define an *Antitarget Region* (see Figure 7.1), $\mathcal{T}$, as the collision zone for both agents, i.e.,

$$\mathcal{T} = \left\{\mathbf{q} : \mathbf{q} \in \Re^{2n}, \|\mathbf{q}_i - \mathbf{q}_j\| \leq r^*\right\}$$

where $\mathbf{q} = [\mathbf{q}_i^T, \mathbf{q}_j^T]^T$ and r^* denotes the minimum safe separation distance between both vehicles. Similarly, we define an *Avoidance Region*, $\Omega \supseteq \mathcal{T}$, as a zone for which the two agents are not

[1] Boundedness of the velocity terms can be claimed by injecting sufficient damping into the system as part of the control law (see Lemma 7.2.1, p. 92).

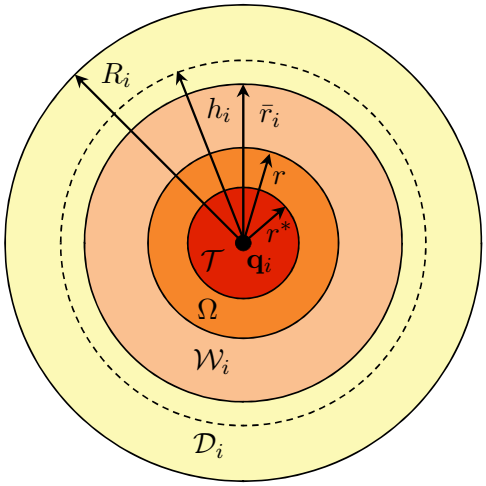

Figure 7.1: Antitarget ($\mathcal{T}$), Avoidance (Ω), Conflict ($\mathcal{W}_i$), and Detection ($\mathcal{D}_i$) Regions for the ith agent.

allowed to enter at any given time. Mathematically,

$$\Omega = \left\{ \mathbf{q} : \mathbf{q} \in \Re^{2n}, \|\mathbf{q}_i - \mathbf{q}_j\| \leq r \right\}$$

where $r \geq r^*$ is the desired minimum separation between both agents. Note that if we design a control policy such that $\mathbf{q}_1$ and $\mathbf{q}_2$ avoid Ω, then we have that they must also avoid $\mathcal{T}$.

Now, consider the dynamic limitations of the ith agent. Since its control inputs and acceleration components are bounded, a control policy aimed to avoid Ω needs to be implemented with enough anticipation, such that the ith vehicle has sufficient time to decelerate and prevent a collision. Consequently, we define a *Conflict Region*, $\mathcal{W}_i$, as

$$\mathcal{W}_i = \left\{ \mathbf{q} : \mathbf{q} \in \Re^{2n}, r < \|\mathbf{q}_i - \mathbf{q}_j\| \leq \bar{r}_i \right\}$$

where $\bar{r}_i > r$ is a lower bound on the distance that the ith agent can come from the other agent and still be able to decelerate and avoid Ω. Thus any collision avoidance strategy for the ith agent must take effect as soon as $\mathbf{q}_1$ and $\mathbf{q}_2$ enter $\mathcal{W}_i$.

Finally, in order for the problem to be well-defined, it is assumed that $\mathcal{W}_i$ lies within the *Detection Region*, $\mathcal{D}_i$, of the ith agent, defined as

$$\mathcal{D}_i = \left\{ \mathbf{q} : \mathbf{q} \in \Re^{2n}, \|\mathbf{q}_i - \mathbf{q}_j\| \leq R_i \right\}$$

where $R_i > \bar{r}_i$ is the detection radius. That is, the ith agent can detect any obstacle or agent inside the Detection Region. In addition, note that whereas $\mathcal{T}$ and Ω are equal for both agents, $\mathcal{W}_i$ and $\mathcal{D}_i$ can differ.

According to the above definitions, we can state the control objective as follows. Given Δ_1, Δ_2 and $\mathcal{T}$, design control inputs $\mathbf{u}_1(t)$ and $\mathbf{u}_2(t)$ such that $[\mathbf{q}_1(t)^T, \mathbf{q}_2(t)^T]^T \notin \Omega$ for all $t \geq 0$, where $\Omega \supseteq \mathcal{T}$.

7.2 Collision Avoidance Control

In order to achieve our control objective, we propose the use of the following control input:

$$\mathbf{u}_i = \left(1 - \frac{\|\mathbf{u}_i^a\|}{\bar{\mu}_i}\right) \mathbf{u}_i^o + \mathbf{u}_i^a - k_i \dot{\mathbf{q}}_i \tag{7.4}$$

where $\mathbf{u}_i^o \in \Re^n$ represents the known objective control law satisfying the constraint $\|\mathbf{u}_i^o(t)\| \leq \bar{\mu}_i$ for all $t \geq 0$ and where k_i is a positive constant given by

$$k_i = \frac{\bar{\mu}_i}{\eta_i}, \qquad \text{for } \bar{\mu}_i = \frac{\mu_i}{2},\ \eta_i > 0.$$

The objective control law $\mathbf{u}_i^o$ is designed such that the ith agent can accomplish its primary task, whereas the term $k_i \dot{\mathbf{q}}_i$ is injected into the system to regulate the maximum velocity of the agent, as it will be shown at the end of this section. The control term $\mathbf{u}_i^a \in \Re^n$ is the avoidance control input designed to guarantee collision-free trajectories. It is computed according to

$$\mathbf{u}_i^a = -\frac{\partial V_{ij}^a(\mathbf{q}_i, \hat{\mathbf{q}}_j)}{\partial \mathbf{q}_i}^T \tag{7.5}$$

where V_{ij}^a, called the avoidance function [102], is given by

$$V_{ij}^a(\mathbf{q}_i, \mathbf{q}_j) = \begin{cases} \Gamma_i \left(\min\left\{0, \dfrac{\|\mathbf{q}_i - \mathbf{q}_j\|^2 - R_i^2}{\|\mathbf{q}_i - \mathbf{q}_j\|^2 - r^2}\right\}\right)^2, & \text{if } \|\mathbf{q}_i - \mathbf{q}_j\| \geq h_i \\ -\bar{\mu}_i \|\mathbf{q}_i - \mathbf{q}_j\| + c_i, & \text{otherwise} \end{cases}$$

for $h_i = \bar{r}_i + \Delta_i$ and

$$\Gamma_i = \frac{\bar{\mu}_i \left(h_i^2 - r^2\right)^3}{4h_i(R_i^2 - h_i^2)(R_i^2 - r^2)}, \qquad\qquad c_i = \Gamma_i \frac{(h_i^2 - R_i^2)^2}{(h_i^2 - r^2)^2} + \bar{\mu}_i h_i.$$

The reader can easily verify that V_{ij}^a is nonnegative, almost everywhere continuously differentiable, and that $\mathbf{u}_i^a$ reduces to

$$\mathbf{u}_i^a = \begin{cases} \mathbf{0}, & \text{if } \|\mathbf{q}_i - \hat{\mathbf{q}}_j\| \geq R_i \\ \dfrac{K_i^a(R_i^2 - \|\mathbf{q}_i - \hat{\mathbf{q}}_j\|^2)}{(\|\mathbf{q}_i - \hat{\mathbf{q}}_j\|^2 - r^2)^3}(\mathbf{q}_i - \hat{\mathbf{q}}_j), & \text{if } h_i \leq \|\mathbf{q}_i - \hat{\mathbf{q}}_j\| < R_i \\ \bar{\mu}_i \dfrac{\mathbf{q}_i - \hat{\mathbf{q}}_j}{\|\mathbf{q}_i - \hat{\mathbf{q}}_j\|}, & \text{if } 0 < \|\mathbf{q}_i - \hat{\mathbf{q}}_j\| < h_i \\ \text{not defined}, & \text{if } \|\mathbf{q}_i - \hat{\mathbf{q}}_j\| = 0 \end{cases} \tag{7.6}$$

where $K_i^a = 4\Gamma_i(R_i^2 - r^2)$. Note that in contrast to the unboundedness of the avoidance functions and control inputs in [102] and Section 6.3, V_{ij}^a and $\mathbf{u}_i^a$ (proposed in this section) are bounded by c_i and $\bar{\mu}_i$, respectively. Similarly, the overall control input $\mathbf{u}_i$ can be shown to be bounded by μ_i.

We now prove that the control law in (7.4) guarantees boundedness of the velocities if $k_i > 0$.

Lemma 7.2.1. *Consider the system in (7.1) with control law (7.4) and (7.6). Let $k_i = \frac{\bar{\mu}_i}{\eta_i}$ for some $\bar{\mu}_i, \eta_i > 0$. Then, for all initial conditions satisfying $\|\dot{\mathbf{q}}_i(0)\| \leq \eta_i$, we have that $\|\dot{\mathbf{q}}_i(t)\| \leq \eta_i$ $\forall t \geq 0$.*

Proof. Consider the following Lyapunov-candidate function

$$V_\eta = \frac{1}{2}\|\dot{\mathbf{q}}_i\|^2.$$

Taking its time derivative we obtain that

$$\dot{V}_\eta = \dot{\mathbf{q}}_i^T \ddot{\mathbf{q}}_i \leq \|\dot{\mathbf{q}}_i\| \bar{\mu}_i - k_i \|\dot{\mathbf{q}}_i\|^2 = \|\dot{\mathbf{q}}_i\| (\bar{\mu}_i - k_i \|\dot{\mathbf{q}}_i\|) < 0, \qquad\qquad \forall \ \|\dot{\mathbf{q}}_i(t)\| > \eta_i.$$

Since $\dot{V}_\eta$ is negative for all $\|\dot{\mathbf{q}}_i\| > \eta_i$, we can conclude that the velocity solutions of (7.1) are bounded by η_i. ∎

7.3 Collision Avoidance under Bounded Uncertainties

In this section we present the main results of this chapter. Generally speaking, we show that the control law in (7.4) and (7.6) guarantees collision-free trajectories for the system in (7.1) given that the design parameters r and $\bar{r}_i$ satisfy a set of inequality constraints. We start addressing the case of noncooperative control, where only one agent effects the avoidance strategy. Then, we present the details for the cooperative case. However, before proceeding to establish strategies for both cases, let us first introduced the following lemma. The lemma will aid us to show that if the ith vehicle has control input given by (7.4) and (7.6), then it will try to evade the other agent.

Lemma 7.3.1. *Consider the dynamical system in (7.1). Assume the ith agent has control input given by (7.4) and (7.6) for* $k_i = \frac{\bar{\mu}_i}{\eta_i}$ *and* $\eta_i > 0$. *Define* $\beta_{ij}(t) = (\mathbf{q}_i(t) - \mathbf{q}_j(t))^T \dot{\mathbf{q}}_i(t)$, $\theta_i \in \left(0, \sin^{-1}\left(\frac{\sqrt{r_\epsilon^2 - \Delta_i^2}}{r_\epsilon}\right)\right)$, *and* $\delta_i = \frac{\theta_i r_\epsilon}{\eta_i + \eta_j}$, *where* $r_\epsilon \in (r, \bar{r}_i]$ *and* $r > \Delta_i$. *Let* $t_0 \leq t_f - \delta_i$ *and suppose that* $\|\dot{\mathbf{q}}_i(t_0)\| \leq \eta_i$, $\|\dot{\mathbf{q}}_j(t)\| \leq \eta_j$ *for some* $\eta_j \geq 0$, $\|\mathbf{d}_i(t)\| \leq \Delta_i \; \forall \, t \geq t_0$, *and* $\|\mathbf{q}_i(t) - \mathbf{q}_j(t)\| \in [r_\epsilon, \bar{r}_i]$ $\forall \, t \in [t_0, t_f]$. *Then,* $\beta_{ij}(t_f)$ *is bounded from below as*

$$\begin{aligned}\beta_{ij}(t_f) \geq \|\mathbf{q}_i(t_f) - \mathbf{q}_j(t_f)\| \Bigg[& -e^{-k_i\delta_i}\eta_i + \frac{\bar{\mu}_i}{r_\epsilon(k_i^2 + \omega_{ij}^2)} \Bigg(k_i\sqrt{r_\epsilon^2 - \Delta_i^2} + \omega_{ij}\Delta_i \\ & - e^{-k_i\delta_i}\left(k_i\sqrt{r_\epsilon^2 - \Delta_i^2}\cos\theta_i - k_i\Delta_i\sin\theta_i + \omega_{ij}\sqrt{r_\epsilon^2 - \Delta_i^2}\sin\theta_i + \omega_{ij}\Delta_i\cos\theta_i \right) \Bigg) \Bigg] \end{aligned} \tag{7.7}$$

where $\omega_{ij} = -\frac{\eta_i + \eta_j}{r_\epsilon}$.

Proof. For ease of notation, let $t_\delta = t_f - \delta_i$, $\mathbf{q}_{ij}(t) = \mathbf{q}_i(t) - \mathbf{q}_j(t)$, and $\hat{\mathbf{q}}_{ij}(t) = \mathbf{q}_i(t) - \hat{\mathbf{q}}_j(t)$. From the assumption that $[\mathbf{q}_i(t)^T, \mathbf{q}_j(t)^T]^T \in \mathcal{W}_i \; \forall t \in [t_0, t_f]$ we have that solutions of (7.1) can be computed as

$$\dot{\mathbf{q}}_i(t_f) = e^{-k_i\delta_i}\dot{\mathbf{q}}_i(t_\delta) + \int_{t_\delta}^{t_f} e^{-k_i(t_f - \tau)}\mathbf{u}_i^a(\tau)d\tau$$

Therefore,

$$\begin{aligned}\beta_{ij}(t_f) =& \mathbf{q}_{ij}(t_f)^T \left(e^{-k_i\delta_i}\dot{\mathbf{q}}_i(t_\delta) + \int_{t_\delta}^{t_f} e^{-k_i(t_f-\tau)}\bar{\mu}_i \frac{\hat{\mathbf{q}}_{ij}(\tau)}{\|\hat{\mathbf{q}}_{ij}(\tau)\|}d\tau \right) \\ \geq & \|\mathbf{q}_{ij}(t_f)\| \left(-\eta_i e^{-k_i\delta_i} + \bar{\mu}_i \int_{t_\delta}^{t_f} e^{-k_i(t_f-\tau)} \frac{\mathbf{q}_{ij}(t_f)^T\hat{\mathbf{q}}_{ij}(\tau)}{\|\mathbf{q}_{ij}(t_f)\|\,\|\hat{\mathbf{q}}_{ij}(\tau)\|}d\tau \right) \\ = & \|\mathbf{q}_{ij}(t_f)\| \left(-\eta_i e^{-k_i\delta_i} + \bar{\mu}_i \int_{t_\delta}^{t_f} e^{-k_i(t_f-\tau)}\cos\phi_{ij}(\tau)d\tau \right) \end{aligned} \tag{7.8}$$

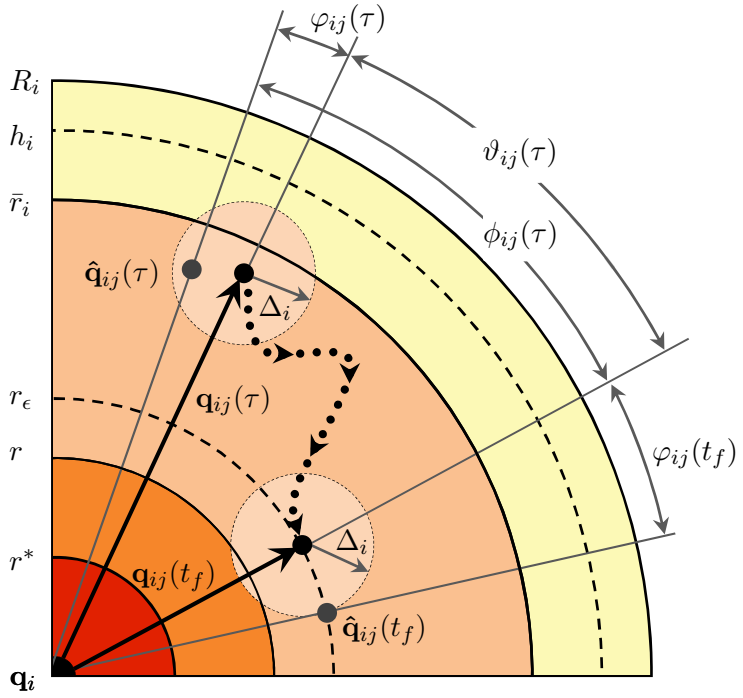

Figure 7.2: Hypothetical motion of $\mathbf{q}_j(\tau)$ with respect to $\mathbf{q}_i(\tau)$ for $t_\delta \leq \tau \leq t_f$. The larger black dots represent the vectors (i.e., distances) $\mathbf{q}_{ij}(\tau)$ and $\mathbf{q}_{ij}(t_f)$, whereas the gray dots denote $\hat{\mathbf{q}}_{ij}(\tau)$ and $\hat{\mathbf{q}}_{ij}(t_f)$.

where $\phi_{ij}(\tau)$ defines the angle between $\mathbf{q}_{ij}(t_f)$ and $\hat{\mathbf{q}}_{ij}(\tau)$ for $\tau \in [t_\delta, t_f]$ and where we used the fact that $\|\dot{\mathbf{q}}_i(t)\| \leq \eta_i \ \forall t$. Now, our main objective in the process of developing the proof is to compute a lower bound on $\int_{t_\delta}^{t_f} e^{-k_i(t_f-\tau)} \cos\phi_{ij}(\tau) d\tau$. In order to do so, we would like to first find an upper bound on $\phi_{ij}(\tau)$ at every instance of time τ. That is, we would like to define a function $\overline{\phi}_{ij}(\tau)$ such that $\phi_{ij}(\tau) \leq \overline{\phi}_{ij}(\tau)$ for all $\tau \in [t_\delta, t_f]$. Therefore, let us consider the illustration in Figure 7.2. Observe that $\phi_{ij}(\tau)$ is always upper bounded by the summation of the angle between $\mathbf{q}_{ij}(t_f)$ and $\mathbf{q}_{ij}(\tau)$ and the angle between $\mathbf{q}_{ij}(\tau)$ and $\hat{\mathbf{q}}_{ij}(\tau)$, denoted as $\vartheta_{ij}(\tau)$ and $\varphi_{ij}(\tau)$, respectively, i.e., $\|\phi_{ij}(\tau)\| \leq \|\vartheta_{ij}(\tau)\| + \|\varphi_{ij}(\tau)\|$. Hence, a suitable function would be

$$\overline{\phi}_{ij}(\tau) = \underbrace{\sup_{t\in[t_\delta,\tau]} \|\vartheta_{ij}(t)\|}_{\overline{\vartheta}_{ij}(\tau)} + \underbrace{\sup_{t\in[t_\delta,\tau]} \|\varphi_{ij}(t)\|}_{\overline{\varphi}_{ij}(\tau)}$$

where $\overline{\vartheta}_{ij}(\tau)$ and $\overline{\varphi}_{ij}(\tau)$ are yet to be determined.

Now, consider $\vartheta_{ij}(\tau)$. Since $\|\mathbf{q}_{ij}(\tau)\| \geq r_\epsilon \ \forall \ \tau \in [t_\delta, t_f]$ and the velocities of the agents are bounded, we have that $\vartheta_{ij}(\tau)$ attains its maximum when the agents approach each other at maxi-

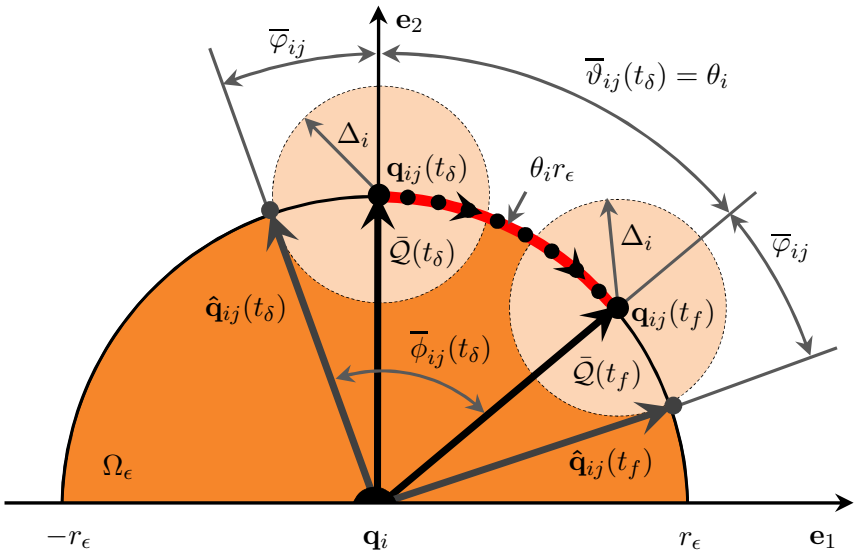

Figure 7.3: Extreme case in Lemma 7.3.1. The agents approach each other at maximum speed along the boundary of Ω_ϵ for $\tau \in [t_\delta, t_f]$.

mum speed along the boundary of Ω_ϵ, where $\Omega_\epsilon = \{\mathbf{q} : \mathbf{q} \in \Re^{2n}, \|\mathbf{q}_{ij}\| < r_\epsilon\}$ (see Figure 7.3 for an illustration). Then, using the arc-length formula to compute the maximum length traveled by the agents and invoking its relation with the central angle ϑ_{ij} we obtain

$$\vartheta_{ij}(\tau) \leq \frac{\int_\tau^{t_f} \|\dot{\hat{\mathbf{q}}}_{ij}(s)\|\, ds}{r_\epsilon} \leq \frac{\int_\tau^{t_f} (\eta_i + \eta_j) ds}{r_\epsilon} = \frac{(\eta_i + \eta_j)(t_f - \tau)}{r_\epsilon} = \overline{\vartheta}_{ij}(\tau)$$

for $\tau \in [t_\delta, t_f]$. Note that $\overline{\vartheta}_{ij}(t_\delta) = \frac{(\eta_i+\eta_j)\delta_i}{r_\epsilon} = \theta_i$ while $\overline{\vartheta}_{ij}(t_f) = 0$. Now, we are left to find $\overline{\varphi}_{ij}(\tau)$.

Since $\|\mathbf{q}_{ij}(\tau)\| \geq r_\epsilon \; \forall \; \tau \in [t_\delta, t_f]$ and $\|\mathbf{d}_i\| \leq \Delta_i < r$, we have that $\varphi_{ij}(\tau)$ is maximized when $\mathbf{q}_{ij}(\tau)$ is close to the boundary of Ω_ϵ. Thus, let us consider the diagram in Figure 7.3, which details this case. First, observe that the maximum angle $\overline{\varphi}_{ij}(\tau)$ is constant whenever $\mathbf{q}_{ij}(\tau)$ lies on the boundary of Ω_ϵ. Consequently, it is sufficient to find $\overline{\varphi}_{ij}(\tau)$ when $\tau = t_\delta$. To this end, let us choose the vectors $\mathbf{e}_1$ and $\mathbf{e}_2$ as an orthonormal basis for the plane containing $\mathbf{q}_{ij}(t_\delta)$ and $\hat{\mathbf{q}}_{ij}(t_\delta)$ and let $\mathbf{e}_2$ be oriented along the same direction and origin as $\mathbf{q}_{ij}(t_\delta)$, as shown in Figure 7.3. Then, $\mathbf{q}_{ij}(t_\delta)$ can be rewritten as $\mathbf{q}_{ij}(t_\delta) = r_\epsilon \mathbf{e}_2$. Similarly, $\hat{\mathbf{q}}_{ij}(t_\delta)$ can be written as $\hat{\mathbf{q}}_{ij}(t_\delta) = c_1\mathbf{e}_1 + c_2\mathbf{e}_2$, where c_1 and c_2 are constants. Now, from the constraint $\|\hat{\mathbf{q}}_{ij}(t_\delta) - \mathbf{q}_{ij}(t_\delta)\| \leq \Delta_i$ (i.e., $\hat{\mathbf{q}}_{ij}(t_\delta) \in \bar{\mathcal{Q}}(t_\delta)$, where $\bar{\mathcal{Q}}(t) = \{\bar{\mathbf{q}} : \bar{\mathbf{q}} \in \Re^{2n}, \|\mathbf{q}_{ij}(t) - \hat{\mathbf{q}}_{ij}(t)\| \leq \Delta_i$ for $\bar{\mathbf{q}}^T = [\mathbf{q}_{ij}^T, \hat{\mathbf{q}}_{ij}^T]^T)$, we have that c_1 and c_2

must satisfy the following equation:

$$c_1^2 + (c_2 - r_\epsilon)^2 \leq \Delta_i.$$

Likewise, we have that $\overline{\varphi}_{ij}$ is maximized when the ratio $|c_1/c_2|$ attains its maximum. It is easy to verify that such conditions are satisfied when

$$c_1 = \pm \frac{\Delta_i}{r_\epsilon}\sqrt{r_\epsilon^2 - \Delta_i^2}, \qquad\qquad c_2 = \frac{r_\epsilon^2 - \Delta_i^2}{r_\epsilon}.$$

Therefore, $\overline{\varphi}_{ij}(\tau) = \overline{\varphi}_{ij}$ can be computed as

$$\overline{\varphi}_{ij} = \cos^{-1}\left(\frac{\mathbf{q}_{ij}(t_\delta)^T \hat{\mathbf{q}}_{ij}(t_\delta)}{\|\mathbf{q}_{ij}(t_\delta)\|\,\|\hat{\mathbf{q}}_{ij}(t_\delta)\|}\right) = \cos^{-1}\left(\frac{\sqrt{r_\epsilon^2 - \Delta_i^2}}{r_\epsilon}\right).$$

Now, let us return to (7.8). Since $\overline{\vartheta}_{ij}(\tau) \leq \theta_i < \sin^{-1}\left(\frac{\sqrt{r_\epsilon^2-\Delta_i^2}}{r_\epsilon}\right)$ and $\overline{\varphi}_{ij}(\tau) = \cos^{-1}\left(\frac{\sqrt{r_\epsilon^2-\Delta_i^2}}{r_\epsilon}\right)$, we have that $\overline{\phi}_{ij}(\tau) = \overline{\vartheta}_{ij}(\tau) + \overline{\varphi}_{ij}(\tau) < \frac{\pi}{2}$. Therefore, $\cos\phi_{ij}(\tau) \geq \cos\overline{\phi}_{ij}(\tau) > 0$ for all τ and

$$\begin{aligned}\int_{t_\delta}^{t_f} e^{-k_i(t_f-\tau)}\cos\phi_{ij}(\tau)d\tau \geq& \int_{t_\delta}^{t_f} e^{-k_i(t_f-\tau)}\cos\overline{\phi}_{ij}(\tau)d\tau \\ =& \frac{1}{k_i^2+\omega_{ij}^2}\left(k_i\cos\overline{\phi}_{ij}(t_f) + \omega_{ij}\sin\overline{\phi}_{ij}(t_f)\right) \\ &- \frac{e^{k_i\delta_i}}{k_i^2+\omega_{ij}^2}\left(k_i\cos\overline{\phi}_{ij}(t_f) + \omega_{ij}\sin\overline{\phi}_{ij}(t_\delta)\right) \qquad (7.9)\end{aligned}$$

where we used the fact that $\dot{\overline{\phi}}_{ij}(t) = \omega_{ij} = -\frac{\eta_i+\eta_j}{r_\epsilon}$ is constant. Also note that $\overline{\phi}_{ij}(t_f) = \overline{\varphi}_{ij}$ and hence

$$\begin{aligned}\cos\overline{\phi}_{ij}(t_f) =& \cos\overline{\varphi}_{ij} = \frac{\sqrt{r_\epsilon^2 - \Delta_i^2}}{r_\epsilon} \\ \sin\overline{\phi}_{ij}(t_f) =& \sin\overline{\varphi}_{ij} = \frac{\|\mathbf{q}_{ij}(t_\delta)\times\hat{\mathbf{q}}_{ij}(t_\delta)\|}{\|\mathbf{q}_{ij}(t_\delta)\|\,\|\hat{\mathbf{q}}_{ij}(t_\delta)\|} = \frac{\Delta_i}{r_\epsilon}.\end{aligned}$$

In order to evaluate $\cos\overline{\phi}_{ij}(t_\delta)$ and $\sin\overline{\phi}_{ij}(t_\delta)$, let us rewrite $\mathbf{q}_{ij}(t_f)$ using $\mathbf{e}_1$ and $\mathbf{e}_2$ as orthonormal basis, i.e.,

$$\mathbf{q}_{ij}(t_f) = r_\epsilon\sin\theta_i\mathbf{e}_1 + r_\epsilon\cos\theta_i\mathbf{e}_2.$$

Then, we have

$$\cos\overline{\phi}_{ij}(t_\delta) = \cos(\theta_i + \overline{\varphi}_{ij}) = \frac{\mathbf{q}_{ij}(t_f)\hat{\mathbf{q}}_{ij}(t_\delta)}{\|\mathbf{q}_{ij}(t_f)\|\,\|\hat{\mathbf{q}}_{ij}(t_\delta)\|} = \frac{\sqrt{r_\epsilon^2 - \Delta_i^2}\cos\theta_i - \Delta_i \sin\theta_i}{r_\epsilon}$$

$$\sin\overline{\phi}_{ij}(t_\delta) = \sin(\theta_i + \overline{\varphi}_{ij}) = \frac{\|\mathbf{q}_{ij}(t_f) \times \hat{\mathbf{q}}_{ij}(t_\delta)\|}{\|\mathbf{q}_{ij}(t_f)\|\,\|\hat{\mathbf{q}}_{ij}(t_\delta)\|} = \frac{\sqrt{r_\epsilon^2 - \Delta_i^2}\sin\theta_i + \Delta_i \cos\theta_i}{r_\epsilon}$$

and returning to (7.9), we obtain

$$\begin{aligned}\int_{t_\delta}^{t_f} e^{-k_i(t_f-\tau)}\cos\phi_{ij}(\tau)d\tau \geq & \frac{1}{r_\epsilon(k_i^2+\omega_{ij}^2)}\left(k_i\sqrt{r_\epsilon^2-\Delta_i^2} + \omega_{ij}\Delta_i - e^{-k_i\delta_i}k_i\sqrt{r_\epsilon^2-\Delta_i^2}\cos\theta_i\right.\\ & \left. + e^{-k_i\delta_i}k_i\Delta_i\sin\theta_i - e^{-k_i\delta_i}\omega_{ij}\sqrt{r_\epsilon^2-\Delta_i^2}\sin\theta_i - e^{-k_i\delta_i}\omega_{ij}\Delta_i\cos\theta_i\right).\end{aligned}$$

Therefore, substituting the above equation into (7.8) yields (7.7), which completes the proof. □

A more conservative yet simpler lower bound on $\beta_{ij}(t)$ than the one given by (7.7) can be computed. Revisiting (7.9), we can alternatively obtain that

$$\begin{aligned}\int_{t_\delta}^{t_f} e^{-k_i(t_f-\tau)}\cos\phi_{ij}(\tau)d\tau \geq & e^{-k_i\delta_i}\int_{t_\delta}^{t_f}\cos\overline{\phi}_{ij}(\tau)d\tau\\ = & -\frac{r_\epsilon e^{-k_i\delta_i}}{\eta_i+\eta_j}\left(\sin\overline{\phi}_{ij}(t_f) - \sin\overline{\phi}_{ij}(t_\delta)\right)\\ = & e^{-k_i\delta_i}\frac{\sqrt{r_\epsilon^2-\Delta_i^2}\sin\theta_i + \Delta_i(\cos\theta_i - 1)}{\eta_i+\eta_j}.\end{aligned}$$

Then, substituting the above inequality into (7.8) would yield

$$\beta_{ij}(t_f) \geq \|\mathbf{q}_i(t_f) - \mathbf{q}_j(t_f)\|\, e^{-k_i\delta_i}\left(\bar{\mu}_i\frac{\sqrt{r_\epsilon^2-\Delta_i^2}\sin\theta_i + \Delta_i(\cos\theta_i - 1)}{\eta_i+\eta_j} - \eta_i\right). \tag{7.10}$$

The above lower bound on β_{ij} is certainly more conservative that the one previously stated in Lemma 7.3.1. However, (7.10) is easier to evaluate than (7.7), which simplifies the design process of the collision avoidance control inputs, as will be shown later in this section.

Remark 7.3.1. *Mathematically, we can interpret* $\frac{\beta_{ij}(t)}{\|\mathbf{q}_{ij}(t)\|}$ *as the scalar projection of the velocity vector* $\dot{\mathbf{q}}_i$ *onto the collision threat vector* $\mathbf{q}_{ij}$*. Accordingly, we can say that the above lemma provides an indication of the direction of the ith agent's velocity vector with respect to the collision threat.*

For instance, if for some time t_f, $\beta_{ij}(t_f) > 0$, then we can conclude that at time t_f the ith agent is moving away from the jth agent.

Having established Lemma 7.3.1, we now proceed to state the main results of this paper. We first start with the noncooperative case, that is, the scenario in which only one agent implements the avoidance control.

Theorem 7.3.1 (Noncooperative Collision Avoidance with Uncertainties)**.** *Consider the two dynamical systems in (7.1). Assume that the velocities of the second agent are bounded by $\eta_2 \geq 0$ and let the control input for the first agent be given by (7.4) and (7.6) with $k_1 = \frac{\bar{\mu}_1}{\eta_1} > 0$. Suppose there exist constants $\eta_1 > \eta_2$, $r \geq r^*$, $\epsilon > 0$, and $\theta_1 \in \left(0, \sin^{-1}\left(\frac{\sqrt{r_\epsilon^2 - \Delta_1^2}}{r_\epsilon}\right)\right)$ such that*

$$\bar{r}_1 = (\theta_1 + 1)(r + \epsilon) < R_1 - \Delta_1 \tag{7.11}$$

and

$$\begin{aligned} -e^{-k_1\delta_1}\left(k_1\sqrt{r_\epsilon^2 - \Delta_1^2}\cos\theta_1 - k_1\Delta_1\sin\theta_1 + \omega_{12}\sqrt{r_\epsilon^2 - \Delta_1^2}\sin\theta_1 + \omega_{12}\Delta_1\cos\theta_1\right) \\ + k_1\sqrt{r_\epsilon^2 - \Delta_1^2} + \omega_{12}\Delta_1 - \frac{r_\epsilon}{\bar{\mu}_1}(k_1^2 + \omega_{12}^2)\left(\eta_2 + e^{-k_1\delta_1}\eta_1\right) \geq 0. \end{aligned} \tag{7.12}$$

Then, if $\mathbf{q}(0) \notin \mathcal{W}_1 \cup \Omega$ for $\mathbf{q}(t) = [\mathbf{q}_1(t)^T, \mathbf{q}_2(t)^T]^T$, $\|\dot{\mathbf{q}}_1(0)\| \leq \eta_1$, and $\|\mathbf{d}_1(t)\| \leq \Delta_1$, we have that $\mathbf{q}(t) \notin \Omega \ \forall t \geq 0$.

Proof. Consider the system in (7.1) with control input given by (7.4) and (7.6) for $i = 1$. Assume that the second agent's velocity is bounded by some $\eta_2 \geq 0$ and that (7.11) and (7.12) hold. Let $k_1 = \frac{\bar{\mu}_1}{\eta_1}$ where $\eta_1 > \eta_2$ and assume that $\|\dot{\mathbf{q}}_1(0)\| \leq \eta_1$. Applying Lemma 7.2.1 we have that $\|\dot{\mathbf{q}}_1(t)\| \leq \eta_1 \ \forall t \geq 0$. Now, let us consider the following Lyapunov candidate function

$$V(t) = \frac{1}{4(\|\mathbf{q}_{12}(t)\|^2 - r^2)^2}. \tag{7.13}$$

Taking its time derivative yields

$$\dot{V}(t) = \frac{\mathbf{q}_{12}(t)^T\dot{\mathbf{q}}_2(t) - \beta_{12}(t)}{(\|\mathbf{q}_{12}(t)\|^2 - r^2)^3} \leq \frac{\|\mathbf{q}_{12}(t)\|\,\eta_2 - \beta_{12}(t)}{(\|\mathbf{q}_{12}(t)\|^2 - r^2)^3}. \tag{7.14}$$

Now, let $\mathbf{q}(0) \notin \mathcal{W}_1 \cup \Omega$ and suppose that for some time $t > 0$, $\|\mathbf{q}_{12}(t)\| \to r_\epsilon = r + \epsilon$ from above. Since $\|\mathbf{q}_{12}(0)\| > \bar{r}_1$ and the velocities of the agents are bounded, it will take the agents some time

Δt to reduce their distance from $\bar{r}_1$ to r_ϵ. Therefore, we have that $\mathbf{q}(\tau) \in \mathcal{W}_1 \ \forall \tau \in [t-\Delta t, t]$, where it is easy to demonstrate that $\Delta t \geq \delta_1 = \frac{\bar{r}_1 - r_\epsilon}{\eta_1+\eta_2} = \frac{\theta_1 r_\epsilon}{\eta_1+\eta_2}$. Then, applying Lemma 7.3.1 and using (7.11) and (7.12), it is easy to show that $\beta_{12}(t) \geq \|\mathbf{q}_{12}(t)\| \, \eta_2$. Returning to (7.14), we finally obtain that $\dot{V}(t) \leq 0$ for $\|\mathbf{q}_{12}\| \leq r_\epsilon$. The fact that $\mathbf{q}_{12}(t)$ is continuous and $\dot{V}(t)$ is non-positive for $\|\mathbf{q}_{12}(t)\| \leq r_\epsilon$ implies that $V(t) < \infty$ (i.e., $V(t)$ is finite for any $t \geq 0$). Hence, the solutions of $\mathbf{q}_{12}(t)$ are uniformly ultimately bounded by r_ϵ, which further implies that $\mathbf{q}(t) \notin \Omega$ for all $t \geq 0$. □

Finding a suitable set of parameters r, ϵ, η_1, and θ_1 (or equivalently, $\bar{r}_1$) satisfying (7.11) and (7.12) can result in a long iterative process. The following claim introduces a more conservative yet simple set of inequalities constraints that will suffice to guarantee collision avoidance in a noncooperative scenario.

Corollary 7.3.1. *Assume* $\exists \ \eta_1 > \eta_2$, $\epsilon > 0$, *and* $\theta_1 \in \left(0, \sin^{-1}\left(\frac{\sqrt{r_\epsilon^2 - \Delta_1^2}}{r_\epsilon}\right)\right)$ *such that (7.11) and*

$$r \geq \max\left\{ r^*, \sqrt{\frac{\left(\alpha_1\left(1 + \frac{\eta_2}{\eta_1} e^{\frac{\theta_1(R_1-\Delta_1)}{\alpha_1}}\right) + \Delta_1(1-\cos\theta_1)\right)^2}{\sin^2\theta_1} + \Delta_1^2 - \epsilon} \right\} \tag{7.15}$$

are satisfied, where $\alpha_1 = \frac{\eta_1(\eta_1+\eta_2)}{\bar{\mu}_1}$. *Suppose that* $\mathbf{q}(0) \notin \mathcal{W}_1 \cup \Omega$, $\|\dot{\mathbf{q}}_1(0)\| \leq \eta_1$, *and* $\|\mathbf{d}_1(t)\| \leq \Delta_1$. *Then,* $\mathbf{q}(t) \notin \Omega \ \forall t \geq 0$.

Proof. The proof follows similar to that of Theorem 7.3.1. It is sufficient to show that $\beta_{12}(t) \geq \|\mathbf{q}_{12}(t)\| \, \eta_2$ for $\|\mathbf{q}_{12}(t)\| \to r_\epsilon$ when using the new inequality constraint in (7.15). Therefore, let us consider (7.10). Using (7.11) and (7.15) yields

$$\beta_{12}(t) \geq \|\mathbf{q}_{12}(t)\| \, \eta_2 e^{-k_1\delta_1} e^{\frac{\theta_1(R_1-\Delta_1)}{\alpha_1}} = \|\mathbf{q}_{12}(t)\| \, \eta_2 e^{\frac{\theta_1(R_1-\Delta_1-r_\epsilon)}{\alpha_1}} > \|\mathbf{q}_{12}(t)\| \, \eta_2.$$

Citing similar arguments as in Theorem 7.3.1, we then conclude that $\mathbf{q}(t) \notin \Omega \ \forall t \geq 0$. □

Up to now, we have addressed the case of noncooperative avoidance. The following theorem establishes a set of sufficient conditions under which cooperative collision avoidance can be claimed.

Theorem 7.3.2 (Cooperative Collision Avoidance with Uncertainties)**.** *Consider the two dynamical systems in (7.1) with control inputs (7.4) and (7.6). Let* $k_i = \frac{\bar{\mu}_i}{\eta_i}$ *and suppose* $\mathbf{q}(0) \notin \mathcal{W}_1 \cup \mathcal{W}_2 \cup \Omega$, $\|\dot{\mathbf{q}}_i(0)\| \leq \eta_i$, *and* $\|\mathbf{d}_i(t)\| \leq \Delta_i$ *for* $i \in \{1,2\}$. *Furthermore, assume that for* $i \in \{1,2\}$ *there exist*

$\eta_i > 0$, $r \geq r^*$, $\theta_i \in \left(0, \sin^{-1}\left(\frac{\sqrt{r_\epsilon^2 - \Delta_i^2}}{r_\epsilon}\right)\right)$ *and an arbitrarily small constant* $\epsilon > 0$ *such that*

$$\bar{r}_i = (\theta_i + 1)(r + \epsilon) < R_i - \Delta_i \tag{7.16}$$

and

$$\left(k_i + \frac{\omega_{ij}\Delta_i}{\sqrt{r_\epsilon^2 - \Delta_i^2}}\right) e^{k_i \delta_i} - \frac{r_\epsilon(k_i^2 + \omega_{ij}^2)}{k_i\sqrt{r_\epsilon^2 - \Delta_i^2}} \geq \left(k_i + \frac{\omega_{ij}\Delta_i}{\sqrt{r_\epsilon^2 - \Delta_i^2}}\right)\cos\theta_i + \left(\omega_{ij} - \frac{k_i\Delta_i}{\sqrt{r_\epsilon^2 - \Delta_i^2}}\right)\sin\theta_i \tag{7.17}$$

for all $i, j, i \neq j$. *Then,* $\mathbf{q}(t) \notin \Omega \; \forall t \geq 0$.

Proof. Consider (7.1) with control inputs (7.4) and (7.6). Since $k_i = \frac{\bar{\mu}_i}{\eta_i}$ and $\|\dot{\mathbf{q}}_i(0)\| \leq \eta_i$, we can apply Lemma 7.2.1 and conclude that $\|\dot{\mathbf{q}}_i(t)\| \leq \eta_i$ for all $i,\ t \geq 0$. Now, consider the Lyapunov candidate function in (7.13). The time derivative of (7.13) along the trajectories of (7.1) is given by

$$\dot{V}(t) = -\frac{\beta_{12}(t) + \beta_{21}(t)}{(\|\mathbf{q}_{12}(t)\|^2 - r^2)^3}. \tag{7.18}$$

Our approach to prove collision avoidance will be to show that $\beta_{ij}(t)$ is positive semi-definite for $i, j \in \{1, 2\},\ i \neq j$, which will be used to demonstrate that $\|\mathbf{q}_{ij}(t)\|$ is bounded from below. For simplicity, let us consider first the case of the ith agent. Assume that $\mathbf{q}(0) \notin \mathcal{W}_1 \cup \mathcal{W}_2 \cup \Omega$ and suppose that for some time $t \geq \delta_i > 0$, $\|\mathbf{q}_{12}(t)\| \to r + \epsilon = r_\epsilon$ from above. Following similar arguments as in Theorem 7.3.1, we have that it will take a time $\Delta t \geq \delta_i = \frac{\bar{r}_i - r_\epsilon}{\eta_i + \eta_j} = \frac{\theta_i r_\epsilon}{\eta_i + \eta_j}$ for the agents to approach each other from a distance $\bar{r}_i$ to a distance r_ϵ. Therefore, $[\mathbf{q}_i(\tau)^T, \mathbf{q}_j(\tau)^T]^T \in \mathcal{W}_i$ for $\tau \in [t - \delta_i, t]$. Consequently, we can apply Lemma 7.3.1 and, after some manipulation and use of (7.16) and (7.17), we can easily show that $\beta_{ij}(t) \geq 0$. Since the above result holds $\forall i, j, i \neq j$, we have that

$$\dot{V}(t) \leq 0, \qquad \text{for } \|\mathbf{q}_{12}(t)\| \leq r_\epsilon.$$

The fact that $\mathbf{q}_{12}(t)$ is continuous and $\dot{V}(t)$ is non-positive for $\|\mathbf{q}_{12}(t)\| \leq r_\epsilon$ implies that $V(t) < \infty$. Hence, we can conclude that $\mathbf{q}_{12}(t)$ is uniformly ultimately bounded by r_ϵ, which also means that $\mathbf{q}(t) \notin \Omega$ for all $t \geq 0$. □

Similar to the noncooperative case, obtaining a set of parameters conforming to (7.17) may require the use of extensive iteration. Therefore, it is in the designer's best interest to find simpler sufficient conditions that will guarantee collision avoidance. The following corollary provides such conditions for the cooperative case.

Corollary 7.3.2. *Assume* $\exists\ \epsilon > 0$ *and* $\theta_i \in \left(0, \sin^{-1}\left(\frac{\sqrt{r_\epsilon^2 - \Delta_i^2}}{r_\epsilon}\right)\right)$ *such that (7.16) holds and*

$$r \geq \max\left\{r^*, \sqrt{\left(\frac{\alpha_i + \Delta_i(1-\cos\theta_i)}{\sin\theta_i}\right)^2 + \Delta_i^2} - \epsilon\right\}, \qquad \forall i \in \{1,2\} \tag{7.19}$$

where $\alpha_i = \frac{\eta_i}{\mu_i}(\eta_i + \eta_j)$. *Suppose that* $\mathbf{q}(0) \notin \mathcal{W}_1 \cup \mathcal{W}_2 \cup \Omega$, $\|\mathbf{d}_i(t)\| \leq \Delta_i$, *and* $\|\dot{\mathbf{q}}_i(0)\| \leq \eta_i$. *Then,* $\mathbf{q}(t) \notin \Omega\ \forall t \geq 0$.

Proof. The proof follows similar to that of Corollary 7.3.1 and Theorem 7.3.2. It suffices to show that $\beta_{ij}(t) \geq 0$ when $\|\mathbf{q}_{ij}(t)\| \to r_\epsilon$ under the given assumptions. To this end, let us revisit (7.10). By substituting (7.19) into (7.10), we obtain that $\beta_{ij}(t) \geq 0$. Since this results holds $\forall i, j$ we can follow the proof of Theorem 7.3.2 and conclude that $\mathbf{q}(t) \notin \Omega\ \forall t \geq 0$. □

Note that the previous statements provide sufficient conditions for collision avoidance in non-cooperative and cooperative scenarios considering bounded sensing uncertainties. The statements require the existence of constants θ_i and r such that a series of inequalities are satisfied. Yet, we have not provided guidelines on how to optimally choose θ_i and r. In general, we would like to choose θ_i and r such that the extent of the Conflict Region is minimized. That is, we want to minimize the distance at which the agents start applying maximum avoidance control. Decreasing the size of $\bar{r}_i$ will reduce the attenuation on the objective control inside the Detection Region.

7.4 Simulation Examples

In this section we present two illustrative examples. The first example addresses a noncooperative avoidance control scenario between two agents. The second example evaluates the extension of the proposed control strategy to a cooperative group comprising four agents.

7.4.1 Example 1: Noncooperative Avoidance Control

Consider a pair of 2-DOF agents with double-integrator dynamics (7.1) and control inputs bounded by $\mu_1 = \mu_2 = 60$ m/s^2. Let the overall control input for both agents be given as in (7.4) with $k_1 = 7.5$ s^{-1} and $k_2 = 15.0$ s^{-1}. Then, the velocities of the first and second agent can be shown to be bounded by $\eta_1 = 4$ m/s and $\eta_2 = 2$ m/s, respectively. Now, consider the case where the first agent implements the proposed avoidance control law (7.6), whereas the second agent does not implement an avoidance strategy, i.e., $\mathbf{u}_2^a(t) = 0 \ \forall t \geq 0$. Assume the minimum separation distance and the detection radius for the first vehicle to be $r^* = 1$ m and $R_1 = 6$ m, respectively. Furthermore, consider the event in which the sensing uncertainty for the first agent is due to a constant sensing delay and is characterized by

$$\mathbf{d}_1(t) = -\int_{t-T_1}^{t} \dot{\mathbf{q}}_2(\tau) d\tau$$

where $T_1 = 0.40$ s denotes the detection delay. It is easy to verify that $\|\mathbf{d}_1\| \leq \Delta_1 = 0.8$ m. Then, the parameters for the avoidance control input $\mathbf{u}_1^a$ can be computed according to Theorem 7.3.1, which yields that the smallest conflict radius $\bar{r}_1$ is obtained when $\theta_1 = 0.81$ rad and $r + \epsilon = 1.94$ m. Choosing $\epsilon = 0.01$ m we obtain that $r = 1.93$ m and $\bar{r}_1 = 3.51$ m.

Finally, we take the objective control input for both agents to be computed as

$$\mathbf{u}_i^o = \begin{cases} \tilde{\mathbf{u}}_i^o, & \text{if } \|\tilde{\mathbf{u}}_i^o\| \leq \bar{\mu}_i = 30 \text{ m/s}^{-2} \\ \dfrac{\tilde{\mathbf{u}}_i^o}{\|\tilde{\mathbf{u}}_i^o\|}, & \text{otherwise} \end{cases}, \qquad \tilde{\mathbf{u}}_i^o = K_p(\mathbf{q}_i^d - \mathbf{q}_i) \tag{7.20}$$

where $\mathbf{q}_1^d = [8 \text{ m}, 7 \text{ m}]^T$ and $\mathbf{q}_2^d = [-8 \text{ m}, -8 \text{ m}]^T$ are the agents' desired final configurations and $K_p = 6$ s^{-1} is the control gain. The initial conditions for the system are set to $\mathbf{q}_1(0 \text{ s}) = [-7 \text{ m}, -8 \text{ m}]^T$, $\mathbf{q}_2(0 \text{ s}) = [8 \text{ m}, 8 \text{ m}]^T$, and $\dot{\mathbf{q}}_i(0 \text{ s}) = [0 \text{ m/s}, 0 \text{ m/s}]^T$. Therefore, the main control objective is to safely drive both systems to a point near each other's initial location.

The response of the two-agent system is illustrated in Figure 7.4. The agents start traveling toward each other near their respective maximum speed, according to their objective control laws. Once the second agent enters the first vehicle's conflict region, the first vehicle starts retreating in opposite direction to avoid a possible collision as illustrated in the right-hand side plot. Meanwhile, the second agent continues undisturbed toward its final destination. Once the second agent is out of the first agent's Detection Region, the first vehicle retakes its path toward its final configuration.

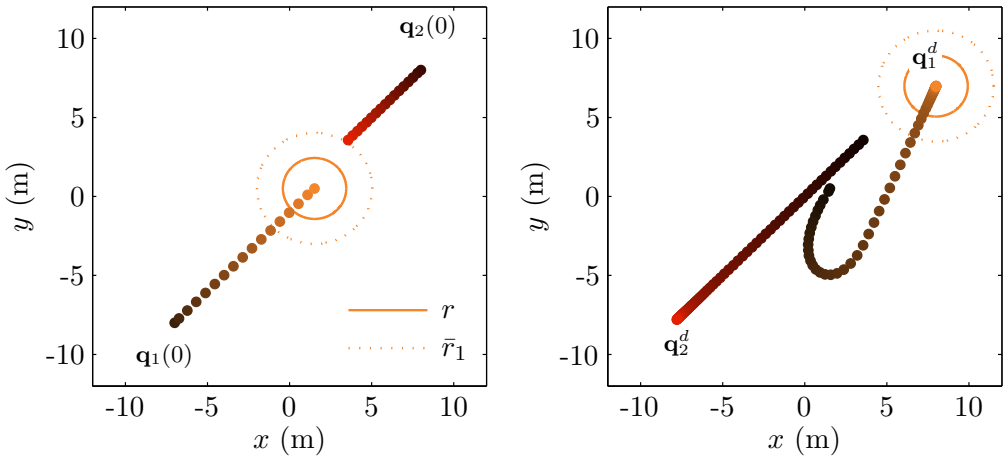

Figure 7.4: Noncooperative collision avoidance example. The left and right plots illustrate the motion of both agents in the intervals $t \in [0.0\text{ s}, 3.2\text{ s}]$ and $t \in [3.2\text{ s}, 20.0\text{ s}]$, respectively. The agents' positions at the initial time of each simulation step in both plots are denoted by the dark-colored circles. The Avoidance and Conflict Region for the first agent at the end of the simulation times are indicated by the solid and dotted lines (i.e., circles), respectively.

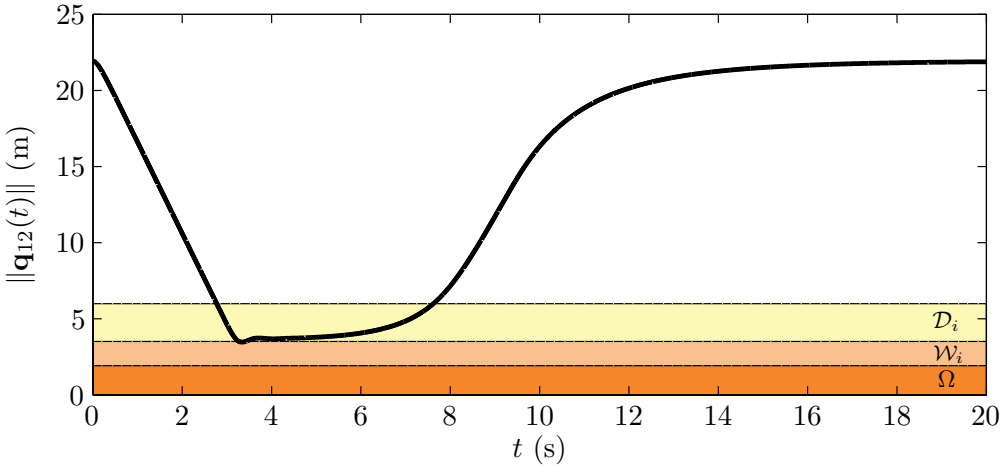

Figure 7.5: Distance between agents for the noncooperative collision avoidance example.

Figure 7.5 plots the distance between both agents at all times. As depicted in the plot, the first vehicle successfully evaded a collision with the other agent.

7.4.2 Example 2: Cooperative Avoidance Control for a Group of Four Agents

In this example, we evaluate a cooperative avoidance control scenario with four agents. The agents have 2-DOF with dynamics governed by (7.1); control inputs given as in (7.4) with $\mu_1 = \mu_2 = 60\text{ m/s}^2$, $\mu_3 = \mu_4 = 80\text{ m/s}^2$, $k_1 = k_2 = 7.5\text{ s}^{-1}$, and $k_3 = k_4 = 10.0\text{ s}^{-1}$; and velocities that can be shown to be equally bounded by $\eta_i = 4\text{ m/s}$. The avoidance control law $\mathbf{u}_i^a$ is considered to be an

extension of (7.6) and is computed as

$$\mathbf{u}_i^a = \begin{cases} \sum_{j,j\neq i}^4 \mathbf{u}_{ij}^a, & \text{if } \left\| \sum_{j,j\neq i}^4 \mathbf{u}_{ij}^a \right\| \leq \bar{\mu}_i \\ \bar{\mu}_i \dfrac{\sum_{j,j\neq i}^4 \mathbf{u}_{ij}^a}{\left\| \sum_{j,j\neq i}^4 \mathbf{u}_{ij}^a \right\|}, & \text{otherwise} \end{cases}$$

where

$$\mathbf{u}_{ij}^a = \begin{cases} \mathbf{0}, & \text{if } \|\mathbf{q}_i - \hat{\mathbf{q}}_j\| \geq R_i \\ \dfrac{K_i^a (R_i^2 - \|\mathbf{q}_i - \hat{\mathbf{q}}_j\|^2)}{(\|\mathbf{q}_i - \hat{\mathbf{q}}_j\|^2 - r^2)^3} (\mathbf{q}_i - \hat{\mathbf{q}}_j), & \text{if } r < \|\mathbf{q}_i - \hat{\mathbf{q}}_j\| < R_i \\ \bar{\mu}_i \dfrac{\mathbf{q}_i - \hat{\mathbf{q}}_j}{\|\mathbf{q}_i - \hat{\mathbf{q}}_j\|}, & \text{if } 0 < \|\mathbf{q}_i - \hat{\mathbf{q}}_j\| \leq r \\ \text{not defined}, & \text{if } \|\mathbf{q}_i - \hat{\mathbf{q}}_j\| = 0 \end{cases}.$$

The reader can easily verify that the above control law simplifies to (7.6) when there is only one agent inside the detection zone. It is assumed that the minimum separation distance and the detection radii for all agents is $r^* = 1$ m and $R_i = 5$ m, respectively. We further assume that each agent can sample the position of other agents and obstacles with a frequency of $f_s = 10$ Hz and subjected to an additional constant process delay of $T_s = 0.20$ s as well as a random noise $\boldsymbol{\zeta}_i$ with uniform distribution on the subset $\mathcal{Z}_i = \{\boldsymbol{\zeta}_i : \boldsymbol{\zeta}_i \in \Re^2, \|\boldsymbol{\zeta}_i\| < 0.3 \text{ m}\}$. Therefore, the sensing uncertainties for the agents can be bounded by

$$\|\mathbf{d}_i(t)\| \leq \Delta_i = \underbrace{T_s \max_{j\neq i}\{\eta_j\}}_{\substack{\text{Constant Delay} \\ 0.8 \text{ m}}} + \underbrace{f_z^{-1} \max_{j\neq i}\{\eta_j\}}_{\substack{\text{Zero-Order-Hold} \\ 0.4 \text{ m}}} + \underbrace{\sup_{t\geq 0} \|\boldsymbol{\zeta}_i(t)\|}_{\substack{\text{Noise} \\ 0.3 \text{ m}}} = 1.5 \text{ m}.$$

The control parameters are computed according to Theorem 7.3.2 as $r + \epsilon = 2.07$ m, $\theta_1 = \theta_2 = 0.57$ rad, and $\theta_3 = \theta_4 = 0.50$ rad. By choosing $\epsilon = 0.01$ m we then have that $r = 2.06$ m, $\bar{r}_1 = \bar{r}_2 = 3.25$ rad, and $\bar{r}_3 = \bar{r}_4 = 2.85$ rad. Finally, the objective control input for all agents is taken as in (7.20) with $K_p = 8$ s^{-2}, $\mathbf{q}_1^d = [0 \text{ m}, 0 \text{ m}]^T$, $\mathbf{q}_2^d = [10 \text{ m}, 10 \text{ m}]^T$, $\mathbf{q}_3^d = [-8 \text{ m}, 10 \text{ m}]^T$, and $\mathbf{q}_4^d = [-10 \text{ m}, -10 \text{ m}]^T$. The four agents are initialized from rest with $\mathbf{q}_1(0 \text{ s}) = [0 \text{ m}, 0 \text{ m}]^T$, $\mathbf{q}_2(0 \text{ s}) = [-10 \text{ m}, -10 \text{ m}]^T$, $\mathbf{q}_3(0 \text{ s}) = [10 \text{ m}, -8 \text{ m}]^T$ and $\mathbf{q}_4(0 \text{ s}) = [10 \text{ m}, 10 \text{ m}]^T$.

Figure 7.6 shows the response of the multi-agent system. As can be seen from the left-top graph; the second, third, and fourth agents start moving toward the center of the graph according to their

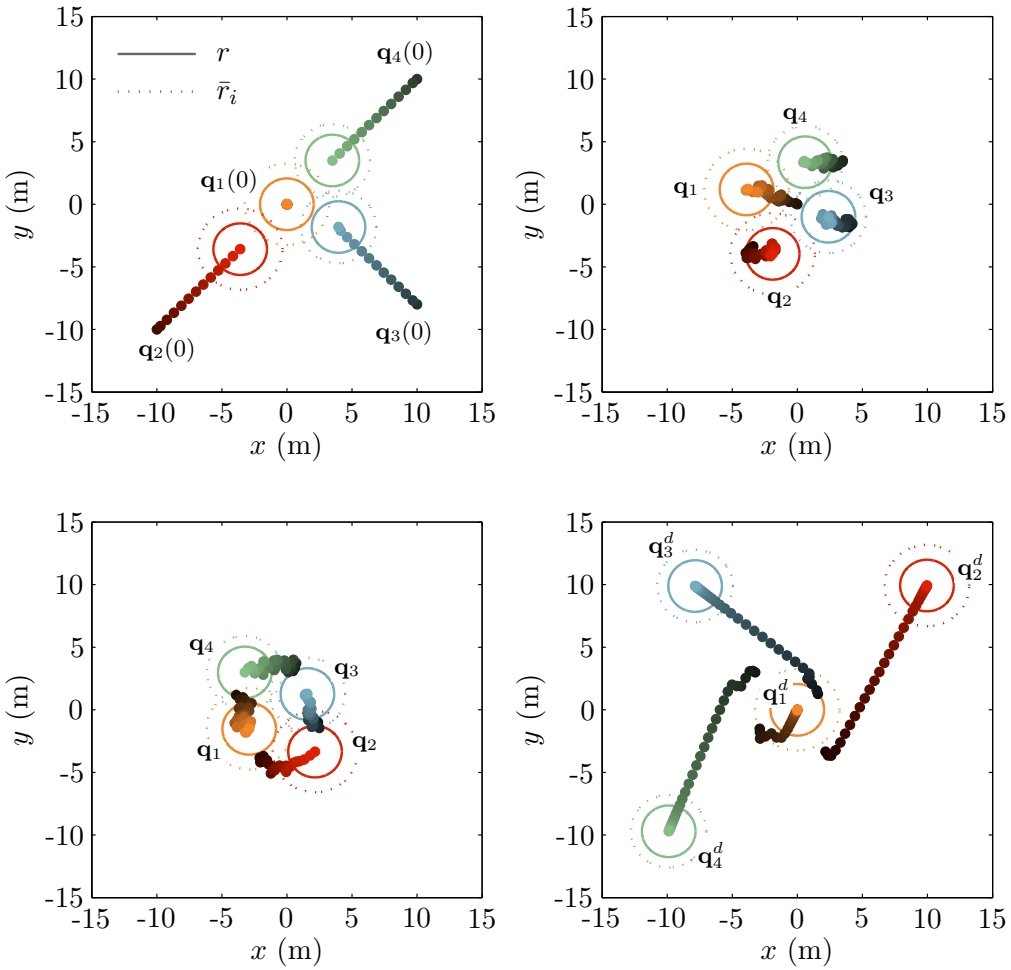

Figure 7.6: Cooperative collision avoidance example. The left-top, right-top, left-bottom, and right-bottom plots illustrate the motion of the four agents in the intervals $t \in [0.0\text{ s}, 2.4\text{ s}]$, $t \in [2.4\text{ s}, 8.0\text{ s}]$, $t \in [8.0\text{ s}, 13.4\text{ s}]$, and $t \in [13.4\text{ s}, 25.0\text{ s}]$, respectively.

corresponding objective control inputs, while the first agent remains stationary at the center in agreement with its control goal. As soon as the agents enter each other's detection and, eventually, conflict regions, all vehicles slow down their motion and start moving in counter-clockwise direction to avoid a collision (see right-top and left-bottom plots). Once the conflict has been resolved, each agent retakes its course toward its final destination, as illustrated in the right-bottom plot of Figure 7.6. The distance among all agents is illustrated in Figure 7.7. None of the agents entered the avoidance region, which implies that no collision took place despite sensing uncertainties of up to 1.5 m.

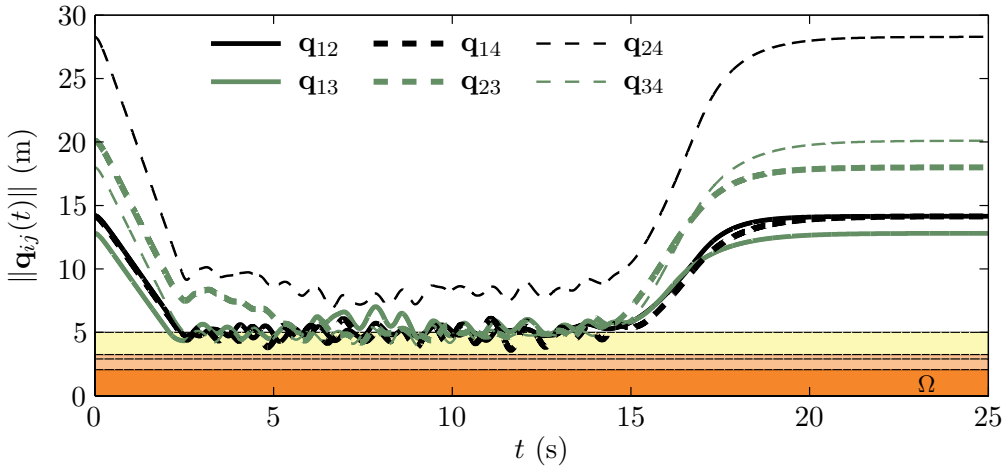

Figure 7.7: Distances among agents for the cooperative collision avoidance example.

7.5 A Cooperative Collision Avoidance Experimental Example

In addition to the previous two examples, we now present experimental results obtained by applying the proposed collision avoidance control law to a pair of unmanned vehicles. The vehicles, illustrated in Figure 7.8, are two E-Flite μ-CX coaxial helicopters with a 0.190 m of rotor diameter and 0.200 m of length. The 3-DOF linearized and simplified models for the two aircraft when in hover are assumed to be identical and given by

$$\ddot{\mathbf{q}}_i(t) = \frac{\bar{\mathbf{u}}_i(t)}{m} = \mathbf{u}_i(t) \tag{7.21}$$

where $m = 0.028$ kg and $\mathbf{q}_i(t) = [x_i(t), y_i(t), z_i(t)]$ (rotational motion around the z axis, i.e., yaw, has been ignored). The helicopters' control inputs are assumed to be limited by $\mu_i = 6$ m/s^2. The minimum safety distance between both vehicles is $r^* = 0.200$ m and the detection radii for the agents are $R_i = 1.210$ m. Uncertainties are considered to originate due to a communication sensing delay almost equal for the two vehicles and which fluctuates between 0.48 s and 0.50 s. The maximum attained velocity reported for both aircraft at maximum constant control $\bar{\mu}_i = 3$ m/s^2 with $k_i = 7.0$ s^{-1} was $\eta_i = 0.6$ m/s. Therefore, sensing uncertainties Δ_i can be estimated to be upper bounded by 0.300 m. The collision avoidance control parameters, chosen according to Theorem 7.3.2 for $\epsilon = 10^{-3}$ m and $\theta_i = 0.73$ rad, are $r = 0.440$ m and $\bar{r}_i = 0.760$ m. The objective

Figure 7.8: Two E-Flite μ-CX coaxial helicopters. Copyright © 2010 Boeing. All rights reserved.

control input is a Proportional-type controller as in (7.20) with gain

$$K_p = \begin{bmatrix} 3.8 & 0 & 0 \\ 0 & 3.8 & 0 \\ 0 & 0 & 1.5 \end{bmatrix} \times 10^{-3}\ \mathrm{s}^{-2}$$

and desired configurations $\mathbf{q}_1^d = [0.9\ \mathrm{m}, 0.0\ \mathrm{m}, 0.6\ \mathrm{m}]$ and $\mathbf{q}_2^d = [-0.9\ \mathrm{m}, 0.0\ \mathrm{m}, 0.6\ \mathrm{m}]$.

The response of the two helicopters in Cartesian coordinates[2] x, y, and z is illustrated in Figure 7.9. The aircraft initialize from opposite positions and start traveling toward each other according to the objective control (see left-top plot). As they enter each other's Conflict Regions, the two vehicles decelerate while trying to solve the potential conflict. As noted in the right-top plot of Figure 7.9, after their initial retreat, the agents approached each other once again coming relatively close to their Avoidance Regions. Eventually, the vehicles are able to safely resolve the conflict and continue toward their final destinations (see left- and right-bottom plots). Figure 7.10, which depicts the 2-norm of the distance between both agents, confirms that the two vehicles successfully evaded entering each other's Avoidance Region. Note that the shortest distance between both aircraft took place at $t = 6.04$ s.

[2]The z axis represents vertical motion. See Figure 7.8 for reference.

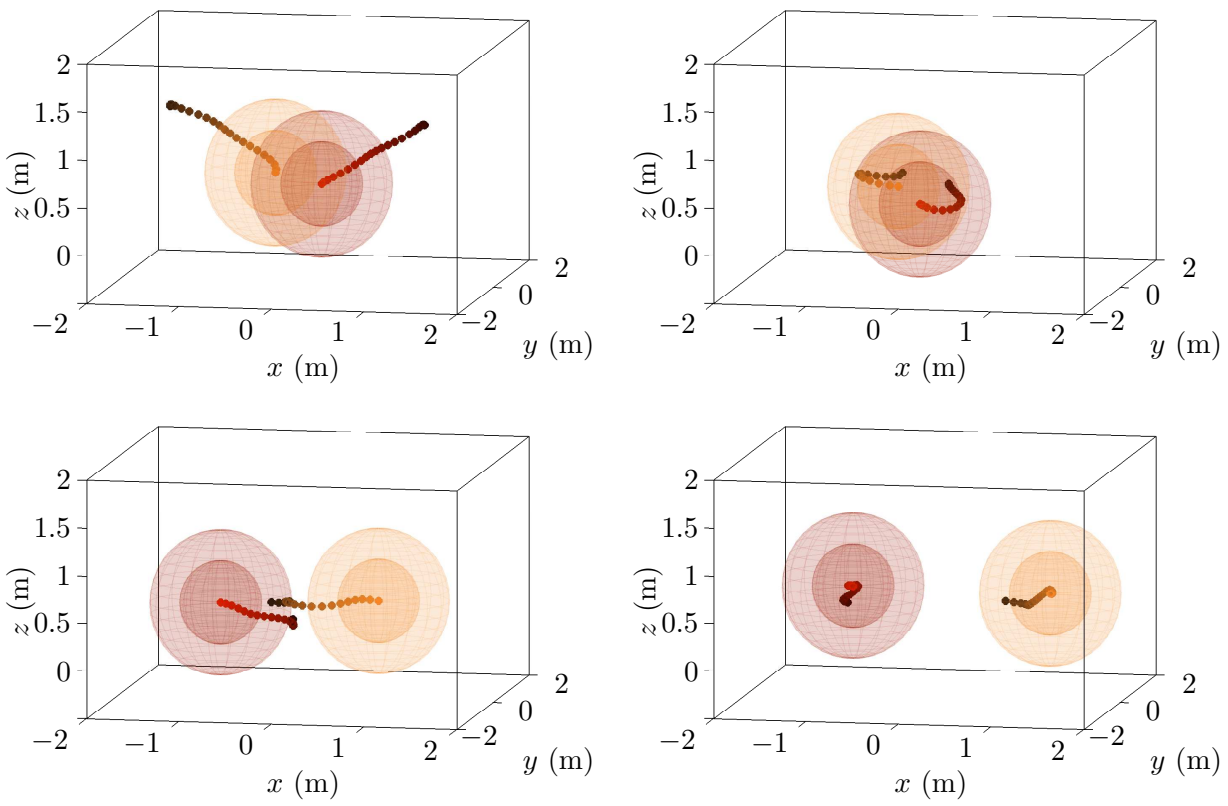

Figure 7.9: Cooperative collision avoidance experimental example. The left-top, right-top, left-bottom, and right-bottom plots illustrate the motion in 3-D for the two aircraft in the intervals $t \in [0.00\text{ s}, 3.66\text{ s}]$, $t \in [3.66\text{ s}, 6.04\text{ s}]$, $t \in [6.04\text{ s}, 9.87\text{ s}]$, and $t \in [9.87\text{ s}, 12.98\text{ s}]$, respectively. The position of the first helicopter, time-spaced by approximately 0.18 s, is represented by the orange circular markers, whereas the position information of the second agent is traced with red markers. Positions at the initial time of each plotted interval are indicated by the darker-colored markers. The agents' Avoidance and Conflict Regions at the end of each plotted interval are depicted by the inner and outer translucent spheres, respectively.

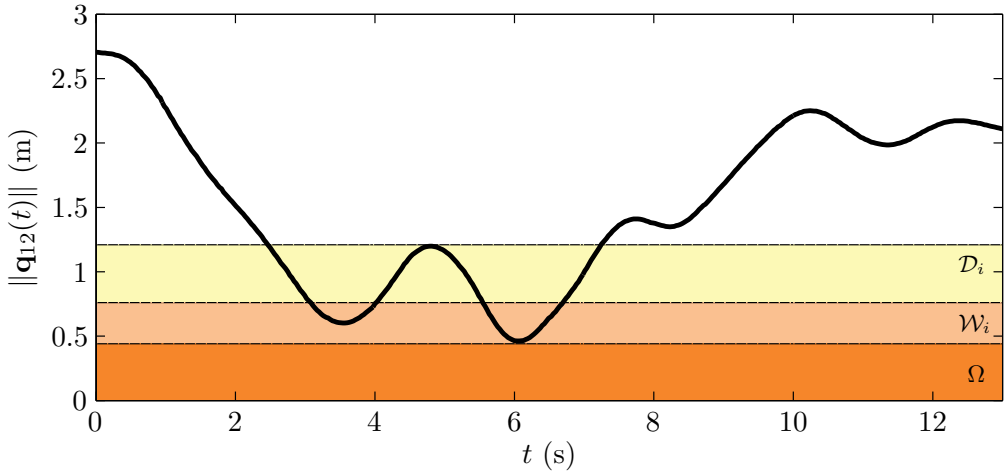

Figure 7.10: Norm of the distance between the two helicopters.

CHAPTER 8

COLLISION AVOIDANCE CONTROL: MULTI-AGENT SYSTEMS

Continuing with the topic of collision avoidance under sensing uncertainties and detection delays, we now formally extend the avoidance control ideas presented in the previous chapter to a group of N Lagrangian systems. We design decentralized, real-time, cooperative avoidance control laws and provide sufficient conditions to guarantee collision-free trajectories under the presence of bounded sensing uncertainties and limited control inputs.

8.1 Multi-Lagrangian System with Bounded Control Inputs and Sensing Uncertainties

In this chapter, we address the task of controlling a group of N n-DOF vehicles with nonlinear Lagrangian dynamics given by

$$M_i(\mathbf{q}_i(t))\ddot{\mathbf{q}}_i(t) + C_i(\mathbf{q}_i(t), \dot{\mathbf{q}}_i(t))\dot{\mathbf{q}}_i(t) = \mathbf{u}_i(t) \tag{8.1}$$

where $\mathbf{q}_i \in \Re^n$ are the generalized coordinates, $M_i \in \Re^{n\times n}$ are the positive definite inertia matrices, $C_i \in \Re^{n\times n}$ are the centrifugal and Coriolis matrices, and $\mathbf{u}_i \in \mathcal{U}_i \subset \Re^n$ are the control inputs for $i = \{1, \cdots, N\}$. We assume that gravitational forces are negligible or compensated via active control and that the magnitudes of the control inputs are radially bounded, i.e., $\exists \mu_i > 0$ such that $\|\mathbf{u}_i(t)\| \leq \mu_i \ \forall i \in \{1, \cdots, N\},\ t \geq 0$. Moreover, we assume that each agent can locate other near agents with a known bounded error. That is, we suppose that the ith agent is able to sense the jth agent as being located at $\hat{\mathbf{q}}_j^i(t) = \mathbf{q}_j(t) + \mathbf{d}_{ij}(t)$ whenever the jth agent is sufficiently close to the ith agent. The time-varying vector $\mathbf{d}_{ij} \in \Re^n$ represents the uncertainty on the localization process (e.g., delays, noise, and quantization) and is considered to be upper bounded by some positive constant Δ_i, i.e., $\|\mathbf{d}_{ij}(t)\| \leq \Delta_i,\ \forall t \geq 0$ and $j \neq i$.

Finally, we make the assumption that the dynamics of the agents satisfy Properties 2.2.1 to 2.2.3.

8.2 Control Objective and Definitions

Our control goal is to design decentralized collision avoidance strategies that guarantee the safe navigation of a group of vehicles with sensing uncertainties. Specifically, we would like to guarantee a minimum safe distance between any two vehicles at all times independently of measurement errors, delays, and noise incurred in the detection process. Additionally, we would like to design the avoidance control strategy to be active only when another vehicle or obstacle is within a short distance. With this notion of relative distances in mind, we recall the following definitions from Chapters 6 and 7.

First, we define the group $\mathcal{N}_i$ as the set of agents in the vicinity of the ith vehicle. We assume that any jth agent in $\mathcal{N}_i$ can be located by the ith vehicle if the former lies within the bounded *Detection Region*, $\mathcal{D}_{ij}$, of the latter given as

$$\mathcal{D}_{ij} = \left\{\mathbf{q} : \mathbf{q} \in \Re^{2n}, \|\mathbf{q}_i - \mathbf{q}_j\| \leq R_i\right\}$$

where $R_i > 0$ is the ith vehicle's detection radius and $\mathbf{q}(t) = [\mathbf{q}_i^T(t), \mathbf{q}_j^T(t)]^T$. In addition, we define an *Antitarget Region*, $\mathcal{T}_{ij}$, as the collision zone for the ith agent, i.e.,

$$\mathcal{T}_{ij} = \left\{\mathbf{q} : \mathbf{q} \in \Re^{2n}, \|\mathbf{q}_i - \mathbf{q}_j\| \leq r_{ij}^*\right\}$$

where $r_{ij}^* \in (0, R_i)$ is the minimum safe distance between the ith vehicle and any jth agent in $\mathcal{N}_i$. Similarly, we define an *Avoidance Region*, $\Omega_{ij} \supseteq \mathcal{T}_{ij}$, as a restricted zone for which any agent in $\mathcal{N}_i$ is forbidden. That is,

$$\Omega_{ij} = \left\{\mathbf{q} : \mathbf{q} \in \Re^{2n}, \|\mathbf{q}_i - \mathbf{q}_j\| \leq r_{ij}\right\}$$

where $r_{ij} \in [r_{ij}^*, R_i)$ is the desired minimum distance between the ith and jth agents. Therefore, any collision avoidance strategy designed to avoid Ω_{ij}, will also avoid $\mathcal{T}_{ij}$.

Finally, since the control input and acceleration for the ith vehicle are bounded, any collision avoidance control law must be effected with enough anticipation, such that the ith vehicle has sufficient time to decelerate and prevent a collision. Hence, we define a *Conflict Region*, $\mathcal{W}_{ij}$, as

$$\mathcal{W}_{ij} = \left\{\mathbf{q} : \mathbf{q} \in \Re^{2n}, r_{ij} < \|\mathbf{q}_i - \mathbf{q}_j\| \leq \bar{r}_{ij}\right\}$$

where $\bar{r}_{ij} \in (r_{ij}, R_i)$ is a lower bound on the distance that the ith agent can come from the jth vehicle and still be able to decelerate and avoid Ω_{ij}. Therefore, any collision avoidance strategy for the ith agent must take effect as soon as $\mathbf{q}_i$ and $\mathbf{q}_j$ enter $\mathcal{W}_{ij}$.

Having defined the Antitarget, Avoidance, Conflict, and Detection regions, we can state the control objective as follows. Given $\{\Delta_1, \cdots, \Delta_N\}$, $\mathcal{T} = \bigcup_{i\in N, j\in\mathcal{N}_i} \mathcal{T}_{ij}$, and $\mathcal{D} = \bigcup_{i\in N, j\in\mathcal{N}_i} \mathcal{D}_{ij}$, design control inputs $\{\mathbf{u}_i(t), \cdots, \mathbf{u}_N(t)\}$ such that $[\mathbf{q}_1^T(t), \cdots, \mathbf{q}_N^T(t)]^T \notin \Omega = \bigcup_{i\in N, j\in\mathcal{N}_i} \Omega_{ij}$ for all $t \geq 0$, where $\Omega \supseteq \mathcal{T}$.

For simplicity, we define $R = \min_i\{R_i\}$, $r^* = \max_i\{r_{ij}^*\}$, and $\Delta = \max_i\{\Delta_i\}$, and let $\bar{r}_{ij} = \bar{r}$ $\forall i \in \{1, \cdots, N\}$, $j \in \mathcal{N}_i$.

8.3 Control Framework

In order to achieve our control objective, we consider the following control input

$$\mathbf{u}_i = \mathbf{u}_i^o + \mathbf{u}_i^a, \qquad \|\mathbf{u}_i\| \leq \mu_i \tag{8.2}$$

where $\mathbf{u}_i^o$ and $\mathbf{u}_i^a$ are the objective and collision avoidance control laws, respectively. The objective input is taken to be a stable control law designed to achieve a particular task such as trajectory tracking or set-point regulation. The collision avoidance input is a control policy aimed to guarantee collision-free transit among agents independently of bounded sensing uncertainties. Ideally, $\mathbf{u}_i^a$ must be designed such that it does not interfere with the objective control $\mathbf{u}_i^o$ when no potential collision is present.

According to this formulation, we propose the objective control law to be computed as

$$\mathbf{u}_i^o = -\bar{\mu}_i \frac{\partial V_i^o(\mathbf{q}_i)}{\partial \mathbf{q}_i} \tag{8.3}$$

where V_i^o is an objective function satisfying the following two properties.

Property 8.3.1. *$0 \leq V_i^o(\mathbf{q}_i) \leq \alpha_i$, for some $\alpha_i > 0$.*

Property 8.3.2. *$\|\partial V_i^o(\mathbf{q}_i)/\partial \mathbf{q}_i\| \leq \beta_i$, for some $\beta_i > 0$.*

On the other hand, we propose the collision avoidance control to be given as

$$\mathbf{u}_i^a = -\bar{\mu}_i \sum_{j\in\mathcal{N}_i} \frac{\partial V_{ij}^a(\mathbf{q}_i, \hat{\mathbf{q}}_j^i)}{\partial \mathbf{q}_i} - \sum_{j\in\mathcal{N}_i} \gamma_i \theta_{ij}(\dot{\mathbf{q}}_i, \mathbf{q}_i, \hat{\mathbf{q}}_j^i) \frac{\dot{\mathbf{q}}_i}{\|\dot{\mathbf{q}}_i\|} \tag{8.4}$$

where

$$\bar{\mu}_i = \frac{\mu_i}{N - 1 + \varepsilon + \beta_i}, \tag{8.5}$$

$$\gamma_i = \varepsilon \bar{\mu}_i, \tag{8.6}$$

$$\theta_{ij}(\dot{\mathbf{q}}_i, \mathbf{q}_i, \hat{\mathbf{q}}_j^i) = \begin{cases} \frac{1}{N-1}, & \text{if } \|\dot{\mathbf{q}}_i\| > 0 \text{ and } \left\|\mathbf{q}_i - \hat{\mathbf{q}}_j^i\right\| \leq R \\ 0, & \text{otherwise} \end{cases} \tag{8.7}$$

for some $\varepsilon \in [0, 1)$ (ideally $\varepsilon < \underline{\beta}$, where $\underline{\beta} = \min_i\{\beta_i\}$). The avoidance function V_{ij}^a, illustrated in Figure 8.1, is defined as

$$V_{ij}^a(\mathbf{q}_i, \mathbf{q}_j) = \begin{cases} \frac{R_\Delta + h}{2} - \|\mathbf{q}_i - \mathbf{q}_j\|, & \text{if } \|\mathbf{q}_i - \mathbf{q}_j\| \leq h \\ \frac{(\|\mathbf{q}_i - \mathbf{q}_j\| - R_\Delta)^2}{2(R_\Delta - h)}, & \text{if } h < \|\mathbf{q}_i - \mathbf{q}_j\| \leq R_\Delta \\ 0, & \text{otherwise} \end{cases} \tag{8.8}$$

where $R_\Delta = R - \Delta$ and $h = \bar{r} + \Delta < R_\Delta$. The reader can easily verify that V_{ij}^a is positive semi-definite, almost everywhere continuously differentiable, and that its partial derivative is given by

$$\frac{\partial V_{ij}^a(\mathbf{q}_i, \mathbf{q}_j)}{\partial \mathbf{q}_i} = \begin{cases} \mathbf{0}, & \text{if } \|\mathbf{q}_i - \mathbf{q}_j\| > R_\Delta \\ \left(1 - \frac{R_\Delta}{\|\mathbf{q}_i - \mathbf{q}_j\|}\right) \frac{\mathbf{q}_i - \mathbf{q}_j}{R_\Delta - h}, & \text{if } h < \|\mathbf{q}_i - \mathbf{q}_j\| \leq R_\Delta \\ -\frac{\mathbf{q}_i - \mathbf{q}_j}{\|\mathbf{q}_i - \mathbf{q}_j\|}, & \text{if } 0 < \|\mathbf{q}_i - \mathbf{q}_j\| \leq h \\ \text{not defined}, & \text{if } \|\mathbf{q}_i - \mathbf{q}_j\| = 0 \end{cases}. \tag{8.9}$$

Note that in contrast to the avoidance function and control inputs in [102], both V_{ij}^a and $\mathbf{u}_i^a$ (proposed herein and depicted in Figure 8.1) are bounded. Moreover, as the next lemma will show, the gradient of the avoidance function (8.9) is locally Lipschitz.

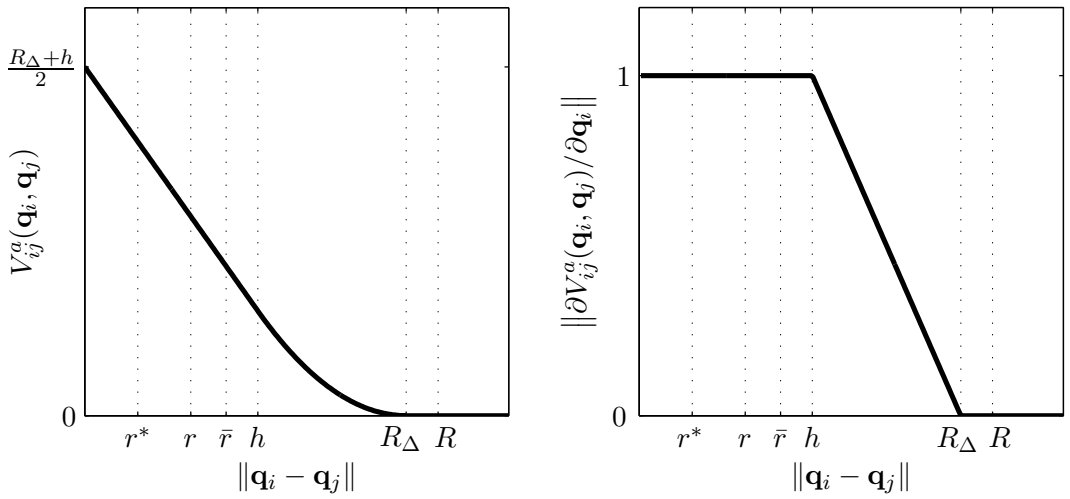

Figure 8.1: Bounded avoidance function and bounded avoidance control.

Lemma 8.3.1. *The gradient $\partial V_{ij}^a(\mathbf{q}_i,\mathbf{q}_j)/\partial\mathbf{q}_i$ is Lipschitz continuous for all $\mathbf{q}_j \in \mathcal{X} = \{\mathbf{q}_j : \mathbf{q}_j \in \Re^n, \|\mathbf{q}_i-\mathbf{q}_j\| \geq r-\Delta\}$ with Lipschitz constant given by*

$$L = \max\left\{\frac{3+2\sqrt{n-1}}{4(r-\Delta)}, \min\left\{\frac{1}{h}+\frac{R_\Delta\sqrt{n}}{h(R_\Delta-h)}, \frac{1}{R_\Delta-h}+\frac{(3+2\sqrt{n-1})R_\Delta}{4h(R_\Delta-h)}\right\}\right\}. \tag{8.10}$$

Proof. Let a_{kl} denote the klth entry of $\frac{\partial^2 V_{ij}^a(\mathbf{q}_i,\mathbf{q}_j)}{\partial\mathbf{q}_i\partial\mathbf{q}_j}$. Then, we have that (8.9) is locally Lipschitz continuous on $\Re^n \times \mathcal{X}$ if

$$\left\|\frac{\partial^2 V_{ij}^a(\mathbf{q}_i,\mathbf{q}_j)}{\partial\mathbf{q}_i\partial\mathbf{q}_j}\right\| = \left\|[a_{kl}]_{n\times n}\right\| \leq L$$

for some nonnegative constant L, except possibly on a set of Lebesgue measure zero. In addition, since $\partial^2 V_{ij}^a(\mathbf{q}_i,\mathbf{q}_j)/\partial\mathbf{q}_i\partial\mathbf{q}_j$ is symmetric, we have that

$$\left\|\frac{\partial^2 V_{ij}^a(\mathbf{q}_i,\mathbf{q}_j)}{\partial\mathbf{q}_i\partial\mathbf{q}_j}\right\|_\infty = \max_k \sum_{l=1}^n |a_{kl}| = \max_l \sum_{k=1}^n |a_{kl}| = \left\|\frac{\partial^2 V_{ij}^a(\mathbf{q}_i,\mathbf{q}_j)}{\partial\mathbf{q}_i\partial\mathbf{q}_j}\right\|_1$$

and, therefore,

$$\left\|\frac{\partial^2 V_{ij}^a(\mathbf{q}_i,\mathbf{q}_j)}{\partial\mathbf{q}_i\partial\mathbf{q}_j}\right\| \leq \sqrt{\left\|\frac{\partial^2 V_{ij}^a(\mathbf{q}_i,\mathbf{q}_j)}{\partial\mathbf{q}_i\partial\mathbf{q}_j}\right\|_1 \left\|\frac{\partial^2 V_{ij}^a(\mathbf{q}_i,\mathbf{q}_j)}{\partial\mathbf{q}_i\partial\mathbf{q}_j}\right\|_\infty} = \left\|\frac{\partial^2 V_{ij}^a(\mathbf{q}_i,\mathbf{q}_j)}{\partial\mathbf{q}_i\partial\mathbf{q}_j}\right\|_1.$$

Hence, the Lipschitz constant L is invariant under the use of $\|\cdot\|_1$, $\|\cdot\|$, or $\|\cdot\|_\infty$.

Now, let us divide the problem in three domains: $\mathcal{X}_1 = \{\mathbf{q}_j : \mathbf{q}_j \in \Re^n, r - \Delta \leq \|\mathbf{q}_i - \mathbf{q}_j\| < h\}$, $\mathcal{X}_2 = \{\mathbf{q}_j : \mathbf{q}_j \in \Re^n, h < \|\mathbf{q}_i - \mathbf{q}_j\| < R_\Delta\}$, and $\mathcal{X}_3 = \{\mathbf{q}_j : \mathbf{q}_j \in \Re^n, \|\mathbf{q}_i - \mathbf{q}_j\| > R_\Delta\}$.

For $\mathbf{q}_i = [q_{i_1}, \cdots, q_{i_n}]^T \in \Re^n$ and $\mathbf{q}_j = [q_{j_1}, \cdots, q_{j_n}]^T \in \mathcal{X}_1$ we have that

$$\left\| \frac{\partial^2 V_{ij}^a(\mathbf{q}_i, \mathbf{q}_j)}{\partial \mathbf{q}_i \partial \mathbf{q}_j} \right\|_1 = \max_l \sum_{k=1}^{n} |a_{kl}|$$

where

$$a_{kl} = \begin{cases} \dfrac{\|\mathbf{q}_i - \mathbf{q}_j\|^2 - (q_{i_k} - q_{j_k})^2}{\|\mathbf{q}_i - \mathbf{q}_j\|^3}, & \text{if } k = l \\ \dfrac{-(q_{i_k} - q_{j_k})(q_{i_l} - q_{j_l})}{\|\mathbf{q}_i - \mathbf{q}_j\|^3}, & \text{if } k \neq l \end{cases}.$$

Therefore,

$$\begin{aligned} \left\| \frac{\partial^2 V_{ij}^a(\mathbf{q}_i, \mathbf{q}_j)}{\partial \mathbf{q}_i \partial \mathbf{q}_j} \right\|_1 \leq & \frac{\left| \|\mathbf{q}_i - \mathbf{q}_j\|^2 - |q_{i_l} - q_{j_l}|^2 \right| + |q_{i_l} - q_{j_l}| \sum_{k=1, k\neq l}^{n} |q_{i_k} - q_{j_k}|}{\|\mathbf{q}_i - \mathbf{q}_j\|^3} \\ = & \frac{\|\mathbf{q}_i - \mathbf{q}_j\|^2 - |q_{i_l} - q_{j_l}|^2 + \sqrt{n-1}\,|q_{i_l} - q_{j_l}|\,\|\mathbf{q}_i - \mathbf{q}_j\|}{\|\mathbf{q}_i - \mathbf{q}_j\|^3} \end{aligned}$$

It is easy to prove that the numerator is maximized when $|q_{i_l} - q_{j_l}| = \frac{\|\mathbf{q}_i - \mathbf{q}_j\|}{2}$. Hence,

$$\left\| \frac{\partial^2 V_{ij}^a(\mathbf{q}_i, \mathbf{q}_j)}{\partial \mathbf{q}_i \partial \mathbf{q}_j} \right\|_1 \leq \frac{\|\mathbf{q}_i - \mathbf{q}_j\|^2 + \frac{\sqrt{n-1}}{2}\|\mathbf{q}_i - \mathbf{q}_j\|^2 - \frac{1}{4}\|\mathbf{q}_i - \mathbf{q}_j\|^2}{\|\mathbf{q}_i - \mathbf{q}_j\|^3} = \frac{3 + 2\sqrt{n-1}}{4\,\|\mathbf{q}_i - \mathbf{q}_j\|}$$

and

$$\left\| \frac{\partial^2 V_{ij}^a(\mathbf{q}_i, \mathbf{q}_j)}{\partial \mathbf{q}_i \partial \mathbf{q}_j} \right\| = \left\| \frac{\partial^2 V_{ij}^a(\mathbf{q}_i, \mathbf{q}_j)}{\partial \mathbf{q}_i \partial \mathbf{q}_j} \right\|_1 \leq L_1 = \frac{3 + 2\sqrt{n-1}}{4(r - \Delta)}, \qquad \text{for } \mathbf{q}_i \in \Re^n, \mathbf{q}_j \in \mathcal{X}_1.$$

Similarly, for the domain $\Re^n \times \mathcal{X}_2$ we have that

$$a_{kl} = \begin{cases} \dfrac{-\|\mathbf{q}_i - \mathbf{q}_j\|^3 + R_\Delta\|\mathbf{q}_i - \mathbf{q}_j\|^2 - R_\Delta(q_{i_k} - q_{j_k})^2}{(R_\Delta - h)\|\mathbf{q}_i - \mathbf{q}_j\|^3}, & \text{if } k = l \\ \dfrac{-R_\Delta(q_{i_k} - q_{j_k})(q_{i_l} - q_{j_l})}{(R_\Delta - h)\|\mathbf{q}_i - \mathbf{q}_j\|^3}, & \text{if } k \neq l \end{cases}.$$

Therefore,

$$\begin{aligned}\left\|\frac{\partial^2 V_{ij}^a(\mathbf{q}_i,\mathbf{q}_j)}{\partial \mathbf{q}_i \partial \mathbf{q}_j}\right\|_1 \leq & \frac{\|\mathbf{q}_i-\mathbf{q}_j\|^2 (R_\Delta - \|\mathbf{q}_i-\mathbf{q}_j\|) + R_\Delta \, |q_{i_l}-q_{j_l}| \sum_{k=1}^n |q_{i_k}-q_{j_k}|}{(R_\Delta - h)\|\mathbf{q}_i-\mathbf{q}_j\|^3} \\ \leq & \frac{\|\mathbf{q}_i-\mathbf{q}_j\|^2 (R_\Delta - \|\mathbf{q}_i-\mathbf{q}_j\|) + R_\Delta \, \|\mathbf{q}_i-\mathbf{q}_j\| \, \|\mathbf{q}_i-\mathbf{q}_j\|_1}{(R_\Delta - h)\|\mathbf{q}_i-\mathbf{q}_j\|^3} \\ \leq & \frac{R_\Delta - \|\mathbf{q}_i-\mathbf{q}_j\| + R_\Delta\sqrt{n}}{(R_\Delta - h)\|\mathbf{q}_i-\mathbf{q}_j\|} \\ = & \frac{1}{R_\Delta - h}\left(\frac{R_\Delta(1+\sqrt{n})}{\|\mathbf{q}_i-\mathbf{q}_j\|} - 1\right)\end{aligned}$$

So for $\mathbf{q}_i \in \Re^n$ and $\mathbf{q}_j \in \mathcal{X}_2$, we have

$$\left\|\frac{\partial^2 V_{ij}^a(\mathbf{q}_i,\mathbf{q}_j)}{\partial \mathbf{q}_i \partial \mathbf{q}_j}\right\| \leq \frac{1}{R_\Delta - h}\left(\frac{R_\Delta(1+\sqrt{n})}{h} - 1\right) = \frac{1}{h} + \frac{R_\Delta\sqrt{n}}{h(R_\Delta - h)}. \tag{8.11}$$

Alternatively, we can compute a different upper bound for (8.11). We left to the reader to verify that

$$\left\|\frac{\partial^2 V_{ij}^a(\mathbf{q}_i,\mathbf{q}_j)}{\partial \mathbf{q}_i \partial \mathbf{q}_j}\right\| \leq \frac{1}{R_\Delta - h} + \frac{R_\Delta}{R_\Delta - h}\frac{3+2\sqrt{n-1}}{4\|\mathbf{q}_i-\mathbf{q}_j\|} \leq \frac{1}{R_\Delta - h} + \frac{(3+2\sqrt{n-1})R_\Delta}{4h(R_\Delta - h)} \tag{8.12}$$

which becomes a less conservative upper bound on the Lipschitz property if $h > \frac{(1+4\sqrt{n}-2\sqrt{n-1})R_\Delta}{8}$. Therefore, by combining (8.11) and (8.12), we obtain that

$$\left\|\frac{\partial^2 V_{ij}^a(\mathbf{q}_i,\mathbf{q}_j)}{\partial \mathbf{q}_i \partial \mathbf{q}_j}\right\| \leq L_2 = \min\left\{\frac{1}{h} + \frac{R_\Delta\sqrt{n}}{h(R_\Delta - h)}, \frac{1}{R_\Delta - h} + \frac{(3+2\sqrt{n-1})R_\Delta}{4h(R_\Delta - h)}\right\}.$$

Finally, since $\frac{\partial V_{ij}^a(\mathbf{q}_i,\mathbf{q}_j)}{\partial \mathbf{q}_i} \equiv \mathbf{0}$ for $\mathbf{q}_i \in \Re^n$ and $\mathbf{q}_j \in \mathcal{X}_3$, we have that $L_3 = 0$. Therefore,

$$\left\|\frac{\partial^2 V_{ij}^a(\mathbf{q}_i,\mathbf{q}_j)}{\partial \mathbf{q}_i \partial \mathbf{q}_j}\right\| \leq \max\{L_1, L_2, L_3\} = L$$

for all $\mathbf{q}_i \in \Re^n$, $\mathbf{q}_j \in \mathcal{X}$, except on the set $\mathbf{q}_j \in \{h, R_\Delta\}$ of measure zero. Thereby, we conclude that (8.9) is locally Lipschitz continuous in $\mathbf{q}_j$ for $\mathbf{q}_j \in \mathcal{X}$ with Lipschitz constant determined by (8.10). □

8.4 Collision Avoidance Analysis

We now claim that the proposed collision avoidance control law, along with the control objective input, guarantees collision-free trajectories for a group of N vehicles with bounded control inputs, limited sensing range, and detection uncertainties.

Theorem 8.4.1 (Collision Avoidance for Multiple Agents with Sensing Uncertainties)**.** *Consider the multi-Lagrangian system in (8.1) with control inputs given by (8.2) to (8.9). Suppose that* $\|\dot{\mathbf{q}}_i(0)\| \leq \eta_i$, $\|\mathbf{q}_i(0) - \mathbf{q}_j(0)\| \geq R$, *and* $\|\mathbf{d}_{ij}\| \leq \Delta \ \forall i, j, \ i \neq j$. *Let* $\varepsilon \in [0, 1)$, $\bar{L} \in \left(0, \frac{\varepsilon}{(N-1)\Delta}\right]$, *and choose* r, h, *and* α_i *such that*

i. $r^* \leq \frac{(3+2\sqrt{n-1})}{4\bar{L}} + \Delta \leq r < R_\Delta$,

ii. $\underline{h} \leq h \leq \bar{h}$, *where*

$$\begin{aligned}
\underline{h} &= \min\left\{\frac{\bar{L}R_\Delta+1-\sqrt{1+\bar{L}^2R_\Delta^2-2\bar{L}R_\Delta\left(1+2\sqrt{n}\right)}}{2\bar{L}}, \frac{\bar{L}R_\Delta-1-\sqrt{1+\bar{L}^2R_\Delta^2-\bar{L}R_\Delta\left(5+2\sqrt{-1+n}\right)}}{2\bar{L}}\right\} > r \\
\bar{h} &= \max\left\{\frac{\bar{L}R_\Delta+1+\sqrt{1+\bar{L}^2R_\Delta^2-2\bar{L}R_\Delta\left(1+2\sqrt{n}\right)}}{2\bar{L}}, \frac{\bar{L}R_\Delta-1+\sqrt{1+\bar{L}^2R_\Delta^2-\bar{L}R_\Delta\left(5+2\sqrt{-1+n}\right)}}{2\bar{L}}\right\} < R_\Delta
\end{aligned}$$

iii. *and* $\sum_{i=1}^N \alpha_i < \frac{R_\Delta+h}{2} - r - \sum_{i=1}^N \frac{\bar{\lambda}_i\eta_i^2}{2\bar{\mu}_i}$, *where* $\overline{\lambda}_i$ *is the larger eigenvalue of* M_i.

Then, $[\mathbf{q}_i^T, \cdots, \mathbf{q}_N^T]^T \notin \Omega \ \forall t \geq 0$.

Proof. Consider the following Lyapunov function

$$V = \sum_{i=1}^N V_i^o(\mathbf{q}_i) + \frac{1}{2}\sum_{i=1}^N \sum_{j\in\mathcal{N}_i} V_{ij}^a(\mathbf{q}_i, \mathbf{q}_j) + \frac{1}{2}\sum_{i=1}^N \frac{1}{\bar{\mu}_i}\dot{\mathbf{q}}_i^T M_i(\mathbf{q}_i)\dot{\mathbf{q}}_i \tag{8.13}$$

Taking its time-derivative and using Property 2.2.1 we obtain

$$\begin{aligned}
\dot{V} = &\sum_{i=1}^N \frac{\partial V_i^{oT}(\mathbf{q}_i)}{\partial \mathbf{q}_i}\dot{\mathbf{q}}_i + \frac{1}{2}\sum_{i=1}^N \sum_{j\in\mathcal{N}_i}\left(\frac{\partial V_{ij}^{aT}(\mathbf{q}_i, \mathbf{q}_j)}{\partial \mathbf{q}_i}\dot{\mathbf{q}}_i + \frac{\partial V_{ij}^{aT}(\mathbf{q}_i, \mathbf{q}_j)}{\partial \mathbf{q}_j}\dot{\mathbf{q}}_j\right) \\
&+ \sum_{i=1}^N \frac{1}{\bar{\mu}_i}\left(\dot{\mathbf{q}}_i^T M_i(\mathbf{q}_i)\ddot{\mathbf{q}}_i + \frac{1}{2}\dot{\mathbf{q}}_i^T \dot{M}(\mathbf{q}_i)\dot{\mathbf{q}}_i\right)
\end{aligned}$$

$$
\begin{aligned}
\dot{V} =& \sum_{i=1}^{N} \frac{\partial V_i^{oT}(\mathbf{q}_i)}{\partial \mathbf{q}_i}\dot{\mathbf{q}}_i + \underbrace{\sum_{i=1}^{N}\sum_{j\in\mathcal{N}_i} \frac{\partial V_{ij}^{aT}(\mathbf{q}_i,\mathbf{q}_j)}{\partial \mathbf{q}_i}\dot{\mathbf{q}}_i}_{\text{Due to symmetry}} \\
&+ \sum_{i=1}^{N}\frac{1}{\bar{\mu}_i}\left(-\bar{\mu}_i\sum_{j\in\mathcal{N}_i}\frac{\partial V_{ij}^{aT}(\mathbf{q}_i,\hat{\mathbf{q}}_j^i)}{\partial \mathbf{q}_i} - \gamma_i\sum_{j\in\mathcal{N}_i}\theta_{ij}(\dot{\mathbf{q}}_i,\mathbf{q}_i,\hat{\mathbf{q}}_j^i)\frac{\dot{\mathbf{q}}_i^T}{\|\dot{\mathbf{q}}_i\|} - \bar{\mu}_i\frac{\partial V_i^{oT}(\mathbf{q}_i)}{\partial \mathbf{q}_i}\right)\dot{\mathbf{q}}_i \\
=& \sum_{i=1}^{N}\sum_{j\in\mathcal{N}_i}\left(\frac{\partial V_{ij}^{aT}(\mathbf{q}_i,\mathbf{q}_j)}{\partial \mathbf{q}_i} - \frac{\partial V_{ij}^{aT}(\mathbf{q}_i,\hat{\mathbf{q}}_j^i)}{\partial \mathbf{q}_i}\right)\dot{\mathbf{q}}_i - \sum_{i=1}^{N}\sum_{j\in\mathcal{N}_i}\frac{\gamma_i}{\bar{\mu}_i}\theta_{ij}(\dot{\mathbf{q}}_i,\mathbf{q}_i,\hat{\mathbf{q}}_j^i)\frac{\dot{\mathbf{q}}_i^T}{\|\dot{\mathbf{q}}_i\|}\dot{\mathbf{q}}_i.
\end{aligned}
$$

Now, applying Lemma 8.3.1 yields

$$
\dot{V} \leq \sum_{i=1}^{N}\sum_{j\in\mathcal{N}_i} L\Delta\,\|\dot{\mathbf{q}}_i\| - \sum_{i=1}^{N}\sum_{j\in\mathcal{N}_i}\frac{\gamma_i}{\bar{\mu}_i(N-1)}\|\dot{\mathbf{q}}_i\| = \sum_{i=1}^{N}\sum_{j\in\mathcal{N}_i}\left(L\Delta - \frac{\varepsilon}{(N-1)}\right)\|\dot{\mathbf{q}}_i\|
$$

where L is the Lipschitz constant for $\partial V_{ij}^{aT}(\mathbf{q}_i,\mathbf{q}_j)/\partial\mathbf{q}_j$. It is easy to show that if we choose r and h according to conditions i and ii, then $L \leq \bar{L} \leq \frac{\varepsilon}{(N-1)\Delta}$ and $\dot{V} \leq 0$. The semi-negative definite property on $\dot{V}(t)$ implies that $V(t) \leq V(0) \leq \sum_{i=1}^{N}\left(\frac{\bar{\lambda}_i\eta_i^2}{2\bar{\mu}_i} + \alpha_i\right)$, $\forall t \geq 0$, where we have made use of Property 2.2.2.

Now assume that (iii) holds and suppose that for at least some pair i,j, $\|\mathbf{q}_i(t) - \mathbf{q}_j(t)\| \to r$. As a consequence, $V(t) \geq V_{ij}^a(t) \to \frac{R_\Delta + h}{2} - r > \sum_{i=1}^{N}\left(\frac{\bar{\lambda}_i\eta_i^2}{2\bar{\mu}_i} + \alpha_i\right)$. Since we reached a contradiction, we conclude that $[\mathbf{q}_i^T(t),\mathbf{q}_j^T(t)]^T \notin \Omega_{ij}$ for all $i,j,\ i\neq j$ and $t \geq 0$. □

Theorem 8.4.1 provides sufficient conditions for the safe navigation of a group of N Lagrangian vehicles. It, however, says nothing about the fulfillment of the objective control. The only conclusion we can deduce regarding the objective control is that whenever the agents are outside of the detection regions, i.e., $[\mathbf{q}_i^T,\cdots,\mathbf{q}_N^T]^T \notin \mathcal{D}$, the collision avoidance control inputs do not affect the objective control laws.

In the following we posit sufficient conditions for collision avoidance of nonlinear vehicles with zero uncertainties but limited sensing range and bounded control inputs. The results along this line are of relevance given that vehicles with bounded control inputs and accelerations cannot react (e.g., evade or escape) instantaneously to a collision threat.

Corollary 8.4.1 (Collision Avoidance for Multiple Agents without Sensing Uncertainties)**.** *Consider the multi-Lagrangian system in (8.1) with control inputs given by (8.2) to (8.9) for $\varepsilon = 0$. Suppose that $\|\mathbf{d}_{ij}(t)\| = \Delta = 0$ and that $\|\dot{\mathbf{q}}_i(0)\| \leq \eta_i$, $\|\mathbf{q}_i(0) - \mathbf{q}_j(0)\| \geq R\ \forall i,j,\ i\neq j$ and assume*

$\exists\ r \geq r^*,\ h < R,\ and\ \alpha_i > 0\ such\ that$

$$\sum_{i=1}^{N} \alpha_i < \frac{R+h}{2} - r - \sum_{i=1}^{N} \frac{\bar{\lambda}_i \eta_i^2}{2\bar{\mu}_i} \tag{8.14}$$

Then, $[\mathbf{q}_i^T, \cdots, \mathbf{q}_N^T]^T \notin \Omega\ \forall t \geq 0.$

Proof. Consider the Lyapunov candidate function given in (8.13). Its time-derivative is computed as

$$\dot{V} = \sum_{i=1}^{N} \frac{\partial V_i^{oT}(\mathbf{q}_i)}{\partial \mathbf{q}_i}\dot{\mathbf{q}}_i + \sum_{i=1}^{N}\sum_{j\in\mathcal{N}_i} \frac{\partial V_{ij}^{aT}(\mathbf{q}_i,\mathbf{q}_j)}{\partial \mathbf{q}_i}\dot{\mathbf{q}}_i + \sum_{i=1}^{N}\left(-\sum_{j\in\mathcal{N}_i} \frac{\partial V_{ij}^{aT}(\mathbf{q}_i,\mathbf{q}_j)}{\partial \mathbf{q}_i} - \frac{\partial V_i^{oT}(\mathbf{q}_i)}{\partial \mathbf{q}_i}\right)\dot{\mathbf{q}}_i \leq 0.$$

Therefore, $V(t) \leq V(0) \leq \sum_{i=1}^{N}\left(\frac{\bar{\lambda}_i\eta_i^2}{2\bar{\mu}_i} + \alpha_i\right)$. Now suppose (8.14) is satisfied and that for at least some pair $i, j, i \neq j$ and some $t \geq 0$, $[\mathbf{q}_i(t), \mathbf{q}_j(t)] \to \Omega_{ij}(t)$. This would imply that $V(t) \geq V_{ij}^a(t) \to \frac{R+h}{2} - r > \sum_{i=1}^{N}\left(\frac{\bar{\lambda}_i\eta_i^2}{2\bar{\mu}_i} + \alpha_i\right)$, which is a contradiction. Consequently, we can conclude that $[\mathbf{q}_i^T(t), \cdots, \mathbf{q}_N^T(t)]^T \notin \Omega(t)\ \forall t \geq 0.$ □

8.5 Example: Collision Avoidance with Detection Delays

To validate the proposed collision avoidance strategy, we simulate the behavior of four 2-DOF vehicles with dynamics governed by

$$m\ddot{\mathbf{q}}_i = \mathbf{u}_i - \rho_i\dot{\mathbf{q}}_i \tag{8.15}$$

where $m = 1.5$ kg, $\rho_1 = \rho_4 = 0.25$ kg/s, $\rho_2 = \rho_3 = 0.10$ kg/s and $\|\mathbf{u}_i\| \leq 100\ \text{kg}\cdot\text{m/s}^2\ \forall i$. The minimum safety distance and detection radius for all vehicles are assumed to be $r^* = 1.5$ m and $R = 20$ m, respectively. In addition, we assume an a priori bound of $\Delta = 0.15$ m on the sensing uncertainty for each agent owed to a 0.05 s delay incurred during the localization process of nearby agents.

8.5.1 Control Law

The control objective is to safely drive the vehicles from an initial configuration to a desired final position. In order to do so, we propose the use of the following objective function

$$V_i^o(\mathbf{q}_i) = \alpha_i \left(1 - \operatorname{sech}\left(\frac{\left\|\mathbf{q}_i - \mathbf{q}_i^d\right\|}{\sigma_i}\right)\right)^{\delta_i} \tag{8.16}$$

where $\alpha_1 = \alpha_2 = 3.0$, $\alpha_3 = \alpha_4 = 2.5$, $\sigma_i = 5$, and $\delta_i = 7$ for $i \in \{1, 2, 3, 4\}$. The desired final configurations are chosen as $\mathbf{q}_1^d = [-8 \text{ m}, -18 \text{ m}]^T$, $\mathbf{q}_2^d = [8 \text{ m}, 18 \text{ m}]^T$, $\mathbf{q}_3^d = [-25 \text{ m}, 0 \text{ m}]^T$, and $\mathbf{q}_4^d = [25 \text{ m}, 5 \text{ m}]^T$. The objective control input (8.3) is then given by

$$\mathbf{u}_i^o = -\frac{\bar{\mu}_i \alpha_i \delta_i}{\sigma_i} \left(1 - \operatorname{sech}\left(\frac{\left\|\mathbf{q}_i - \mathbf{q}_i^d\right\|}{\sigma_i}\right)\right)^{\delta_i - 1} \operatorname{sech}\left(\frac{\left\|\mathbf{q}_i - \mathbf{q}_i^d\right\|}{\sigma_i}\right) \tanh\left(\frac{\left\|\mathbf{q}_i - \mathbf{q}_i^d\right\|}{\sigma_i}\right) \frac{\mathbf{q}_i - \mathbf{q}_i^d}{\left\|\mathbf{q}_i - \mathbf{q}_i^d\right\|} \tag{8.17}$$

if $\|\mathbf{q}_i - \mathbf{q}_i^o\| \neq 0$ and $\mathbf{u}_i^0 = \mathbf{0}$ otherwise. The collision avoidance control input for the four agents is computed according to Theorem 8.4.1. The parameters are summarized in Table 8.1 where we have chosen $\varepsilon = 0.16$ and assumed that initial velocities for all agents are bounded by $\eta_i = 2$ m/s.

Table 8.1: Collision Avoidance Control Parameters

Agent (i)	**Parameter**						
$N = 4$	$\overline{\lambda}_i$ (kg)	$\bar{\mu}_i$ (N)	γ_i (N)	r (m)	h (m)	L	β_i
1	1.5	29.46	4.71	3.67	10.19	0.356	0.234
2	1.5	29.46	4.71	3.67	10.19	0.356	0.234
3	1.5	29.80	4.78	3.67	10.19	0.356	0.196
4	1.5	29.80	4.78	3.67	10.19	0.356	0.196

8.5.2 Simulation Results

The responses of the four agents to the objective and collision avoidance control inputs are represented in Figure 8.2. The agents start from positions $\mathbf{q}_1(0 \text{ s}) = [18 \text{ m}, 22 \text{ m}]^T$, $\mathbf{q}_2(0 \text{ s}) = [-21 \text{ m}, -14 \text{ m}]^T$, $\mathbf{q}_3(0 \text{ s}) = [16 \text{ m}, -20 \text{ m}]^T$, and $\mathbf{q}_4(0 \text{ s}) = [2 \text{ m}, 25 \text{ m}]^T$ with initial velocities given by $\dot{\mathbf{q}}_i(0 \text{ s}) = 2\frac{\mathbf{q}_i^d}{\|\mathbf{q}_i^d\|}$ m/s. Notice that shortly after their initial state, the first and fourth agents entered each other's Detection Region, whereas the second and third vehicles accelerated

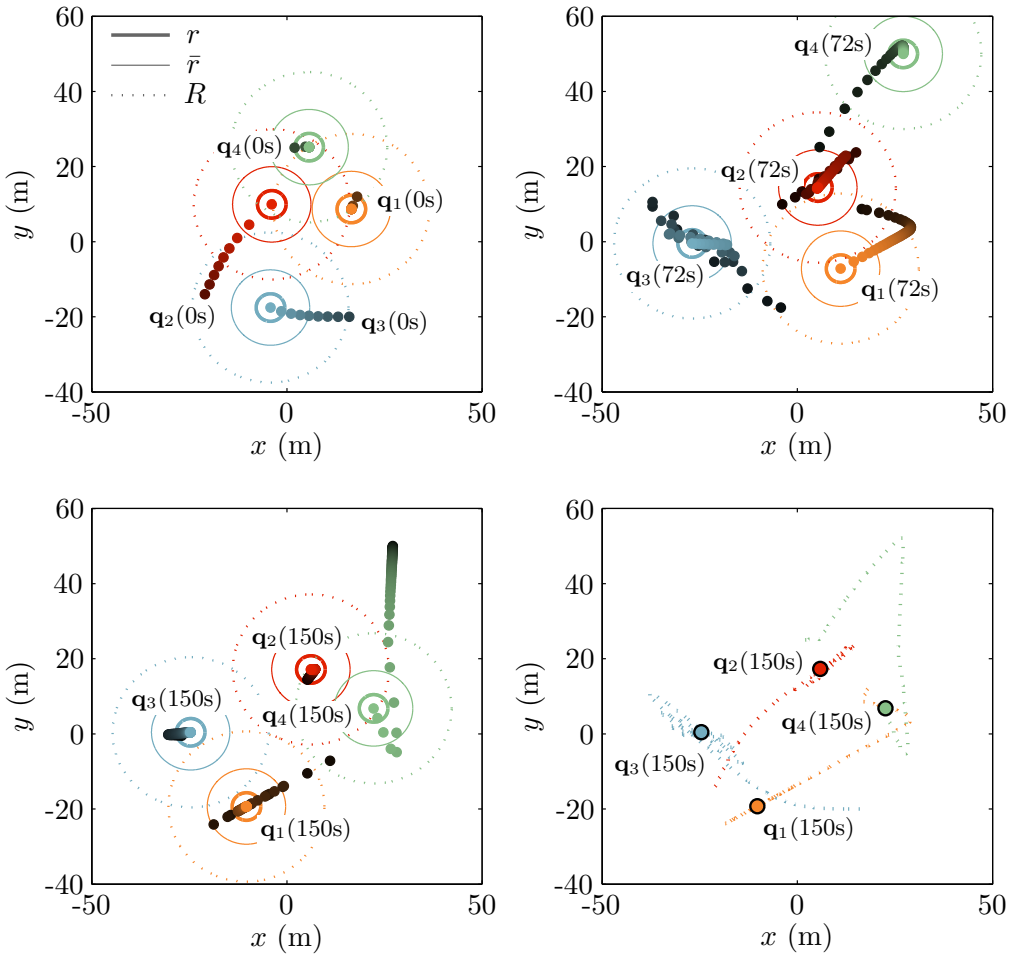

Figure 8.2: Multi-agent collision avoidance example with sensing uncertainties. The left-top, right-top, and left-bottom plots illustrate the motion of the four agents at the intervals $t \in [0\text{ s}, 12\text{ s}]$, $t \in [12\text{ s}, 72\text{ s}]$, and $t \in [72\text{ s}, 150\text{ s}]$, respectively, where each mark is time-spaced by 1.5 s. The initial positions of the four agents at each plotted simulation interval are indicated by the dark-colored dots. The Avoidance, Conflict, and Detection Regions for all all agents at the end of the simulation intervals are delimited by the bold, thin, and dashed lines, respectively. The right-bottom figure illustrates the complete trajectory.

freely toward their final destination (see left-top plot and contrast the distance traveled by all agents). As the second agent comes to the proximity of the first and fourth agents, it ends entering their Detection Regions. Consequently, the first and fourth vehicles move away from the second agent to prevent a collision, as can be seen in the right-top figure. Once the four agents are safely apart, they are finally able to continue toward their final configurations.

Figure 8.3 illustrates the distances between the four agents at all times. Note that the first, second, and fourth agents entered each other's Detection Regions at different intervals of time, whereas the third vehicle did not interact with any other agent. In addition, note that the second

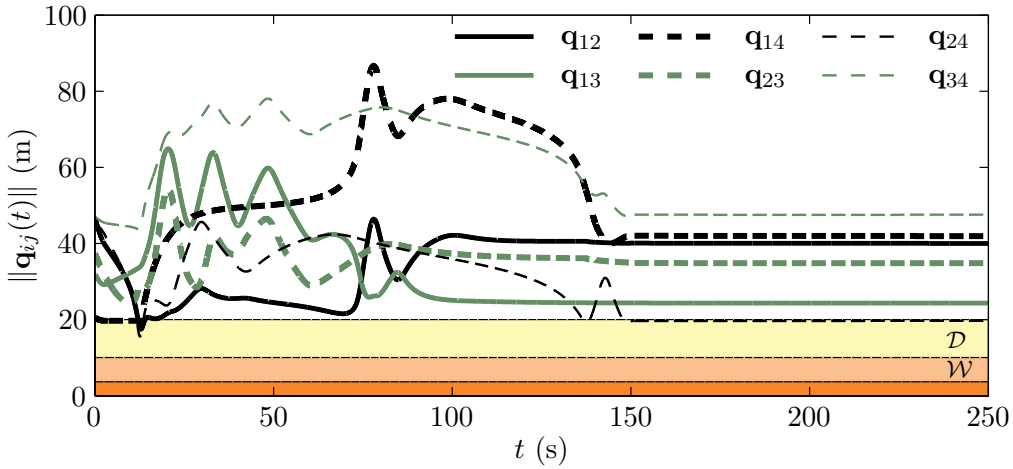

Figure 8.3: Distances among agents with sensing uncertainties.

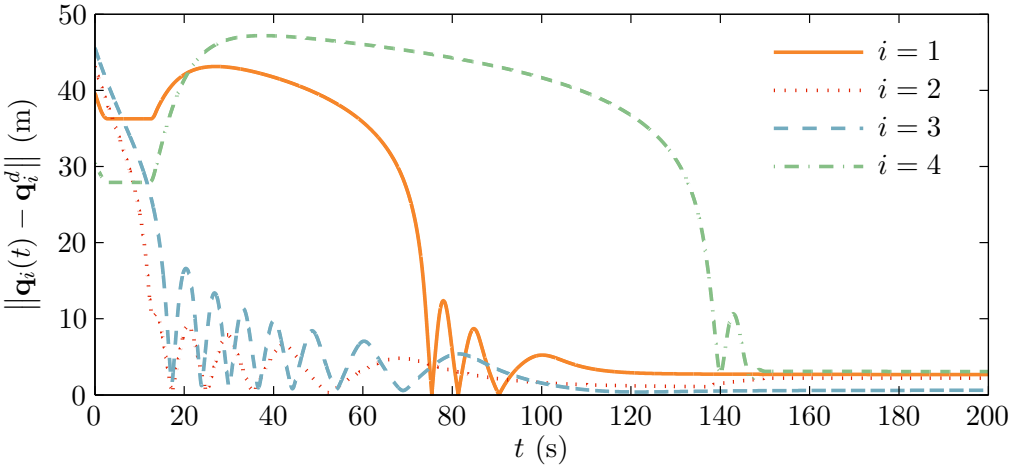

Figure 8.4: Norm of the difference between the position of the vehicles and their desired configuration.

and fourth agents remained within each other's Detection Regions after the systems reached an apparent steady-state. Yet, no collision took place. The errors between the positions of the vehicles and the desired destinations are also shown in Figure 8.4. The fourth agent successfully reached its final destination as expected since its path was not disturbed by any collision threat. The final constant error exhibited by the second and fourth vehicles is a result of their steady nonzero collision avoidance input which represents a conflict with their objective control. On the other hand, the quasi-steady error of the first agent is owed to the slow convergence rate of the objective control input near the desired destination, and it should continue progressing toward zero.

8.6 Example: Collision Avoidance without Sensing Uncertainties

Similar to the previous example, we now simulate the response of the four-agents described in (8.15) assuming zero uncertainties, i.e., perfect sensing. We take the objective functions and control inputs to be given as in (8.16) and (8.17) with $\alpha_1 = \alpha_2 = 2.8$, $\alpha_3 = \alpha_4 = 2.3$, $\sigma_i = 10$, and $\delta_i = 2\ \forall i$. The desired final configurations are chosen as $\mathbf{q}_1^d = [-6.00\text{ m}, -13.50\text{ m}]^T$, $\mathbf{q}_2^d = [6.00\text{ m}, 13.50\text{ m}]^T$, $\mathbf{q}_3^d = [-18.75\text{ m}, 0.00\text{ m}]^T$, and $\mathbf{q}_4^d = [18.75\text{ m}, 3.75\text{ m}]^T$. The Detection Region for all agents is assumed to be bounded by $R = 15$ m.[1] Finally, the cooperative collision avoidance control inputs are computed according to Corollary 8.4.1 and (8.4), where we have chosen $\varepsilon = 0$, $r = 2$ m, and $h = 10$ m.

8.6.1 Simulation Results

The response of the four vehicles is presented in Figure 8.5. The agents are taken to start from positions $\mathbf{q}_1(0\text{ s}) = [13.50\text{ m}, 16.50\text{ m}]^T$, $\mathbf{q}_2(0\text{ s}) = [-15.75\text{ m}, -10.50\text{ m}]^T$, $\mathbf{q}_3(0\text{ s}) = [12.00\text{ m}, -15.00\text{ m}]^T$, and $\mathbf{q}_4(0\text{ s}) = [1.50\text{ m}, 18.75\text{ m}]^T$ with the same initial velocities as in the example in Section 8.5. Notice that, at first (see left-top plot), the agents are relatively free to move toward their desired configurations with little interaction. Then, at time $t \approx 17$s, the first and second agent are shown to come into close proximity to the third vehicle. However, the vehicles are able to solve the conflict and converge to their final destinations. Figure 8.6 confirms that the agents avoided any potential collision. As can be seen in the plot, the four agents entered each other's Detection Region at different intervals of time. In particular, the second and fourth agents repeatedly entered into each other's Detection Region. This behavior can be attributed to the close proximity of their final destination.

Figure 8.7 depicts the error between the position of the four agents with respect to their desired final location. Observe that the errors eventually converge to zero. Their slow convergence rates can be attributed to the small magnitude of the objective control inputs near their desired locations.

[1] Note that the desired configurations and detection radius have the same values as in the previous example but scaled by a factor of $\frac{3}{4}$. Having zero uncertainty allows for the treatment of cases with smaller Detection Regions.

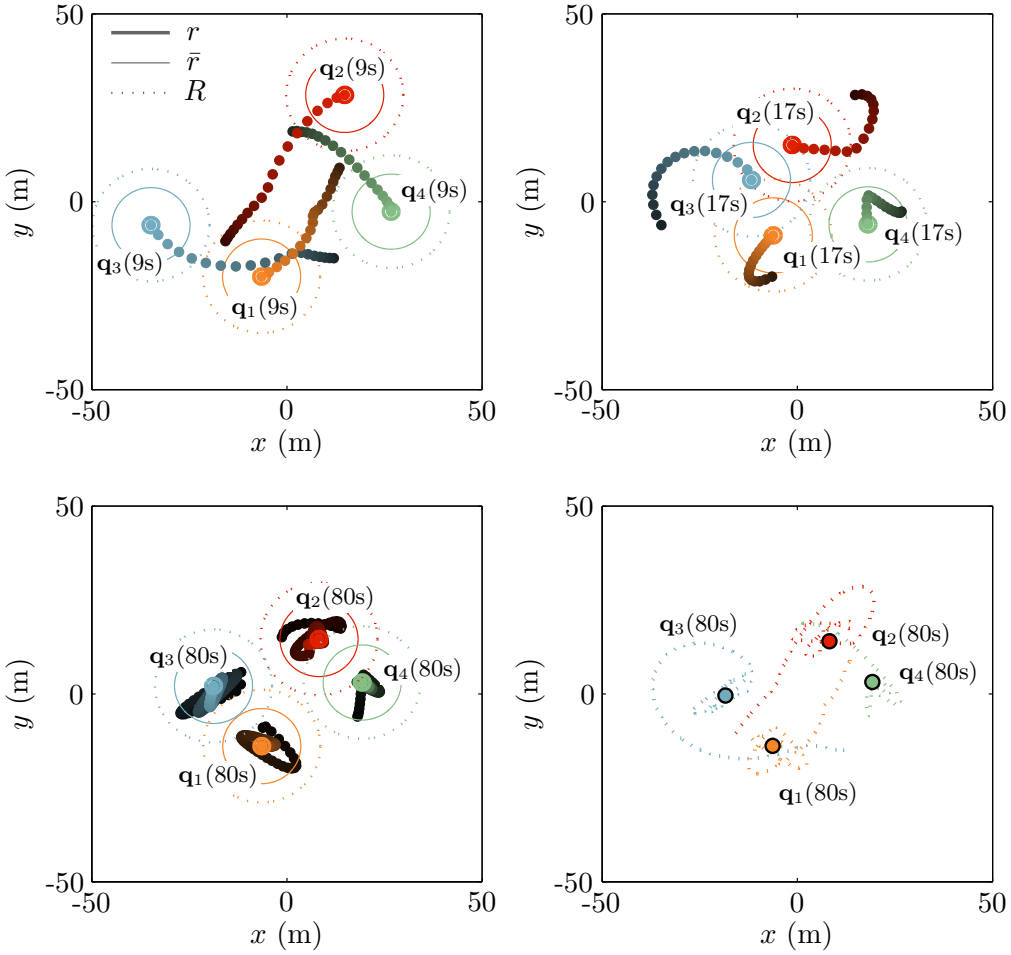

Figure 8.5: Multi-agent collision avoidance example with perfect sensing. The left-top, right-top, and left-bottom plots illustrate the motion of the four agents at the intervals $t \in [0\text{ s}, 9\text{ s}]$, $t \in [9\text{ s}, 17\text{ s}]$, and $t \in [17\text{ s}, 80\text{ s}]$, respectively, where each mark is time-spaced by 0.5 s. The initial positions of the four agents at each plotted simulation interval are indicated by the dark-colored dots. The Avoidance, Conflict, and Detection Regions for all all agents at the end of the simulation intervals are delimited by the bold, thin, and dashed lines, respectively. The right-bottom figure illustrates the complete trajectory.

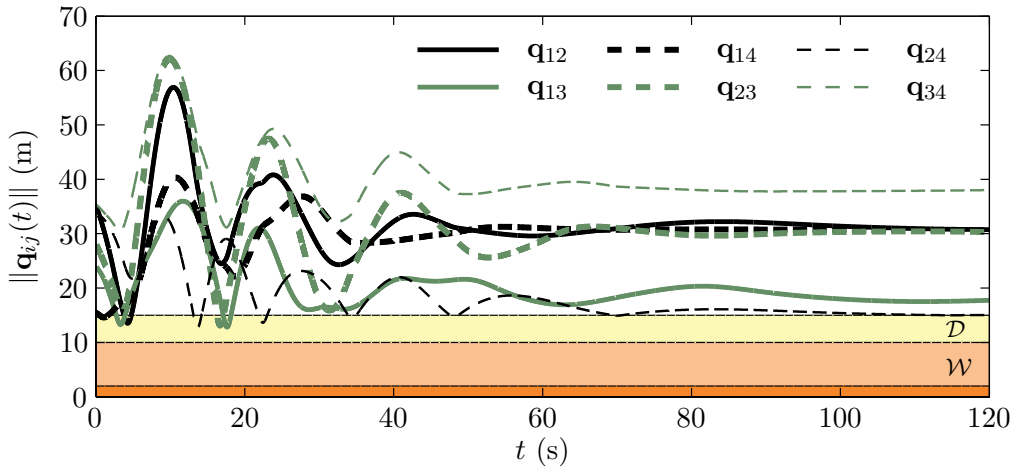

Figure 8.6: Distances between agents with perfect sensing.

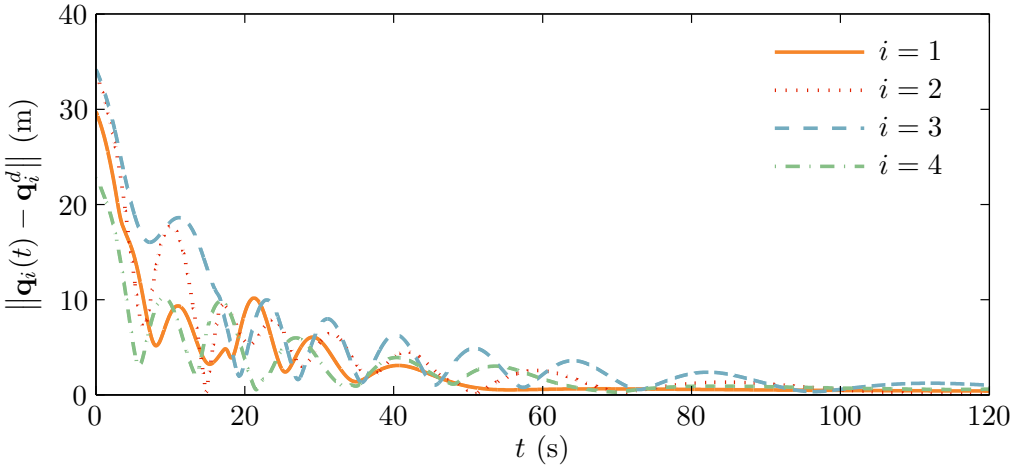

Figure 8.7: Norm of the error between the position of the agents and their desired configuration.

CHAPTER 9

CONCLUSIONS AND RECOMMENDATIONS

This chapter summarizes the work of this thesis. Our major contributions to NCS technology are highlighted, and a list of future related, research directions are suggested.

9.1 Conclusions

Throughout this dissertation, we have presented and validated original control solutions for single as well as multiple networked Lagrangian systems with time delay inputs. By using passivity concepts and Lyapunov-based analysis, we have studied different control challenges within NCSs such as stability of time delay nonlinear systems, bilateral teleoperation, multi-agent coordination, and collision avoidance. We have also studied the effects of delays and data transmission errors on the performance of nonlinear NCSs. The following is a summary of the contributions.

9.1.1 Nonlinear Systems with Control Input Delays

We started in Chapter 3 with the introduction of a passivity-based MRRC framework that guarantees asymptotic stability and state tracking convergence of nonlinear dissipative Lagrangian systems with input and state feedback delays. The proposed controller utilizes the scattering transformation to passify the energetic coupling between plant and controller independently of the delay, and introduces a state tracking compensator that enforces full state convergence for unknown initial conditions, computational errors, and transmission losses. Simulation tests with robotic manipulators as well as experiments with a coaxial helicopter employing the MRRC framework yielded satisfactory results.

In Chapter 4 we extended the passivity-based MRRC formulation to the general case of multiple agents. Within this context, we showed that the stability, formation, and motion coordination of a network of heterogeneous agents can be attained independently of arbitrarily large constant

communication delays. Simulation results on formation control and trajectory tracking with time-delay omni-directional vehicles were presented.

9.1.2 Bilateral Teleoperation

In Chapter 5 we considered an SMSS bilateral teleoperation system with communication delays. We introduced a novel control framework that builds on passivity-based control and wave scattering transformation to stabilize and coordinate the motion of an SMSS teleoperator with arbitrarily large constant coupling delays. By exploiting the independent-passivity property of the wave impedance on wave-based teleoperation architectures, we introduced a time-varying wave impedance control framework that passively changes the wave impedance from any small value, suitable for free motion tasks, to a sufficiently large value, ideally for a transparent interaction with stiff environments. Furthermore, the control strategy is proved to achieve closed-loop stability of the teleoperation system and to enforce smooth position tracking and static force reflection independently of delays, even for a non-passive human operator. Indeed, we showed using the paradigm of input-to-state stability that the coordination error between master and slave is ultimately bounded and that this bound decreases with an increase of the impedance value. We presented simulation and experimental results on nonlinear manipulators that illustrated and evidenced the claimed position error compensation.

Our attention to SMSS bilateral teleoperation is shifted to multi-slave teleoperation systems in Chapter 6. Specifically, we presented a distributed bilateral control architecture that enforces closed-loop stability, slaves-to-master motion coordination, formation control, static force reflection, and collision avoidance for a group of slave robots coupled to a single human-controlled master robot with communication constant delays. The controller synthesizes the use of a PD-based controller, which guarantees closed-loop stability, motion coordination, and static force reflection, with the use of avoidance functions that impose collision-free trajectories for the slave agents. The control framework was then validated via experiments with two coaxial helicopters coupled to a haptic device and teleoperated in an obstructed environment. The operator was given the ability to alter the geometry of the vehicles' formation according to the topology of the remote environment. The reported results were satisfactory under network round-trip delays of up to 124 ms.

9.1.3 Collision Avoidance with Sensing Uncertainties

In Chapter 7 we provided sufficient conditions and developed real-time cooperative and noncooperative collision avoidance strategies for a pair of agents with sensing uncertainties (e.g., localization errors due to communication time-varying delays, quantization, and noise). We explicitly considered the case where position information from nearby agents and obstacles is unreliable (i.e., inaccurate) and developed bounded control inputs based on avoidance functions that guarantee collision-free trajectories for both vehicles. The designed avoidance control strategies can be appended to any other stable control law (i.e., main control objective) and are active only when the vehicle is close to another agent or obstacle. Simulation results are presented to validate the proposed control formulation and evaluate its extension to the general case of multiple agents. An experiment with two coaxial helicopters with half a second of sensing delay is also presented with satisfactory reported results.

The collision avoidance control for two agents is later reformulated for the case of N vehicles in Chapter 8. By using bounded Lyapunov functions, we showed that, if sufficiently large avoidance and detection regions are defined, we can design decentralized, cooperative collision avoidance control laws that guarantee collision-free trajectories for a group of nonlinear Lagrangian systems. Moreover, outside of the detection regions, these avoidance control strategies do not interfere with any other objective control. We also extended the analysis to Lagrangian systems with zero uncertainty but bounded control inputs. Simulation results with four agents demonstrated the effectiveness of the proposed avoidance control strategy.

9.2 Recommended Future Research Directions

There are many research directions that stem from the results presented in this dissertation. The following are some suggestions.

- In Chapter 3, we assumed the delayed information of the control input could be decoded from the system's output or, that at least, the round-trip delay was known in order to reconstruct the delayed control input and develop the passivity-based MRRC framework. An immediate extension to the control framework would be to derive sufficient conditions for stability for unknown, possible time-varying delay inputs, as well as to evaluate its sensitivity to data transmission losses and time-varying delays.

- The full-state compensator proposed in Section 3.3.1, guarantees state convergence between the time delay nonlinear plant and the reference model, given that the system does not reach steady-state before the compensation task is consumed. In the future, we suggest investigating properties on the reference signal that will guarantee state convergence. An alternative would be to impose the reference signal to be persistently exciting [164].

- Modifications to the transparency compensation control technique for bilateral teleoperators introduced in Chapter 5, such that time-varying delayed and lossy communication channels are considered, would be an appealing extension.

- How to achieve collaboration from multiple operators working from different locations? An interesting task within bilateral teleoperation is to evaluate the integration and cooperation of multiple master robots as well as multiple operators.

- Theoretical considerations on how to control dynamic and switching formations would be an appealing extension to the PD-based control proposed in Chapter 6.

- How to develop robust control strategies for systems with delayed inputs? Along a similar research line, how can we integrate the MRRC framework with the collision avoidance policies presented in Chapters 7 and 8? These are research questions we suggest can be investigated.

- Providing a bound on the maximum number of vehicles for which the cooperative collision avoidance control strategies can be applied would be an additional consideration. This bound will clearly depend on the sensing range, the uncertainties, and the limits on the control inputs.

- Finally, it would be appealing to extend the control methodologies proposed in this dissertation to nonholonomic systems such as car-like vehicles and airplanes.

REFERENCES

[1] W. Zhang, M. S. Branicky, and S. M. Phillips, "Stability of networked control systems," *IEEE Control Syst. Mag.*, vol. 21, no. 1, pp. 84–99, Feb. 2001.

[2] P. Antsaklis and J. Baillieul, "Guest editorial: Special issue on networked control systems," *IEEE Trans. Automat. Control*, vol. 49, no. 9, pp. 1421–1423, Sep. 2004.

[3] P. Antsaklis and J. Baillieul, "Special issue on technology of networked control systems," *Proc. IEEE*, vol. 95, no. 1, pp. 5–8, Jan. 2007.

[4] S. Graham, G. Baliga, and P. R. Kumar, "Abstractions, architecture, mechanisms, and a middleware for networked control," *IEEE Trans. Automat. Control*, vol. 54, no. 7, pp. 1490–1503, July 2009.

[5] J. P. Hespanha, P. Naghshtabrizi, and Y. Xu, "A survey of recent results in networked control systems," *Proc. IEEE*, vol. 95, no. 1, pp. 138–162, Jan. 2007.

[6] J. Baillieul and P. J. Antsaklis, "Control and communication challenges in networked real-time systems," *Proc. IEEE*, vol. 95, no. 1, pp. 9–28, Jan. 2007.

[7] M. S. Branicky, S. M. Phillips, and W. Zhang, "Stability of networked control systems: Explicit analysis of delay," in *Proc. IEEE Am. Control Conf.*, Chicago, IL, June 2000.

[8] V. Volterra, "Sur la théorie mathématique des phénomenes héréditares," *J. Math. Pures Appl.*, vol. 7, no. 9, pp. 249–298, 1928, (in French).

[9] N. Minorsky, "Directional stability of automatically steered bodies," *J. Am. Soc. Naval Engrs.*, vol. 34, no. 2, pp. 280–309, May 1922.

[10] H. L. Hazen, "Theory of servo-mechanisms," *J. Franklin Inst.*, vol. 218, no. 3, pp. 279–331, Sep. 1934.

[11] S. I. Niculescu, *Delay Effects on Stability: A Robust Control Approach*, ser. Lecture Notes in Control and Information Sciences, M. Thoma and M. Morari, Eds. London: Springer Verlag, 2001, vol. 269.

[12] A. Callender, D. R. Hartree, and A. Porter, "Time-lag in a control system," *Philosoph. Trans. Royal Soc. London*, vol. 235, no. 756, pp. 415–444, July 1936.

[13] E. Staff, "The damping effects of time lag," *The Engineer*, vol. 163, p. 439, Apr. 16, 1937.

[14] N. Minorsky, "Self-excited oscillations in dynamical systems possessing retarded actions," *J. Applied Mech.*, vol. 9, pp. A65–A71, 1942.

[15] Y. Z. Tsypkin, "The systems with delayed feedback," *Avthomathika i Telemech*, vol. 7, pp. 107–129, 1946.

[16] A. D. Myshkis, "General theory of differential equations with delay," *Am. Math. Soc. Transl.*, vol. 55, pp. 1–62, 1951, (Russian version published in 1949).

[17] J. K. Hale, "History of delay equations," in *Delay Differential Equations and Applications*, ser. Nato Science Series, O. Arino, M. L. Hbid, and E. A. Dads, Eds. The Netherlands: Springer-Netherlands, 2006, pp. 1–28.

[18] O. J. M. Smith, "A controller to overcome dead time," *Instrum. Soc. Am. J.*, vol. 6, no. 2, pp. 28–33, Feb. 1959.

[19] B. S. Razumikhin, "Stability in first approximation of systems with lag," *J. Appl. Math. Mech.*, vol. 22, no. 2, pp. 215–229, 1958.

[20] N. Krasovskii, *Stability of Motion. Applications of Lyapunov's Second Method to Differential Systems and Equations with Delay.* Stanford, California: Stanford University Press, 1963, (translated by J. L. Brenner).

[21] K. Gu and S.-I. Niculescu, "Survey on recent results in the stability and control of time-delay systems," *J. Dyn. Syst. Meas. Control*, vol. 125, no. 2, pp. 158–165, June 2003.

[22] J.-P. Richard, "Time-delay systems: An overview of some recent advances and open problems," *Automatica*, vol. 39, no. 10, pp. 1667–1694, 2003.

[23] T. C. Yang, "Networked control system: A brief survey," *Proc. IEE Control Theory Appl.*, vol. 153, no. 4, pp. 403–412, July 2006.

[24] T. B. Sheridan, "Teleoperation, telerobotics and telepresence: A progress report," *Control Eng. Pract.*, vol. 3, no. 3, pp. 205–214, Feb. 1995.

[25] P. F. Hokayem and M. W. Spong, "Bilateral teleoperation: An historical survey," *Automatica*, vol. 42, no. 12, pp. 2035–2057, Dec. 2006.

[26] N. E. Leonard, D. A. Paley, F. Lekien, R. Sepulchre, D. M. Fratantoni, and R. E. Davis, "Collective motion, sensor networks, and ocean sampling," *Proc. IEEE*, vol. 95, no. 1, pp. 48–74, Jan. 2007.

[27] R. Olfati-Saber, J. A. Fax, and R. M. Murray, "Consensus and cooperation in networked multi-agent systems," *Proc. IEEE*, vol. 95, no. 1, pp. 215–233, Jan. 2007.

[28] L. Hetel, J. Daafouz, and C. Iung, "Stabilization of arbitrary switched linear systems with unknown time-varying delays," *IEEE Trans. Automat. Control*, vol. 51, no. 10, pp. 1668–1674, Oct. 2006.

[29] M. B. G. Cloosterman, N. van de Wouw, W. P. M. H. Heemels, and H. Nijmeijer, "Stability of networked control systems with uncertain time-varying delays," *IEEE Trans. Automat. Control*, vol. 54, no. 7, pp. 1575–1580, July 2009.

[30] W. Heemels and N. van de Wouw, "Stability and stabilization of networked control systems," in *Networked Control Systems*, ser. Lecture Notes in Control and Information Sciences, A. Bemporad, M. Heemels, and M. Johansson, Eds. Springer Berlin/Heidelberg, vol. 406, pp. 203–253.

[31] J. Cao, S. Zhong, and Y. Hu, "Novel delay-dependent stability conditions for a class of MIMO networked control systems with nonlinear perturbations," *Appl. Math. Comput.*, vol. 197, no. 2, pp. 797–809, Apr. 2008.

[32] D. Muñoz de la Peña and P. D. Christofides, "Lyapunov-based model predictive control of nonlinear systems subject to data losses," *IEEE Trans. Automat. Control*, vol. 53, no. 9, pp. 2076–2089, Oct. 2008.

[33] T. Matiakis, S. Hirche, and M. Buss, "Control of networked systems using the scattering transformation," *IEEE Trans. Control Syst. Technol.*, vol. 17, no. 1, pp. 60–67, Jan. 2009.

[34] R. Luck and A. Ray, "Experimental verification of a delay compensation algorithm for integrated communication and control systems," *Int. J. Control*, vol. 59, no. 6, pp. 1357–1372, 1994.

[35] O. Beldiman, G. C. Walsh, and L. Bushnell, "Predictors for networked control systems," in *Proc. IEEE Am. Control Conf.*, Chicago, IL, June 2000.

[36] S. Munir and W. J. Book, "Internet-based teleoperation using wave variables with prediction," *IEEE/ASME Trans. Mechatron.*, vol. 7, no. 2, pp. 124–133, June 2002.

[37] Y. Tipsuwan and M. Y. Chow, "Control methodologies in networked control systems," *Control Eng. Pract.*, vol. 11, no. 10, pp. 1099–1111, Oct. 2003.

[38] P. F. Hokayem and C. T. Abdallah, "Inherent issues in networked control systems: A survey," in *Proc. IEEE Am. Control Conf.*, June 2004, pp. 4897–4902.

[39] X.-H. Ji, "A survey of recent results in networked systems analysis and design," in *Proc. Chinese Control Decision Conf.*, May 2010, pp. 1931–1935.

[40] C. Abdallah, P. Dorato, and J. Benitez-Read, "Delayed positive feedback can stabilize oscillatory systems," in *Proc. IEEE Am. Control Conf.*, June 1993, pp. 3106–3107.

[41] A. Thowsen, "An analytic stability test for a class of time-delay systems," *IEEE Trans. Automat. Control*, vol. 26, no. 3, pp. 735–736, June 1981.

[42] R. Ortega, A. Loría, P. J. Nicklasson, and H. Sira-Ramírez, *Passivity-Based Control of Euler-Lagrange Systems: Mechanical, Electrical, and Electromechanical Applications.* London, UK: Springer-Verlag, 1998.

[43] B. Mirkin, E. L. Mirkin, and P.-O. Gutman, "Model reference adaptive control of nonlinear plant with dead time," in *Proc. IEEE Conf. Decision Control*, Dec. 2008, pp. 1920–1924.

[44] F. Mazenc and P.-A. Bliman, "Backstepping design for time-delay nonlinear systems," *IEEE Trans. Automat. Control*, vol. 51, no. 1, pp. 149–154, Jan. 2006.

[45] X. Zhang and Z. Cheng, "Output feedback stabilization of nonlinear systems with delays in the input," *Appl. Math. Comput.*, vol. 167, no. 2, pp. 1026–1040, Aug. 2005.

[46] G. Niemeyer and J. J. E. Slotine, "Stable adaptive teleoperation," *IEEE J. Oceanic Eng.*, vol. 16, no. 1, pp. 152–162, Jan. 1991.

[47] T. Matiakis, S. Hirche, and M. Buss, "Independent-of-delay stability of nonlinear networked control systems by scattering transformation," in *Proc. IEEE Am. Control Conf.*, Minneapolis, MN, June 2006, pp. 2801–2806.

[48] S. Hirche, T. Matiakis, and M. Buss, "A distributed controller approach for delay-independent stability of networked control systems," *Automatica*, vol. 45, no. 8, pp. 1828–1836, 2009.

[49] N. Chopra and M. W. Spong, "Delay-independent stability for interconnected nonlinear systems with finite $\mathcal{L}_2$ gain," in *Proc. IEEE Conf. Decision Control*, Dec. 2007, pp. 3847–3852.

[50] N. Chopra, "Passivity results for interconnected systems with time delay," in *Proc. IEEE Conf. Decision Control*, Dec. 2008, pp. 4620–4625.

[51] N. Chopra, "Control of robotic manipulators with input/output delays," in *Proc. IEEE Am. Control Conf.*, June 2009, pp. 2024–2029.

[52] C. Secchi and C. Fantuzzi, "Energy shaping over networks for mechanical systems," in *Proc. IEEE Conf. Decision Control*, Dec. 2007, pp. 647–652.

[53] R. M. Murray, "Recent research in cooperative control of multivehicle systems," *J. Dyn. Syst. Meas. Control*, vol. 129, no. 5, pp. 571–583, Sep. 2007.

[54] V. Kumar, D. Rus, and S. Singh, "Robot and sensor networks for first responders," *IEEE Pervasive Comput.*, vol. 3, no. 4, pp. 24–33, 2004.

[55] G. Kantor, S. Singh, R. Peterson, D. Rus, A. Das, V. Kumar, G. Pereira, and J. Spletzer, "Distributed search and rescue with robot and sensor teams," in *Field and Service Robotics*, ser. Springer Tracts in Advanced Robotics, S.Yuta, H. Asama, S. Thrun, E. Prassler, and T. Tsubouchi, Eds. Springer Berlin - Heidelberg, 2006, pp. 529–538.

[56] T. Balch and R. C. Arkin, "Behavior-based formation control for multirobot teams," *IEEE Trans. Robot. Automat.*, vol. 14, no. 6, pp. 926–939, Dec. 1998.

[57] W. B. Dunbar and R. M. Murray, "Distributed receding horizon control for multi-vehicle formation stabilization," *Automatica*, vol. 42, no. 4, pp. 549–558, 2006.

[58] A. Y. Pogromsky, "Passivity based design of synchronizing systems," *Int. J. Bifurcat. Chaos*, vol. 8, no. 2, pp. 295–319, 1998.

[59] A. Jadbabaie, J. Lin, and A. S. Morse, "Coordination of groups of mobile autonomous agents using nearest neighbor rules," *IEEE Trans. Automat. Control*, vol. 48, no. 6, pp. 988–1001, June 2003.

[60] R. Olfati-Saber and R. M. Murray, "Flocking with obstacle avoidance: Cooperation with limited communication in mobile networks," in *Proc. IEEE Conf. Decision Control*, Maui, HI, Dec. 2003, pp. 2022–2028.

[61] R. Olfati-Saber and R. M. Murray, "Consensus problems in networks of agents with switching topology and time-delays," *IEEE Trans. Automat. Control*, vol. 49, no. 9, pp. 1520–1533, Sep. 2004.

[62] N. Chopra and M. W. Spong, "Passivity-based control of multi-agent systems," in *Advances in Robot Control: From Everyday Physics to Human-Like Movements*, S. Kawamura and M. Svinin, Eds. Springer Berlin - Heidelberg, 2006, pp. 107–134.

[63] N. Chopra and M. W. Spong, "Output synchronization of nonlinear systems with time delay in communication," in *Proc. IEEE Conf. Decision Control*, San Diego, CA, Dec. 2006, pp. 4986–4992.

[64] J. Hu and Y. Hong, "Leader-following coordination of multi-agent systems with coupling time delays," *Physica A*, vol. 374, no. 2, pp. 853–863, Feb. 2007.

[65] D. Lee and M. W. Spong, "Agreement with non-uniform information delays," in *Proc. Am. Control Conf.*, Minneapolis, MN, June 2006, pp. 756–761.

[66] Y. Hongwang, Z. Yufan, and P. Weiyun, "Coordination of multiagent systems with time-varying delays," in *Proc. Chinese Control Conf.*, July 2008, pp. 76–80.

[67] C.-L. Liu and Y.-P. Tian, "Coordination of multi-agent systems with communication delays," in *Proc. IFAC World Congress*, Seoul, Korea, July 2008, pp. 10 782–10 787.

[68] S.-J. Chung and J. J. E. Slotine, "Cooperative robot control and concurrent synchronization of Lagrangian systems," *IEEE Trans. Robot.*, vol. 25, no. 3, pp. 686–700, June 2009.

[69] K. Peng and Y. Yang, "Leader-following consensus problem with a varying-velocity leader and time-varying delays," *Physica A*, vol. 388, no. 2-3, pp. 193–208, Jan. 2009.

[70] H. Yan and L. Gao, "Leader-following consensus of multi-agent systems with and without time-delay," in *Proc. WCICA*, July 2010, pp. 4342–4347.

[71] C.-L. Liu and F. Liu, "Consensus of second-order multi-agent systems with input delay," in *Proc. Chinese Control Decision Conf.*, May 2010, pp. 1261–1266.

[72] D. Lee, "Semi-autonomous teleoperation of multiple wheeled mobile robots over the Internet," in *Proc. ASME Dyn. Syst. Control Conf.*, Ann Arbor, MI, Oct. 2008.

[73] P. F. Hokayem, D. M. Stipanović, and M. W. Spong, "Reliable control of multi-agent formations," in *Proc. Am. Control Conf.*, New York City, NY, July 2007, pp. 1882–1887.

[74] P. F. Hokayem, D. M. Stipanović, and M. W. Spong, "Semiautonomous control of multiple networked Lagrangian systems," *Int. J. Robust Nonlin.*, vol. 19, no. 18, pp. 2040–2055, Dec. 2009.

[75] E. J. Rodríguez-Seda, J. J. Troy, C. A. Erignac, P. Murray, D. M. Stipanović, and M. W. Spong, "Bilateral teleoperation of multiple mobile agents: Coordinated motion and collision avoidance," *IEEE Trans. Control Syst. Technol.*, vol. 18, no. 4, pp. 984–992, July 2010.

[76] D. A. Lawrence, "Stability and transparency in bilateral teleoperation," *IEEE Trans. Robot. Automat.*, vol. 9, no. 5, pp. 624–637, Oct. 1993.

[77] R. W. Daniel and P. R. McAree, "Fundamental limits of performance for force reflecting teleoperation," *Int. J. Robot. Res.*, vol. 17, no. 8, pp. 811–830, 1998.

[78] L. F. Peñín, K. Matsumoto, and S. Wakabayashi, "Force reflection for time-delayed teleoperation of space robots," in *Proc. IEEE Int. Conf. Robot. Autom.*, San Francisco, CA, Apr. 2000, pp. 3120–3125.

[79] C. D. Onal and M. Sitti, "Teleoperated 3-D force feedback from the nanoscale with an atomic force microscope," *IEEE Trans. Nanotechnol.*, vol. 9, no. 1, pp. 46–54, Jan. 2010.

[80] N. R. Parker, S. E. Salcudean, and P. D. Lawrence, "Application of force feedback to heavy duty hydraulic machines," in *Proc. IEEE Int. Conf. Robot. Autom.*, Atlanta, GA, May 1993, pp. 375–381.

[81] G. H. Ballantyne, "Robotic surgery, telerobotic surgery, telepresence, and telementoring," *Surgical Endoscopy*, vol. 16, no. 10, pp. 1389–1402, Oct. 2002.

[82] J. Rosen and B. Hannaford, "Doc at a distance," *IEEE Spectrum*, vol. 43, no. 10, pp. 34–39, Oct. 2006.

[83] S. C. Jacobsen, M. Olivier, F. M. Smith, D. F. Knutti, R. T. Johnson, G. E. Colvin, and W. B. Scroggin, "Research robots for applications in AI, teleoperation and entertainment," in *Experimental Robotics VIII*, ser. Springer Tracts in Advanced Robotics, B. Siciliano and P. Dario, Eds. Springer Berlin - Heidelberg, 2003, pp. 2–20.

[84] N. Murakami, A. Ito, J. D. Will, M. Steffen, K. Inoue, K. Kita, and S. Miyaura, "Development of a teleoperation system for agricultural vehicles," *Comput. Electron. Agr.*, vol. 63, no. 1, pp. 81–88, Aug. 2008.

[85] K. Schilling, H. Roth, and O. J. Rösch, "Mobile mini-robots for engineering education," *Global J. Eng. Educ.*, vol. 6, no. 1, pp. 79–84, 2002.

[86] T. B. Sheridan, "Telerobotics," *Automatica*, vol. 25, no. 4, pp. 487–507, July 1989.

[87] T. B. Sheridan, *Telerobotics, Automation, and Human Supervisory Control*. Cambridge, MA: MIT Press, 1992.

[88] D. Lee and M. W. Spong, "Bilateral teleoperation of multiple cooperative robots over delayed communication networks: Theory," in *Proc. IEEE Int. Conf. Robot. Autom.*, Barcelona, Spain, Apr. 2005, pp. 360–365.

[89] D. Lee, O. Martinez-Palafox, and M. W. Spong, "Bilateral teleoperation of multiple cooperative robots over delayed communication networks: Applications," in *Proc. IEEE Int. Conf. Robot. Autom.*, Barcelona, Spain, Apr. 2005, pp. 366–371.

[90] O. Martínez-Palafox and M. W. Spong, "Bilateral teleoperation of a formation of nonholonomic mobile robots under constant time delay," in *Proc. IEEE/RSJ Int. Conf. Intell. Robots Syst.*, St. Louis, MO, Oct. 2009, pp. 2821–2826.

[91] P. F. Hokayem, "Reliable control of multi-agent systems," Ph.D. dissertation, Univ. Illinois at Urbana-Champaign, Illinois, USA, 2007.

[92] Y. Cheung, J. H. Chung, and N. P. Coleman, "Semi-autonomous formation control of a single-master multi-slave teleoperation system," in *Proc. IEEE Symp. Comput. Intell. Control Autom.*, Apr. 2009, pp. 117–124.

[93] O. M. Palafox and M. W. Spong, "Bilateral teleoperation of a formation of nonholonomic mobile robots under constant time delay," in *Proc. IEEE/RSJ Int. Conf. Intell. Robots Syst.*, St. Louis, MO, 2009.

[94] G. N. Desouza and A. C. Kak, "Vision for mobile robot navigation: A survey," *IEEE Trans. Pattern Anal. Mach. Intell.*, vol. 24, no. 2, pp. 237–267, Feb. 2002.

[95] J. C. Kinsey, R. M. Eustice, and L. L. Whitcomb, "A survey of underwater vehicle navigation: Recent advances and new challenges," in *Proc. IFAC Conf. Manoeuvring Control Mar. Craft*, Lisbon, Portugal, Sep. 2006.

[96] M. M. Hunt, W. M. Marquet, D. A. Moller, K. R. Peal, W. K. Smith, and R. C. Spindell, "An acoustic navigation system," Woods Hole Oceanographic Institution, Woods Hole, MA, Tech. Rep. WHOI-74-6, Dec. 1974.

[97] L. L. Whitcomb, D. R. Yoerger, and H. Singh, "Combined Doppler/LBL based navigation of underwater vehicles," in *Proc. Int. Symp. Unmanned Untethered Submersible Techn.*, Aug. 1999.

[98] J. A. Volpe, "Vulnerability assessment of the transportation infrastructure relying on the Global Positioning System," NTSC, U.S. Department of Transportation, Tech. Rep. NAV-CEN, Aug. 2001.

[99] G. Leitmann and J. Skowronski, "Avoidance control," *J. Optim. Theory Appl.*, vol. 23, no. 4, pp. 581–591, Dec. 1977.

[100] I. M. Mitchell, A. M. Bayen, and C. J. Tomlin, "A time-dependent Hamilton-Jacobi formulation of reachable sets for continuous dynamic games," *IEEE Trans. Automat. Control*, vol. 50, no. 7, pp. 947–957, July 2005.

[101] J. A. Sethian, *Level Set Methods and Fast Marching Methods: Evolving Interfaces in Computational Geometry, Fluid Mechanics, Computer Vision, and Materials Science.* Cambridge: Cambridge University Press, 2002.

[102] D. M. Stipanović, P. F. Hokayem, M. W. Spong, and D. Šiljak, "Cooperative avoidance control for multiagent systems," *J. Dyn. Syst. Meas. Control*, vol. 129, pp. 699–707, Sep. 2007.

[103] S. Mastellone, D. M. Stipanović, C. R. Graunke, K. A. Intlekofer, and M. W. Spong, "Formation control and collision avoidance for multi-agent non-holonomic systems: Theory and experiments," *Int. J. Robot. Res.*, vol. 27, no. 1, pp. 107–126, Dec. 2008.

[104] P. F. Hokayem, D. M. Stipanović, and M. W. Spong, "Coordination and collision avoidance for Lagrangian systems with disturbances," *Appl. Math. Comput.*, vol. 217, no. 3, pp. 1085–1094, Oct. 2010.

[105] D. V. Dimarogonas, S. G. Loizou, K. J. Kyriakopoulos, and M. M. Zavlanos, "A feedback stabilization and collision avoidance scheme for multiple independent non-point agents," *Automatica*, vol. 42, no. 2, pp. 229–243, Feb. 2006.

[106] P. Panyakeow and M. Mesbahi, "Decentralized deconfliction algorithms for unicycle UAVs," in *Proc. Am. Control Conf.*, Baltimore, MD, June 2010, pp. 794–799.

[107] R. Olfati-Saber, "Flocking for multi-agent dynamic systems: Algorithms and theory," *IEEE Trans. Automat. Control*, vol. 51, no. 3, pp. 401–420, Mar. 2006.

[108] K. D. Do, "Bounded controllers for formation stabilization of mobile agents with limited sensing ranges," *IEEE Trans. Automat. Control*, vol. 52, no. 3, pp. 569–576, Mar. 2007.

[109] K. D. Do, "Output-feedback formation tracking control of unicycle-type mobile robots with limited sensing ranges," *Robot. Autonomous Syst.*, vol. 57, no. 1, pp. 34–47, Jan. 2009.

[110] O. Khatib, "Real-time obstacle avoidance for manipulators and mobile robots," *Int. J. Robot. Res.*, vol. 5, no. 1, pp. 90–98, 1986.

[111] D. E. Koditschek and E. Rimon, "Robot navigation functions on manifolds with boundary," *Adv. Appl. Math.*, vol. 11, no. 4, pp. 412–442, Dec. 1990.

[112] D. M. Stipanović, "A survey and some new results in avoidance control," in *Proc. Int. Workshop Dyn. Control*, Tossa de Mar, Spain, 2009, pp. 166–173.

[113] H. R. Everett, "Survey of collision avoidance and ranging sensors for mobile robots," *Robot. Autonomous Syst.*, vol. 5, no. 1, pp. 5–67, May 1989.

[114] M. Adams, W. S. Wijesoma, and A. Shacklock, "Autonomous navigation: Achievements in complex environments," *IEEE Instrum. Meas. Mag.*, vol. 10, no. 3, pp. 15–21, June 2007.

[115] S. Li and G. Tao, "Feedback based adaptive compensation of control system sensor uncertainties," *Automatica*, vol. 45, no. 2, pp. 393–404, Feb. 2009.

[116] H. P. Moravec, "Sensor fusion in certainty grids for mobile robots," *AI Mag.*, vol. 9, no. 2, pp. 61–74, 1988.

[117] A. Elfes, "Using occupancy grids for mobile robot perception and navigation," *IEEE Computer*, vol. 22, no. 6, pp. 46–57, 1989.

[118] E. Frew and R. Sengupta, "Obstacle avoidance with sensor uncertainty for small unmanned aircraft," in *Proc. IEEE Conf. Decision Control*, Paradise Island, Bahamas, Dec. 2004, pp. 614–619.

[119] R. Bis, H. Peng, and G. Ulsoy, "Vehicle occupancy space: Robot navigation and moving obstacle avoidance with sensor uncertainty," in *Proc. ASME Dyn. Syst. Control Conf.*, Hollywood, CA, Oct. 2009.

[120] E. J. Rodríguez-Seda, P. O. López-Montesinos, D. M. Stipanović, and M. W. Spong, "Passivity-based model reference robust control for a class of nonlinear systems with input and state measurement delays," in *Proc. IEEE Am. Control Conf.*, Baltimore, MD, June 2010, pp. 6585–6592.

[121] E. J. Rodríguez-Seda and M. W. Spong, "A time-varying wave impedance approach for transparency compensation in bilateral teleoperation," in *Proc. IEEE/RSJ Int. Conf. Intell. Robots Syst.*, St. Louis, MO, Oct. 2009, pp. 4609–4615.

[122] E. J. Rodríguez-Seda, D. M. Stipanović, and M. W. Spong, "Collision avoidance control with sensing uncertainties," in *Proc. Am. Control Conf.*, 2011, to appear.

[123] V. D. Tourassis and C. P. Neuman, "Properties and structure of dynamic robot models for control engineering applications," *Mech. Mach. Theory*, vol. 20, no. 1, pp. 27–40, Jan. 1985.

[124] R. Ortega and M. W. Spong, "Adaptive motion control of rigid robots: A tutorial," in *Proc. IEEE Conf. Decision Control*, Dec. 1988, pp. 1575–1584.

[125] F. Ghorbel, B. Srinivasan, and M. W. Spong, "On the uniform boundedness of the inertia matrix of serial robot manipulators," *Int. J. Robot. Res.*, vol. 15, no. 1, pp. 17–28, Jan. 1998.

[126] A. van der Schaft, *$\mathcal{L}_2$-Gain Stability and Passivity Techniques in Nonlinear Control*. London, UK: Springer-Verlag, 2000.

[127] B. Lehman, "Stability of chemical reactions in a CSTR with delayed recycle stream," in *Proc. IEEE Am. Control Conf.*, June 1994, pp. 3521–3522.

[128] J. S. Ansary, "Stability of differential-difference equations representing heat exchanger and certain other systems," *Int. J. Control*, vol. 17, no. 1, pp. 193–198, Dec. 1972.

[129] H. Khalil, *Nonlinear Systems*. New Jersey: Prentice Hall, 2002.

[130] M. W. Spong, S. Hutchinson, and M. Vidyasagar, *Robot Modeling and Control*. New York: John Wiley and Sons, 2006.

[131] E. J. Rodríguez-Seda, D. Lee, and M. W. Spong, "Experimental comparison study of control architectures for bilateral teleoperators," *IEEE Trans. Robot.*, vol. 25, no. 6, pp. 1304–1318, Dec. 2009.

[132] B. Mettler, *Identification Modeling and Characteristics of Miniature Rotorcraft*. Dordrecht, The Netherlands: Kluwer Academic Publishers, 2003.

[133] J. J. Troy, C. A. Erignac, and P. Murray, "Closed-loop motion capture feedback control of small-scale aerial vehicles," in *AIAA Infotech@Aerospace Conf.*, Rohnert Park, CA, May 2007.

[134] J. J. Troy, C. A. Erignac, and P. Murray, "Haptics-enabled UAV teleoperation using motion capture systems," *ASME J. Comput. Inf. Sci. Eng.*, vol. 9, no. 1, pp. 0 110 031–0 110 037, Mar. 2009.

[135] J. A. Vázquez and M. Velasco-Villa, "Path-tracking dynamic model based control of an omnidirectional mobile robot," in *Proc. IFAC World Congress*, Seoul, Korea, July 2008, pp. 5365–5370.

[136] R. L. Williams, B. E. Carter, P. Gallina, and G. Rosati, "Dynamic model with slip for wheeled omnidirectional robots," *IEEE Trans. Robot. Automat.*, vol. 18, no. 3, pp. 285–293, June 2002.

[137] W. R. Ferrell, "Remote manipulation with transmission delay," *IEEE Trans. Hum. Factors Electron.*, vol. 6, no. 1, pp. 24–32, Sep. 1965.

[138] C. Secchi, S. Stramigioli, and C. Fantuzzi, "Digital passive geometric telemanipulation," in *Proc. IEEE Int. Conf. Robot. Autom.*, Taipei, Taiwan, Sep. 2003, pp. 3290–3295.

[139] W. R. Ferrell, "Delayed force feedback," *Hum. Factors*, vol. 8, no. 5, pp. 449–455, Oct. 1966.

[140] R. J. Anderson and M. W. Spong, "Bilateral control of teleoperators with time delay," in *Proc. IEEE Conf. Decision Control*, Austin, TX, Dec. 1988, pp. 167–173.

[141] G. M. H. Leung, B. A. Francis, and J. Apkarian, "Bilateral controller for teleoperators with time delay via μ-synthesis," *IEEE Trans. Robot. Automat.*, vol. 11, no. 1, pp. 105–116, Feb. 1995.

[142] P. Buttolo, P. Braathen, and B. Hannaford, "Sliding control of force reflecting teleoperation: Preliminary studies," *Presence*, vol. 3, no. 2, pp. 158–172, 1994.

[143] W. S. Kim, B. Hannaford, and A. K. Bejczy, "Force reflection and shared compliant control in operating telemanipulators with time delay," *IEEE Trans. Robot. Automat.*, vol. 8, no. 2, pp. 176–185, Apr. 1992.

[144] Y. Yokokohji and T. Yoshikawa, "Bilateral control of master-slave manipulators for ideal kinesthetic coupling-formulation and experiment," *IEEE Trans. Robot. Automat.*, vol. 10, no. 5, pp. 605–620, Oct. 1994.

[145] Y. Yokokohji, T. Imaida, and T. Yoshikawa, "Bilateral teleoperation under time-varying communication delay," in *Proc. IEEE/RSJ Int. Conf. Intell. Robots Syst.*, Oct. 1999, pp. 1854–1859.

[146] K. Hashtrudi-Zaad and S. E. Salcudean, "Analysis of control architectures for teleoperation systems with impedance/admittance master and slave manipulators," *Int. J. Robot. Res.*, vol. 20, no. 6, pp. 419–445, June 2001.

[147] D. J. Lee and M. W. Spong, "Passive bilateral teleoperation with constant time delays," *IEEE Trans. Robot.*, vol. 22, no. 2, pp. 269–281, Apr. 2006.

[148] I. G. Polushin, P. X. Liu, and C.-H. Lung, "A control scheme for stable force-reflecting teleoperation over IP networks," *IEEE Trans. Syst., Man, Cybern.*, vol. 36, no. 4, pp. 930–939, Aug. 2006.

[149] G. Niemeyer and J. J. E. Slotine, "Telemanipulation with time delays," *Int. J. Robot. Res.*, vol. 23, no. 9, pp. 873–890, Sep. 2004.

[150] S. Hirche and M. Buss, "Human perceived transparency with time delay," in *Advances in Telerobotics*, ser. Springer Tracts in Advanced Robotics, M. Ferre, M. Buss, R. Aracil, C. Melchiorri, and C. Balaguer, Eds. Springer Berlin - Heidelberg, 2007, pp. 191–209.

[151] P. Arcara and C. Melchiorri, "Control schemes for teleoperation with time delay: A comparative study," *Robot. Autonomous Syst.*, vol. 38, no. 1, pp. 49–64, Jan. 2002.

[152] E. Nuño, R. Ortega, N. Barabanov, and L. Basanez, "A globally stable PD controller for bilateral teleoperators," *IEEE Trans. Robot.*, vol. 24, no. 3, pp. 753–758, June 2008.

[153] P. Arcara and C. Melchiorri, "Comparison and improvement of control schemes for robotic teleoperation systems with time delay," in *Advances in Control of Articulated and Mobile Robots*, ser. Springer Tracts in Advanced Robotics, B. Siciliano, O. Khatib, and F. Groen, Eds. Springer Berlin - Heidelberg, 2004, pp. 39–60.

[154] C. Secchi, S. Stramigioli, and C. Fantuzzi, "Position drift compensation in port-Hamiltonian based telemanipulation," in *Proc. IEEE/RSJ Int. Conf. Intell. Robots Syst.*, Beijing, China, Oct. 2006, pp. 4211–4216.

[155] N. Chopra, M. W. Spong, and R. Lozano, "Adaptive coordination control of bilateral teleoperators with time delay," in *Proc. IEEE Conf. Decision Control*, Paradise Island, Bahamas, Dec. 2004, pp. 4540–4547.

[156] N. A. Tanner and G. Niemeyer, "Online tuning of wave impedance in telerobotics," in *Proc. IEEE Conf. Robot. Automat. Mechatron.*, Singapore, Dec. 2004, pp. 7–12.

[157] P. J. Walsh, "Feedback linearization of a robotic manipulators," M.S. thesis, Univ. Illinois Urbana-Champaign, 1994.

[158] A. Jaritz and M. W. Spong, "An experimental comparison of robust control algorithms on a direct drive manipulator," *IEEE Trans. Control Syst. Technol.*, vol. 4, no. 6, pp. 627–640, Nov. 1996.

[159] D. Lee and P. Y. Li, "Passive bilateral control and tool dynamics rendering for nonlinear mechanical teleoperators," *IEEE Trans. Robot.*, vol. 21, no. 5, pp. 936–951, Oct. 2005.

[160] M. A. Srinivasan and C. Basdogan, "Haptics in virtual environments: Taxonomy, research status, and challenges," *Computers & Graphics*, vol. 21, no. 4, pp. 393–404, 1997.

[161] P. Buttolo, R. Oboe, and B. Hannaford, "Architectures for shared haptic virtual environments," *Computers & Graphics*, vol. 21, no. 4, pp. 421–429, 1997.

[162] R. J. Adams and B. Hannaford, "A two-port framework for the design of unconditionally stable haptic interfaces," in *Proc. IEEE/RSJ Int. Conf. Intell. Robots Syst.*, Victoria, B.C., Aug. 1998, pp. 1254–1259.

[163] W. A. McNeely, K. D. Puterbaugh, and J. J. Troy, "Six degree-of-freedom haptic rendering using voxel sampling," in *Proc. ACM SIGGRAPH*, Los Angeles, CA, July 1999, pp. 401–408.

[164] P. A. Ioannou and J. Sun, *Robust Adaptive Control*. Upper Saddle River, NJ: Prentice-Hall, 1996.